Solar thermal energy systems for building integration

Helena Gajbert

Division of Energy and Building Design
Department of Architecture and Built Environment
Lund University
Faculty of Engineering LTH, 2008
Report EBD-T--08/10

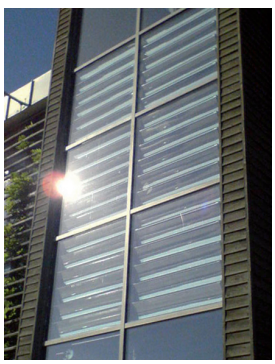

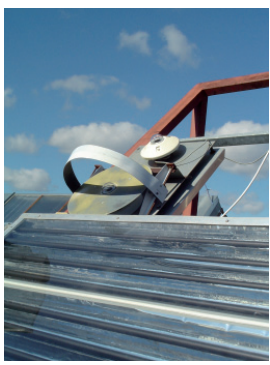


Lund University

Lund University, with eight faculties and a number of research centres and specialized institutes, is the largest establishment for research and higher education in Scandinavia. The main part of the University is situated in the small city of Lund which has about 105 000 inhabitants. A number of departments for research and education are, however, located in Malmö. Lund University was founded in 1666 and has today a total staff of 6 000 employees and 42 500 students attending 90 degree programmes and 1 000 subject courses offered by 74 departments.

Division of Energy and Building Design

Reducing environmental effects of construction and facility management is a central aim of society. Minimising the energy use is an important aspect of this aim. The recently established division of Energy and Building Design belongs to the department of Architecture and Built Environment at the Lund University, Faculty of Engineering LTH in Sweden. The division has a focus on research in the fields of energy use, passive and active solar design, daylight utilisation and shading of buildings. Effects and requirements of occupants on thermal and visual comfort are an essential part of this work. Energy and Building Design also develops guidelines and methods for the planning process.

Solar thermal energy systems for building integration

Helena Gajbert

Licentiate thesis

Keywords

building integration, concentrating collector, incidence angle dependence, optical efficiency, parabolic reflector, photovoltaic-thermal system, solar collector, solar simulator, solar thermal energy, solar thermal system, thermal performance.

The English language corrected by L. J. Gruber BSc(Eng) MICE MIStructE.
Layout: Hans Follin, LTH, Lund.
Cover photo: Helena Gajbert, Bengt Perers and Martin Råberg

Printed by KFS AB, Lund 2008

Report No EBD-T--08/10
Solar thermal energy systems for building integration.
Department of Architecture and Built Environment, Division of Energy and Building Design,
Lund University, Lund

ISSN 1651-8136
ISBN 978-91-85147-29-8

Lund University, Lund Institute of Technology
Department of Architecture and Built Environment
Division of Energy and Building Design
P.O. Box 118
SE-221 00 LUND
Sweden

Telephone: +46 46 - 222 73 52
Telefax: +46 46 - 222 47 19
E-mail: ebd@ebd.lth.se
Home page: www.ebd.lth.se

Abstract

Solar thermal energy has the potential to make a significant contribution to the energy supply for space heating and hot water production, even in locations at higher latitudes, and in this way to reduce the use of fossil fuels. It is therefore very important to increase the use of this technology.

By integrating solar collectors into building envelopes, the cost effectiveness of the collectors can be increased, as building material and labour costs can be reduced. By also using concentrating reflectors the cost effectiveness can be further increased.

The aim of this work is to identify cost effective design criteria for building integrated solar collectors and solar thermal systems. It is hoped that the outcome will give guidance and inspiration to product developers, architects, designers and constructors and thereby help boost the solar thermal market and increase the use of solar thermal systems.

The presented work includes an investigation of solar thermal systems for highly insulated buildings, performed for the International Energy Agency, Solar Heating and Cooling Programme, Task 28, in which solar thermal systems are designed for apartment buildings at high latitudes. Design advice is given based on Polysun simulations and parametric studies of various design parameters. Special attention was paid to dimensioning of the collector area to avoid overheating.

The thermal performance of three designs of collectors for non-insulated roofs with cold attics underneath has been evaluated from measurments. The idea is to produce a thin, cheep and flexible roof-integrated collector for easy installation. The results show that the annual thermal energy yield would be 320, 330 and 280 kWh/m^2 respectively for the three collectors A, B and C, at 50°C operating temperature. The corresponding yield per absorber area is 360, 680 and 1140 kWh/m^2 respectively. As the material costs should be low, there is a potential for the production of these solar collectors, Collector B in particular, as cost effective building elements. However, further investigations for improved efficiency are suggested.

The characteristics of a solar simulator have been investigated in order to show how suitable it is for use as a light source for indoor measurements of concentrating collectors for evaluation of their incidence angle

dependence. It is here concluded that accurate results can be achieved for lower angles of incidence but for higher angles, above 35°-40°, outdoor measurements are more reliable.

A large solar thermal system, with façade-integrated collectors in several directions, connected to the flow side of the district heating grid in Malmö, Sweden, has been studied, e.g. from measured data, and described. WINSUN simulations were performed to validate that the plant works as expected, which was confirmed by the results. The simulated annual output of 174 kWh/m²a from the system agreed well with the measured output, 180 kWh/m^2a. The results from each of the collectors are also described and a small parametric study is given. The good accuracy of these results implies that WINSUN and Meteonorm data can be used for relatively good estimations of a complex system design when climate data is unavailable.

The geometrical design of a concentrating PV/thermal hybrid collector for integration in a wall element is optimised for maximal energy output by short circuit current measurements of thin film photovoltaic cells and MINSUN simulations. The results show that the annual energy output could increase from 70 kWh/m^2 for a vertical reference cell to 120 kWh/m^2 absorber area. Results for a number of geometries are presented.

Table of contents

* Papers I, II and III were published in Sustainable Solar Housing, Vol.1, Strategies and Solutions, by Earthscan (an imprint of James & James Ltd), 8-12 Camden high street, London NW1 0JH, UK, www.earthscan.co.uk.

Preface

This work was mainly financed by the Swedish Energy Agency. Other sponsors are NCC Construction Sweden, who financed part of the work on Paper IV, and Nordic Energy Research, who supported my participation in the REBUS project (Competitive Solar Heating Systems for Residential Buildings).

I want to thank everyone who has helped me with this work.

First of all I want to thank my supervisors, Prof. Björn Karlsson, Dr. Håkan Håkansson and Dr. Bengt Perers, who have given me great support in my work and from whom I have learned very much. Björn has given me good ideas and valuable feedback throughout the project. Håkan has helped me with the experimental work and often given me technical advice. Bengt has been a great support, especially in my work on Paper VI and with the installation of the test rig. I also want to thank Dr. Bengt Hellström who has often given me useful advice.

I have enjoyed working with, Johan Nilsson, Maria Hall, Tobias Rosencrantz and Andreas Fieber in co-authoring different papers.

I want to thank Johan Smeds, Robert Hastings, Maria Wall, and all the participants of the IEA-SHC project Task 28 – Sustainable solar housing, for good collaboration and interesting meetings.

Most of the measurements for this work were carried out at Energy and Building Design but some data was obtained from measurements performed at the test laboratory of Vattenfall Utveckling at Älvkarleby, in which Peter Krohn has been very helpful. Stefan Larsson is acknowledged for his dedicated work with the development of the test rig.

My participation in the REBUS project has taught me a lot about the solar energy research of our neighbour countries and I want to thank the participants of this group.

Martin Råberg, Per Rosén, Elsa Anderson and Simon Furbo have given me valuable information and technical data of different kinds.

I also want to thank all my colleagues at Energy and building design who have given me very good company during this time.

Last but not least, I want to thank my family and my friends, especially Mattias, for their fantastic support and for putting up with my long working hours. You are wonderful!

List of symbols

Latin symbols

A	Area (m^2)
a	Absorber width (m)
b_0	Incidence angle modifier coefficient (-)
C_g	Geometrical concentration ration (-)
c_p	Specific heat capacity (J/kg, K)
F'	Collector efficiency factor (-)
$F'U$	Over all heat loss coefficient of a solar collector (W/m^2K)
$F'U_0$	First heat loss coefficient of a solar collector (W/m^2K)
$F'U_1$	Second heat loss coefficient of a solar collector (W/m^2K^2)
G	Global irradiance (W/m^2)
G_b	Beam irradiance (W/m^2)
G_d	Diffuse irradiance (W/m^2)
G_{sc}	Solar constant (W/m^2a)
h	Height (m)
I	Current (A)
I_{sc}	Short circuit current (A)
I_{mp}	Current at maximal power (A)
K	Optical efficiency (influenced by reflector and glazing) (-)
K_b	Incidence angle modifier for beam irradiance (-)
K_d	Incidence angle modifier for diffuse irradiance (-)
L_l	Local meridian (°)
L_{st}	Standard meridian (°)
$\dot{m}$	Mass flow rate (kg/s)
$(mC)_e$	Effective thermal capacity for a solar collector (J/m^2K)
n	Day number (-)
q	Power (W/m^2)
R	Resistance (Ω)
R_T	Optical efficiency in the transverse plane - influenced by the reflector only (-)
S	Absorbed energy in a solar collector (W/m^2)
T	Temperature (°C)
T_a	Ambient temperature (°C)

T_f	Mean temperature of the absorber fin (°C)
T_{in}	Temperature at the inlet to the collector (°C)
T_m	Mean fluid temperature in the collector (°C)
T_{out}	Temperature at the outlet from the collector (°C)
t	Time (s)
U	Heat loss coefficient (W/m^2K)
V	Voltage (V)
V_{oc}	Open circuit voltage (V)
V_{mp}	Voltage at maximal power (V)

Greek symbols

α	Solar altitude angle, angle between solar vector and the horizontal plane (°)
α_{NS}	The solar altitude angle projected in the north-south-vertical plane (°)
β	Slope (°)
γ	Azimuth angel (°)
γ_s	Solar azimuth angel (°)
ΔT	Temperature difference between the collector and the ambient air (°C)
δ	Declination (°)
η	Efficiency (-)
η_0	Optical efficiency (-)
η_{0b}	Optical efficiency for beam irradiation (-)
η_{0d}	Optical efficiency for diffuse irradiation (-)
θ	Angle of incidence (°)
$\theta_{a/2}$	Acceptance half angle
θ_L	Angle of incidence in the longitudinal plane (°)
θ_{NS}	Angle of incidence in the north-south-vertical plane (°)
θ_T	Angle of incidence in the transverse plane (°)
θ_Z	Zenit angle (º)
λ	Latitude (°)
ν	Tilt angle of optical axis (°)
ρ	Density (kg/m^3)
$(\tau\alpha)_n$	Optical losses at normal incidence (-)
ϕ	Flow rate (m^3/s)
ω	Time angle (°)

Acronymns

AG	Analog ground
CIGS	Copper-indium-gallium-diselenide, CuInGaSe2
CPC	Compound parabolic concentrator
DHW	Domestic hot water
EPS	Expanded polystyrene
FF	Fill factor (-)
HEX	Heat exchanger
SF	Solar fraction (-)
VOC	Volatile organic compound

List of papers

I. Gajbert, H. (2007) Using active solar energy in S*ustainable Solar Housing, Vol.1, Strategies and Solutions*, Hastings, R. & Wall, M. (editors) pp 28-32, ISBN 978-1-84407-325-2, Earthscan, London.

II. Gajbert, H. & Smeds, J. (2007) Apartment buildings in the cold climate, renewable energy strategy in *Sustainable Solar Housing, Vol. 1, Strategies and Solutions*, Hastings, R. & Wall, M. (editors) pp 156-170, ISBN 978-1-84407-325-2, Earthscan, London.

III. Smeds, J. & Gajbert, H. (2007) Apartment buildings in the cold climate, conservation strategy in *Sustainable Solar Housing, Vol. 1, Strategies and Solutions*. Hastings, R. & Wall, M. (editors) pp 150-156, ISBN 978-1-84407-325-2, Earthscan, London.

IV. Gajbert, H., Karlsson, B. & Nilsson J. (2006) Design and evaluation of solar collectors for integration on non-insulated roofs. Submitted to *Solar Energy Materials & Solar Cells*.

V. Gajbert, H., Håkansson, H. & Karlsson, B. (2004) Measurement of concentrating solar collectors using a solar simulator with parallel light. *Proceedings of Eurosun 2004*, Freiburg, Germany.

VI. Gajbert, H., Perers, B. & Karlsson, B. (2005) Design and performance of a large solar thermal system with façade-integrated collectors in several directions, connected to the district heating system. *Proceedings of Northsun 2005*, Vilnius, Lithuania.

VII. Gajbert H., Hall, M. & Karlsson, B. (2007) Optimisation of reflector and module geometries for static, low-concentrating, façade-integrated photovoltaic systems. Published in *Solar Energy Materials & Solar Cells 91* (19), pp 1788-1799.

VIII. Fieber, A., Gajbert, H., Håkansson, H., Nilsson, J., Rosencrantz, T. & Karlsson, B. (2004) Design, building integration and performance of a hybrid solar wall element. *Proceedings of Eurosun 2004*, Freiburg, Germany.

IX. Furbo, S., Thür, A., Fiedler, F., Bales, C., Rekstad, J., Meir, M., Blumberga, D., Rochas, C., Karlsson, B. & Gajbert, H., Competitive solar heating systems for residential buildings, *Proceedings of Northsun 2005*, Vilnius, Lithuania.

1 Introduction

1.1 Background

The ongoing climate changes, caused by the resource consuming life style in our modern society, put us and future generations at great risk and we are given an enormous problem to deal with. It is of the highest importance that the problem is addressed urgently and effectively. The use of fossil fuels must be significantly reduced and renewable energy sources must be implemented on a large scale throughout our society.

Today approximately 80% of the primary energy use in the world is provided by fossil fuels and only about 13% by renewable energy sources. The energy use within the building and service sector accounts for a large share of the total energy use, approximately 40% both in Sweden and in the European Union (Swedish Energy Agency, 2006). This energy demand can be lowered significantly by using improved building construction techniques and a great part of the energy used for space heating and domestic hot water can be supplied by solar thermal energy, which is not only renewable, but also clean in the sense that the conversion phase does not give rise to any green house gas emissions.

The solar thermal market has an immense potential for growth (ESTIF, 2007). The solar energy received by the earth during one hour is more than the total annual energy demand worldwide. It is obvious that we could profit from solar energy to a far greater extent than what is done today. The biggest problem has been that the cost of solar thermal systems has not been low enough to make these systems competitive on the market. This trend is starting to change with rising energy prices, but it is not changing fast enough.

In order to widen and increase the use of solar thermal energy there are several ways to deal with the issue. Legislation is one way, already practised in some European countries. Governmental subsidies are another way, in which continuity is very important.

Although the collectors of today are already highly developed it is also important to continue the development of collectors and system designs in order to improve their efficiency, quality, life expectancy, profitability etc.

A higher market growth could be achieved by the introduction of more cost-effective solar collectors. By integrating solar collectors into building elements, both building materials and the time for installation work can be saved, making the collectors more cost-effective. It can also make the collectors more attractive.

The cost-effectiveness of solar collectors can also be increased by using concentrating collectors. By replacing some of the expensive absorber by cheaper metallic reflectors to concentrate the irradiation onto the absorber, there is a potential to lower the production cost for the collectors. A reduced absorber surface also means lower heat losses.

Sun-tracking collectors with a high concentration ratio would collect the most irradiation per absorber area. However, for building integrated elements, all moving parts should be avoided. Therefore a static system with lower concentration is more suitable for building integration.

1.2 Objectives

The purpose of this work is to find good design characteristics for cost-effective solar thermal systems, with the focus on the design of concentrating building-integrated solar thermal collectors. The work has been divided between studies of solar system designs and the design and evaluation of solar collectors. The objective is to find a collector design that can be developed into a cost-effective product. It is mainly the technical characteristics that are investigated, while the economic aspects are given less attention.

A couple of previously studied collector designs are further investigated and three new collector designs are developed for integration on non-insulated roofs. The collectors are evaluated by indoor and outdoor measurements, with the aim to create cheap, flexible collectors implying simple production and mounting methods.

The geometry of a concentrating façade-integrated solar collector, which could be used either for photovoltaic cells, thermal absorbers or as a photovoltaic/thermal hybrid, has been optimised by measurements and simulations for maximal annual energy output in the Swedish climate.

A necessary part of the work has been to study the characteristics of the solar simulator at Energy and Building Design, Lund University, in order to find how suitable it is to use for evaluations of the incidence angle dependence of concentrating collectors.

Another important part of the work has been to construct a solar collector test rig in order to facilitate and improve the repetitiveness of the collector measurements performed.

Design features of solar thermal systems for houses with very low energy demand have been investigated by simulations and analyses within the framework of the International Energy Agency and the Solar Heating and Cooling programme (IEA-SHC), Task 28 - Sustainable Solar Housing.

The design and performance of a large solar thermal system with façade-integrated collectors, producing heat for the district heating grid in Malmö, has been studied. Important design features of the system have been described and simulations and analyses have been performed to verify the system performance.

1.3 Outline

A theoretical background with facts and formulas concerning solar irradiation, solar angles, heat transfer, optical concentration of light etc. is presented in Chapter 2.

The measurement techniques, tools and experimental methods are described in Chapter 3.

The work performed for IEA-SHC, Task 28 - Sustainable Solar Housing - is presented in Chapter 4, starting with an introduction to the work within Task 28. Section 4.2 presents the content of Section 2.5 in the handbook, Sustainable Solar Housing, Vol 1, Strategies and Solutions, an outcome of the project. This is basically an introduction to how active solar thermal energy can be utilised within buildings, focusing on buildings with very low energy demand. Section 4.3 is the simulation work performed to design solar thermal systems for buildings with limited energy use (presented in Sections 8.6 and 8.7 in the handbook). This contains simulation results of the energy performance of solar thermal systems for apartment buildings in the Stockholm climate. Design advice is given for this type of buildings in the end of this chapter. The chapters from the handbook are also presented as Papers I, II and III.

Chapter 5 is about the evaluation of three slightly different solar collectors designed for integration in non-insulated roofs, also presented in Paper IV. Commonly used corrugated steel makes up the frame of these collectors, two of which have concentrating reflectors to enhance the irradiation on the absorbers during the heating season and thereby achieve a better balance of the energy yield over the year. The design, evaluations and results are presented.

Chapter 6 presents the work performed to investigate how suitable a solar simulator is for applications concerning the evaluation of the incidence angle dependence of concentrating collectors. Some issues that were noted about the accuracy of measurements at high angles of incidence

have been investigated by using a photodiode array. The results are also presented in Paper V.

Chapter 7 is a summary of Paper VI - a study and evaluation of a solar thermal system connected to the district heating system in Malmö. These solar collectors are integrated in the façade in five different directions as they were installed to replace the old façade material. Simulations of the collector output have been performed as well as analyses of data from the plant. The control features of the system are discussed as well as the simulation results.

Chapter 8 presents the work of Paper VII, which is an optimisation of the reflector and module geometry of a façade-integrated photovoltaic/thermal hybrid solar collector. The work contains experimental measurements and results which have also been used in simulations performed to find the maximal annual energy yield.

Chapter 9 contains a summary and discussion of the work.

2 Theoretical background

2.1 Solar thermal market development

2.1.1 Historic development

The basic theory of solar heating is simple and has been known and used for a very long time. The ancient Greeks used passive solar energy to heat their homes in the 4th century BC and there were ideas of how to actively convert solar energy to heat already in the 18th century, when scientists tested the highest temperature they could achieve in a "hot box", an insulated box with a glass lid. In the 19th century people began to use solar water heaters consisting of black painted metal tanks that were put on the roofs. However, with this technique it took a long time to heat the water and as soon as the sun went down the water would cool down again. Eventually, the technique with the "hot box" and the water tanks were combined in the world's first commercial solar water heater, which was patented in 1891 by Clarence Kemp from Baltimore, USA. This collector was made of black painted metal tanks that were put in boxes with glass lids, capturing the sunlight. It sold very well and the technique was further developed by several actors. In 1909 William J. Bailey developed a system similar to the solar systems used today, where the tank and the solar collector were separated into two units and the insulated storage tank could be placed inside the house, keeping the water hot much longer than previously used systems. (Butti & Perlin, 1980)

In the following years, the market for solar thermal energy started to grow in the USA, but collapsed as gas and electricity became availably at low price. In the 1950:s, 1960:s and 1970:s more attention was paid to solar thermal energy in countries all around the world. The technology was introduced in Japan, where the market increased very quickly. Also in Australia and in countries around the Mediterranean Sea, e.g. Israel, Turkey, Cyprus and Greece, people started to use solar water heaters. These are areas where the market has been strong for a long period (ESTIF, 2006). In 1973, when the oil embargo took place and the price of oil increased dramatically the solar water heater industry was revived in many places.

After the price of oil had stabilized in the mid 1980s the sales of solar collectors decreased. (Butti and Perlin, 1980; Dessus & Pharabod, 2000).

2.1.2 Recent development

Since 1990 there has been a favourable development in the solar thermal market in many countries, mainly in China and Europe (Swedish Ministry of Enterprise, Energy and Communications, 2007). In 2004 over 140 million m^2 collectors were installed worldwide, of which 76% were glazed collectors (flat plate and evacuated tube collectors). This corresponds to 99 GWth[1] installed capacity, an annual energy yield of 58 MWh, replacing 9.3 billion litres of oil and thereby saving 25 million tons of CO_2 annually. China is completely dominating the world market, both in annual sales – with impressively 78 % of the world market (ESTIF, 2006) – and in terms of installed capacity. 44% of the total capacity world wide is installed in China, followed by USA (20%), Japan (5.5%), Turkey (5.2%), Germany (4.6%), Australia (3.4%), Greece (2.1%) and Austria (2.0%). In China the dominating collector type is evacuated tube collectors in thermo siphon systems, whereas unglazed collectors heating swimming pools are those most commonly used in USA and Australia. In Europe, Japan, Turkey and Israel the glazed flat plate collectors are dominating. The countries with the highest installed collector capacity per capita are Cyprus (with 63 MW_{th} per 100 000 inhabitants), Israel (52 MW_{th}), Greece, Austria and Barbados (19 MW_{th}) (Figures from 2004). (Weiss et al., 2006[2])

The European market is now growing extremely fast. It increased by 44% from 2005 to 2006, when 3 million m^2 glazed collectors were sold (Eur'ObservER, 2007). This can be compared to the European collector sales of 0.3 million m^2 annually at the end of the 1980s (Dalenbäck, 2005). The installed capacity of glazed solar thermal collectors exceeded 20 million m^2 (14 MW_{th}) at the end of 2006 (Eur'ObservER, 2007).

It seems unlikely that the target of 100 000 000 m^2 installed collector capacity in the EU by 2010, which was presented in the European Commission's White Paper from 1997, will be reached. The aim is to reach 12% renewable energy in the EU by 2010, a target which was then considered ambitious but realistic (European Commission, 1997). However, some

[1]Experts from seven countries have agreed on a factor of 0.7 kW_{th}/m^2 collector area to derive the nominal capacity from solar collectors. The decision was based on tests results and operating conditions specified in the European Code EN 12975-2. More information on www.iea-shc.org and www.estif.org.

[2]These figures are based on a survey conducted in 41 countries estimated to represent 85-90% of the solar thermal market worldwide and 57% of the world's population.

European countries are excellent role models. If every European country followed the Austrian model, where 15% of all detached houses have solar thermal systems, the target would have been reached already. In fact, two new objectives for installed solar thermal collectors, to be accomplished by 2020, have been defined by ESTIF (European Solar Thermal Industry Federation) and published in January 2007 in their "Solar Thermal Action Plan". The minimum objective of reaching an installed capacity of 91 GW_{th} (130 million m^2) in Europe is based on the Austrian collector density of 199 kW_{th} per 1000 inhabitants and the ambitious objective of reaching 320 GW_{th} (457 million m^2) is based on having 1 m^2 installed collector per inhabitant (ESTIF, 2007).

As the problems with global warming and limited oil resources have attracted more and more attention, a growing number of municipalities, regions and countries are starting to take action by introducing legislation on financial support systems. Germany has for long been the leading European country in annual sales, followed by Greece and Austria. These are countries were governmental economic support systems have been generous, continuous and reliable. The high energy prices have created a favourable market climate and encouraged many small scale production units to act and to grow. In Austria, for example, private initiatives and campaigns have also played an important role for this development. (Thür and Weiss, 2005; Dalenbäck, 2005; Eur'ObservER, 2007).

The markets in France and Spain are now growing very fast, mainly due to investment programmes and legislation. In France a simple tax deduction system, which enables 50% of the investment costs to be recovered, has recently been introduced and the new Spanish building code, introduced in 2006 (CTE – Código Técnico de la Edificatión), makes it obligatory to use solar thermal energy to cover 30-70% of the hot water demand in all new constructions or completely renovated buildings. Portugal and India have also introduced legislation similar to that in Spain, something that has been applied in Israel since 1980. The Chinese government has set up a target that 20-30% of the population shall have access to solar heated hot water in 2015, which would require the installation of about 250 million m^2 solar collectors. (Eur'ObservER, 2007; Swedish Ministry of Enterprise, Energy and Communications, 2007)

In Sweden the total area of installed solar thermal collectors is approximately 200 000 m^2 (0,15 GW_{th},) and also here the market is growing. The sales of glazed collectors increased by 26% between 2005 and 2006 (ESTIF, 2006; Eur'ObservER, 2007). Here is also a large potential for solar installations on the existing buildings. If solar thermal systems were to be installed in all buildings in Sweden, the potential for replacing bought energy by solar thermal energy has been estimated to 12 TWh,

which would require approximately 40 million m^2 of solar collectors (Kjellsson, 2004).

The growing market for solar collectors does not only reduce the green house gas emissions, but it also creates jobs and increases industrial growth. (Eur'ObservER, 2007)

The solar thermal collectors sold today are significantly improved in comparison to those introduced in the late 1970s, mainly due to international cooperation in testing and certification (Solar Keymark) (Swedish Ministry of Enterprise, Energy and Communications, 2007). Today's collectors are highly developed with only low heat losses, enabling heat generation even at lower irradiation. The use of absorbers with selective surfaces have significantly improved the efficiency of solar collectors as they offer high solar absorbance and yet a very low thermal emittance. This is achieved by double layers of coatings on the absorbers giving high reflectance and low emittance for radiation of longer wave lengths and low reflectance and high absorbance for solar radiation. The glazing is often low in iron content and antireflective treated, which gives higher transmittance.

There is also a wide variety of designs of the solar thermal systems that are in operation. The system design developments have led to increased efficiency of the solar thermal energy systems. Pumps of suitable dimensions and characteristics have for long been hard to find, but now the increased market demand has given incentives for development of better suited components.

2.2 Solar irradiation

By fusion in the sun, hydrogen atoms are combined to helium while energy is liberated and radiated as electromagnetic radiation. The spectrum of the sun's radiation is very similar to that of a blackbody at approximately 5780 K, and its emissivity can be regarded as equal to 1. The radiation is distributed in all directions from the sun and the radiation that falls on the earth outside the atmosphere is 1367 W/m^2 (Duffie & Beckman, 1991), also referred to as the solar constant, G_{sc}. This is a yearly average, as the irradiance varies slightly over the year (from 1322 in July to 1412 W/m^2 in December), due to the earth's slightly elliptic orbit around the sun and to changes in solar activity (Duffie & Beckman, 1991). As different atmospheric gases, e.g. CO_2 and water vapour, absorb and scatter solar radiation of different wave lengths, the irradiance that reaches the earth after passing through the atmosphere is reduced to approximately 1000 W/m^2. The solar spectrum extends from 0.3 μm to 3.0 μm and

includes near infrared radiation, visible light and ultraviolet radiation and the highest intensity is in the area of visible light, at approximately 0.5 µm. The solar spectrum in Figure 2.1 shows the radiation from the sun before and after it passes through the atmosphere. It also shows the absorption of solar radiation by atmospheric gases.

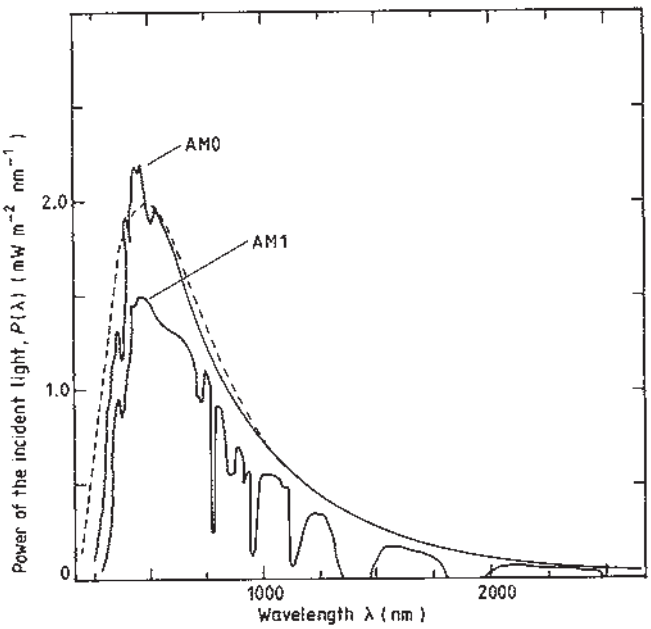

Figur 2.1 *The solar spectrum before (AM0) and after (AM1) passing through the atmosphere.*

At higher latitudes, the angle of incidence of the solar irradiance on the earth's surface is higher, which results in lower irradiance to the ground. The distance through which solar radiation has to travel in the atmosphere is also longer at higher latitudes, which means that more energy is absorbed and reflected before reaching the earth. Because of these two effects, average irradiance and annual irradiation are lower at high latitudes. The irradiance is also reduced depending on cloudiness, humidity and the concentration of particles in the air. As the total annual global irradiation (on a horizontal surface) varies from 640 to over 2300 kWh/m² depending on the location, there are naturally very different opportunities of using solar energy. In Sweden, the annual irradiation measured on a horizontal surface is between 950 and 1000 kWh/m^2. In the Mediterranean area the global annual irradiation is 1400-1800 kWh/m² and in some areas it can

be over 2300 kWh/m², as can be seen in Figures 2.2 and 2.3 (Meteotest, 2006).

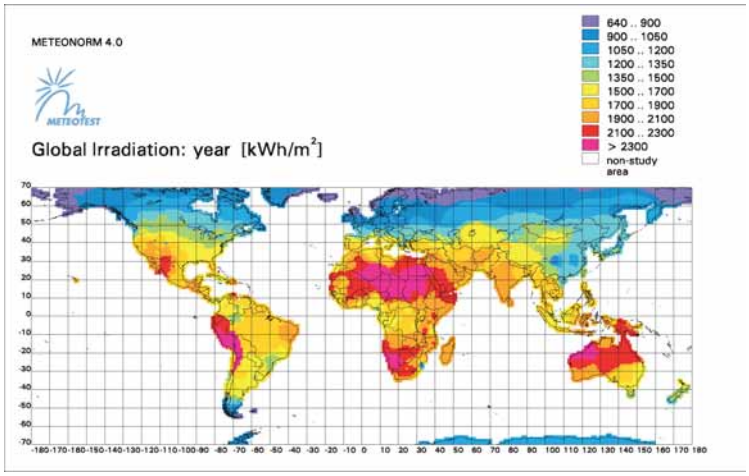

Figure 2.2 *The annual global irradiation throughout the world, measured on a horizontal surface. (Figure from Meterotest 2006).*

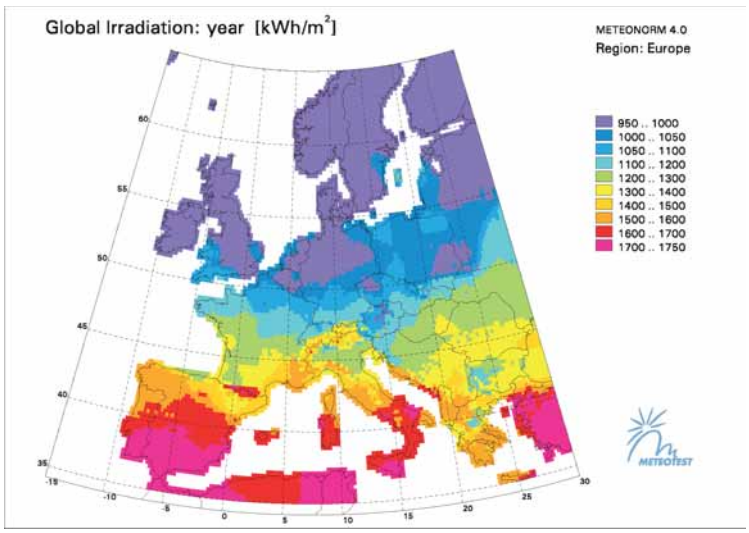

Figure 2.3 *The annual global irradiation in Europe, measured on a horizontal surface. Figure from Meteotest (2006).*

2.3 Solar angles

As the apparent location of the sun varies over the day and over the year, the angle of incidence of solar irradiance on a specific surface varies. To the right in Figure 2.4 the incoming irradiance on a horizontal surface can be seen in relation to the cardinal points, east (E), west (W), south (S), north (N) and to the zenith axis (Z). The solar irradiance is here imagined as a vector, the solar vector. The angle of incidence to a surface is denoted θ and if a horizontal surface is considered, this angle can also be referred to as the zenith angle, θ_z, as shown to the right in the figure. α is the solar altitude angle or the solar height. The azimuth angle of a surface, γ, is the angle between the normal to the surface projected in the horizontal plane and the south axis. The solar azimuth angle, γ_s, describes the location of the sun relative to the south axis (i.e. the angle between the solar vector projected in the horizontal plane and the south axis).

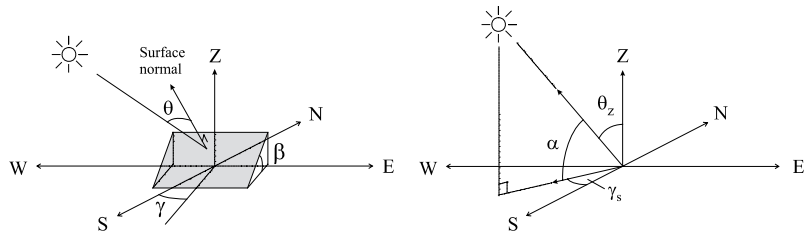

Figure 2.4 *The slope of a surface, β, the surface's azimuth angle, γ, and the sun's angle of incidence to the surface, θ, are shown in the left figure. To the right, the azimuth angle of the sun, γ_s, the solar altitude angle (or the solar height), α, and the zenith angle, θ_z, i.e. the sun's angle of incidence to the horizontal, are shown.*

The sun's angle of incidence, altitude angle and azimuth angle can be calculated according to the following equations (Duffie & Beckman, 1991).

The declination, δ, i.e. the angle between the direction of the solar irradiation and the equatorial plane, varies between -23.45° and 23.45° according to Equation 1. The inclination of the earth's axis is 23.45°. The time of year is here expressed by the day number, *n*.

$$\delta = 23{,}45 \cdot \sin\left(\frac{360 \cdot (284 + n)}{365}\right) \qquad \text{Eq. (1)}$$

The solar time is a way of expressing time based on the assumption that the sun is in the south at 12.00 o'clock.

Solar time – standard time = $4(L_{st}-L_l) + E$ (time difference in minutes) Eq. (2)

The equation of time, E, is used to compensate for the difference between solar time and standard time that is caused by the earth´s elliptic orbit around the sun and by the tilt of the axis of the earth. L_{st} is the standard time meridian (positive in west, $L_{st} = -15^o$ in Sweden) and L_l is the local meridian.

$$E = 229.2 \cdot (0.000075 + 0.001868 \cdot \cos(B) - \\ - 0.032077 \cdot \sin(B) - 0.014615 \cdot \cos(2B) - \\ - 0.04089 \cdot \sin(2B)) \qquad \text{Eq. (3)}$$

$B = 360(n\text{-}1)/365$ (in degrees) Eq. (4)

The time angle, ω, describes the sun's position east or west of the local meridian (positive angles west of the meridian) and can be calculated as in Equation 5, where *hh* stands for hours and *mm* for minutes, in normal time.

$$\omega = 15 \cdot (hh - 12) + \frac{mm + E}{4} + L_{st} - L_l \qquad \text{Eq. (5)}$$

Knowing the declination and the time angle, the solar altitude angle, α, and the solar azimuth angle, γ_s, can be calculated by Equations 6 and 7, for which the latitude, λ, must be known.

$$\alpha = \arcsin(\cos(\delta) \cdot \cos(\omega) \cdot \cos(\lambda) + \sin(\delta) \cdot \sin(\lambda)) \qquad \text{Eq. (6)}$$

$$\tan(\gamma_s) = \frac{\cos(\delta) \cdot \sin(\omega)}{(\cos(\delta) \cdot \cos(\omega) \cdot \sin(\lambda) - \sin(\delta) \cdot \cos(\lambda))} \qquad \text{Eq. (7)}$$

For calculation of the angle of incidence, θ, on a tilted surface, with the tilt angle β, and surface azimuth angle γ, Equation 8 or 9 can be used.

$$\theta = \arccos(\cos(\delta)\sin(\omega)\sin(\beta)\sin(\gamma) + \\ + \cos(\delta)\cos(\omega)\sin(\lambda)\sin(\beta)\cos(\gamma) - \\ - \sin(\delta)\cos(\lambda)\sin(\beta)\cos(\gamma) + \\ + \cos(\delta)\cos(\omega)\cos(\lambda)\cos(\beta) + \\ + \sin(\delta)\sin(\lambda)\cos(\beta)) \qquad \text{Eq. (8)}$$

$$\theta = \arccos(\cos(\alpha)\sin(\beta)\cos(\gamma_s - \gamma) + \sin(\alpha)\cos(\beta)) \qquad \text{Eq. (9)}$$

When static concentrators for solar collectors are designed, it is important to consider the variation in the solar altitude and the angles of incidence on the surface in question. It is often useful to use α_{NS}, the projection of the solar altitude angle in the meridian plane (the north-south vertical plane). In order to calculate this angle, a coordinate system with the axes X, Y and Z is imagined (X representing south, Y east and Z the zenith axis). The coordinates are transformed from spherical to Cartesian according to Equations 10-12. These angles and coordinate systems are illustrated in Figure 2.5. The projected solar altitude angle is then derived according to Equation 13.

$$X = \cos(\alpha) \cdot \cos(\gamma_s) \qquad \text{Eq. (10)}$$

$$Y = \cos(\alpha) \cdot \sin(\gamma_s) \qquad \text{Eq. (11)}$$

$$Z = \sin(\alpha) \qquad \text{Eq. (12)}$$

$$\tan(\alpha_{NS}) = \frac{\sin(\alpha)}{\cos(\alpha) \cdot \cos(\gamma_s)} = \frac{\tan(\alpha)}{\cos(\gamma_s)} \qquad \text{Eq. (13)}$$

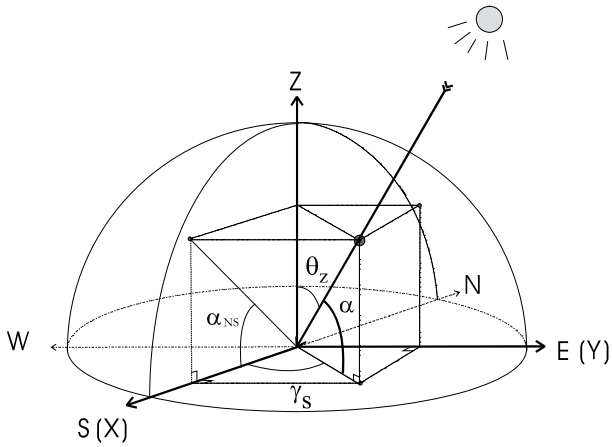

Figure 2.5 *The solar altitude angle, α, the solar altitude angle projected in the north-south vertical plane, α_{NS}, the solar azimuth angle, γ_s, and the zenith angle,θ_z, in relation to the cardinal points and the zenith axis.*

The projected solar altitude angle, α_{NS}, varies over the day as shown in Figure 2.6, showing data from Stockholm (60° latitude). The curves represent different months. At the equinox, α_{NS} in Stockholm is constant 30° during the whole day. In summer this angle is highest in the morning and in the evening, and in winter the highest angle is at noon.

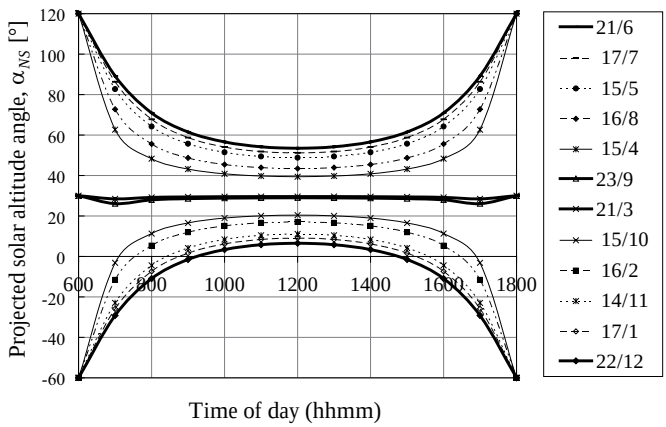

Figure 2.6 *The projected solar altitude angle, α_{NS}, shown over the day for different months of the year for a location at latitude 60°.*

At high latitudes the irradiation from low solar altitude angles gives a relatively high contribution to the annual irradiation. In Stockholm, Sweden (latitude 59.4°N), the highest amount of irradiation on a vertical south-facing surface is from projected solar altitude angles, α_{NS}, between 50° and 55° according to Rönnelid (1998) from 1983-1991, shown in Figure 2.7a. In Figure 2.7b, the irradiation on a south-facing surface tracking around an east-west axis is shown. The irradiation is considerably reduced during the winter due to the cloudy climate and absorption of the radiation in the atmosphere (Rönnelid et al., 1999). This explains the low irradiation for α_{NS} =7°.

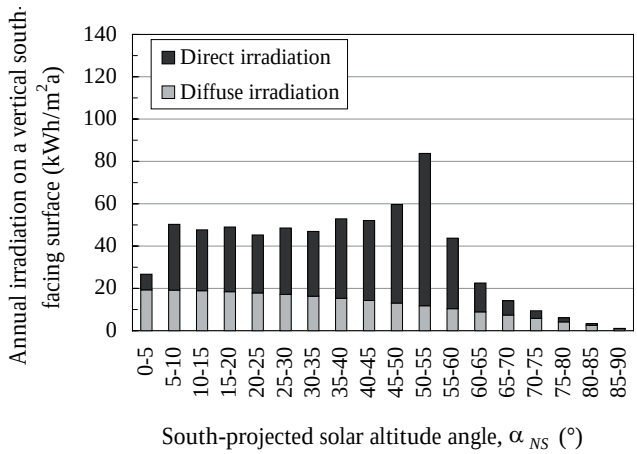

Figure 2.7a *The annual solar irradiation from different projected solar altitude angles, α_{NS}, on a vertical south-facing surface. Data collected in Stockholm 1983-1991 (Rönnelid, 1998).*

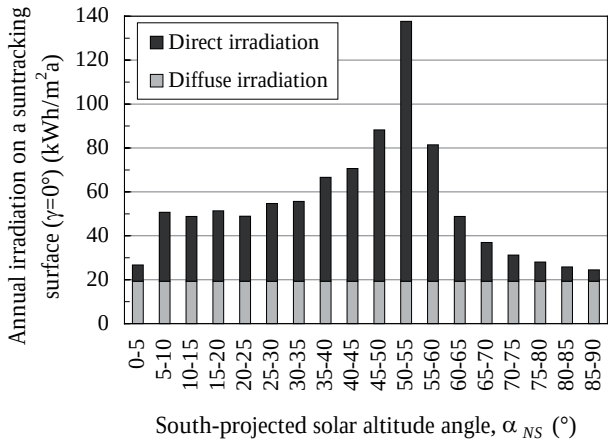

Figure 2.7b *The annual solar irradiation from different projected solar altitude angles, α_{NS}, on a surface tracking around an east-west axis. Data collected in Stockholm 1983-1991 (Rönnelid, 1998).*

2.4 Heat transfer and thermal performance of solar collectors

The thermal performance of a solar thermal collector is determined based on its optical properties and its insulating capacity. When irradiation falls on the collector, a part of it is lost through optical losses, e.g. reflection in the glazing, absorption in the glazing and also reflections in the absorber. There are also multiple reflexes between the glazing and the absorber. The remaining irradiation is absorbed in the absorber, from where the heat is transported, mainly through conduction and convection, to the heat transfer medium. Thereafter the heated liquid is pumped to a heat storage tank. The absorber loses heat, mainly through convection and radiation, but also due to conductive heat losses, and the insulation of both the collector and the piping is very important.

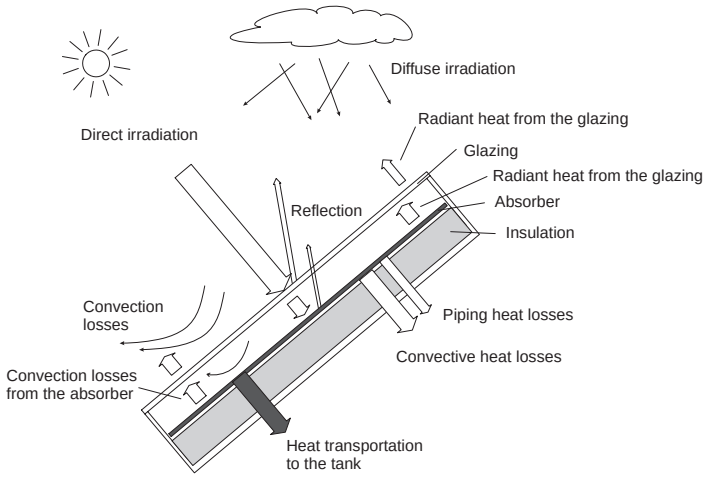

Figure 2.8 The heat transfer processes in a solar collector.

The power, q, from a solar collector is the solar radiation absorbed by the absorber, reduced by the heat losses. This is described by Equation 14, where S is the absorbed radiation, T_f is the temperature of the absorber fin and T_a is the temperature of the ambient air. U is the heat loss coefficient (W/m^2K) describing the collector's insulation capacity.

$$q = S - U \cdot (T_f - T_a) \qquad \text{Eq. (14)}$$

2.4.1 Irradiance

The global solar irradiation, G, is the sum of the direct irradiation from the sun, also referred to as beam irradiation, G_b, and the diffuse irradiation, G_d. The ground reflected irradiation, G_g, which is often small enough to be neglected, is sometimes separated from the diffuse irradiation but it is often included in the diffuse irradiation model, as in this case also.

The momentary efficiency of a solar collector is calculated by the ratio of the power to the irradiance.

$$\eta = \frac{q}{G} \qquad \text{Eq. (15)}$$

2.4.2 Optical losses

The optical efficiency of the collector describes the losses of irradiation in the collector due to reflection and absorption in the glass cover and the absorber. For a concentrating collector there are optical losses also in the reflector. The optical efficiency can also be referred to as the zero-loss efficiency, i.e. the efficiency in an ideal case, when the temperature difference between the absorber and the ambient air is zero, so that the heat losses are eliminated leaving only the optical losses.

Optical losses in the glass cover

The glass covering the absorber reduces the irradiation on the absorber since part of the irradiation is reflected on the glass surfaces and part of it is absorbed in the glass, while the rest of the light is transmitted. Flat clear 4 mm glass panes have a transmittance of approximately 83% at normal incidence. The development of glass material by anti-reflection treatment and by reduction of the iron content has resulted in increased transmittance. Glass panes with reduced iron content have a transmittance of approximately 90% at normal incidence. It is also becoming more common to use antireflection treated glass, which has transmittances of up to 95% (Brogren et al., 2000).

Optical losses in reflectors

The reflectance of metals is high and weakly angle dependent. The optical losses in reflectors of various materials, e.g. steel or aluminium, has been investigated in several studies. The steel reflectors have been found to have reflectances of around 65% and to be very durable. Aluminium reflectors have reflectances of up to 90% but are less durable outdoors. Below a glass the anodised aluminium reflectors have been shown to be long-term stable (Brogren et al., 2000).

Absorbed energy from solar radiation

The absorbed energy in the collector, S, in Equation 16, is the total irradiance reduced by the optical losses in the collector. In order to describe the incidence angle dependence of the absorbed energy, there are different models, which are attempts to describe the transmittance of the glazing for different angles of incidence. The parameters K_b and K_d are the incidence angle modifiers for beam and diffuse irradiance. The term $(\tau\alpha)_n$ describes the optical losses at normal incidence. Multiple reflexes between the glazing and the absorber are also included in this term.

$$S = (\tau\alpha)_n (K_b \cdot G_b + K_d \cdot G_d) \quad \text{Eq. (16)}$$

The most commonly used model of the incidence angle modifier for beam irradiance, K_b, is expressed in Equation 17, which is valid for incidence angles below 60°. For incidence angles over 60°, the curve declines linearly to 90°. The incidence angle modifier coefficient, b_0, is characteristic for the glazing.

$$K_b = 1 - b_0 \cdot \left(\frac{1}{\cos\theta} - 1 \right) \quad \text{Eq. (17)}$$

The collector efficiency factor, *F'*, is used to compensate for the heat losses that arise because the temperature of the absorber flange is higher than the temperature of the fluid in the absorber. *F'* is a temperature dependent parameter which includes various heat resistances in the absorber and influences both the absorbed energy and the heat losses, due to the collector characteristics. If *F'* is taken into account, the power, *q*, can be expressed as in Equation 18, where the difference between the mean liquid temperature, T_m, and the temperature of the surrounding air, T_a, is used instead of (T_f-T_a). This is the more commonly used expression. T_m is also easy to establish by measurements of the inlet and outlet liquid temperatures, T_{in} and T_{out} , of the collector. The power can therefore be developed into Equation 20. The term (T_m-T_a) is often referred to as ΔT.

$$q = F'S - F'U \cdot (T_m - T_a) \quad \text{Eq. (18)}$$

$$T_m = \left(\frac{T_{in} + T_{out}}{2} \right) \quad \text{Eq. (19)}$$

$$q = F'(\tau\alpha)_n K_b G_b + F'(\tau\alpha)_n K_d G_d - F'U(T_m - T_a) \quad \text{Eq. (20)}$$

By less detailed expression of the irradiation, the power can be written as in Equation 21.

$$q = \eta_0 \cdot G - F'U \cdot \Delta T \quad \text{Eq. (21)}$$

The incidence angle dependent term, K_b, and the term $F'(\tau\alpha)_n$ are put together and are referred as η_{0b}, the optical efficiency or the "zero-loss efficiency" for beam irradiation. Sometimes it is also referred to as $F'(\tau\alpha)_e$, where e denotes effective.

$$\eta_{0b} = F'(\tau\alpha)_e = F'(\tau\alpha)_n \cdot K_b \qquad \text{Eq. (22)}$$

In the same way the incidence angle modifier for diffuse irradiance, K_b, and $F'(\tau\alpha)_n$ are often written together as η_{0d}. The power can then be expressed as in Equation 23.

$$q = \eta_{0b} \cdot G_b + \eta_{0d} \cdot G_d - F'U \cdot (T_m - T_a) \qquad \text{Eq. (23)}$$

2.4.3 Thermal heat losses from the collector

Heat is lost from the solar collector through the top, the back and the edges of the collector and can thus be described as in Equation 24 (subscripts *b* for back, *t* for top and *e* for edges).

$$U = U_b + U_t + U_e \qquad \text{Eq. (24)}$$

The overall temperature dependent heat loss coefficient, *F'U*, can also be written as:

$$F'U = F'U_0 + F'U_1 \cdot (T_m - T_a) \qquad \text{Eq. (25)}$$

The term describing the heat losses can thus be written as:

$$F'U \cdot (T_m - T_a) = F'U_0 \cdot (T_m - T_a) + F'U_1 \cdot (T_m - T_a)^2 \qquad \text{Eq. (26)}$$

There are also cumulative temperature changes in the collector that affect the power. The term $(mC)_e\, dT/dt$ is the heat capacity of the collector, multiplied by the temperature increase of the collector. By adding this term, the expression of the collector power can be developed into Equation 27.

$$q = \eta_{0b} G_b + \eta_{0d} G_d - F'U_0 (T_m - T_a) - F'U_1 (T_m - T_a)^2 - (mC)_e \frac{dT_m}{dt} \qquad \text{Eq. (27)}$$

2.4.4 Evaluation of thermal performance from measured data

Evaluations of the thermal performance of solar collectors are performed by measurements of the liquid temperatures at the inlet and outlet, the ambient temperature, the flow rate and the diffuse and global irradiance in the collector plane, according to standard procedures (in Sweden according to SS-EN 12975-2). The overall efficiency of the collector can then be determined from Equation 28, where $\dot{m}$ is the mass flow rate, c_p is the specific heat capacity and A is the collector area. As the density of the liquid is temperature dependent it should be determined for the temperature in the flow meter. The value of c_p should be determined at the mean temperature of the liquid in the collector.

$$\eta = \frac{\dot{m} \cdot c_p \cdot (T_{out} - T_{in})}{G \cdot A} \qquad \text{Eq. (28)}$$

The total optical efficiency, η_0, can be calculated from measurements of thermal performance by rearranging Equation 21 into Equation 29.

$$\eta_0 = \frac{q + F'U(T_m - T_a)}{G} \qquad \text{Eq. (29)}$$

A more specific evaluation of the measured data can be performed by multilinear regression, MLR, according to the model described by Perers (1993). The model is based on Equation 27, which for a flat plate collector can be written as in Equation 30. From the monitored parameters, the collector power, q, the diffuse and direct irradiance, G_b and G_d, the mean collector temperature, T_m, and the ambient temperature, T_a, the parameters $F'(\tau\alpha)_n$, b_0, K_d, $F'U_0$, $F'U_1$ and $(mC)_e$ are derived by MLR.

$$q = F'(\tau\alpha)_n \cdot \left(1 - b_0 \cdot \left(\frac{1}{\cos(\theta)} - 1\right)\right) \cdot G_b + F'(\tau\alpha)_n \cdot K_d \cdot G_d - \\ - F'U_0 \cdot (T_m - T_a) - F'U_1 \cdot (T_m - T_a)^2 - (mC)_e \cdot \frac{dT_m}{dt} \qquad \text{Eq. (30)}$$

For *concentrating collectors* (non-tracking), the optical efficiency for beam irradiation is strongly dependent on the angle of incidence of the irradiation in the transverse plane. This means that Equation 23 and K_b cannot be applied to describe the angular dependence. A detailed angular

dependence of the optical efficiency should therefore be calculated and established from measurements in order to set up a model for predicting the collector power. The optical efficiency for beam irradiation can be calculated from Equation 31.

$$\eta_{0b}(\theta) = \frac{q - \left(\eta_{0d} G_d - F'U_0 (T_m - T_a) - F'U_1 (T_m - T_a)^2 - (mC)_e \frac{dT_m}{dt} \right)}{G_b} \qquad \text{Eq. (31)}$$

Optical efficiency of concentrating photovoltaic systems

For concentrating photovoltaic systems, the optical efficiency can also be calculated from measurements of the short-circuit current from the photovoltaic cells in the concentrating system, $I_{sc,\,conc}$, and from a reference cell of equal type and size that is placed in the same direction as the glazing of the concentrating system, $I_{sc,\,ref}$. As the short-circuit current is proportional to the irradiance on the cell, the relation between these currents gives a measure of the influence of the reflector. Knowing the geometric concentration ratio, *C*, the optical efficiency can be calculated according to Equation 32.

$$\eta_0 = \frac{I_{sc,conc}}{C \cdot I_{sc,ref}} \qquad \text{Eq. (32)}$$

2.5 Optical concentration of light

Light can be concentrated by non-imaging or imaging optics. Imaging optics is used to transform light in an ordered way whereas non-imaging optics is about transforming light from one area to another without concerns regarding the paths of the rays. Either lenses or reflectors can be used for concentration of light. (Welford and Winston, 1989)

Optical concentration of irradiation by mirrors can be used to increase the irradiation on a solar absorber and thereby increase the energy output.

The technique to concentrate sunlight by using mirrors has been known for a long time, and was e.g. used at the world exhibition in Paris in 1878 (Dessus, 2000). Since then, many types of concentrators have been developed. Parabolic mirrors are often used in solar energy applications (Winston, 2001), either as two-dimensional troughs, often extended in the east-west direction, or as three-dimensional sun-tracking dishes, which are often used for power generation in combination with a conventional steam turbine.

The geometric concentration ratio of a concentrator is the ratio between the aperture area, A_1 and the area of the receiver, A_2, i.e. the absorber (see Figure 2.10).

$$C = \frac{A_1}{A_2} \qquad \text{Eq. (33)}$$

The concentration can also be described by the ratio between the irradiance on the receiver, G_2, and the irradiation on the aperture, G_1.

$$C = \frac{G_2}{G_1} \qquad \text{Eq. (34)}$$

The maximum concentration of an ideal two-dimensional concentrator is given by Equation 35 (Welford and Winston, 1989), where $\theta_{a/2}$ is the half-acceptance angle that is illustrated in Figure 2.10.

$$C_{\max,2D} = \frac{1}{\sin\theta_{a/2}} \qquad \text{Eq. (35)}$$

2.5.1 Parabolic reflectors

The parabolic shape is suitable for the design of reflectors for concentrating collectors as all irradiation that is parallel to the optical axis (the y-axis in Figure 2.9), will be reflected to the focal point, F (case a). Irradiation coming from the right hand side of the optical axis in Figure 2.9 (case b) will be reflected to a point along the focal length, P, which is the distance between Origo and F. Irradiation from the left hand of the optical axis will be reflected back out (case c). The parabola is mathematically described by Equation 36 the distance between the focal point and a certain point on the parabola, *r*, is calculated by Equation 37 and ϕ denotes the angle between *r* and the optical axis.

$$y = \frac{x^2}{4p} \qquad \text{Eq. (36)}$$

$$r = \frac{P}{\cos^2\left(\frac{\phi}{2}\right)} \qquad \text{Eq. (37)}$$

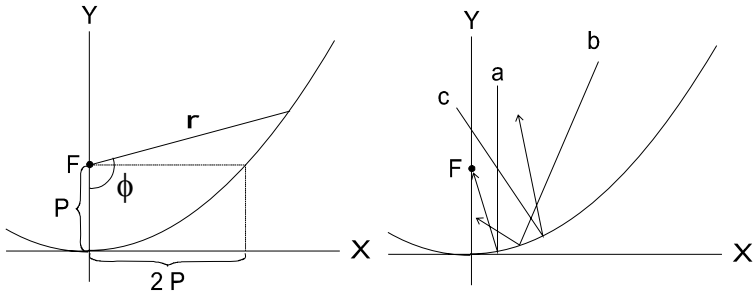

Figure 2.9 *The parabola. The y-axis is the optical axis of the parabola, F is the focal point, p is the focal length, and r is a vector from F to a point on the parabola. ϕ denotes the angle between r and the optical axis.*

The Compound Parabolic Concentrator (CPC) is based on two parabolic reflectors with the focal points at the edges of the absorber as shown to the left in Figure 2.10. The concentration ratio of an ideal CPC is given by Equation 35. The geometry of the CPC can be modified to enhance concentration from certain solar angles while suppressing the irradiation from others. This is the purpose of the MaReCo (Maximum Reflector Collector) (Karlsson and Wilson, 2000), which is shown to the right in Figure 2.10. This collector is designed for static conditions and well adapted for the Swedish climate where most of the annual irradiation comes from projected solar altitude angles (α_{NS}) of 50-55° (Figure 2.7). The angles of the optical axes and the slope of the truncation of the two parabolas give the specific acceptance interval. The stand-alone-MaReCo reflects all irradiation from solar altitude angles between 20° and 65° onto the bifacial absorber.

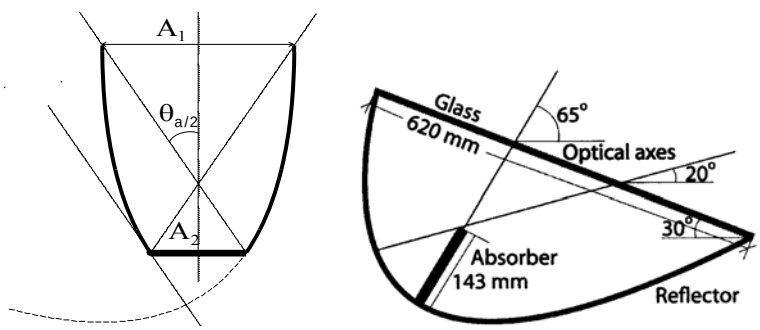

Figure 2.10 *A CPC and a stand-alone MaReCo (Maximum Reflector Collector).*

Another collector is designed for integration in a 30° tilted roof. A single reflector is used to reflect light to a bifacial absorber. The lower part of the reflector is parabolic up to the optical axis and the upper part is circular. The inclination of the optical axis sets the limits of the acceptance interval of the collector. The design to the left in Figure 2.11 reflects light from solar altitude angles between 0° and 60°. From higher altitude angles, the light will fall directly on the absorber but no light will be reflected to the back side of the absorber.

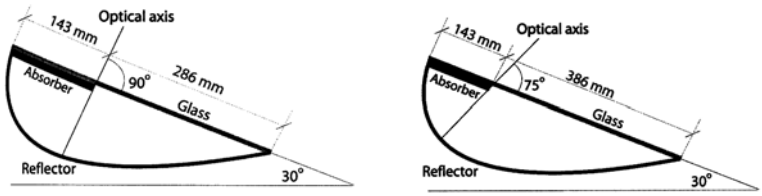

Figure 2.11 *Two concentrating collectors designed for tilted roofs. The right collector is optimised for spring and autumn performance.*

The design to the right in the figure has a lower inclination of the optical axis and thus a smaller acceptance interval, only from 0° to 45°, which implies that the reflector will mainly be in use from autumn to spring. This evens out the seasonal variations in the collector output.

A façade integrated concentrating collector

Concentrating collectors can also be integrated in façade elements. An example of a wall element including façade and insulation is illustrated in Figure 2.12. The geometry for this reflector is a parabola where the tilt angle of the optical axis, ν, here is 25° and a vertical glass surface truncates the parabola from the focal point. The absorber tilt angle β is 20°.

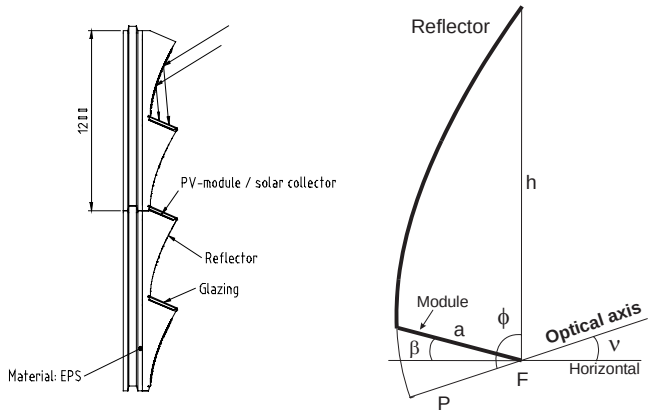

Figure 2.12 *A concentrating solar collector, integrated in an insulated façade element. The geometry of the reflector is a tilted parabola with the optical axis tilted 25°.*

The concentration ratio can be calculated from the expressions of the absorber width, *a*, and the height of the reflector, *h*, which are described by Equations 38 and 39, both derived from Equation 37. The geometrical concentration ratio is here 2.96.

$$a = \frac{P}{\cos^2\left(\frac{\nu + \beta}{2}\right)} \qquad \text{Eq. (38)}$$

$$h = \frac{P}{\cos^2\left(\frac{\nu + 90}{2}\right)} \qquad \text{Eq. (39)}$$

$$C = \frac{h}{a} = \frac{\cos^2\left(\frac{\nu + \beta}{2}\right)}{\cos^2\left(\frac{\nu + 90}{2}\right)} \qquad \text{Eq. (40)}$$

The collector can concentrate light from angles of incidence between 25° and 65°. At lower angles, a small part will fall directly on the absorber and the rest is reflected back out. At angles of incidence higher than 65° the incoming irradiance will fall directly onto the absorber.

2.5.2 The involute

The involute curve can be described as the shape drawn when unwinding a string that has been wound around a circular object, if a pen is attached to the outer end of the string, as shown in Figure 2.13. (The string is here unwound counter clockwise.) Thus, each point on the circle gives a corresponding point on the involute at the end of a line tangent to the point on the circle. Each line has the length of the circular arc reaching to the starting point of the circle (at σ=0°). *r* is the radius of the circle. The coordinates of the involute are given by Equations 41 and 42. (The equations are derived from the figure in Appendix A.I). The involute is further described by Welford and Winston (1989).

All irradiation falling on an involute-shaped reflector with a tubular absorber at the location of the circle will be reflected on to the absorber.

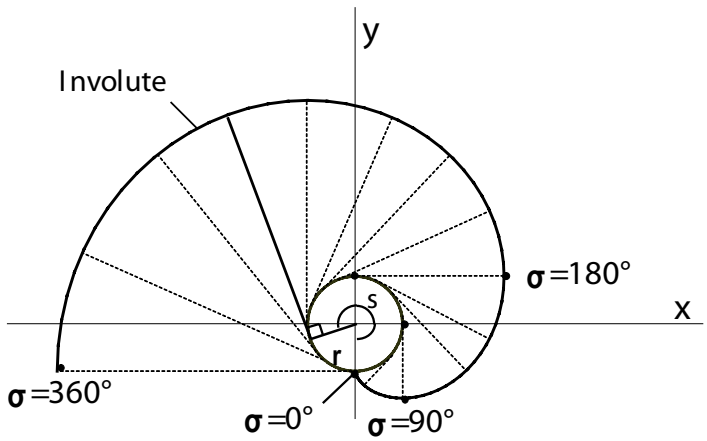

Figure 2.13 The involute curve.

$$x = r\sin\sigma - r\sigma\cos\sigma \qquad \text{Eq. (41)}$$

$$y = -r\cos\sigma - r\sigma\sin\sigma \qquad \text{Eq. (42)}$$

In order to create a suitable reflector shape for a pipe absorber for a roof-integrated solar collector the shape of an involute has been used in combination with a semi-parabola (see Figure 2.14 and also Paper IV). The semi parabola is described in Appendix A.II. The parabolic part of the reflector is heavily truncated to decrease the height of the collector. This

means that the concentration is decreased but also that irradiance from outside the original acceptance interval will reach the absorber.

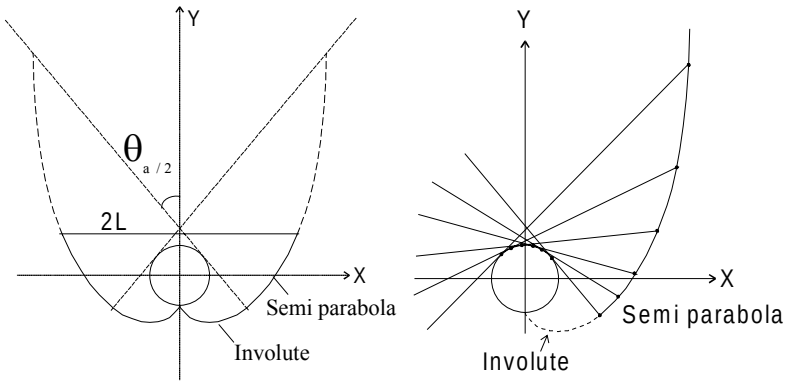

Figure 2.14. A geometrical shape made up of an involute and a semi parabola. The reflector is truncated to get the opening width 2L. All irradiation from angles of incidence up to the half-acceptance angle, $\theta_{a/2}$, will be reflected onto the pipe absorber.

The optical acceptance of the truncated concentrator is one (i.e. all irradiation will be reflected onto the tubular absorber) when the beam comes from inside the acceptance interval, i.e. from angles of incidence up to $\theta_{a/2}$. (See Figure 2.15 to the left.) The maximum geometrical concentration ratio is then equal to 1/sin ($\theta_{a/2}$) (Equation 35).

When irradiation from outside the acceptance interval falls on the collector surface, it is only the irradiation that falls on the half of the aperture area, *L*, minus the area *S* in Figure 2.15 that will be reflected onto the absorber. The rest of the irradiation is reflected back out. This means that the maximal optical acceptance is equal to *(L-S)/2L*.

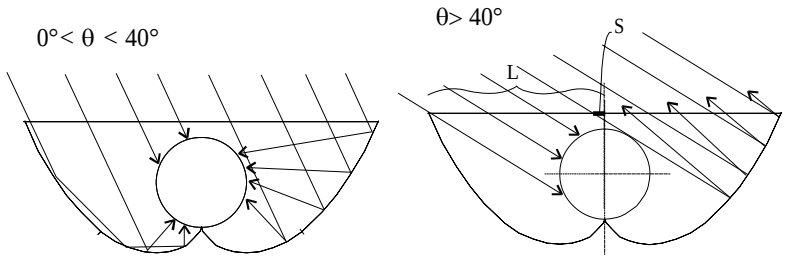

Figure 2.15 *The geometrical acceptance of the concentrating pipe collector with a reflector made up of an involute and a semi parabola. All irradiation from within the acceptance interval between 0° and 40° will be reflected onto the pipe - the acceptance is 1. When irradiation from outside the acceptance interval falls on the collector, a part falls directly onto the pipe absorber and a part of it is reflected back out, reducing the acceptance to (L-S)/2L.*

2.5.3 Incidence angle dependence for concentrating collectors

For asymmetric 2D concentrating collectors, the optical efficiency is dependent on the angles of incidence in both the transverse and the longitudinal planes, as illustrated in Figure 2.16. Here θ_L is the longitudinal angle and θ_T is the transverse projected angle of incidence. The optical efficiency of such collectors can be modelled by a biaxial model (Equation 43) that accounts for the different angular dependencies.

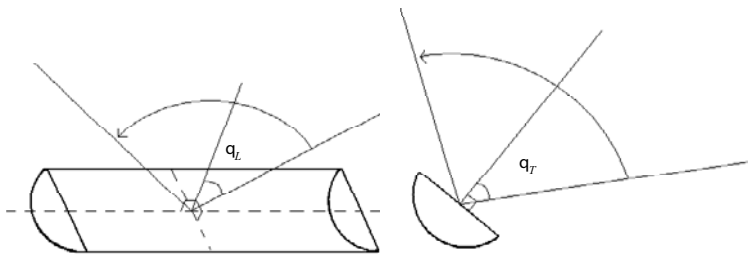

Figure 2.16 *The longitudinal incidence angle, θ_L, and the transversal incidence angle, θ_T, of a 2D concentrating collector.*

$$K(\theta_L,\theta_T) = K_L(\theta_L,0)K_T(0,\theta_T) \qquad \text{Eq. (43)}$$

This model was presented by McIntire (1982) and it estimates the optical efficiency *K* by measurements of the optical efficiency in the longitudinal and transverse directions. However, this model does not calculate the angular dependence of the glazing in a correct way as the effect of the glazing can be included twice using this model.

A modification of the model has been proposed by Nilsson et al. (2006) (Equation 44). This model is based on separate measurements of the optical efficiency of the reflector and the glazing.

$$K(\theta_L,\theta_T) = f_L(\theta) \cdot R_T(\theta_T) \qquad \text{Eq. (44)}$$

$K(\theta_L, \theta_T)$ is the optical efficiency for any given angle of incidence, depending on the angles of incidence in the longitudinal and transverse planes.

$f_L(\theta)$ gives the influence of the glazing for varying angles of incidence. $f_L(\theta)$ is obtained by measuring the angular optical efficiency in the longitudinal plane at a given θ_T, when the effect of the reflector is equal for all angles θ_T. $f_L(\theta)$ can also be estimated from the K_b function (Equation 17) which gives the influence of the glazing if its b_0 value is known.

$R_T(\theta_T)$ gives the influence of the reflector (in the transverse plane) and is obtained by measuring the optical efficiency of the collector for varying angles in the transverse plane when $\theta_L = 0°$, and without glazing. If a glass cover is used to protect the collector, the resulting function is $K(\theta_L = 0, \theta_T)$, which is influenced by both the glazing and the reflector, as shown in Equation 45. Then, $R_T(\theta_T)$ will be obtained by division by $f_L(\theta_T)$, as shown in Equation 46.

$$K(0,\theta_T) = f_L(\theta_T) \cdot R_T(\theta_T) \qquad \text{Eq. (45)}$$

$$R_T(\theta_T) = \frac{K(0,\theta_T)}{f_L(\theta_T)} \qquad \text{Eq. (46)}$$

This means that the ratio between the measured dependencies in the θ_T and θ_L directions gives the influence of the reflector only. The complete expression for the angular dependence is shown in Equation 47, which also explains Equation 44.

$$K(\theta_L,\theta_T) = f_L(\theta) \cdot \frac{K(0,\theta_T)}{f_L(\theta_T)} = f_L(\theta) \cdot R_T(\theta_T) \qquad \text{Eq. (47)}$$

2.5.4 Reflector material

Mirrors based on anodised or coated sheet aluminium are often used as reflectors because of their good solar reflectance, manufacturing flexibility and low cost. Aluminium reflectors offer specular solar reflectance of up to 87 % initially, while their reflectance later on depends on exposure to climatic conditions and on the possible use of a protective coating. This type of reflector also has good mechanical properties. However, their corrosion resistance is limited, which may cause problems. There are several other booster reflector materials available on the market, which give considerably higher solar reflectance than anodised aluminium. For example, Miro sheets from Alanod have a solar reflectance of 90 % at normal incidence. (Brogren et al., 2000)

2.6 Concentrating hybrid PV/thermal collectors

The combination of a photovoltaic absorber and a thermal absorber is interesting as the energy that cannot be used by the solar cell can be utilised for heat production.

In concentrating systems the concentration ratio varies over the cell surface and can be very high at the focus, resulting in high temperatures. The efficiency of photovoltaic cells decreases with increasing cell temperature as the voltage and the fill factor, *FF*, of the cell (given by Equation 48) decreases. The efficiency of the cell is proportional to $I_{sc} \cdot V_{oc} \cdot FF$ and the reduction in efficiency with temperature is -0.4%/K (Nilsson, 2005). Too high temperatures can also result in damage to the module. Cooling is therefore necessary in concentrating photovoltaic systems.

There are several cooling methods available, but work by Edenburn (1980) and Rönnelid et al. (1999) indicate that active water cooling is the most cost-effective method for low-concentrating line-focusing systems. A hybrid absorber can thus have a positive effect as it provides cooling for the solar cell and makes use of the thermal energy.

The fill factor describes how well the cell's I-V (current-voltage) curve (Figure 2.17) coincides with the ideal curve. For an ideal I-V curve, I_{sc} is constant until V_{oc} is reached and then it drops to zero.

$$FF = \frac{I_{mp} \cdot V_{mp}}{I_{sc} \cdot V_{oc}} \qquad \text{Eq. (48)}$$

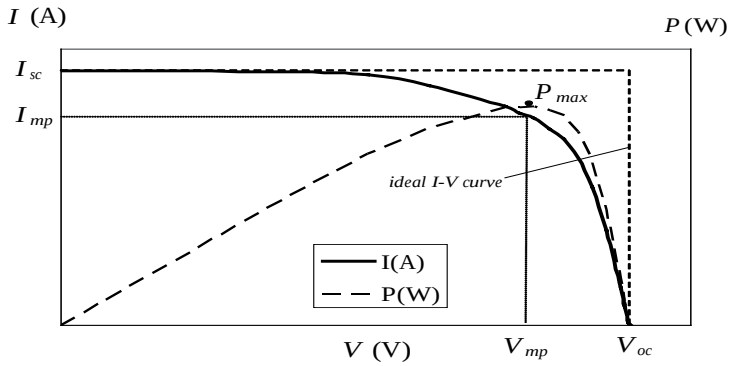

Figure 2.17 *The current-voltage (I-V) curve of a photovoltaic cell. I_{sc} is the short-circuit current, V_{oc} is the open circuit voltage, I_{mp} and V_{mp} are the current and voltage at the maximum power. The fill factor, FF, is dependent on the shape of this curve. For an ideal I-V curve, I_{sc} is constant until V_{oc} is reached and then it drops to zero.*

2.7 Building integration of solar collectors

The designs of solar collectors should be adapted with regard to the interests of the building industry and the private users.

For new buildings it is preferable to integrate the collector as much as possible in the building element, in order to save building material and reduce the labour cost for mounting the collectors. Prefabrication of the collectors integrated in wall or roof building elements is desirable as series production increases the economic benefits. The mounting of the building elements, including collectors, can then be performed easily and quickly.

Service and replacement of components are difficult for building integrated materials and a guaranteed long durability of the optical properties is desirable. It is therefore important to perform lifetime tests on a material intended for use in building-integrated systems, preferably including outdoor tests and tests of accelerated ageing, to prove the optical durability of the reflector materials (Nostell et al., 1998).

It is also important to ensure that the building envelope is of high insulation quality, which means that the collector must be well insulated.

When a solar collector is to be mounted on an existing building, is it important that the installation can be performed quickly and safely, but correctly.

Regardless of the integration level, it is important to keep the maintenance requirements as low as possible in order for the collectors to be attractive to customers. It is also crucial that the airtightness and load-bearing capacity of the construction are not impaired by the integration of the collector.

Leakage from the collectors and the attachments must be avoided. Leakage occurs most frequently at the attachments or where the roof is penetrated. The durability of the collector should preferably be as high as that of the rest of the building envelope. It must also withstand temperature changes and ageing. If it is necessary to replace parts of the collector, it must be possible for this to be done easily.

The safety of operation is very important and design features that could cause operational problems must be avoided. An example is glycol free drain back systems, which can give rise to freezing problems.

Prefabrication, simple transportation and mounting are desirable features of the collectors. Loose details on the elements should be avoided and general solutions for the attachment of the collectors should preferably be part of the design in order to avoid the specification of special solutions for each project. Ease of connection of the coupling of the solar system components to the building's heating system and control system is desirable.

Another issue concerning the system's integration in the building is the location of the tank. It should preferably be placed as close to the collectors as possible. Thermosyphon systems, where the tank is connected directly above the collectors, are widely used in warmer climates.

As for all solar systems, it is important to avoiding shading. Roofs are in this respect generally better than walls on moderately high buildings. The orientation of the collectors is of course very important. In Sweden the optimal tilt angle is 35-50°. A higher angle will reduce the seasonal changes over the year and a larger collector will be required if flat plate collectors are used. A concentrating collector can be designed to reduce the seasonal changes even if placed on a flat roof.

An attractive collector design or a design that makes the collector harmonize with the building design is also an important issue on the market.

Today the market for building integrated solar collectors is on the increase, mainly in countries such as Germany and Austria. Large companies are using solar cells, solar thermal collectors and solar windows that are integrated into highly flexible and attractive building elements that are easily adapted to any building type. A few examples of building integration of solar collectors are shown in Figures 2.18 and 2.19.

Figure 2.18 *Building integration of solar thermal collectors in façades (to the left and in the middle) and of photovoltaics in solar screens (to the right). (Photo: Schüco Internation KG).*

Figure 2.19 *Building integrated photovoltaics in Bunkeflostrand in Malmö, Sweden. (Photo: Schüco Internation KG).*

3 Measurement techniques

This chapter describes the measurement set-ups, the techniques and equipment used for the experimental measurements performed for this work. The simulation programs used are also described in this chapter. Further information is presented in the other chapters. The measurements were partly made outdoors and partly indoors in the laboratory using a solar simulator. Measurements have also been carried out at the Älvkarleby test facility.

3.1 Measurement set-up

3.1.1 Outdoor measurements using the test rig

Concentrating collectors have been evaluated from outdoor measurements using a test rig (described in Section 3.2.3). These measurements were carried out on the roof of the EBD laboratory. During the measurements the collector to be evaluated was mounted on a south-facing stand, adjustable for different tilt angles. Two pyranometers for global and diffuse irradiation were mounted in the collector plane and a static shading ring was mounted in front of the pyranometer measuring diffuse inradiation so that the sensor was constantly shaded regardless of the collector tilt, as shown in Figure 3.1.

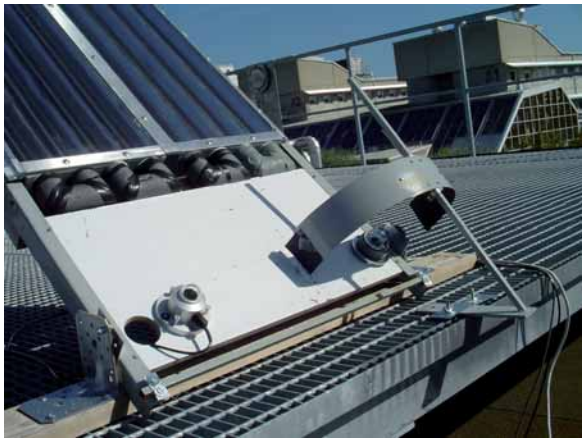

Figure 3.1 *The two pyranometers for measurements of the hemispherical and diffuse irradiation, mounted in the collector plane.*

The inlet temperature of the collector was measured with a Pt 100 sensor and the temperature difference between the inlet and outlet temperature was measured by two Pt 100 sensors and a resistance bridge (as described in Section 3.2.4). This technique gives a more accurate output when differences between inlet and outlet are measured at low temperature. The logger on the test rig was programmed to control the inlet temperature so that it is kept constant. Air vents were placed on the collector outlet and inlet as shown in Figure 3.2.

Figure 3.2 *Insulated air vents and Pt 100 sensors on the collector inlet and outlet.*

Evaluation of incidence angle dependence

Measurements of the transverse incidence angle dependence of a concentrating collector were performed with the collector mounted so that the absorbers are directed in the north-south vertical plane, tilted so that the normal of the glazing is oriented towards south, as shown in Figures 3.3 and 3.4.

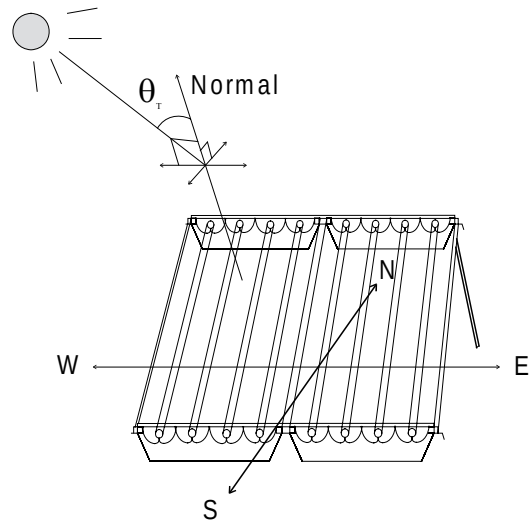

Figure 3.3 *The set-up for measurements of the transverse incidence angle dependence.*

The collector tilt was then constantly adjusted during the measurement (basically by rotation around an east-west oriented axis) so that the sun was in an east-west plane perpendicular to the front of the solar collector. This means that the incidence angle in the longitudinal plane, θ_L, is zero. Also, the incidence angle is minimised and equals the transverse incidence angle θ_T (for this collector in the east-west direction) at all times. The transverse incidence angle can therefore be calculated from Equation 49, which gives the incidence angle as a function of the declination and the time angle for a tracking surface in a plane rotated about a horizontal east-west oriented axis that is continuously adjusted to minimize the incidence angle (Duffy & Beckman, 1991).

$$\cos(\theta) = (1 - \cos^2\delta \cdot \sin^2\omega)^{\frac{1}{2}} \qquad \text{Eq. (49)}$$

Figure 3.4 *A solar collector mounted on the roof of the EBD Laboratory and adjusted to different tilt angles.*

The results were verified by checking an incidence angle indicator. The calculated and measured angles showed good correspondence and this method appears to work well, which is beneficial as data from a high number of incidence angles can be collected in a short time.

The incidence angle indicator

In order to read the incidence angles during outdoor measurements, an aluminium plate with a pin that gives a shadow from the sunlight on a marked scale of angular intervals was designed and carefully mounted on the collector frame (see Figure 3.5). The reading on the scale gives a good indication of the incidence angle. This device was always mounted with the pin oriented in the collector plane, regardless of the orientation of the collectors.

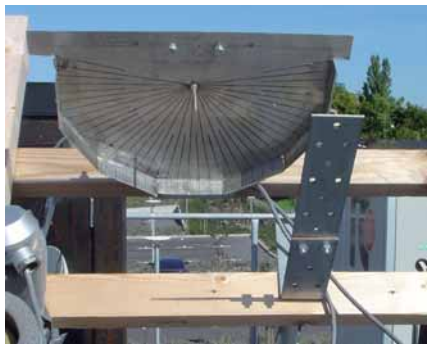

Figure 3.5 *The device for measuring the transverse incidence angle on the glazing of the collector.*

3.1.2 Long-term outdoor measurements at the Älvkarleby test facility

For the roof integrated collectors of corrugated steel described in Chapter 5, the evaluations were partly performed from long-term outdoor measurements at a test facility for solar collectors at Älvkarleby, Sweden (60.5°N, 17.4°E). The collectors were then mounted on a 45° tilted stand directed towards south, as shown in Figure 3.6, with the absorbers in the east-west direction, which means that the transverse incidence angles are in the north-south vertical plane. The temperatures of the ambient air and the collector inlet and outlet, the flow rates and the global and diffuse irradiation were measured and monitored at ten minute intervals. The global and diffuse irradiance were measured in the collector plane, as shown in Figure 3.7, which also shows the air vents at the inlet and after the outlet of the collectors.

Figure 3.6 *The collectors mounted outdoors at the Älvkarleby test facility.*

Figure 3.7 *The pyranometer mounted in the collector plane (to the left) and the inlet piping with an air trap and a vent (to the right).*

The tilts of the collectors were constant during these measurements. The temperatures were measured by Pt 100 sensors and the flow rates were measured by inductive flow meters. An advanced data logger system collects the data at all hours during the evaluation period.

3.1.3 Early measurements

Experimental set-up

In the beginning of the project, before the test-rig was designed and built, measurements were performed using the set-up illustrated in Figure 3.8. This set-up has been used for both indoor and outdoor measurements.

During these measurements, small (0.6×1.0 m) collector prototypes of the Collectors A, B and C, described in Chapter 5, were used. In these measurements the collectors were however equipped with insulation on the back. The prototype of the concentrating Collector C used in these measurements was later replaced by a prototype with a smoother reflector.

The global irradiance was measured with a pyranometer in the collector plane. The collector is connected to a pump and to an expansion vessel that also serves as filter and device for refilling the collector circuit with water. A Campbell logger, model CR10X, was used for data collection. A

PID-regulator and an amplifier were used to maintain the inlet temperature constant during the measurements.

The inlet temperature was measured with a Copper/Constantan thermocouple and the low temperature difference between T_{out} and T_{in} was measured with a thermopile. The outlet temperature was then calculated from these two registered values.

If the registered inlet temperature is too high the regulator gives a signal to the pump in the cooling circuit to operate and if it is too low it gives a signal to the electric heater to operate. The cooling works by circulation through a branched circuit in which an air-cooled heat exchanger is connected. A fan is used to enhance the cooling process. An inductive flow meter connected to a flow display measures the flow rate. As cooling below ΔT = 0°C (T_m-T_a) is not necessary for these measurements, this type of passive cooling was adequate. The regulation to keep a constant inlet temperature was found to work best when a temperature sensor was placed close to the mixing zone after the cooling circuit.

The measured irradiance, the flow rate, T_{in}, T_{out} and T_a were registered and the mean zero-loss efficiency, η_0, was calculated for each measured transverse incidence angle, giving the transverse incidence angle dependence of the collector.

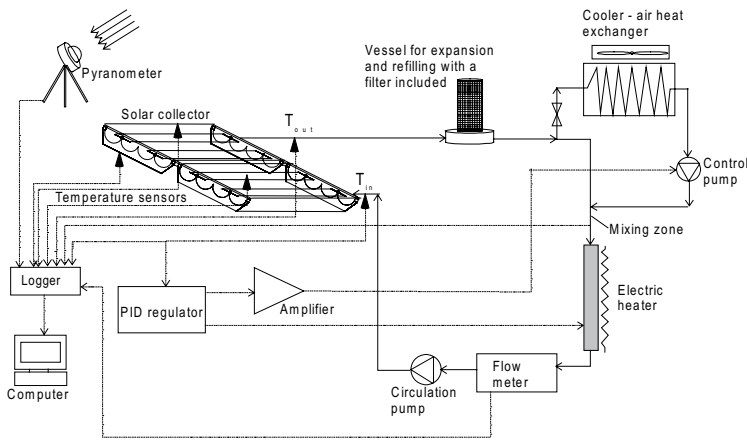

Figure 3.8 System set-up for the early indoor measurements.

Outdoor measurements for determining the optical efficiency

This measurement set-up was applied for outdoor measurements intended to determine the optical efficiency at various transverse incidence angles and to verify the results from indoor measurements.

An adjustable stand, shown in Figure 3.9, was used to change the tilt of the collector during the measurements. The collector and the pyranometer were directed towards the solar azimuth, which means that the solar altitude angles represented the transverse incidence angles. An indicator of the incidence angles similar to the one shown in Figure 3.5 was mounted on the side of the collector.

As it is important to keep the heat losses minimal, to get an accurate value of the zero-loss efficiency, the flow was circulated through the heat exchanger providing passive cooling to the ambient air. The collected data was relatively stable and ΔT was kept as low as possible. The average value of ΔT was 2.5°C and the maximum value was 6.5°C at an average operating temperature of 7.5°C.

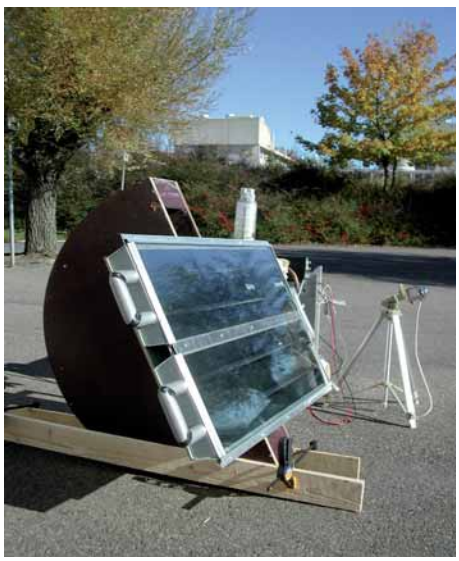

Figure 3.9 *An outdoor measurement outside the laboratory in Lund.*

The results from these measurements were used together with results from the dark-hour evaluations of the $F'U$ value to derive the value of optical efficiency. As ΔT is already very close to 0°C, good accuracy is achieved.

Indoor measurements with the solar simulator

Indoor measurements of the thermal performance were carried out with the same measurement set up. Both the transverse incidence angle dependence and the *F'U* value were evaluated. During the indoor measurements, the collector to be tested was mounted on an adjustable stand at the pivot point in front of the solar simulator (see Figure 3.10). The simulator was raised to different heights (0°-70°), often in 5° or 10° intervals, so as to simulate different solar altitude angles. Occasionally the collectors were placed vertically on a rotating stand in front of the simulator. The incidence angles were then simulated by rotating the collectors. The irradiance was measured with pyranometers placed both in the collector plane and perpendicularly in front of the solar simulator. During some of these measurements, a photo diode array was placed on the collector surfaces in order to get more accurate values of the total irradiance on the test area (described in Section 3.2.2).

Evaluations of the U-value

The value of *F'U* was derived from both indoor and outdoor measurements. The operating temperature of the water in the collector was varied and the results of efficiency for different values of ΔT (i.e. T_m-T_a) were used to estimate *F'U*. This evaluation was also performed in the dark, giving the "dark hour *F'U*-value" of the collector. During these measurements, an electric heater was used to heat the water to a constant temperature. The negative power from the cooling of the collector, i.e. the heat losses achieved at different operating temperatures, was monitored and used to determine *F'U*.

This is a stable repeatable method which however gives a slightly different result of the *F'U*-values compared with the results of *F'U*-values measured with irradiation. This difference is due to the opposite heat flow direction between the fluid and the absorber surface. This effect is explained by Hellström (2005).

3.2 Measuring equipment

3.2.1 The solar simulator

A large solar simulator which provides parallel light - which is an almost unique characteristic for a solar simulator - and is adjustable for solar al-

titude angles has been used for some measurements in this work (Figure 3.10).

The simulator can be raised to simulate different solar altitude angles between 0° and 73.5°. Simultaneously, the platform in front of the lamps can be rotated, which makes it possible to simulate the sun's course during the day.

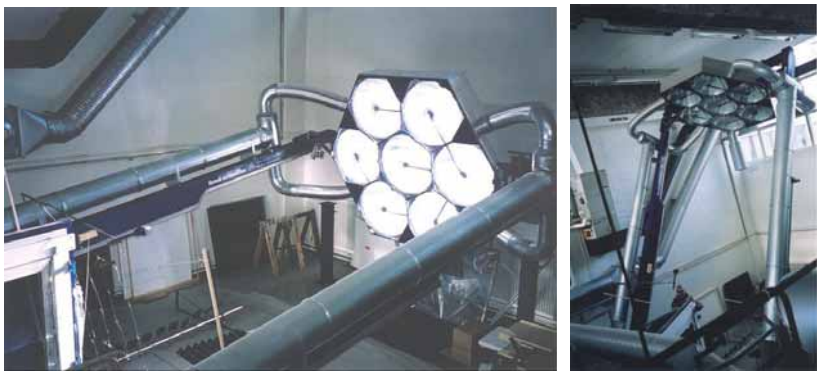

Figure 3.10 *The solar simulator in a horizontal position and raised to the maximum elevation of 73.5°.*

The seven metal-halide lamps use large reflectors, formed in the shape of paraboloids, that render the light nearly parallel. The lamps used are 2.5 kW Philips discharge lamps. This model is called MSR by the manufacturer, which denotes Metal halide Short arch Rare earth. The lamps provide radiation with spectral characteristics similar to those of sunlight (see Figure 3.11) in the range that is visible to the human eye – 400-700 nm. The UV radiation as well as most of the long wave radiation is filtered off in the glass in front of the lamps. (Håkansson 2003 a)

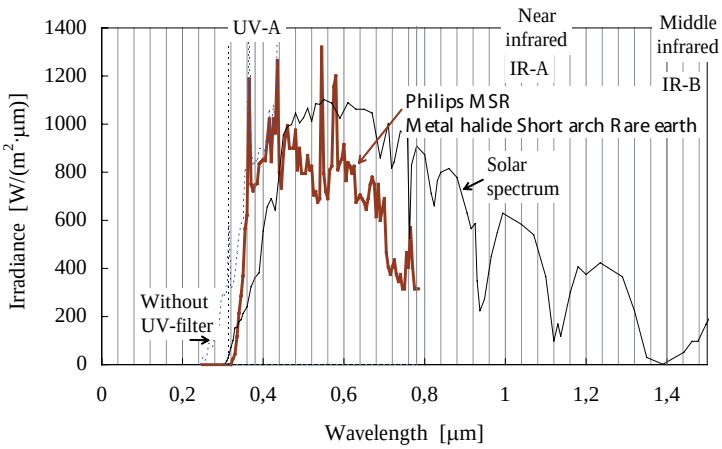

Figure 3.11 *The spectral distribution of the lamps of the solar simulator (Philips discharge lamps, 2.5 kW).*

The simulator was originally designed for simulation of solar irradiance for evaluations of solar shadings, but as the parallel light is an important characteristic when the incidence angle dependence of concentrating collectors is evaluated, it is desirable to use it also for this purpose. The facility to evaluate solar collectors indoors makes the measurements independent of unwanted climate changes and facilitates the repetitiveness of the experiments.

3.2.2 Measurements of irradiance

Hemispherical and diffuse solar irradiance has been measured with two pyranometers, including a shading ring on the pyranometer measuring diffuse irradiance. The direct irradiance was calculated from these data. The pyranometers were calibrated based on two new and calibrated pyranometers. Basically, the same techniques were used during indoor and outdoor measurements. During the measurements the pyranometers were placed in the collector plane. For indoor measurements a second pyranometer was placed directly in front of the simulator measuring the hemispherical irradiance. As the diffuse irradiance is very low this gives mainly the direct irradiance.

Photodiode array

An alternative way of measuring the irradiance during indoor measurements has been developed in order to compensate for the slightly non-uniform light distribution from the solar simulator. This method is based on using an array consisting of six photodiodes connected in parallel. It was placed on the glazed surface of the collectors during the measurement. The placing of the photodiodes divides the front area of the solar collector into smaller areas of approximately equal size with one photodiode placed in the centre of each area. With this arrangement, the average current from the photodiode array should be a relatively good representation of the average irradiance on the collector surface. The spectrum of the silicon photodiodes (S1337-66BR) is between 300-1100 nm, with the peak at 950 nm.

3.2.3 The solar collector test rig

A rig for testing solar collectors has been designed and built within the project. The rig facilitates both stationary and dynamic collector testing with good reproducibility of the measurements. The system components are set up as shown in Figures 3.12 and 3.13.

Figure 3.12 The solar collector test rig.

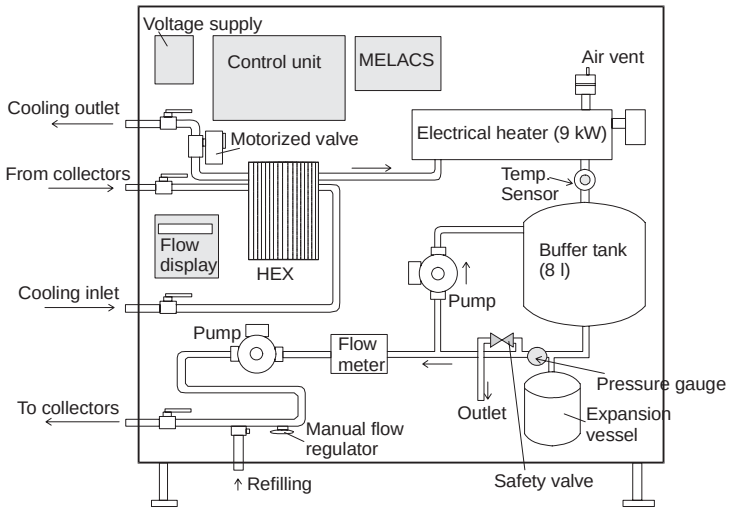

Figure 3.13 *The test rig for solar collectors includes a heat exchanger for cooling, an electric heater, a buffer tank, expansion vessel, a flow meter, pumps and control units including a MELACS logger. A motorized valve is used for the control of the cooling circuit.*

The main purpose of the system design is to provide good temperature control. The temperature to the solar collector should be kept as constant as possible during measurements. The rig is also constructed so that it is easy to connect different solar collectors to the inlet and outlet pipes.

A heat exchanger for cooling the hot water from the collector outlet is connected to the rig. A motor driven valve controls the flow of cold water to the heat exchanger, which has been fitted with two water hoses (the inlet is from the tap to the heat exchanger and the outlet is connected to the floor drain). After the water has passed the cooler, it is passed through a 9 kW electric heater, where the temperature can be further adjusted. An air vent is also connected to the heater as this is the highest point of the water flow in the test rig. The temperature sensor controlling the cooling and heating of the water is placed after the heater, just before the buffer tank of 8 litres. The purpose of using a tank is to mix the water and add an extra thermal capacitance to keep the inlet temperature to the collector constant. An inductive flow meter with a flow rate display for manual flow adjustments is placed on the test rig, just before the outlet to the collector. The rig is also equipped with two circulation pumps, an expansion vessel, a pressure safety valve and a temperature control sensor of microchip

type (LM35). A three-phase 400V AC voltage is connected to the voltage supply. The test rig is designed for a pressure of 1.5 bar.

Two control units are placed on the test rig, see Figure 3.14. The MELACS (the Micro Energy Logger And Control System) control unit contains the main control functions - the processor, a multiplexer, an AD-converter etc. The left control unit receives the information from the MELACS to manage the control of the motorized valve, the electric heater and the pumps. It contains three drive units for each of the three phases of the 400V AC voltage, an I/O module that controls the pumps and two voltage buffer circuits that control the motorized valve and the heater. Three-phase voltage is delivered from this unit to the pumps and to the electric heater.

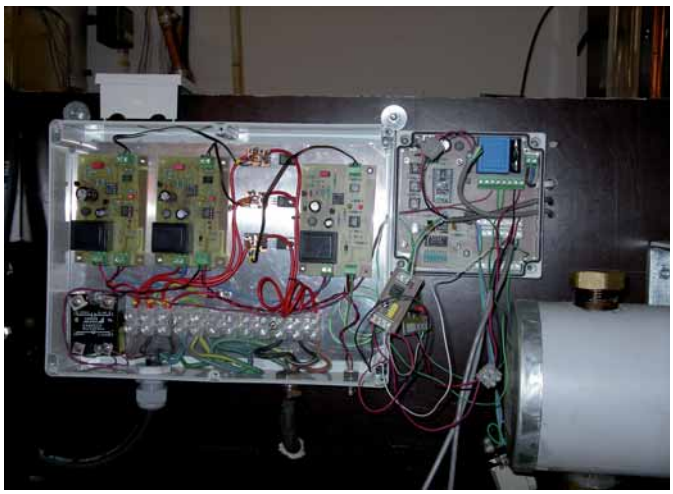

Figure 3.14 *The control board for the cooling and heating applications is at the left in the picture and the smaller MELACS microcontroller is shown at the right.*

The control system MELACS is a microcomputer system including a data logger with an independent battery backup system. The MELACS, which can operate independently of the PC, uses the Basic Stamp microcomputer from Parallax and is programmed in picbasic. The MELACS Microcontroller is developed by Stefan Larsson at the Älvkarleby laboratory (Larsson, 2006).

3.2.4 Temperature measurements

The stability of the inlet temperature to the solar collector must be very high if disturbances from the collector thermal capacitance to the measured thermal output and efficiency are to be eliminated. This is even more important since most of the evaluated collectors are small prototypes, which require relatively low flow rates. Copper/Constantan thermocouples, Pt 100 sensors, a thermopile and temperature sensor of microchip type (LM35) have been used for measuring temperature during different measurements. Two methods that have been used to achieve higher accuracy in the measurements of the critical temperature difference, T_{out}-T_{in}, are described below.

Resistance bridge measurements

Low temperature differences can be very difficult to measure accurately. At high incidence angles the temperature difference is often very small. An error of less than 0.1 K is desirable. In order to measure the low temperature difference between the inlet (T_{in}) and the outlet (T_{out}) of a solar collector, a resistance bridge was set up, according to the illustration in Figure 3.15. A voltage is given over C and D. The resistances R_1 and R_2 are equal (and in the range of 2.4 kΩ when U_{in}= 5V) and the two Pt 100 temperature sensors must be calibrated to give equal resistance for various temperatures. The difference in voltage is measured over A and B. As long as the temperatures of the two Pt 100 sensors are equal, there is no voltage difference between A and B. As these Platinum sensors show extremely linear temperature dependence (they give a resistance of 100 Ω at 0°C) a change in T_{out} alters the resistance R_3 proportionally and changes the voltage potential at point A (and vice versa for T_{in} and point B), which gives the difference in voltage potential over A and B. This way the temperature difference between the Pt 100 sensors is represented by the output signal from the voltage meter. A trim potentiometer is used to balance the resistances before the measurement in case the resistances of the Pt 100 sensors R_3 and R_4 are not exactly equal at 0°C. (The methodology is further described by Frank (1959) and Doebelin (1990)). The two Pt 100 sensors used for a bridge measurement were calibrated in a calorimeter bath between 20°C and 60°C. The zero temperature deviation after 24 hours was 0.0006 °C.

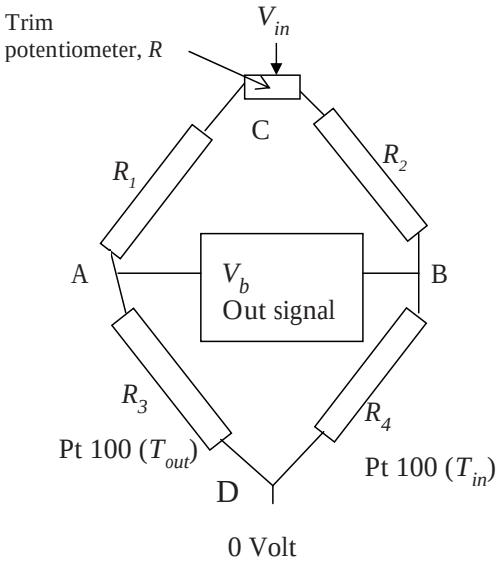

Figure 3.15 *The resistance bridge set up to measure the temperature difference between two Pt 100 sensors.*

Temperature difference from thermopiles

Another way to achieve good accuracy of the measured data when the temperature difference between the inlet and outlet of the collector is low is to use a thermopile, which gives good relative accuracy (shown in Figure 3.16). In some of the measurements a thermocouple was placed in the inlet and thermopiles were mounted at the inlet and outlet, measuring the temperature difference between the inlet and the outlet. The outlet temperature was then calculated from these two registered values.

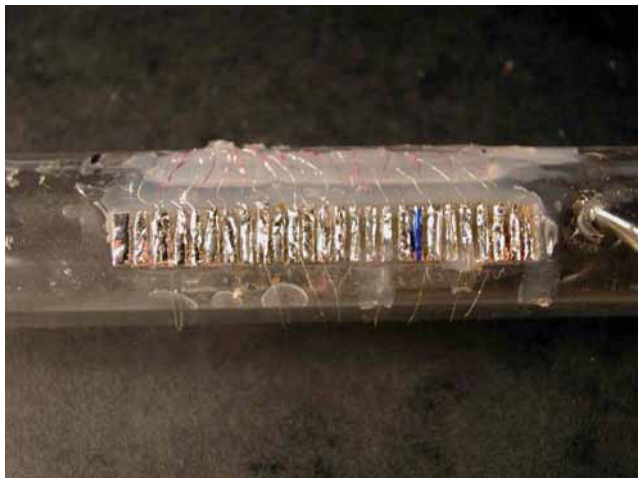

Figure 3.16 *The thermopile used for measurements of the temperature difference (T_{out}-T_{in}) of solar collectors. The thermopile is protected from the fluid with a thin silicon rubber hose.*

Absolute temperature

In order to get an accurate value of the inlet temperature of the collector, the absolute temperature was measured with a Pt 100 sensor that was set up according to the illustration in Figure 3.17.

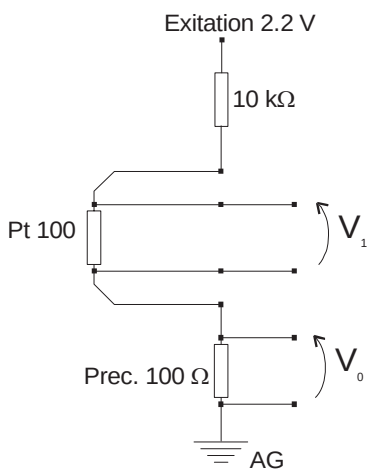

Figure 3.17 *The four-wire measurement set up for measurements of the absolute temperature using a Pt 100 temperature sensor.*

An excitation voltage of 2.2 V is given to the resistor of 10 kΩ. The use of this very large resistance reduces the influence of the Pt 100 sensor´s resistance on the current, which becomes very low. The low current means that errors due to internal heating are avoided. The resistance of the Pt 100 sensor is 100 Ω at 0°C and increases as temperature rises above 0°C, as shown in Equation 50. A precision resistor of 100 Ω is also connected to the circuit and to ground. The current can thereby be calculated by Equation 51. *T* is here measured in °C.

$$R_{Pt100} = 100 + 0.385 \cdot T \qquad \text{Eq. (50)}$$

$$I = \frac{2.2}{10000 + 100 + 100 + 0.385 \cdot T} \qquad \text{Eq. (51)}$$

The voltages over the Pt 100 resistor and the 100 Ω precision resistor are measured and the relation between them equals the relation of their resistances, which means that the temperature is given by Equation 52.

$$\frac{V_{Pt100}}{V_{prec.}} = \frac{I \cdot R_{Pt100}}{I \cdot R_{prec.}} = \frac{100 + 0.385 \cdot T}{100} \qquad \text{Eq. (52)}$$

3.2.5 Flow rate

Inductive flow meters from Enermet/Kamstrup MP115 have been used for all measurements. These flow sensors give a high pulse frequency already at low flow rates and therefore a high resolution in the data.

3.2.6 Data logger system

A logger CR10X from Campbell has been used in all measurements in combination with the software PC208W. The accurate logger measurement sampling interval is 10 seconds. Two minute averages are stored in the logger.

3.3 Computer programs

3.3.1 The MINSUN simulation tool

MINSUN is a simulation tool for calculation of the solar irradiation on surfaces and the energy output from solar collectors (Adsten, 2002; Chant and Håkansson, 1985; Perers, 1993; Perers and Karlsson, 1993). It is specially developed for simulating solar collectors with a complicated angular dependence. The program considers the characteristic parameters of solar collectors and the longitudinal and transverse incidence angle dependence can be included as input data, which makes it suitable for simulations of concentrating collectors.

The program uses climate data for a typical reference year of the Stockholm climate from 1983 to 1992, provided by the Swedish Meteorological and Hydrological Institute Stockholm (SMHI). MINSUN calculates the monthly and annual irradiation on any given surface. It also gives the energy output of the solar collector in question in kWh/m^2 per month and year.

Hourly climate data of direct and diffuse irradiation is used to calculate the total annual irradiation on a specified surface. The total absorbed irradiance, *S*, is obtained by multiplying the direct and diffuse irradiance by incidence angle modifiers for beam and diffuse irradiance. MINSUN can calculate the incidence angle modifier for direct irradiance as a product of the functions $R_T(\theta_T)$ and $f(\theta)$. The optical losses $(\tau\alpha)_n$ are here included in the expression $R_T(\theta_T)$. The functions are given numerically at angular intervals of 5°. The incidence angle modifier for diffuse irradiance, K_d, is given as a constant value or obtained by integrating $R_T(\theta_T)\, f_L(\theta)$ over an isotropic sky. This means that Equation 53 gives the useful irradiance *S* on the cell. For concentrating collectors this expression is then multiplied by the concentration ratio, *C*.

$$S(\theta_T, \theta_L) = (R_T(\theta_T)\, f_L(\theta)\, I_b + K_d I_d) \qquad \text{Eq. (53)}$$

The function R_T, which represents the angular dependence of the reflector, is obtained from measurements of the optical efficiency in the transverse plane with θ_L=0. The function f_L, which represents the angular dependence of the glazing, is obtained from measurements of the optical efficiency in a plane where θ_L is constant. This means that f_L can be conveniently modelled as a conventional K_b function (Equation 17).

3.3.2 WINSUN

WINSUN is a simulation program based on TRNSYS/TRNSED/PRESIM that calculates the theoretical monthly and annual energy output from solar collectors using a dynamic collector model. Synthetic weather data based on long-term average data is used in the program. The collector performance parameters, the orientation of the collectors etc. are used as input data. The monthly average operating temperatures of the collector throughout the year can also be used. The energy output for the period is returned as monthly and annual values.

TRNSYS, the basis of the program, is a dynamic systems simulation tool where complex energy systems can be set up and simulated. TRNSYS is used internationally by researchers within several different fields of work.

3.3.3 Polysun

Polysun 3.3 is a simulation program for solar thermal energy systems developed by Institut für Solartechnik, SPF, in Rapperswil, Switzerland (Polysun, 2002). There are eight main types of solar system designs to choose from, including hot water systems and systems including space heating. The program uses climate data from Meteonorm 95, which is available from locations all over Europe and for a few other locations as well. It is possible to vary a number of parameters from pipe dimensions, hot water consumption (including circulation and habits of energy use), heat exchanger parameters, pump characteristics, tank dimensions for a tank with 12 layers (for which the heat transfer and mixing by temperature inversion are considered), furnace dimensions, features of the control systems etc. The program holds a library of solar collectors that are available on the market, which can be used in the simulations, and it is possible to insert own collector characteristics (for symmetric collectors). The heat demand of the building can be calculated roughly by the program from choices of the construction type of the building, the indoor and design temperatures and the temperatures at the inlet and outlet of the radiant heating system. However, when Polysun was used in this work it was adapted to use Excel input files containing hourly data for a year of the heat demand of the building and of the outdoor temperature. Output files from DEROB-LTH containing these data were then used to simulate the energy demand of very specifically defined building constructions.

Polysun 3.3 is a convenient tool as it has a user-friendly graphical interface and short calculation time. The results given by Polysun are energy balances for the entire system and also for the tank and the collector loop

separately. These data are available as annual or monthly values for the period of one year. Also time related graphs of different temperatures and powers are shown, which makes it possible to estimate whether or not the system will reach stagnation.

4 Solar thermal systems in high performance houses

4.1 Introduction

This chapter presents the work performed by the author for the International Energy Agency, IEA, Task 28 – Sustainable Solar Housing. The work is also presented in the handbook of Task 28, "*Sustainable Solar Housing, Vol 1: Strategies and solutions*" (Hastings & Wall, 2007). The objective of Task 28 has been to spread information about energy effective housing design. The buildings presented in the book are designed with the focus on minimising energy use by constructing the building envelope for very low transmission losses, using efficient mechanical systems and heat recovery systems and finally by using renewable energy to cover the small remaining energy demand. The main objective of the handbook is to give inspiration and guidance to architects, constructors, consultants and students in these fields, with the hope that it will help to turn the trends in the building sector towards lower energy use, particularly lower use of energy from fossil fuels.

Here presented are the contents of the author's work within Task 28, also presented in the following sections in *Sustainable Solar Housing, Vol 1: Strategies and Solutions.*

- Section 2.5. Using active solar energy (Gajbert, 2007). A presentation of different aspects of solar thermal energy use in high performance buildings. Here presented in Section 4.2.

- Section 8.6 Apartment Building in the Cold Climate, Conservation Strategy (Smeds & Gajbert, 2007). Simulations of the solar thermal domestic hot water system for an extremely well insulated building were performed by the author. Here presented in Section 4.3.3.

- Section 8.7 Apartment building in the cold climate, Renewable energy strategy (Gajbert & Smeds, 2007). A design solution of a solar thermal

system for a high performance building is presented as well as a parametric study of several features of the system. Here presented in Sections 4.3.4 and 4.3.5.

In order to put the separate chapters into context for the reader, some brief summaries of other parts of the handbook are also included, such as the design and the energy demand of the reference apartment building for the cold climate, which was designed within the project. The other building solutions discussed here were designed by Johan Smeds.

4.2 Active use of solar thermal energy

From Section 2.5 in Sustainable Solar Housing, Vol 1, Strategies and Solutions

Heat captured by an active solar heating system can cover a significant part of the energy demand of high-performance (h.p.) houses, i.e. buildings with very low energy demand. Because the space heating demand of such buildings is very low, the year-round energy demand for domestic hot water (DHW) becomes relatively important. An active solar system can cover a large part of this energy demand, often more than 50%, since the demand also occurs in summer. The question is whether or not to design the solar system as a combi system that also contributes to the space heating, which means that a water-based heat distribution system is required. A key issue then is estimating the space heating contribution realistically, given the shorter heating period of high performance housing.

4.2.1 Solar thermal system designs

If a water-based heating system is preferred, a solar combi system is a good option. It provides flexibility to the heating system as it is built up around a joint storage tank, serving both the DHW and space heating systems and it can be heated by both the solar collectors and auxiliary energy sources connected to the tank, depending on conditions. There are many interesting combi system designs on the market, varying by region and the locally used auxiliary energy sources (Weiss, 2003). The system illustrated in Figure 4.1 uses a wood pellet boiler and an electric resistance heater as auxiliary energy sources to back up the solar circuit. The tank is equipped with a device to enhance thermal stratification. The domestic hot water is heated by an external heat exchanger.

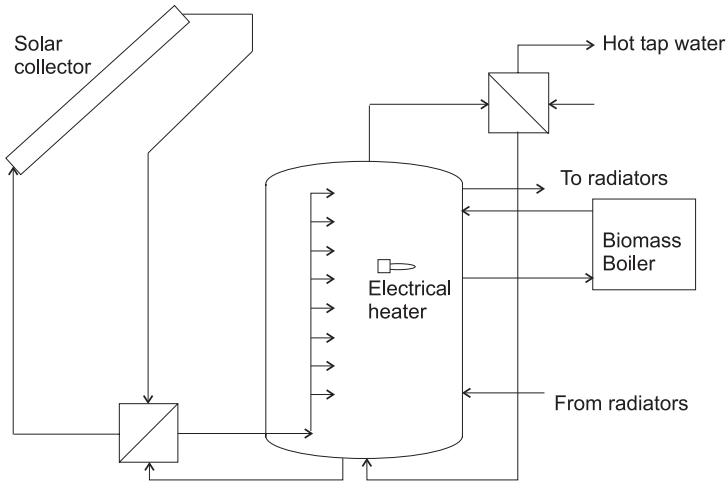

Figure 4.1 *A solar combi system with a joint storage tank for the DHW and space heating systems.*

A critical design condition for solar thermal systems is the case of minimum heat demand and maximum solar gains, as often occurs in summer. To minimize the system overheating in such instances the solar system should be designed to just cover the summer energy demand, accepting a small solar coverage in winter. An important advantage is that the combustion backup heating can be shut down during the summer. Thereby, short cycling of the backup system in summer can be eliminated, increasing the life expectancy of the system.

The shorter heating season of a high performance building results in a more pronounced seasonal mismatch between solar gains and space heating demand than is the case for conventional houses. This is illustrated in Figure 4.2, which shows a typical picture of the energy demand of a high performance house and a standard house in a cold (Stockholm) climate. The DHW demand is here assumed constant over the year although it is often slightly lower in summer, e.g. due to vacations.

As shown by the figure, it is often only a small part of the heating demand of h.p. houses that can be supplied directly by solar energy from a solar thermal system as the small solar gains during the heating season are also needed for hot water production. As it is not only the heating demand but also the peak power requirement of h.p. houses that is very low, it might be sufficient to heat the house simply by an electric heater or a water-to-air heat exchanger of low power in the supply air duct. An expensive water-based radiant heating system can then be avoided. A solar

thermal system would then be suitable for heating the hot water. It could also be connected to a heat exchanger for supply air.

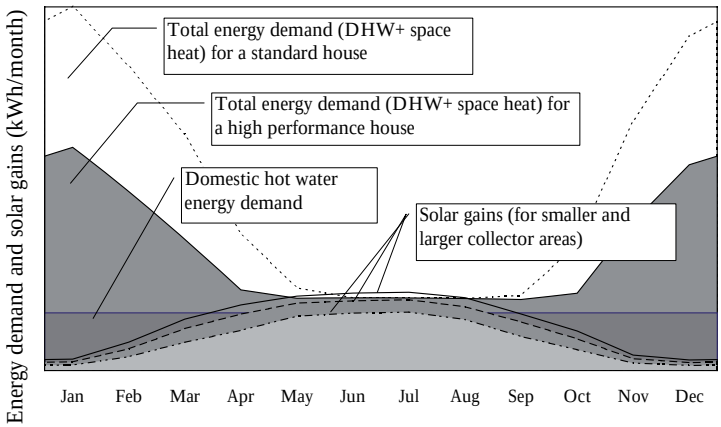

Figure 4.2 *Seasonal variations in solar gains and space heating demand in standard housing versus high performance housing.*

Because of the seasonal mismatch between solar gains and heating demand, it is common to over dimension the solar collectors used in combi systems to increase the solar gains in the heating season. This means that the collectors risk being overheated. This can be avoided by installing a larger storage tank than the system design would otherwise require. However, this approach is expensive, takes up more space and leads to higher tank heat losses.

There are also good control solutions available, for example the use of partial evaporation to empty the collector during stagnation. Active removal of energy transported via the steam during stagnation is also possible with a small-volume heat sink. Alternatively, the tank can be cooled down by circulating the heat transfer medium through the collectors at night or by using an air cooler. (Weiss, 2003; Hausner and Fink, 2002). However, the more cautious design strategy is not to over dimension the collector area.

An advantage of a combi system is that during the heating season, when energy for space heating is withdrawn from the tank, the operating temperature in the collectors can be lowered, increasing the collector efficiency. This typically occurs in autumn and spring.

This gain in efficiency can be maximized if the system includes an option to deliver solar energy directly to low temperature surface heating, e.g. floor heating. When there is a heating demand and the collector

temperature is sufficient, as often in spring or autumn, the flow from the collectors can be directed to the low temperature surface heating system, which means that the collectors can be operated at low temperature and thus be more efficient. This requires a good control strategy. Figure 4.3 shows an example of the design of such systems, which are common in France, Denmark and Germany (Weiss, 2003).

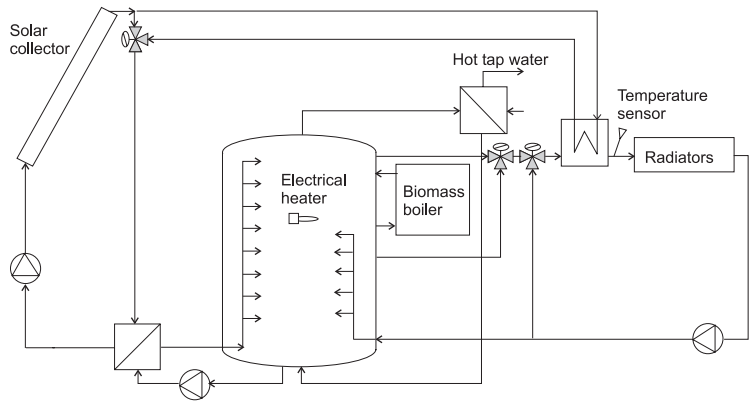

Figure 4.3 *A solar combi system with the option to deliver solar heat directly to the heating system without passing through the tank first.*

One way to better balance the solar gains against the heating demand is to mount the collectors vertically on the façade or to mount them with a high tilt. This positioning makes better use of low winter sun angles and suppresses summer overheating. This results in a more even distribution of the solar gains over the year, but a larger collector area is required to cover the summer domestic hot water demand. Figure 4.4 shows how the solar fraction (the part of the heating demand which is supplied by solar energy) increases with increased collector area for collectors tilted 40° and 90°. It shows that with a vertical collector the solar fraction can be increased if the collector area is increased. However, a larger collector will be necessary in order to get the same solar fraction as with a 40° tilted collector.

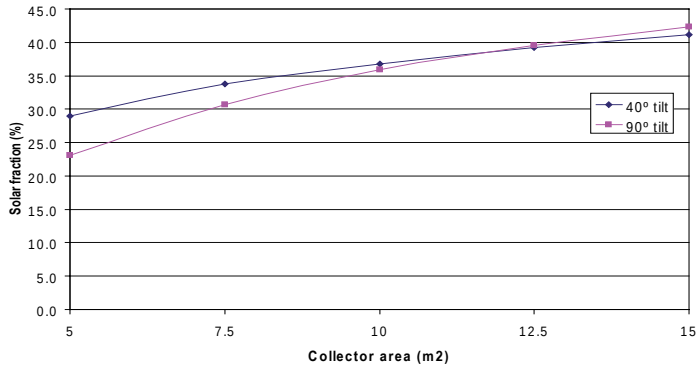

Figure 4.4 *Effect of collector tilt and area on solar fraction. Results from Polysun simulations of a combi system for a single family house in the cold climate. (T. Boström).*

A larger collector area is possible without risking overheating if the collector tilt angle is increased in relation to the optimal tilt angle, which approximately lies between 35° in southern latitudes (latitudes around 45°) and 45° in northern latitudes (latitudes around 60°). The suitable collector area and collector tilt angle are further discussed in Section 4.3.5.

Where buildings are closely spaced, a micro heating grid with a central solar system may be plausible. Collectors on the buildings can then share a large, semi-seasonal solar storage tank enabling some summer solar gain excess to be stored for the autumn. The large tank volume has an advantageous surface to volume ratio reducing tank heat loss. Also, a shared system can even out peak demands or supply excesses, resulting from the inhabitants' different habits of energy use. Disadvantages are the relatively high heat losses of the pipe network relative to the very small space heating demand, and the investment and administrative costs for meeting such a small demand. Such micro heat distribution grids for row-houses have proven effective in demonstration projects in Germany (Russ, 2005).

4.2.2 Collector types

There are many reliable and efficient collectors of different types on the market today:

Flat plate collectors have been highly optimized with selective coated absorbers, low-iron, anti-reflective coated glazing, durable frames and gaskets and effective back insulation.

Evacuated tube collectors, with their extremely good insulation, can operate at higher temperatures with only very small heat losses. Because the losses are so small, evacuated tube collectors can deliver heat even at very low irradiance levels occurring in winter and during overcast periods. They are thus very suitable for high performance houses with their shortened heating season. The individual tubes can be rotated to an optimal absorber tilt angle, allowing great flexibility in their placing. However, the separation between tubes must avoid one shadowing the next. Heat pipe collectors need to be mounted with a slight tilt to allow for gravity flow. A critical issue is snow retention on the tubes. A façade-mounted system minimizes this problem (Kovacs and Pettersson, 2002).

Concentrating collectors can also be envisioned, though such systems are not commercially available for housing. Prototype systems have been built and tested e.g. in Sweden, Great Britain and Australia. A low-cost reflector increases the irradiance on the absorber. The system geometry can be optimized for spring and autumn solar angles. While this suppresses the summer performance, the solar gains are better balanced against the heating demand over the year. Using an evacuated tube collector as the target of the reflector is a promising solution.

Solar air collectors, while interesting for conventional buildings or renovations, are difficult to justify economically for high performance houses. The heat exchanger of the ventilation system competes with the solar air collectors. One system or the other must operate with decreased efficiency. A plausible configuration would be an entire roof slope covered with a low cost, sheet-metal, solar air collector. During summer an air-to-water heat exchanger should easily cover all or most of the energy demand for water heating. In the autumn and spring the system could supply much of the space heating. Precast hollow-core concrete floor planks or large core masonry walls can also serve for heat storage and distribution (Morhenne, 2000).

4.2.3 Tank location

The tank location is an important design decision. On the one hand, it is sensible to locate it inside the insulated envelope of the building. Heat losses from even a very well insulated tank are therefore not lost to the ambient air but remain within the building (though this is a disadvantage in summer). Short pipe runs keep circulation heat losses small. A good location for the tank could be in or next to the bathroom. The warm tank surface improves the comfort in the bathroom. Comfort here is critical, because this is often where exhaust air for the whole living space is extracted, and the occupant may feel cold after showering. Also, the pipe run

is minimized between the tank and one of the largest points of demand. This decreases pipe heat losses and offers the convenience of hot water being quickly available at the tap. An upper floor bathroom is ideal, as the pipe run to roof collectors is also minimized. However, the insulated building interior is a very expensive volume to sacrifice for a tank, so the basement may be the preferred location. This otherwise cold space can then be slightly heated, improving comfort for the many uses found for a basement. Pipe runs from the tank should be within the heated building envelope as much as possible.

4.2.4 Regional design differences

It is easiest to market a solar combi system in regions where home owners prefer hot water radiant heating, particularly low temperature systems. Regions where oil or wood pellet heating is preferred have proved to be good markets for combi systems, often even large systems. Solar combi systems have been widely sold in Germany, Austria, Switzerland, Sweden, Denmark and Norway. It seems more difficult to market combi systems in regions where mainly direct electricity or gas is used for heating, in the Netherlands for example (Weiss, 2003).

In warmer climates, the space heating demand of h.p. houses is even lower but the solar energy can also be used a little bit longer in spring and autumn, as the general illustration in Figure 4.5 shows.

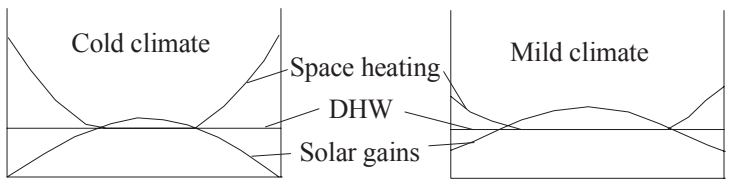

Figure 4.5 *The general differences between colder and milder climates; the solar gains are better balanced against the space heating demand in the milder climate.*

4.3 Design of solar heating systems

4.3.1 Introduction

The work within Task 28 - Subtask B

Within the framework of IEA, Task 28, subtask B, high performance houses have been designed and analysed. The results of all the buildings are presented in the handbook.

Designs of three house types - single family houses, row houses and apartment buildings - in three different climates - "the cold climate" (Stockholm), "the temperate climate" (Zurich) and "the mild climate" (Milan) - have been investigated. Reference buildings with standard insulation quality were set up for each of the nine building types. Targets to meet were set up after thorough discussions and investigations. Thereafter the design process of the high performance houses for the different cases began. (Wall, 2007)

The applied design approaches - energy conservation and renewable energy supply

A general advice for building designers who want to reduce the energy demand of a building is to start by designing a well insulated building envelope and to ensure good heat recovery systems, so that the heating demand of the building is reduced as much as possible, and secondly to ensure that renewable energy is used for the remaining energy supply. As there may be limitations of different kinds, e.g. in the budget for the building materials or the heating systems, the feasibility of grid connection etc., it is useful to know how the use of primary energy can be reduced to a low level in different cases. Therefore two design approaches are differentiated and applied in this work - *the conservation strategy* and *the renewable energy strategy*.

When the conservation strategy is applied, the main focus is to reduce the thermal losses from the building by investing most resources in the building envelope. Thick insulation, building materials with low thermal conductivity, low-e-coated windows and efficient heat recovery systems are used, all in order to reduce the energy demand. Another means of reducing the energy demand is to choose low-consuming household appliances. With these measures, large energy savings can be accomplished, without reducing comfort or quality.

When the renewable energy strategy is applied, the focus is set on supplying the required energy with renewable energy, here with the focus on solar thermal energy and bio fuel, which lowers the non-renewable

primary energy demand significantly. In comparison with the conservation strategy, a slightly lower insulation level of the building envelope may be acceptable, as the target of non-renewable primary energy use (discussed below) can still be reached.

The targets to meet

Two targets were set for the buildings before the design process. The main target is that the annual use of non-renewable primary energy for space heating and hot water production and the electricity for mechanical systems must not exceed 60 kWh/m^{2}a. Targets for the maximum space heating demand were then set up and different buildings were designed to meet these targets. For the conservation strategy the maximum space heating demand is 15 kWh/m^{2}a. However, an extremely well insulated apartment building requiring only 6 kWh/m^{2}a is also designed for the cold climate. For the renewable energy strategy, the maximum space heating demand was set higher, to 20 kWh/m^{2}a.

The author's assignments

The author was assigned to work on the design of the solar heating systems for two apartment buildings in the cold (Stockholm) climate, one for the conservation strategy and one for the renewable energy strategy. These building constructions (including mechanical ventilation systems) had previously been designed by Johan Smeds, using the simulation program DEROB-LTH (Kvist, 2005). The results of space heating demand from these simulations were used by the author in the simulations of the solar thermal heating system, using Polysun 3.3 (Polysun, 2002), which had been slightly adapted so that output data of space heating demand from DEROB-LTH could be used as input data. Hourly Stockholm climate data from Meteonorm (Meteotest, 2004) were used for both the Polysun and the DEROB-LTH simulations. For general assumptions and parameters used in the DEROB-LTH and Polysun simulations, see Appendix B.

Most of the simulation work performed by the author was carried out for the design of a solar combi system for the building in Solution 2, the renewable energy strategy. A sensitivity analysis of different parameters of the solar system, such as the type, size and orientation of the collectors, the tank size, flow rates etc., was performed for this system. A solar thermal hot water system was also designed for the extremely well insulated building in Solution 1a.

Definitions and design assumptions

All the buildings presented in this chapter have the same basic structure based on reinforced concrete and wooden frame facades with mineral

wool. It is mainly the insulation thickness that is varied. The apartment buildings were all designed with a floor area of 1600 m^2, which is divided into 16 apartments of 100 m^2 each. The average number of occupants in each apartment is 3 people (two adults and one child). The domestic hot water demand is assumed to be 40 litres per day and person.

The energy terms presented in the result tables are defined as follows:

The net energy is the energy required for services such as maintaining the building at the specified internal temperature, lighting or ventilating a space etc. Internal gains from inhabitants, electric appliances and circulation losses were taken into account in the simulations of space heating demand in DEROB-LTH. The presented figure of space heating demand is thus the remaining heating demand. The tank losses and losses from the collector loop on the other hand have not been considered as internal gains since the tank and boiler are assumed to be placed in the basement outside the thermal envelope of the building.

The total energy use of the building includes the net energy and the system heat losses. It can also be described as the sum of the delivered energy and the energy produced and used on site, including renewable forms, but excluding passive gains. Energy delivered back to the market is not included.

The delivered energy is the energy supplied to the building from the last market agent.

Both the *emissions of CO_2 equivalents* and the *non-renewable primary energy use* are directly related to the total energy use. *Primary energy* is the energy used on site, for which losses from the extraction, distribution and conversion to heat are taken into account. The presented results of non-renewable primary energy include only the share of the primary energy that is based on non-renewable energy sources. Energy required for space heating, water heating and for the mechanical systems is included. Circulation heat losses and losses from the boiler are also included. The conversion losses of an electric heater in the tank are assumed to be zero. (Petersdorf & Primas, 2007)

The conversion factors to calculate the primary energy and the CO_2 equivalents from different energy sources were set up by a group within the project which has studied LCA reports agreement. The factors used are based on the GEMIS tool (GEMIS, 2004) where average values for 17 European countries are used. These factors are related to the lower heating value (LHV) for which condensation energy is not included. This means that the theoretical efficiency of a heating system with a condensing gas furnace can be higher than 100%. However, the efficiencies set here are 100% for a gas furnace, 98% for an oil furnace and 85 % for a pellet boiler. The factor used for calculating the non-renewable primary energy is 2.35

for electricity and 0.14 for bio pellets (Petersdorf & Primas, 2007). These conversion factors are also presented in Appendix B.III.

4.3.2 The cold climate apartment reference building

The reference apartment building for the cold Stockholm climate has reinforced concrete structure and wooden frame facades with mineral wool, as the other apartment buildings designed for the cold climate. Air-filled triple glazed windows with a frame ratio of 30% are used and the U-value of the whole building envelope is 0.35. There is no heat recovery in the exhaust air ventilation system, which provides 0.5 ach (air changes per hour). District heating is used for heating DHW and space heating. (Smeds, 2007)

Calculations of the space heating demand of the reference house were performed using the Bilanz program and according to EN832 (Heidt, 1999). The annual space heating demand is 70000 kWh/a or 44 kWh/m^2a and the maximum power requirement is 46 kW or 29 W/m^2. The total energy use (for space heating, DHW, system losses and mechanical systems) is 81 kWh/m^2a. The use of non-renewable primary energy is 70 kWh/m^2a (112600 kWh/a) and the corresponding emissions of CO_2 equivalents are 20 kg/m^2a. (Smeds, 2007)

4.3.3 Design solution 1a – Conservation strategy: A solar DHW system for an extremely well insulated building

From Section 8.6 in Sustainable Solar Housing, Vol 1, Strategies and Solutions.

A solar domestic hot water system was designed for an extremely well insulated apartment building in the cold climate. This building has a space heating demand of only **6.5 kWh/m^2a**, which is even lower than the target of the conservation strategy, and the peak power for space heating is limited to **10 W/m².** The energy for space heating is supplied by electric resistance heating.

The building design

A similar building but with extremely high insulation level was also designed for the project. The U-value of the whole building envelope is only 0.21 (to be compared with 0.41 for the building of the renewable energy strategy). The U-value of the windows is 0.92 for frame and glass. The

windows have a frame ratio of 30%, triple glazing, one low-e coating and they are filled with krypton. The U-value of the walls is 0.13, the roof, 0.09 and the floor, 0.12 (excluding ground). More detailed U-values and construction data are shown in Appendix B.I.I. Also for this building, a balanced mechanical ventilation system with 80% heat recovery and a bypass for summer ventilation is used. The only heat distribution system is the supply air duct, where electric heating is installed.

Solar thermal system design

A solar domestic hot water system is designed for this building. The solar system consists of 60 m² collectors, a storage tank of 6 m³ and an electric heater of 8 kW in the tank. The collector is an advanced flat plate collector and the same collector parameters as in Solution 2 are used (see Table 4.4 – collector no 3.) The heat from the solar circuit is delivered to the storage tank via an external heat exchanger. A stratification device is placed in the tank to improve stratification. The hot water is taken directly from the top of the tank and a three-way-valve is used to mix it with cold water. Daily peaks in hot water consumption are taken into consideration.

Energy Performance

The space heating demand of this building is 10300 kWh/a (6.5 kWh/m²a) according to simulation results from DEROB-LTH. The space heating demand for each month of the year is shown in Figure 4.6. The highest heat load occurs in January and is 16 kW (10 W/m²). The net heat demand for domestic hot water is approximately 37800 kWh/a (23.6 kWh/m²a) which means that the DHW demand is much larger than the space heating demand.

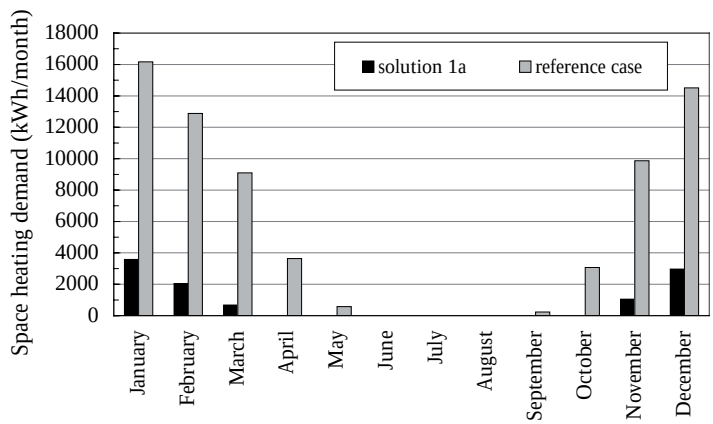

Figure 4.6 Monthly values of the space heating demand for the building of

solution 1a and of the reference building.

The total energy use for DHW and space heating, system losses and mechanical systems is 63200 kWh/a (39.5 kWh/m^{2}a). The system losses consist mainly of losses from the hot water storage tank (1.5 kWh/m²a), but also of pipe heat losses in the distribution system. After taking the solar contribution for DHW into account the delivered energy is 34200 kWh/a (21.4 kWh/m^{2}a), which is provided by electricity. This results in a total use of non-renewable primary energy of 80300 kWh/a (55 kWh/m²a) and CO_2 equivalent emissions of 10 kg/m²a, see Table 4.1.

Table 4.1 Total energy demand, non-renewable primary energy demand and CO_2 equivalent emissions for the apartment building with electric resistance space heating and solar DHW system with electrical backup. The energy terms are defined in 4.3.1.

Net Energy (kWh/m²a)		Total Energy Use (kWh/m²a)				Delivered energy (kWh/m²a)		Non renewable primary energy		CO_2 equivalent emissions	
		Energy use		Energy source				factor (-)	(kWh/m²a)	factor (kg/kWh)	(kg/m²a)
Mechanical systems	5.0	Mechanical systems	5.0	Electricity	5.0	Electricity	5.0	2.35	11.8	0.43	2.2
Space heating	6.5	Space heating	6.5	Electricity	6.5	Electricity	18.3	2.35	43.0	0.43	7.9
DHW	23.6	DHW	23.6	Electricity	11.8						
		Tank and circulation losses	5.5	Solar	17.3						
		Conversion losses	0.0								
Total	35.1		40.6		40.6		23.3		54.8		10.0

4.3.4 Design solution 2 - Renewable energy strategy: A solar thermal system for DHW and space heating,

From Section 8.7 in Sustainable Solar Housing, Vol 1, Strategies and Solutions.

This section presents a design solution of an apartment building in the cold climate (Stockholm) and the solar and bio fuel based heating system designed for this building. The solution is based on the renewable energy strategy, for which the maximum space heating demand of the building was **20 kWh/m^{2}a.** The use of renewable energy should make it possible to reach the target of non-renewable energy use of **60 kWh/m^{2}a.** For this solution a solar combi system with a bio fuel boiler is used for the thermal energy supply of both DHW and space heating. The design of

the solar thermal heating system was performed primarily with regard to low auxiliary energy use in summer, avoidance of overheating and economic aspects.

The building design

This apartment building is similar to the reference building, with reinforced concrete structure and wooden frame facades with mineral wool. The U-value of the whole building envelope is 0.41, which is even higher than the reference building. However, the building has a balanced mechanical ventilation system with heat recovery of 80%, which reduces the ventilation losses, and a bypass for summer ventilation is installed. The ventilation rate is 0.45 ach and the infiltration rate is 0.05. The double glazed windows, with U-value of 1.34 for frame and glass, have a frame ratio of 30%, one low-e coating and are filled with air. The U-value of the walls is 0.27, the roof, 0.29 and the floor, 0.30 (excluding ground). The heating set point is 20°C, the maximum room temperatures: 23°C during winter and 26°C during summer (assumes use of shading devices and window ventilation) (See more details in Appendix B.I.III).

The solar and bio fuel heating system

A solar combi system is designed for this building, i.e. a solar thermal system where the space heating system and the domestic hot water (DHW) system are combined, here by a joint storage tank, to which both solar collectors and auxiliary energy sources are connected. The solar thermal heating system consists of 50 m² collectors placed on a south-facing roof, tilted 40°. The collector is an advanced flat plate collector. (The collector parameters are shown in Table 4.4, for collector number 3.) The storage tank is 4 m³, there is a 35 kW pellet boiler and an electric heater of 5 kW connected to the tank for increased operational flexibility. The heat from the collector circuit is delivered to the tank via an external heat exchanger coupled to a stratifying device, which improves the important thermal stratification in the tank. Another external heat exchanger is used for heating the DHW, taking water from the top of the tank and returning it at the bottom. The heat transfer medium in the collector circuit is a mixture of 50% water and 50% glycol. Water from the tank is used for the radiant heating system in the building. The system is illustrated in Figure 4.7.

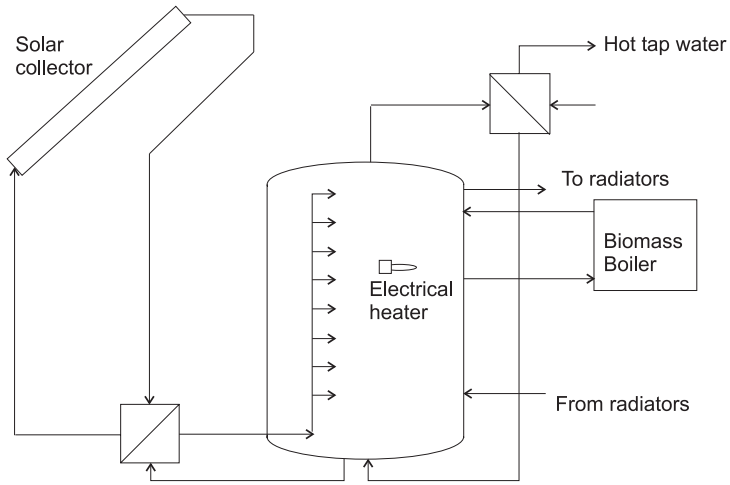

Figure 4.7 *The design of the suggested solar combi system with a pellet boiler and an electric heater as auxiliary heat sources, two external heat exchangers, one for the DHW and one for the solar circuit. The latter is attached to a stratifying device in the tank.*

The electric heater and the biomass boiler are mainly working alternately, heating the upper part of the tank when necessary. When only very little auxiliary heat is required during short periods, as often in the summer, the biomass boiler operation mode with frequent starts and stops causes unnecessary energy losses and it is therefore suitable to shut off the furnace during summer, when solar energy can cover most of the energy demand. The electric heater can then be a good backup during cold and cloudy days. The electric heater can also be used parallel with the boiler if needed on extremely cold winter days.

Energy Performance

The space heating demand of the building is 30400 kWh/a, or 19.0 kWh/m^{2}a, according to simulations results from DEROB-LTH, which is below the limit of maximum space heating demand. The monthly space heating demand for this high performance case in comparison to a reference building according to the current building code of year 2001 is shown in Figure 4.8. The annual peak load occurs in January and is 26.8 kW (17 W/m^2).

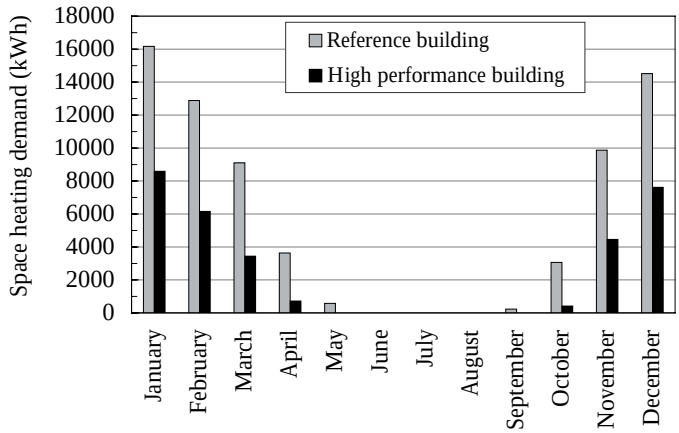

Figure 4.8 *Monthly values of the space heating demand during one year. The annual total space heating demand is 30400 and 70000 kWh/a respectively for the high performance building and the reference building.*

The net energy demand for domestic hot water is assumed to be 37800 kWh/a (23.6 kWh/m²a). The DHW demand is thus larger than the space heating demand.

The system losses consist mainly of losses from the hot water storage tank, but also from circulation losses in the distribution system for DHW. The tank and circulation losses are 1.2 and 4.4 kWh/m^{2}a respectively. The efficiency of the biomass boiler is set to 85%, resulting in conversion losses of 5.5 kWh/m^{2}a.

As shown in Table 4.2, the net energy required for DHW, space heating and mechanical systems is 47.6 kWh/m^{2}a (76200 kWh/a). Adding tank, boiler and system losses gives a total energy use of 58.7 kWh/m²a (93900 kWh/a).The total auxiliary energy demand (electricity and pellets), including the conversion losses in the pellet boiler, is 36.4 kWh/m^{2}a (58300 kWh/a), of which 36.2 kWh/m^{2}a (57900 kWh/a) are provided by biomass in the pellet boiler and approximately 0.3 kWh/m^{2}a (400 kWh/a) by the electric heater.

The active solar gains are 17.3 kWh/m²a (27600 kWh/a) and the solar fraction of the heating system is 35%, since the simulation result of the same building, but without solar collectors, would require 77400 kWh/a (described in section 4.3.5).The electricity use for mechanical systems is 5.0 kWh/m²a (8000 kWh/a).

Due to the solar contribution, the delivered energy is reduced to 41.4 kWh/m^{2}a (66200 kWh/a). The total use of non-renewable primary energy is approximately 17 kWh/m^{2}a (27900 kWh/a) and the CO_2 equivalent emissions are 3.8 kg/m^{2}a (6100 kg/a). Compared to the reference building, the non-renewable energy use and CO_2 equivalent emissions are considerably lower; see Table 4.3 and Figure 4.9.

Table 4.2 Total energy demand, non-renewable primary energy demand and CO_2 equivalent emissions for the apartment building. The energy terms are defined in 4.3.1.

Net Energy (kWh/m²a)	Total Energy Use (kWh/m²a)		Delivered energy (kWh/m²a)	Non renewable primary energy		CO_2 equivalent emissions	
	Energy use	Energy source		factor (-)	(kWh/m²a)	factor (kg/kWh)	(kg/m²a)
Mechanical systems 5.0	Mechanical systems 5.0	Electricity 5.0	Electricity 5.0	2.35	11.8	0.43	2.2
Space heating 19.0	Space heating 19.0	Electricity 0.3	Electricity 0.3	2.35	0.6	0.43	0.1
		Solar 17.3	Solar 0.0	0.00	0.0	0.00	0.0
DHW 23.6	DHW 23.6	Bio pellets 36.2	Bio pellets 36.2	0.14	5.1	0.04	1.6
	Tank and circulation losses 5.6						
	Boiler conversion losses 5.5						
Total 47.6	58.7	58.7	41.4		17.4		3.8

Table 4.3 A comparison between the high performance house and the reference house regarding energy use and CO_2-equivalent emissions.

Building	Net energy (kWh/m²a)	Total energy use (kWh/m²a)	Delivered energy (kWh/m²a)	CO_2 equivalent emissions (kWh/m²a)
High performance building	47.6	58.7	41.4	3.8
Reference building	72.4	81.2	81.2	20.5

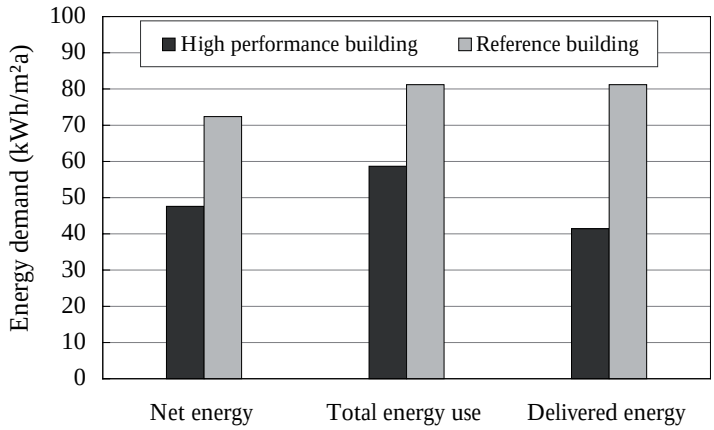

Figure 4.9 *An overview of the net energy, the total energy use and the delivered energy for the high performance building and the reference building.*

4.3.5 Sensitivity analysis of the solar system for Solution 2

As the performance of the solar energy system is strongly affected by the system design parameters, e.g. collector area, tank volume, slope and direction of the collectors and collector type of the solar heating system, some of the most important results from the Polysun simulations performed during the design of the system are presented here. Unless otherwise stated, the parameters of the simulated systems are the same as for the system solution described above. The "auxiliary energy", which is shown in many of the figures, is the heat output from the auxiliary energy system, thus including heat for DHW heating, space heating and also heat losses from the piping and the tank. It does not include the conversion losses from the heat production (i.e. combustion and heat exchanger losses in a wood pellet furnace).

Collector area

When a solar thermal system is designed, the collector area and tank volume should preferably be considered both individually and as a unit. The collector area is however the more important feature to optimise in order to minimise the auxiliary energy use.

Polysun simulations of a solar combi system have been performed with varying collector areas and with a constant storage tank volume. The aim was to find a collector size that is large enough to almost cover the summer heating demand, i.e. the DHW demand, while still maintaining a relatively low risk of stagnation in the collectors.

The solar fraction, *SF*, is calculated according to Equation 54. The parameters *Aux* and Aux_0 represent the auxiliary energy required with (*Aux*) and without (Aux_0) the solar system. In Polysun, the value of Aux_0 was obtained by setting the collector area to zero, which resulted in an annual auxiliary energy demand of 77400 kWh per year and 11600 kWh during the summer months (June, July and August).

$$SF = 1 - \frac{Aux}{Aux_0} \qquad \text{Eq. (54)}$$

In Figure 4.10 it is shown how the calculated solar fractions for the whole year and also for the summer months, June, July and August, increase with increasing collector area.

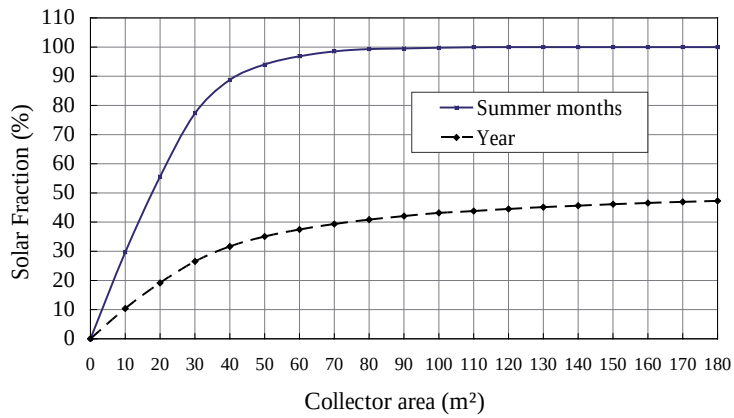

Figure 4.10 *The solar fraction of the system for the whole year and for the summer months.*

In order to lower the risk of stagnation and overheating, 50 m² seems a suitable collector size. The pellet boiler can still be turned off during summer, although a small amount of electricity may be needed during a few colder days. The solar fraction during the three summer months will

then be 95%. If a solar fraction of 100% in the summer were to be attained, the risk of overheating and stagnation would be large. Even though good control strategies can mitigate these problems, it is still desirable to avoid the problem completely. If a solar heated swimming pool for summer use were connected to the system, the problems of overheating and stagnation could be reduced and a larger collector area could be used, giving higher solar gains over the whole year. Figure 4.11 shows monthly values of the auxiliary energy demand during summer for different system dimensions.

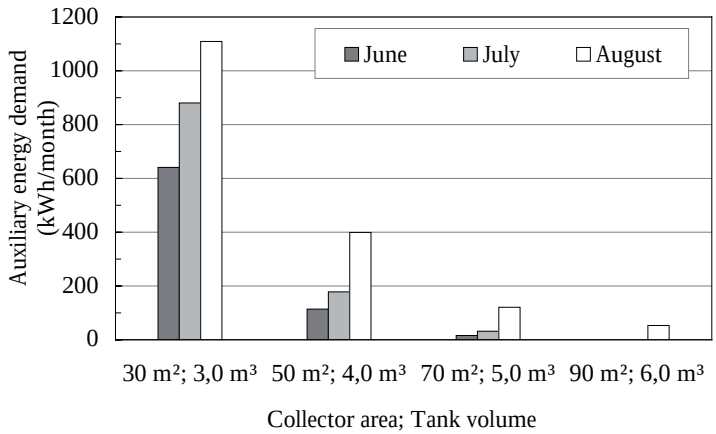

Figure 4.11 *Monthly values of auxiliary energy demand for solar systems of different dimensions.*

In Figure 4.12, the energy saved due to the installation of the collectors is shown for the marginal collector area, i.e. the extra savings made with an increase in collector area by 10 m².

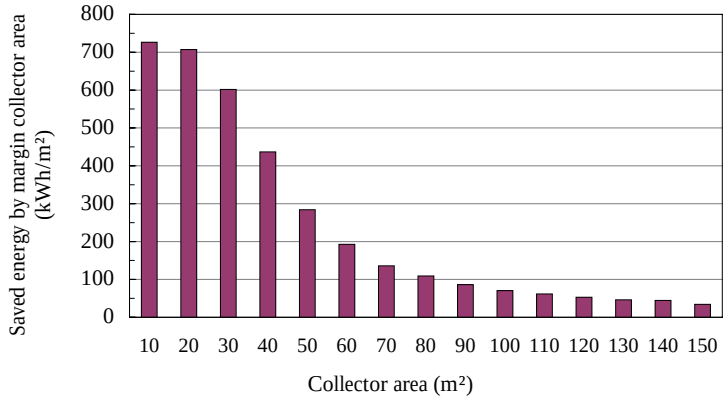

Figure 4.12 *The energy savings per marginal collector area, i.e. the amount of additional energy saved if 10 m² is added to the collector area, read from left to right.*

The resulting non-renewable primary energy demand and CO_2-equivalent emissions when solar combi systems of different dimensions are used can be seen in Figure 4.13. The tank volumes were optimised for each case.

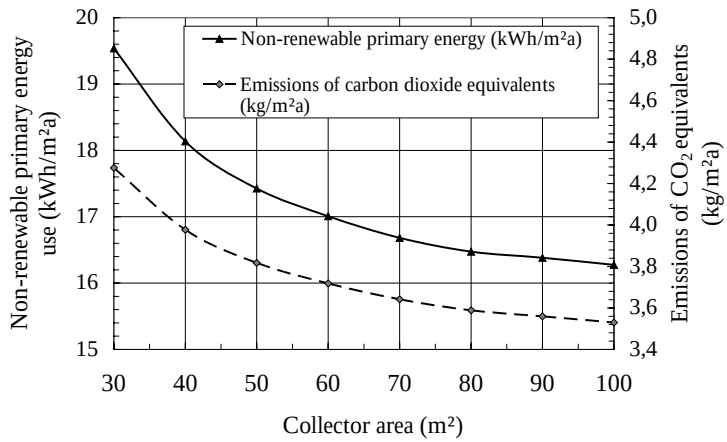

Figure 4.13 *The resulting non-renewable primary energy demand and CO_2-equivalent emissions for different collector areas.*

If the solar system had been installed in the reference building (described in Section 7.2 in the handbook) instead, the auxiliary energy demand would be much higher, as can be seen in Figure 4.14, where the auxiliary

energy demands of the two buildings are shown for different solar system dimensions. Again the tank volumes were optimised for each case.

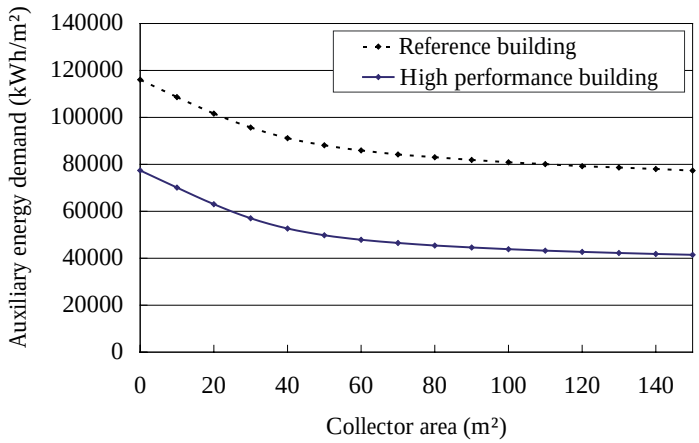

Figure 4.14 *Annual auxiliary energy demand per floor area for different system dimensions based on Polysun simulations.*

In Figure 4.15 the overview of the energy demands of the high performance building and the reference building are shown as well as the solar gains of collectors of 30, 50 and 70 m^2. Note that the heat for DHW, circulation losses and tank losses is valid for 50 m^2 collector area. For a larger collector, the tank losses will be slightly higher.

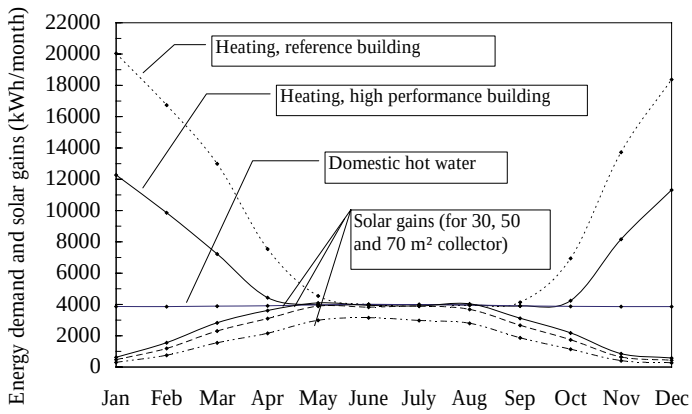

Figure 4.15 *The energy demands and solar gains of the high performance building and the reference building. The solar gains are shown for different collector areas.*

Storage tank volume

For economic reasons it is important to consider the storage tank volume. A larger tank is much more expensive though the impact on the auxiliary energy use is rather small, as shown in Figure 4.16. The tank could preferably be designed based on the daily energy demand, due to the limited storage time capacity. The tank should not be too small in view of the risk of overheating and because of lowered storage capacity. On the other hand, an oversized tank might give rise to a higher auxiliary energy demand in order to heat the tank and also because of the higher heat losses. A high insulation level is therefore important and it becomes more important, the larger the tank is.

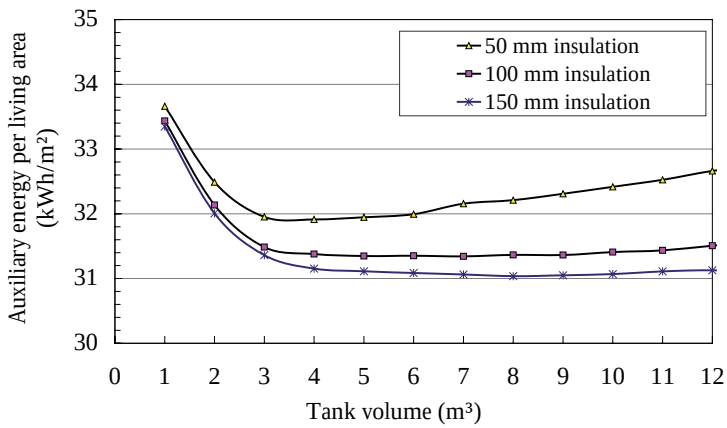

Figure 4.16 *The influence of tank volume and tank insulation level. The figure shows the auxiliary energy demand per living area for different tank volumes.*

Simulation results for collector areas between 50 and 100 m², with varying tank volumes, are shown in Figure 4.17 where the chosen system is marked with a circle. These results too show that the collector area has a much larger influence on the auxiliary energy use than the tank volume. For the larger collectors, some energy can be saved by choosing a larger tank. The suggested system with 50 m² collector area and a storage volume of 4 m³ would entail neither overheating nor excessive tank losses, according to the simulation results.

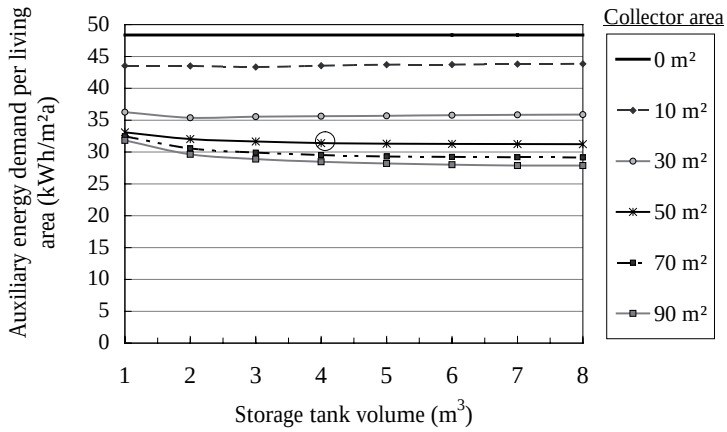

Figure 4.17 *Annual auxiliary energy per living area for different system dimensions based on Polysun simulations.*

Collector tilt

The tilt of the collector determines how large the collector should be in order to cover the summer demand. In order to maintain a solar fraction of 95% during the summer months, the required collector size increases as the collector tilt is increased or decreased from 30- 40°, which is the tilt where the smallest collector area (50 m^2) is needed. This is illustrated in Figure 4.18.

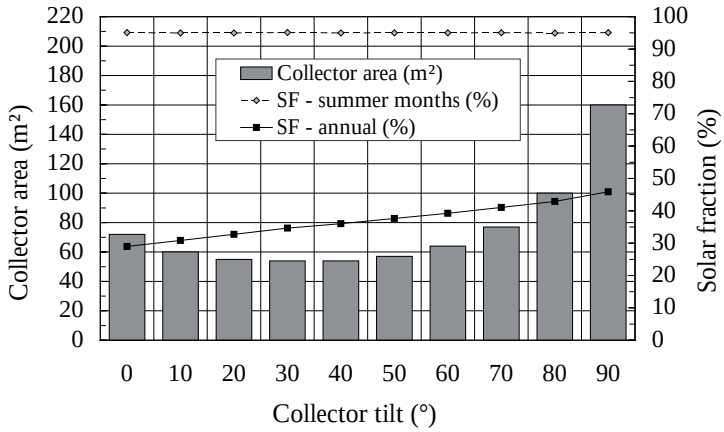

Figure 4.18 *The graph shows the collector area required for differently tilted collectors in order to get a solar fraction of 95% during summer, i.e. an appropriate area which does not imply boiling in the tank. The solar fraction for the whole year and the constant solar fraction in summer are shown.*

When highly tilted or vertical collectors are used, the solar gains will be better balanced against the seasonal heating demand as more of the winter space heating demand will be covered. However, this requires a larger collector area in order to cover the summer demand. For a very large collector with a high tilt angle, energy can be saved in total over the year, thus implying a higher annual solar fraction. A good, yet very expensive, solution would therefore be to use a vertical wall mounted collector of very large size. The benefits of this are naturally much higher for combi systems than for DHW systems. There are generally no benefits in using a horizontal collector, or a collector with a very low tilt.
Looking further at two mounting options for good building integration; either to mount the collectors on the 40° tilted roof or vertically on the wall, tilted 90°, it can be seen in Figure 4.19 how the auxiliary energy demand decreases with increasing system size. The 40° tilt gives rise to a lower demand of auxiliary energy on an annual basis and the difference is more significant in smaller systems. Furthermore, the risk of snow cover should be considered if a very low tilt angle is used. The risk of snow cover is even larger for evacuated tube collectors.

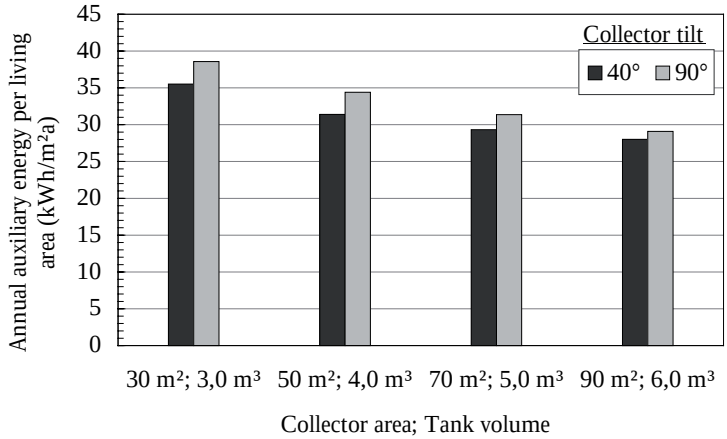

Figure 4.19 *Results from simulations of systems with differently tilted collectors, 40° for the roof mounted and 90° for the wall mounted collectors.*

Azimuth angle

If the deviation from south, i.e. the azimuth angle, is varied, the auxiliary energy demand and solar fraction change according to Figure 4.20.

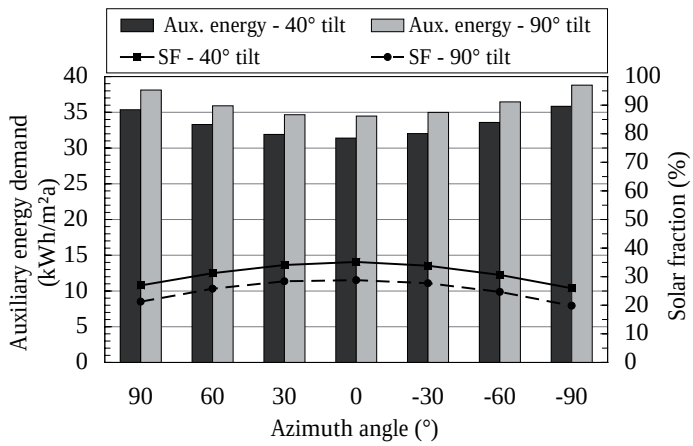

Figure 4.20 *The auxiliary energy demand and solar fractions of systems with different azimuth angles.*

Collector performance

The choice of collector is very important for the system performance. Simulations have been performed with collectors of different types, from older collector types without a selective surface to the most advanced evacuated tube collectors available, with characteristics and simulation results listed in Table 4.4. The results are also shown in Figure 4.21. In the suggested system an advanced flat plate collector with a selective surface, antireflection treated glass and highly efficient thermal insulation (number 3 in Table 4.4) is used. When compared to an older collector type without selective surface, the chosen collector increases the solar fraction from 26.4% to 35.1%. If an evacuated tube collector is used, the solar fraction increases even more. For the suggested solar heating system an evacuated tube collector of 35 m² would be sufficient. Evacuated tube collectors are very efficient, but also often very expensive.

Table 4.4 Collector parameters and corresponding solar fraction and auxiliary energy.

Collector type	η_0 (-)	c_1 (W/m^2K)	c_2 (W/m^2K^2)	KCH1 (-)	KCH2 (-)	Specific heat capacity (kJ/m^2K)	Solar fraction (%)	Auxiliary energy (kWh/a)	Auxiliary energy (kWh/m²a)
1. Advanced evacuated tube collector	0.88	1.41	0.013	0.92	1.15	7.84	40,5	46053	28.8
2. Evacuated tube collector	0.77	1.85	0.004	0.9	1.00	5.71	36.7	49004	30.6
3. Advanced flat plate collector	0.85	3.7	0.007	0.91	0.91	6.32	35.1	50232	31.4
4. Flat plate collector	0.8	3.5	0.015	0.9	0.9	6.32	33.1	51767	32.4
5. Flat plate collector - no selective surface	0.75	6,00	0.03	0.9	0.9	7,00	26.4	56976	35.6

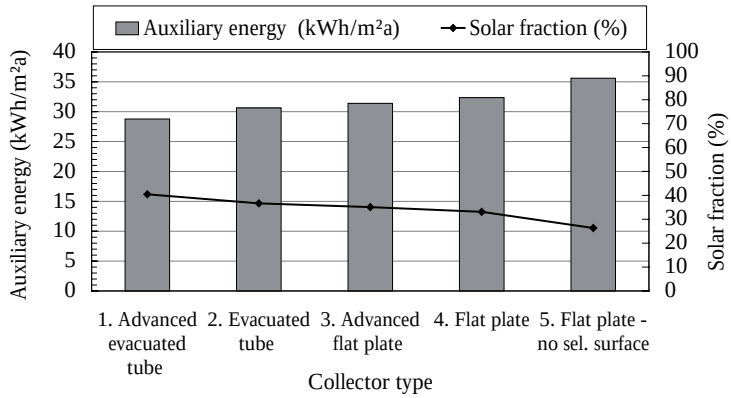

Figure 4.21 Results from simulations of systems with different collector types.

Concentrating collectors

By using concentrating reflectors to enhance the irradiance on the absorber, the output from the collectors can be increased. If the geometry of the collectors excludes irradiation from higher solar angles, the collector could improve the seasonal balance by increasing the winter performance and suppressing the summer performance. It is interesting to apply this strategy to evacuated tube collectors, which have the potential to deliver energy during lower irradiance levels and which are also relatively expensive at the present time. An estimation of the effect this would give rise to was investigated for an evacuated tube collector (with collector characteristics according to Collector type 1 in Table 4.4). Polysun simulations were performed assuming a double collector area from October to March and with the collector tilted 70° and 90°. The area was chosen so as to imply a solar fraction of 95 % during summer. The results shown in Table 4.5 indicate that the reflector gives rise to energy savings of 11 %, if it is tilted either 70° or 90°.

Table 4.5 The auxiliary energy demand for an evacuated tube collector with and without reflectors.

	70°, 42 m^2		90°, 56 m^2	
	Without reflector	With reflector	Without reflector	With reflector
Total annual auxiliary energy (kWh/a)	47538	42297	45643	40570
Solar fraction (%)	38.6	45.4	41.0	47.6

Design of the collector loop heat exchanger and flow rate

The design of the storage tank and its connected components is also important for the system efficiency, as different types of heat exchangers work optimally at different flow rates. The flow rate in the collector loop should not be too low, so as not to cause laminar flow, air traps and/or increased heat losses. Therefore, if the heat from the collectors is transferred to the tank through an internal heat exchanger, a high flow rate gives rise to a lower auxiliary energy demand, as shown in Figure 4.22.

The efficiency of the solar heating system is improved if an external heat exchanger is used instead, and even better if a stratifying device is used. In a smaller tank the importance of a stratifying device is more significant. In these cases, a low flow rate is better, since the fluid inserted into the tank may otherwise cause mixing of the stratified water. However, the flow rate should not be too low. The optimum can be seen in Figure 4.22. Lower flow rates also contribute to a lower electricity use for the pump, and the dimensions of the pipes are reduced and they are therefore less expensive.

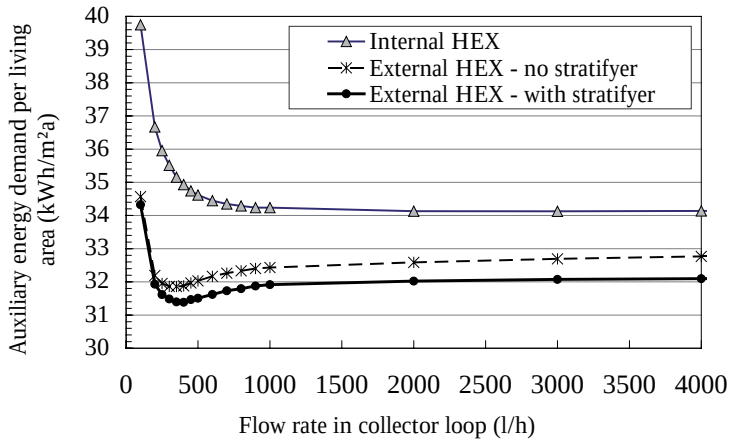

Figure 4.22 *The auxiliary energy demand, with varied flow rate and type of heat exchanger in the solar circuit.*

Non-renewable energy use – for solar DHW systems and combi systems

In order to compare our solar combi system with a solar DHW system, simulations were also performed for two different a solar DHW system for the same building construction as for the combisystem. One of these DHW systems is combined with an electric heater in the DHW tank and electricity also for space heating. The other system is combined with district heating for both DHW and space heating. The use of non-renewable energy and the emissions of CO_2 equivalents are shown in Figures 4.23 and 4.24, which clearly show that the most environmentally friendly design is the solar combi system with a pellet boiler. This system reaches the targets of non-renewable primary energy of maximum 60 kWh/m^{2}a (floor area) by far and only a small collector is required in order to reach this target. If a solar DHW system combined with electricity for space heating were applied the target would not be reached. For a solar DHW system combined with district heating for space heating, the solar collectors would have to be at least 40 m^2 in order to reach the target, as shown in Figure 4.23.

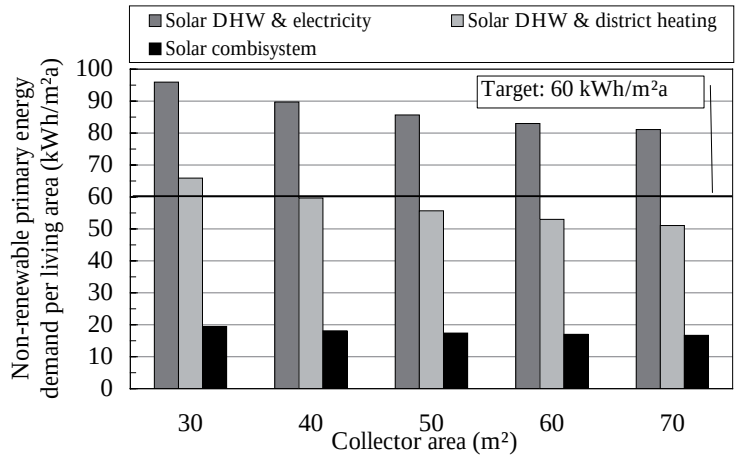

Figure 4.23 *The use of non-renewable primary energy for three different energy system designs; the combi system in question, with a pellet boiler and an electric heater, a solar DHW system combined with district heating and a solar DHW system combined with electric heating.*

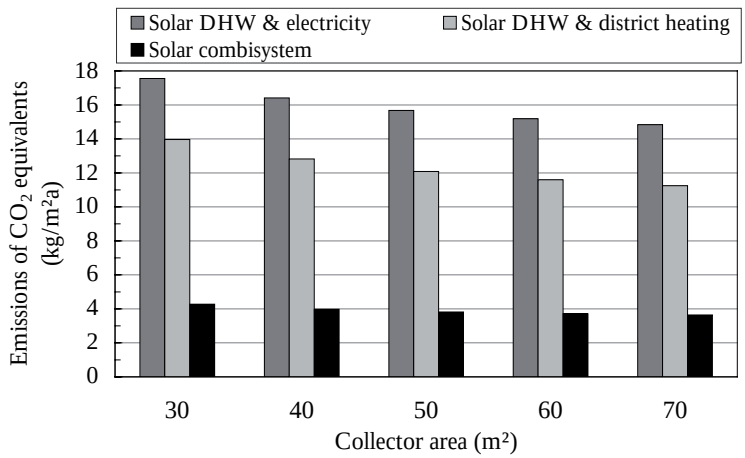

Figure 4.24 *The emissions of CO_2 equivalents for three different energy system designs; the combi system in question, with a pellet boiler and an electric heater, a solar DHW system combined with district heating and a solar DHW system combined with electric heating.*

4.3.6 Comparison between the different solutions

The results for the different solutions have also been compared and analysed. These figures are also presented in Section 8.1 in the handbook (Smeds, 2007). First a short overview of the design and heat load of the reference building and the different solutions.

Table 4.6 The designs of the solutions and the reference building.

	Reference building	Solution 1a	Solution 1b	Solution 2
U-value of the whole building (W/m^2K)	0.35	0.21	0.34	0.41
Space heating demand (kWh/m^2a)	44	6.5	13.4	19.0
Heating system	District heating for DHW and space heating	Electric resistance heating of the supply air. Solar DHW system with electric backup.	District heating for DHW and space heating.	Solar combi system with biomass boiler for DHW and space heating.

The results of non-renewable energy use and emissions of CO_2 equivalents for the different solutions of buildings and heating systems are presented in Figures 4.25 and 4.26. All the solutions have substantially lower energy demand than the reference building and all the solutions meet the targets of non-renewable primary energy use.

The total energy demand and the delivered energy are lowest for Solution 1a, due to the extremely well insulated building envelope. However, it is for Solution 2 that the lowest emissions of CO_2 equivalents and non-renewable primary energy use are achieved, due to the extensive use of renewable energy.

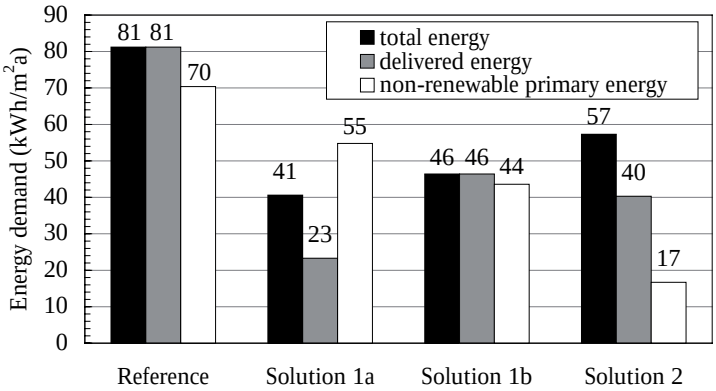

Figure 4.25 *Overview of the total energy demand, the delivered energy and the non-renewable primary energy demand for the apartment buildings. The reference building is connected to district heating. (Smeds, 2007)*

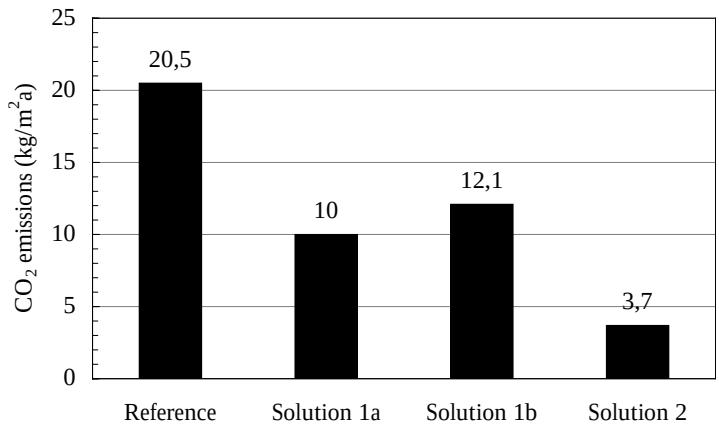

Figure 4.26 *Overview of the CO_2 emissions for the apartment buildings. The reference building is connected to district heating. (Smeds, 2007).*

4.4 Conclusions

The thermal energy from a solar combi system can provide a significant part of the total energy demand of a high performance building. If the space heating demand is specifically examined, it is seen that solar energy can also contribute to some extent to the space heating supply even for a well-insulated building. However, the relatively low space heating demand (although higher in the cold climate) and the short heating season makes it unreasonable to over dimension the solar system to cover much more than the domestic hot water demand (which is a large part of the total demand in a h.p. house and more constant over the year). The solar system should therefore preferably be designed so as to cover most of the energy demand in summer, both for solar combi systems and solar DHW systems. This way the furnace can be switched off in the summer, avoiding inefficient operation.

The building design and the choice of heat distribution system set the context for the design of a solar heating system. If the space heating demand is so low that is could be supplied merely by heating the incoming air, e.g. by electric resistance heating and heat recovery, a solar domestic hot water system is more easily argued, given the costs of a radiant heating system.

If a water-based radiant heating system is preferred, it is suitable to design a solar combi system, where a joint storage tank combines the domestic hot water system and the space heating system. The tank can be heated both by the solar collector and by auxiliary heat sources, thus providing flexibility to the system. The combined storage tank can give beneficial effects due to the higher energy withdrawal from the tank, which could lower the temperature in the collector circuit and thereby increase the collector efficiency somewhat during the heating season. The solar energy can also be used more efficiently if the collectors can be directly connected to a low-temperature radiant heating system, e.g. a floor heating system.

For a solar DHW system a collector tilt of 40-50º is suitable in the cold climate. For combi systems a higher collector tilt or façade integrated collectors improves the seasonal balance between space heating demand and solar gains, although a larger collector area is required to cover the summer demand.

The simulations performed during the design of the solar thermal system of Solution 2 (renewable energy strategy), for an apartment building in the cold climate, showed that a combi system with a collector area of 50 m^2 and a storage tank of 4 m^3 should be suitable. The system was designed to cover 95% of the energy demand in summer, so that the risk of stagnation is relatively low and the auxiliary pellet furnace can be switched off during the summer. The parametric study shows how much

the collector area needs to be increased when the tilt angles are higher or lower than the optimal angle for summer production.

Generally, a suitable collector area for the energy demand of the building in Solution 2 is between 30 and 80 m^2 (0.6 – 1.8 m^2/occupant) and a suitable tank volume is between 3000 and 5000 l (60-100 l/occupant). However, this much depends on user behaviour.

The parametric study also shows that the volume of the storage tank has a rather low influence on the energy output, although a minimum volume is crucial.

As regards the heat transfer from the collector circuit to the storage tank, the simulation results show that an external heat exchanger with a stratifying device in the tank should preferably be used, as it saves more energy compared to using internal heat exchangers in the tank. For internal heat exchangers a higher flow rate gives higher output while a lower flow is more beneficial when an external heat exchanger is used, as the tank water can be kept well stratified.

For Solution 2, the result of non-renewable energy demand is very low, only 17.4 kWh/m^2a, which is far below the target of 60 kWh/m^2a. Also, the emissions of CO_2-equivalents to the atmosphere are very low, 3.8 kg/m^2a. The alternative solar DHW systems simulated for the same building as the solar system would give rise to much higher use of non-renewable primary energy. For a solar DHW system combined with auxiliary electricity for DHW and for the space heating, the target would not be reached at all for a reasonable collector size. If the space heating were supplied by district heating, the target could be reached for a collector area of 40 m^2.

For Solution 1a (a building with U-value 0.21 and a solar DHW system with electric resistance heating for the remainng DHW demand and the space heating) the non-renewable energy demand is 54.8 kWh/m^2a and the emissions of CO_2-equivalents are 10 kg/m^2a.

When the construction of the building envelope is compared to current building standards, it is clear that today's apartment buildings could live up to the targets of space heating demand set by the IEA if they were built very airtight and if efficient ventilation heat exchangers were used. The comparison between the reference building, Solution 1a, Solution 2 and another building, Solution 1b (which has U-value 0.34 and which uses district heating) shows that they all meet the targets of non-renewable energy use but it is Solution 2 that gives the lowest non-renewable energy use and the lowest emissions of CO_2-equivalents. As this building has the highest space heating demand, it is interesting to see that the non-renewable primary energy demand can be lowered so much, relative to the other solutions. This indicates the huge importance of using renewable energy.

There is not one optimum design for an energy efficient building and in each situation factors such as user behaviour, climatic conditions, political regulations, building standards and the availability of different energy network systems, such as natural gas or district heating, are important to consider. Depending on the circumstances, the design strategy should be adapted so that a realistic and long-term sustainable development is introduced in the built environment.

Generally, the strategy of renewable energy use is suitable for retrofit buildings where increased insulation is not a reasonable solution. For the design of new buildings the conservation strategy gives more opportunities for the future as the well insulated building envelope provides opportunities for further reductions in energy use by changing the energy systems to use more renewable energy.

District heating systems use a large share of renewable fuels in Scandinavia; approximately 80% of the fuel is renewable. If the building is situated in an urban area with such a district heating system, the district heating is to be preferred to the use of biomass boilers, as biomass boilers can give rise to some emissions from the furnaces, something that may be against the regulations in certain urban areas. However, the purification of the exhaust gases is very good today and modern furnaces are often designed to use optimal oxygen amounts in the combustion process. If a biomass boiler is to be used, it should be an "environmentally approved" boiler and it should be coupled to a thermal heat storage tank in order to achieve an effective and controlled combustion process and to minimise the emissions of VOC and particles (Johansson et al., 2003).

A solar thermal heating system can be combined or integrated with most other heating systems and there is a large potential to lower the primary energy use and the impact on the environment by using solar collectors. Capturing and using energy from the sun is thus a very natural and marketable concept for sustainable, low energy housing.

5 Solar collectors for integration on non-insulated roofs

Three solar collectors have been designed for non-insulated roofs in order to provide a cost-effective and easily installed solar collector. The collectors were tested outdoors and the measurement results and analysis are presented in this chapter and in Paper IV: *Design and evaluation of solar collectors for integration on non-insulated roofs* (Gajbert et al., 2007), which was presented at the conference *NorthSun 2005* in Vilnius. The paper has been submitted to Solar Energy Materials and Solar Cells. Some additional results from measurements and simulations are also presented in this chapter.

5.1 Introduction

Non-insulated roofs with cold attics underneath are one of the largest available potential locations for installation of solar thermal collectors in Sweden. Solar thermal collectors for building integration are often very well insulated in order to contribute to the thermal comfort in the building. For collectors integrated on non-insulated roofs less insulation material is sufficient for the insulation of the collector. There is therefore a potential for development of a cost-effective, thin collector with lower use of insulation material, suitable for easy integration in non-insulated roofs.

The objective of this work is to design a thin, cost-effective solar thermal collector for integration into a roofing material. It should be flexible for production in variable lengths and have potential to be developed into a cost effective product. Prefabrication and simple mounting are desirable features for building integrated collectors.

Three similar collectors for non-insulated roofs have been designed and constructed as small scale prototypes. By using low-concentrating reflec-

tors in two of the collectors the absorber material is used more efficiently. Existing roofing sheet is used for the collector bottoms, which means that no separate collector box is required. This and the fact that the absorber area is reduced enable the collector to be produced at low cost.

The thermal performance and the incidence angle dependence of the collectors were evaluated from measurements and the potential energy production from the collectors was calculated using the MINSUN simulation program.

5.2 The collector designs

The three collectors, including absorbers, reflectors and the expanded polystyrene (EPS) insulation material, are designed to fit in a commonly used corrugated sheet steel roofing material in order to facilitate the installation and to integrate the collector into the building element.

The designs of the three collectors are similar but two of them are designed with concentrating reflectors and one is a flat plate reference collector. All collectors are covered with a 4 mm acrylic sheet with a relatively low transmittance. It is assumed that this sheet will be replaced by a glass cover with higher transmittance in a full scale collector. A description of the collectors follows.

5.2.1 Collector A

Standard size Sunstrip absorbers of 143 mm are used in the reference collector, Collector A, shown in Figures 5.1 and 5.2. Underneath is 50 mm insulation of EPS material. For the other designs the thickness of the insulation is determined by the reflector geometry.

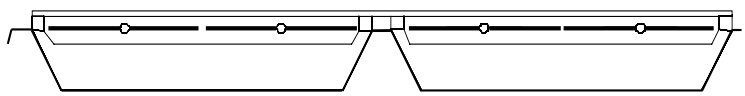

Figure 5.1 *Collector A – the flat plate reference collector. Two absorber plates fit into each compartment of the corrugated steel roof.*

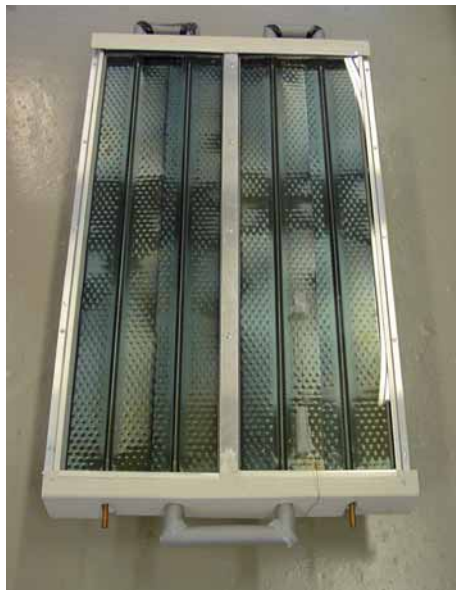

Figure 5.2 *Collector A has standard Sun-strip absorbers of 143 mm.*

5.2.2 Collector B

The concentrating Collector B (Figures 5.3 and 5.4) has a Sunstrip absorber of half width (71.5 mm) combined with circular shaped concentrating reflectors, resulting in a factor of 2.0 between the glazed area and single side absorber area, i.e. the geometrical concentration ratio. The physical concentration is 1.0, since the absorber is bifacial.

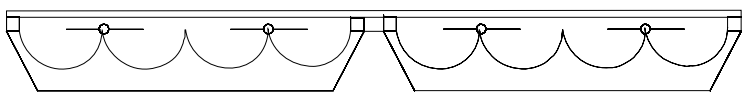

Figure 5.3. *Collector B – a concentrating collector with narrow strip absorbers and circular reflectors.*

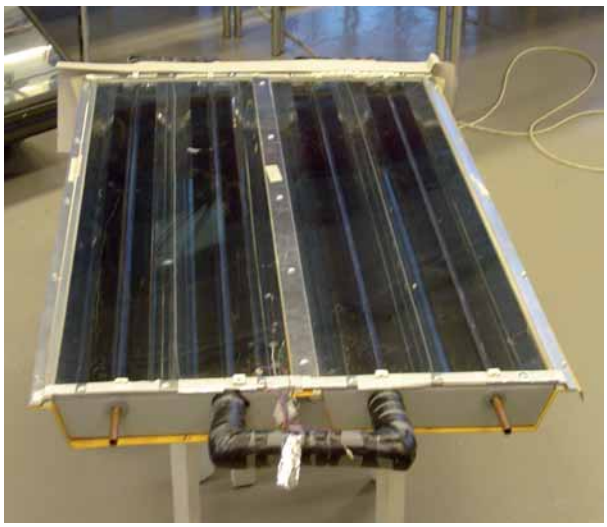

Figure 5.4 *Collector B, with circular concentrators and narrow 71.5 mm Sun-strip absorbers.*

5.2.3 Collector C

The absorbers of the concentrating Collector C are copper pipes with an aluminium foil with a selective surface paint on an aluminium foil, produced by the Swedish Company Skultuna Flexible, taped onto it. The pipe diameter is 180 mm. The absorbance, α, is 0.92 and the emittance, ε, is 0.20.

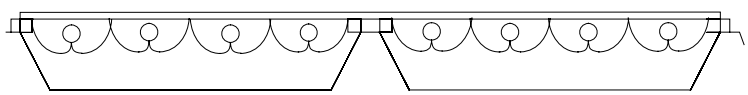

Figure 5.5 *Collector C – a concentrating collector with tube absorbers, selective surface and CPC-reflectors.*

Four copper pipes with reflectors of anodized aluminium (with a reflectance of 0.85) fit into each compartment of the corrugated steel, shown in Figure 5.6.

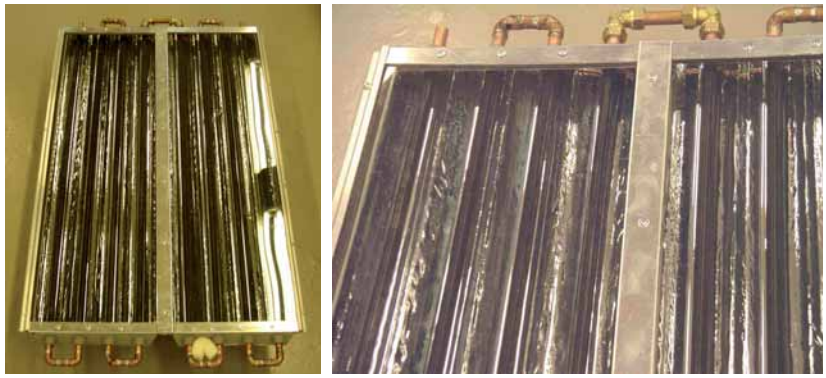

Figure 5.6 *Collector C, showing the tube absorbers with selective surface.*

The geometrical design of the concentrating reflector is an involute (Winston and Welford, 1989) (See further description in Section 2.5.2) combined with a truncated quasi parabola, resulting in a geometrical concentration ratio of 1.3 between the glazed area and the tube area. It is the lowest part of the reflector that is an involute (see Figure 5.7). The involute is based on a pipe of 150 mm in diameter and an acceptance angle of 40°. A slightly larger copper pipe, of 180 mm, is then used as absorber. The parabola is then truncated at 10 mm above the top of the pipe. This geometry gives an acceptance interval of 80°, i.e. the acceptance half-angle, $\theta_{a/2}$ is 40°.

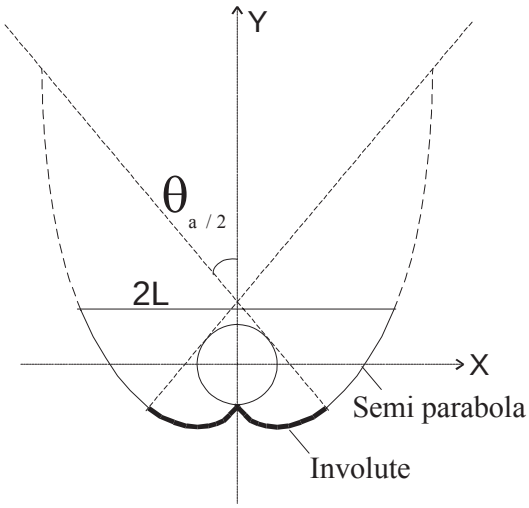

Figure 5.7. *The shape of the truncated reflector used in Collector C, which is a combination of an involute and a parabola with an acceptance half-angle, $\theta_{a/2}$, of 40°.*

If large collectors with straight wide tube absorbers are used, it will be easier to connect them in series. The use of wide pipes in the collectors means that the pressure drop will be low, which is very beneficial as components of lower dimensions, such as pumps etc., can be used, which also reduces the cost of the system.

5.2.4 Orientation

With these collector designs, the collectors could be oriented either in the east-west or in the north-south direction. For Collectors A and B, this orientation of the absorbers should not have any impact on the energy output, as they accept all irradiation that hits the glass. If only a small part of the roof is used as collector, it would be more suitable to place them in the north-south direction, as it facilitates the water run-off on the corrugated steel.

For Collector C, which has a limited acceptance of irradiation in the transverse plane, this will have a small impact on the energy output, although the 80º of acceptance it has will not exclude much of the irradiation, if mounted in the north-south direction. Therefore, if an entire roof is constructed as a collector, it is suitable to mount it with the absorbers in the east-west direction, and this is what Collector C is intended for.

5.3 Experimental work and evaluations

The thermal performance and the incidence angle dependence of the collectors have been evaluated by both indoor and outdoor measurements. Long-term outdoor measurements have been performed with larger collector prototypes in the Älvkarleby test facility and several indoor and outdoor measurements have been performed in the laboratory in Lund. From the long-term outdoor measurements, the thermal performances of the collectors were evaluated by multi linear regression, MLR. The results were used to set up a model of the expected collector output and it was also used for MINSUN simulations of the annual energy output. Ray tracing simulations of Collector C were performed in ZEMAX by Johan Nilsson. The methods are further described in Chapter 3.

5.3.1 Long-term measurements and MLR

Long-term outdoor measurements

Long-term outdoor measurements of larger collector prototypes were performed at the test facility in Älvkarleby (60.5°N, 17.4°E) during the period from 2005-04-02 to 2005-05-10. Three collector prototypes (Collectors A, B and C) of the size 1.0 × 2.0 m were mounted facing towards south with the absorbers directed in the east-west plane. For further method description see Section 3.1.2.

MLR analysis

From the long-term outdoor measurements, the thermal performances of the collectors were evaluated by Multi Linear Regression, MLR, according to the model described by Perers (1993), which is based on Equation 30. It should be noted that values from measurements even during hours of lower irradiance are accounted for in these analyses. The monitored parameters of the collector power, q, the diffuse and direct irradiance, G_b and G_d, the mean collector temperature, T_m, and the ambient temperature, T_a, are used as input in the MLR calculations. The parameters $F'(\tau\alpha)_n$, b_0, K_d, $F'U_0$, $F'U_1$ and $(mC)_e$ given are results from the MLR. The parameters $F'U$ and η_{0b} are thereafter calculated. The results for the three collectors are shown in Table 5.1.

Table 5.1 The results from the MLR analysis based on long-term outdoor measurements.

Collector	η_{0b} [-]	η_{0d} [-]	$F'U$ [W/m²K]	$F'U_0$ [W/m² K]	$F'U_1$ [W/m²K]	mC_e [J/kgK]	b_0 [-]
A	0.76	0.65	5.84	4.90	0.017	6834	0.125
B	0.72	0.62	4.93	4.27	0.012	5617	0.134
C	0.72	0.58	5.79	5.29	0.009	19148	0.154

The MLR analysis shows that the concentrating collectors, B and C, have a lower optical efficiency than the reference, Collector A. This is explained by reflectance losses and deviations from the ideal optical design. The pipes of Collector C are slightly displaced from the centre of the reflector, which affects the beam efficiency. Collector C shows a lower diffuse efficiency, which is normal for concentrating collectors. Collector B, with a narrow absorber, shows the lowest heat loss factor *F'U*, while the *F'U* values of Collector C and Collector A are comparable. The collectors A and B contain the same volume of water, while Collector C with the tube absorber contains four times more water per collector area. This is also reflected in the very high specific heat parameter, $(mC)_e$, of Collector C. The longitudinal incidence angle dependence is basically equal to K_b using the b_0 value from these MLR results. This is explained in Section 5.3.5, Figure 3.19. The incidence angle dependence in the longitudinal plane, given by the b_0 value, is similar for all the collectors.

5.3.2 Model accuracy

In order to verify the accuracy of the measurement results, a model of the expected collector power was set up based on the results from the MLR analysis. The model was compared with measurements from the 6th of May 2005, a day with varying weather and low temperature. Figures 5.8-5.10 show the measured and modelled collector power over time. Figures 5.11-5.13 show the modelled power on the Y-axis and the measured values on the X-axis, with data from the period 2005-04-02 to 2005-05-10. The good agreement between modelled and measured power of the collectors that can be seen in these graphs indicates that the evaluation model works satisfactorily.

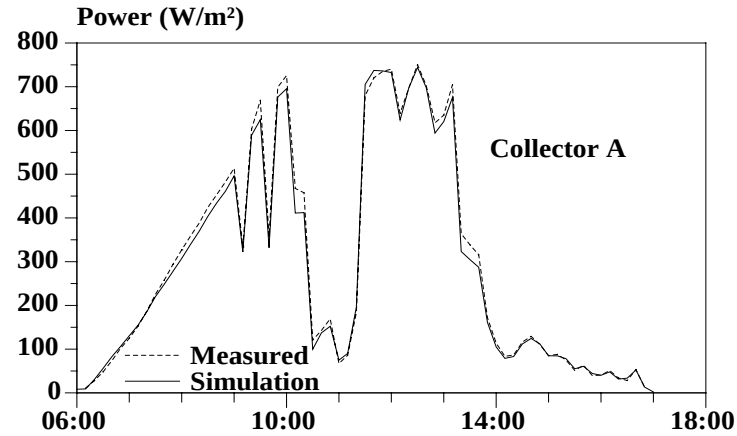

Figure 5.8 *Measured and simulated power of Collector A over time, 6th of May 2006.*

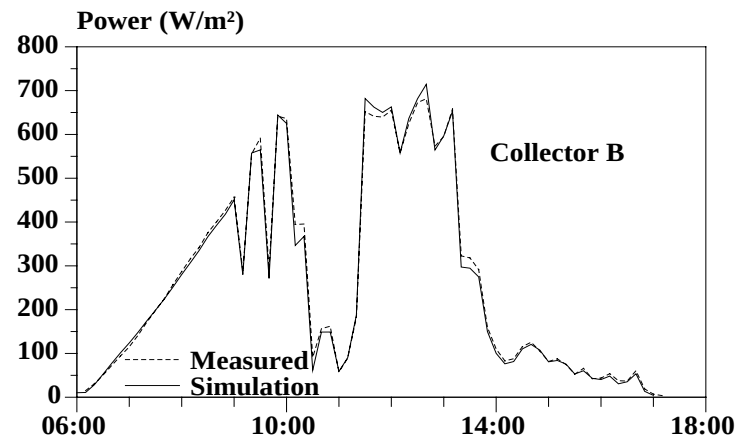

Figure 5.9 *Measured and simulated power of Collector B over time, 6th of May 2006.*

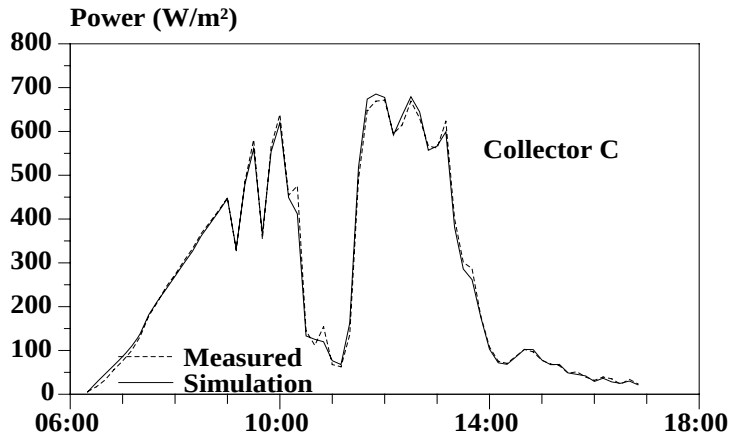

Figure 5.10 *Measured and simulated power of Collector C over time, 6th of May 2006.*

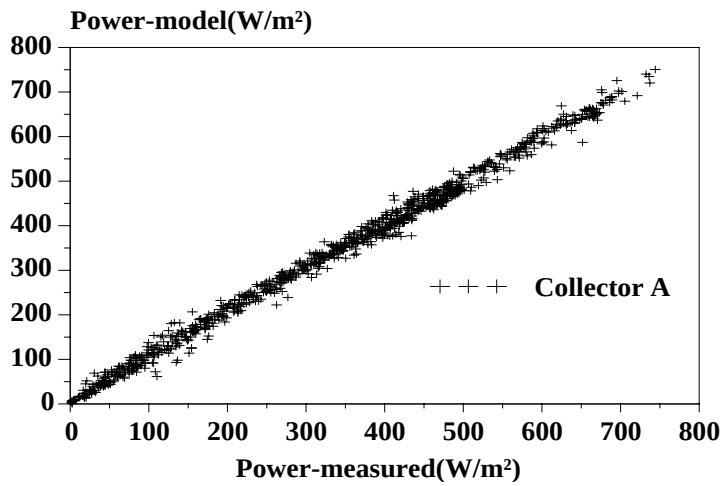

Figure 5.11 *Measured and modelled power for Collector A. Data from the period 2005-04-02 to 2005-05-10.*

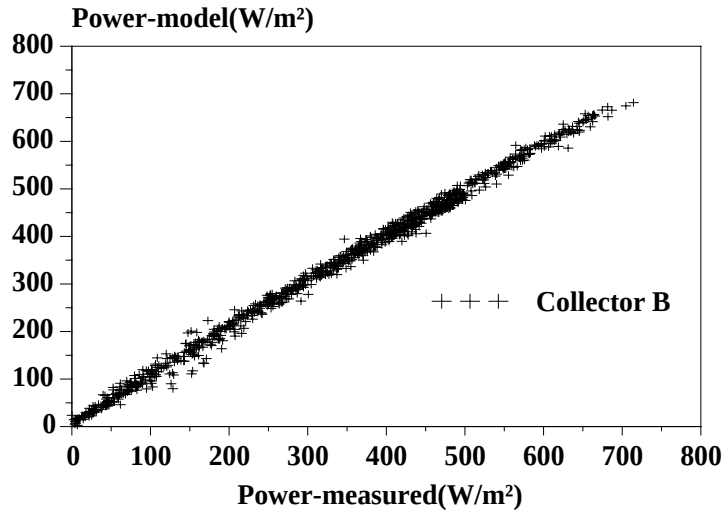

Figure 5.12 *Measured and modelled power for Collector B. Data from the period 2005-04-02 to 2005-05-10.*

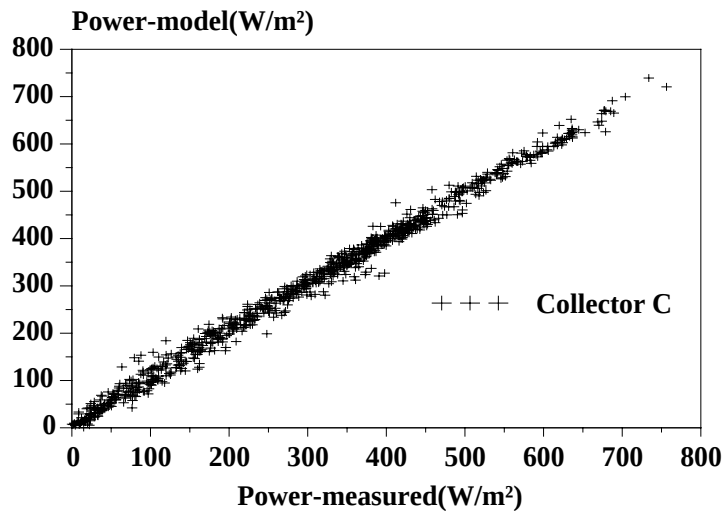

Figure 5.13 *Measured and modelled power for Collector. Data from the period 2005-04-02 to 2005-05-10.*

5.3.3 Thermal inertia of the collectors

The thermal inertia of Collector C is greater than that of Collectors A and B, since the absorber tube of Collector C is wider and contains more water, giving a larger constant $(mC)_e$. This is confirmed by the comparison of the modelled and the monitored collector power from the long-term measurements on 25th April 2005, during a sudden temperature drop, see Figures 5.14-5.16, where the model follows the measurements well. Figure 16 shows that the power of Collector C exhibits a strong peak, while the other collectors show just a small response to the decrease in temperature. These properties are also shown by the very high $(mC)_e$ value of Collector C from the MLR analysis.

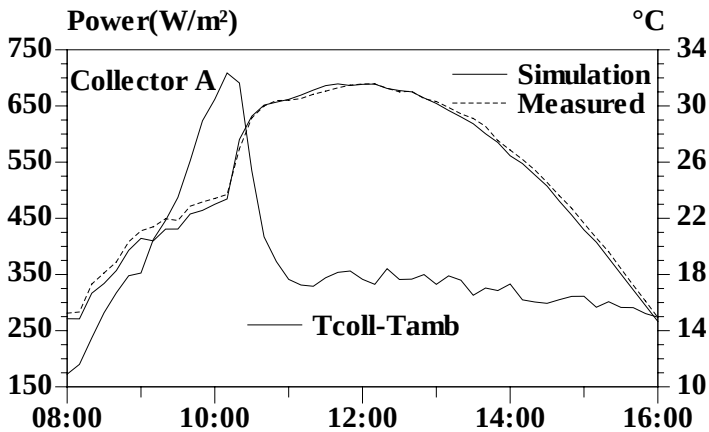

Figure 5.14. The relative collector temperature and the measured and modelled power of Collector A during a temperature peak.

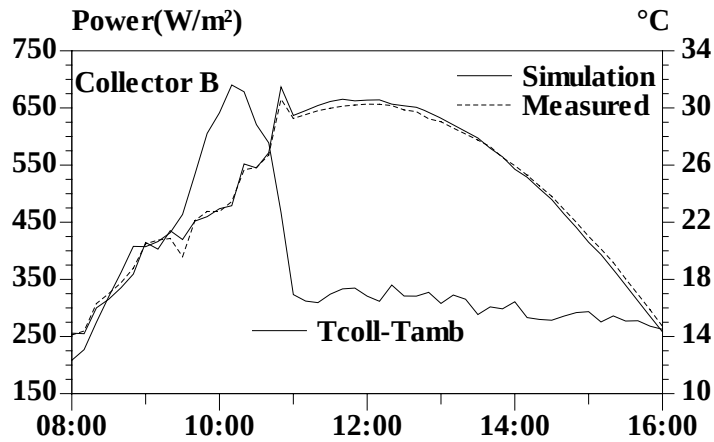

Figure 5.15. The relative collector temperature and the measured and modelled power of Collector B during a temperature peak.

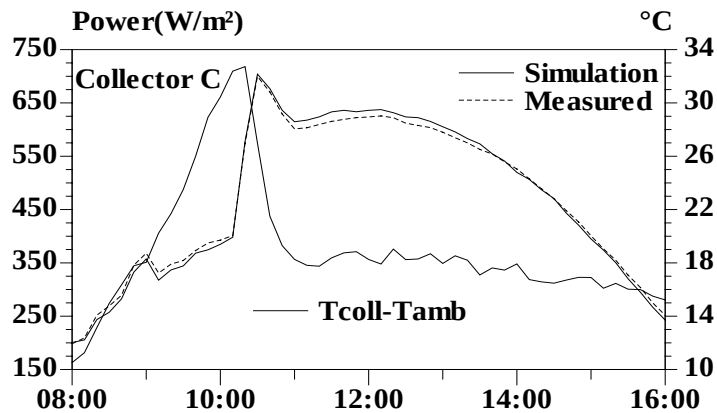

Figure 5.16. The relative collector temperature and the measured and modelled power of Collector C during a temperature peak.

5.3.4 Monitoring of efficiency graphs

Results from the long-term outdoor measurements

The standard efficiency curves of the three collectors are determined from the long-term measurements during periods of near normal incidence, stable temperatures and for irradiance higher than 900 W/m^2. The results are shown in Figure 5.17.

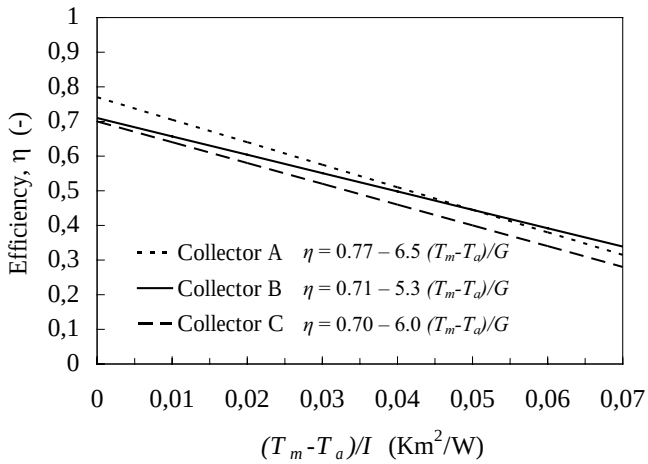

Figure 5.17 *The efficiency of the three collectors as a function of $(T_m-T_a)/I$. The slope of the graph is the value of the heat loss coefficient F'U and the value where the graph crosses the Y-axis is the value of the optical efficiency, η_0.*

Good agreement is shown between the results of optical efficiency, η_0, derived from these graphs, and the results from the MLR. The *F´U* values from these efficiency graphs at high irradiances are systematically higher than the corresponding data from the MLR, which includes data measured during all hours of operation. This is because an increase in absorbed irradiance causes an increase in the temperature difference between the fin and the heat carrier fluid, which increases *F´U* (Hellström, 2005). This effect was confirmed by measuring *F´U* from cooling the collectors during dark hours, which resulted in even lower *F´U* values, shown in Table 5.2. The dependence of *F´U* on the irradiance is strongest for Collector A, which has a low *F´*-value because of the wide absorber.

Table 5.2 The heat loss coefficient F´U derived from the efficiency graphs from the long-term measurements, from the MLR analysis and from the dark hour measurements.

Collector	*F'U* from efficiency curves [W/m²K]	*F'U* from MLR [W/m² K]	*F'U* measured in darkness [W/m²K]
A	6.5	5.84	5.5
B	5.3	4.93	4.8
C	6.0	5.79	5.5

Results from measurements using the test rig

Outdoor measurements on the smaller (0.6 × 1.0 m) prototype of Collector C were performed in Lund, both in daylight and during dark hours as described in Section 3.1.1. The test rig was used and the power and temperatures were recorded at three different operating temperatures. Figure 5.18 shows results from dark hour measurements. The heat losses are shown as negative values of power on the Y axis. On the X-axis is ΔT, the difference between the mean fluid temperature in the collector and the ambient air temperature. *F'U* is determined from the slope of the graph to 6.5 W/m²K. The fact that this is higher than the *F'U* value derived from the MLR analyses based on long-term measurements (with large prototypes) is explained by the higher area-to-volume ratio of the smaller prototypes.

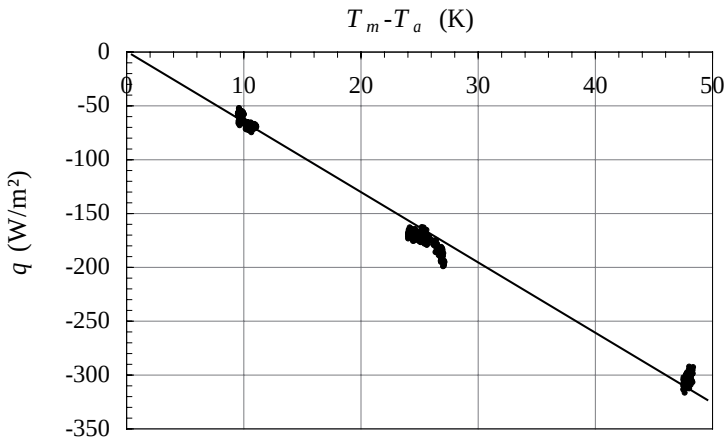

Figure 5.18. The heat losses of the small prototype of Collector C as a function of (T_m- T_a), from dark hour measurement. The slope of the graph is equal to F'U, which is 6.5 W/m²K.

Results from early measurements

Earlier performed indoor measurements during dark hours on all the small collector prototypes (see Section 3.1.3) show *F'U* values of 4.5 W/m²K for all prototypes. Similar outdoor measurements (using the same set-up) show the same results. The difference between the results from the measurements using the test rig and the early measurements may seem high, but it can be explained by the use of back insulation on the collector during the early measurements, which gives a lower *F'U* value.

5.3.5 Longitudinal incidence angle dependence

The longitudinal incidence angle dependence was evaluated using data from the long-term measurements, where the collectors were mounted with the absorbers in the east-west direction. Data from May 1, 2005, when the transverse incidence angle of the irradiance was nearly constant during the whole day (shown in Figure 5.19), show how the incidence angle coincides with the longitudinal incidence angle during most of the time. The transverse incidence angle hardly varies at all. This leads to the conclusion that the collector efficiency is mostly dependent on variations in the longitudinal incidence angle. This means that the reflectors of Collector B and C have a very small or no impact on the b_0 values. The

b_0 values obtained from the MLR-analysis represents only the effect of the incidence angles on the glazing. Therefore the longitudinal incidence angle dependence can be described by K_b, with the b_0 values obtained from the MLR-analysis.

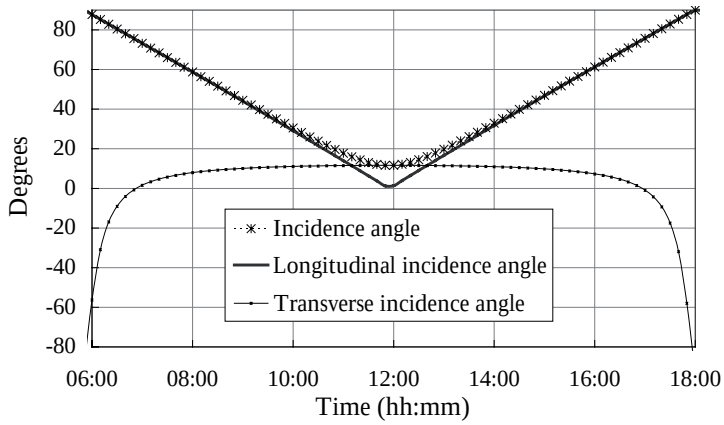

Figure 5.19 *The incidence angles on the collector surfaces, measured on April 1, 2005. The incidence angle coincides with the longitudinal incidence angle during most of the time and the transverse incidence angle hardly varies at all.*

The angular dependence of η_{0b}, with corrections for the contribution from diffuse irradiance and heat losses (according to Equation 31), are presented in Figures 5.20 and 5.21. The data is from April 26, 2005. In Figure 21 the zero-loss efficiency is shown as a function of $[(1/\cos\theta) -1]$. Here, the b_0 values are equal to the slopes of the graphs.

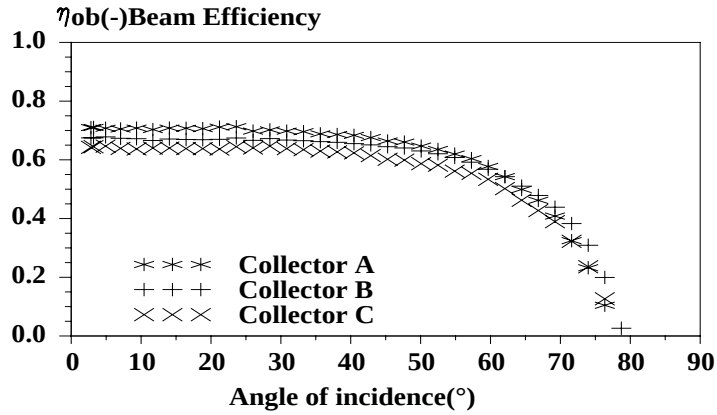

Figure 5.20 *The zero-loss beam efficiency, η_{0b}, shown as a function of the incidence angle.*

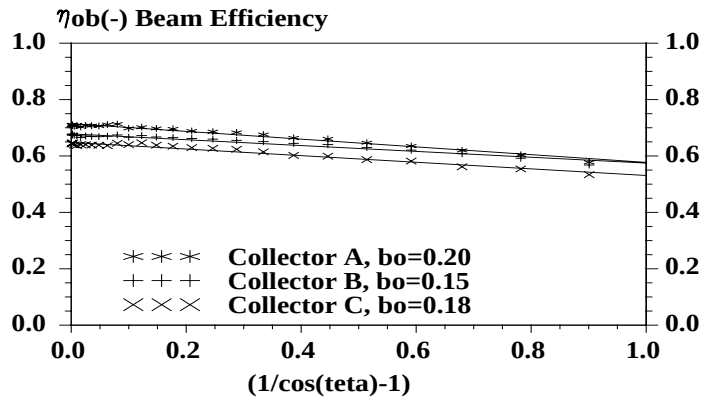

Figure 5.21 *The zero-loss beam efficiency, η_{0b}, shown as a function of (1/cos θ-1). b_0 is derived from the slopes of the graphs.*

It is shown that all the collectors have similar angular dependence in the longitudinal direction. For Collectors A, B and C, b_0 is equal to 0.20, 0.15 and 0.18 respectively. These are higher values than the corresponding values obtained from the MLR analysis. An explanation for this is that

the MLR results are, to a high degree, determined from angles where high power is achieved, i.e. incidence angles below 30°, which correspond to values of the function [(1/cosθ) -1] lower than 0.15. In Figure 5.21, it is clearly shown that the slopes giving the b_0 values are very low for these values. The b_0 values from the MLR are thus more representative of the whole range of longitudinal incidence angles.

5.3.6 Incidence angle dependence in the transverse plane

Results from outdoor measurements using the test rig

The incidence angle dependence in the transverse plane of an identical but smaller (0.6 × 1.0 m) prototype of the concentrating Collector C has been evaluated based on outdoor measurements using the test rig and equipment described in Section 3.1.1. Figure 5.22 shows measurement results of optical efficiency for beam irradiance from September 1st 2005, plotted against the transverse incidence angles, θ_T.

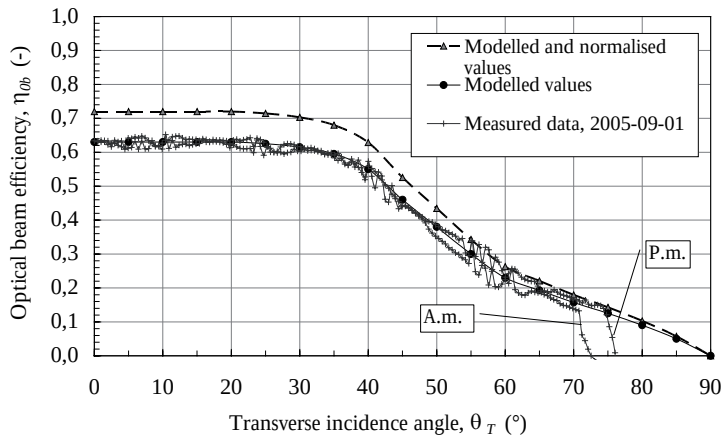

Figure 5.22 *The transverse incidence angle dependence of the small prototypes of the concentrating Collector C. Measured data from a.m. and p.m. on September 1st, 2005. The modelled transverse incidence angles, and the normalization to data from the larger collectors, are also shown.*

As expected, the optical efficiency is highest and almost constant within the acceptance interval (i.e. when the transverse incidence angle is between 0° and 40°) and thereafter it decreases. A slight difference between values of measured data from a.m. and p.m. can be seen. This difference can be explained by the obstruction in the horizon, the sun is descending before reaching 90°, and by the difficulty of measuring at low incidence angles.

The figure also shows the model of the expected optical efficiency for different transverse incidence angles that was set up based on the measured data. The model of transverse incidence angle dependence was adjusted to descend gradually to 0 at 90° from the abrupt drop between 70° and 80°. The model was also normalized to match the MLR results of η_{0b} at normal incidence, which meant multiplying all values of η_{0b} by 1.14. This was done because the long-term measurements are considered more accurate due to the larger size and the better precision during the production of the prototypes.

A complete model to predict the collector power could now be set up (as in Equation 27) with these modelled results of the transverse incidence angle dependence for beam irradiation, $\eta_{0d}(\theta_T)$, (using the normalized values for larger collectors and the original values for the smaller prototypes) and the results of η_{0d}, $F'U$ and mC_e from the MLR analysis.

The model was validated by comparing measured data of the collector power from another day, August 18, 2005, with the modelled values. As can be seen in Figure 5.23, the model agrees well with measured data.

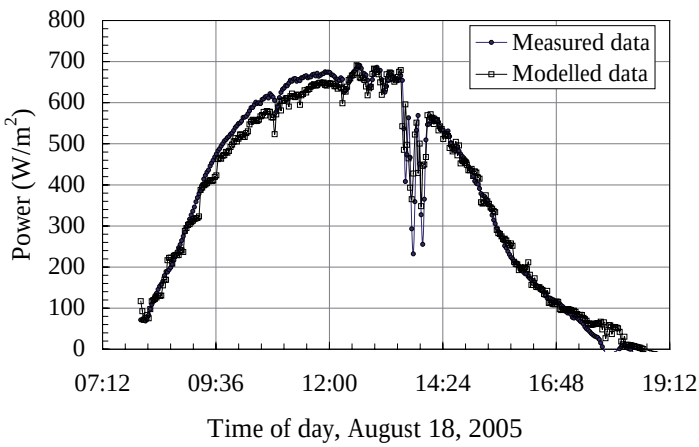

Figure 5.23 *Measured and modelled data of the collector power during August 18, 2005.*

Results from early measurements

The results of zero-loss efficiency for normal irradiance from the early measurements (described in Section 3.1.3) are shown in Table 5.3. The results are based on global irradiance on a tilted surface.

Table 5.3 The zero-loss efficiency at normal incidence angle.

Collector	Collector A	Collector B	Collector C
η_0 (%)	72	73	59

Collector B shows similar optical efficiency as the reference, Collector A. This was expected as Collector B has a low concentration ratio and the same acceptance interval as Collector A (180°). Therefore, it shows that the optics is good. Collector C, on the other hand, shows a lower optical efficiency at normal irradiance, which is explained by non-ideal reflector optics. The prototype of Collector C used here was replaced by one with smoother reflector before the measurements with the test rig were performed.

The efficiency, η_0, for different transverse angles of incidence, θ_T, is plotted in Figure 5.24.

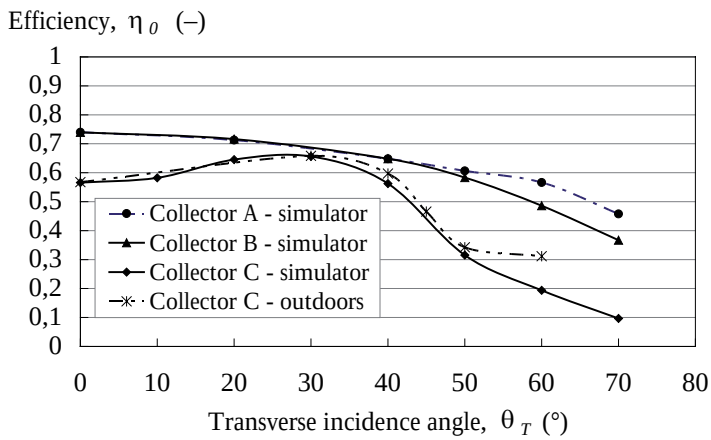

Figure 5.24 *The measured incidence angle dependence of the three collectors in the transverse direction. The collectors A and B are tested indoors with the solar simulator and collector C is tested both indoors and outdoors.*

Collectors A and B exhibit a similar angular dependence in the transverse direction as in the longitudinal and transverse direction. The concentrating Collector C, with a tubular absorber, is clearly influenced by the limited acceptance interval, and shows that for angles above 40°, the efficiency decreases. However, Collector C shows a relatively low efficiency for normal irradiance. An explanation for this is that the absorber pipes may have been slightly dislocated from their original position. The results from outdoor and indoor measurements of Collector C agree well up to transverse incidence angles, θ_T, of 50°. The difference at higher angles is explained by the low accuracy during measurement on small areas at high angles of incidence. This is due to the somewhat uneven light distribution of the solar simulator used in indoor measurements and the movement of the light pattern during the elevation of the simulator during measurements. The outdoor measurements are therefore more reliable at high incidence angles.

5.3.7 Ray tracing simulations

Ray tracing simulations of Collector C were performed in ZEMAX by Johan Nilsson in order to show the theoretical transverse incidence angle dependence. Detailed data of the collector geometry was used for the simulations. In the first simulation only the reflectance of the reflector was considered and set to 0.85. A second simulation was also performed, where also the transmittance of the glazing and the absorbance of the absorber were included. The transmittance was set to 0.9 and the absorbance to 0.9. The incidence angle dependence of the transmittance and the absorbance was accounted for by a variation from 0.9 at normal incidence to 0.0 at 90° incidence, similar to the K_b function. Simulations of the light distribution pattern on the absorber surface were also performed for various incidence angles.

Ray tracing results

Figure 5.25 shows the ray tracing results of theoretical optical efficiency, η_{0b}, of Collector C for varying transverse incidence angles, compared to the normalized model shown in Figure 5.22. The ray tracing simulation including reflectance, transmittance and absorptance corresponds relatively well with the model. The deviations are explained by the slightly imperfect reflector shape. The simulation that only considers the influence of the reflector gives very much higher values.

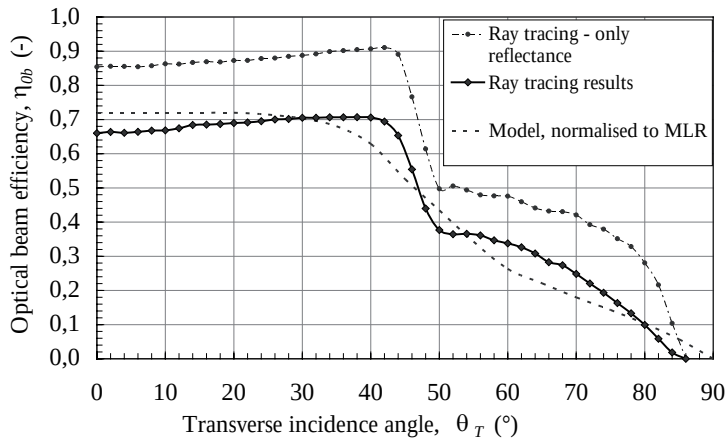

Figure 5.25 *Ray tracing results and the modelled values of optical efficiency for beam irradiation for varying transverse incidence angles for Collector C.*

In Figures 5.26 - 5.33 the results from the ray tracing simulations of irradiance on the absorber and the light distribution pattern for incidence angles of 0°, 20°, 45° and 60° are shown. In the figures showing irradiance, the X-axis shows the pixels along the absorber surface, which were used in the simulation, clockwise from the top.

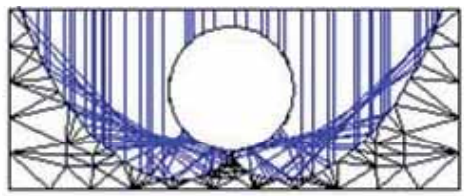

Figure 5.26 *Light distribution pattern for the incidence angle θ_T of 0°.*

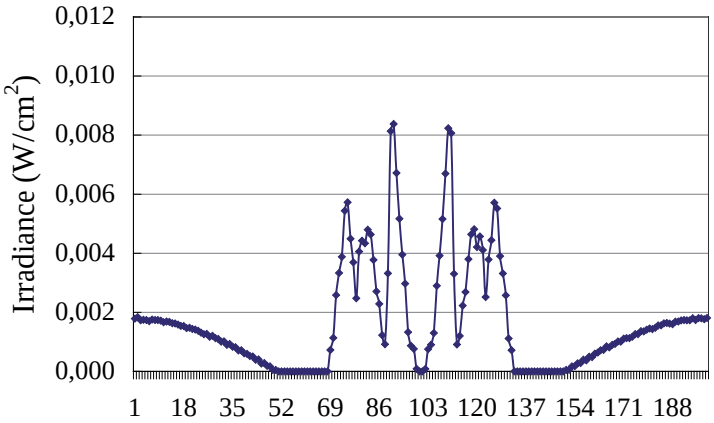

Figure 5.27 *The irradiance along the tube absorber for incidence angles θ_T of 0°.*

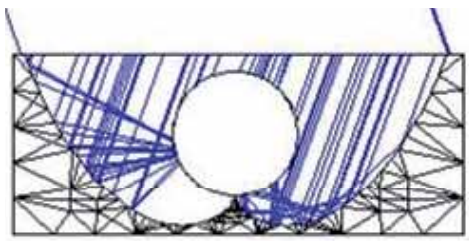

Figure 5.28 *Light distribution pattern for the incidence angle θ_T of 20°.*

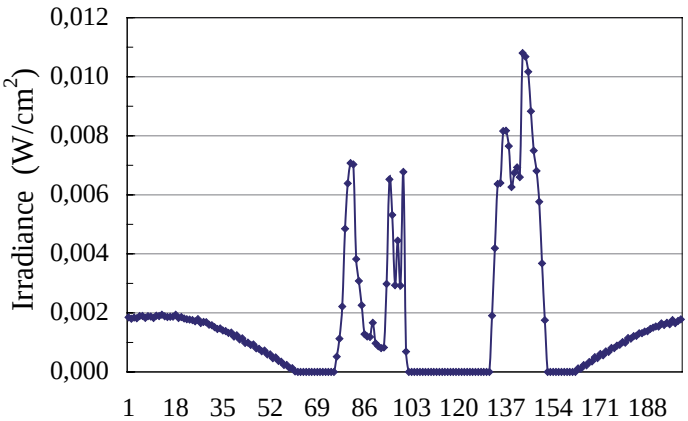

Figure 5.29 *The irradiance along the tube absorber for incidence angles θ_T of 20°.*

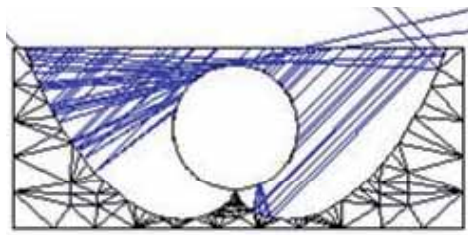

Figure 5.30 *Light distribution pattern for the incidence angle θ_T of 45°.*

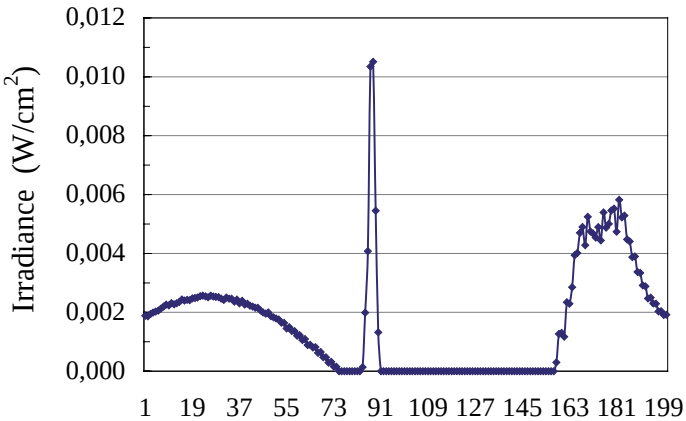

Figure 5.31 *The irradiance along the tube absorber for incidence angles θ_T of 45°.*

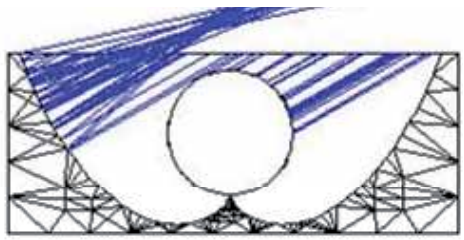

Figure 5.32 *Light distribution pattern for the incidence angle θ_T of 60°.*

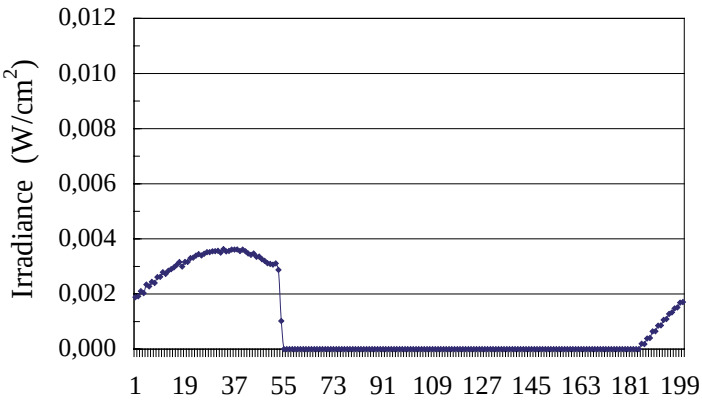

Figure 5.33 *The irradiance along the tube absorber for incidence angles θ_T of 60°.*

5.3.8 MINSUN simulations of annual energy output

The MINSUN simulation program (see Section 3.3.1) was used to calculate the expected annual energy output from the collectors. The parameters derived by the MLR analysis (Table 5.1) were used as input data. Simulations were performed for all three collectors. For Collectors A and B, the K_b function with the b_0 values from the MLR results was used to describe the incidence angle dependence. For Collector C simulations were performed with the influence of both the longitudinal and the transverse incidence angle dependence. The tilt of the surface was varied in order to show the effect of installing the collectors on roofs of different tilt angles.

Annual energy output - MINSUN simulation results

The simulation results show that the maximum annual energy output per glazed collector area would be 320 kWh/m^2, 330 kWh/m^2 and 280 kWh/m^2 respectively for Collectors A, B and C, at an operating temperature of 50°C and with a collector tilt of 45°. If calculated per absorber area, the corresponding yield would be 360, 680 and 1140 kWh/m^2 absorber respectively for Collectors A, B and C. (The absorber area of Collector C is based on the pipe diameter).

While Collectors A and B show higher performance per glazed area than Collector C, both Collectors B and C, Collector C in particular, show high energy output per absorber area. The low energy output per collector area of Collector C could be explained by a slight dislocation of the absorber, which means that a lot of the irradiation could be reflected back out from the collector.

The influence of the roof tilt on the annual energy output is shown in Figure 5.34. The optimal tilt angle of the roof is 45° and for tilt angles between 35° and 50° the annual output is not reduced by more than 2%.

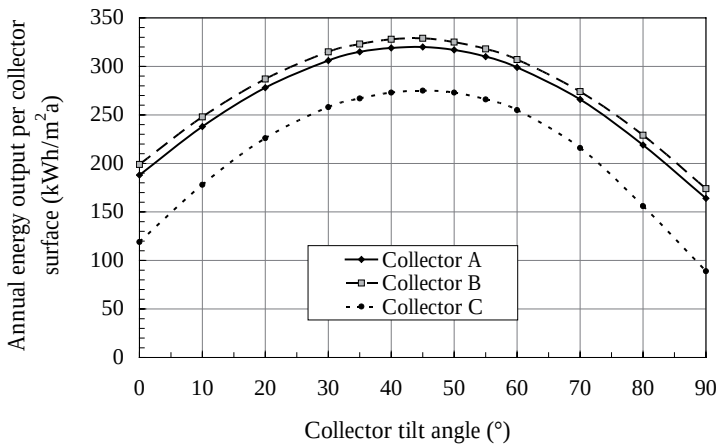

Figure 5.34 *Simulation results showing the annual energy output for the collectors on differently tilted roofs, at an operating temperature of 50°.*

5.4 Conclusions

The thermal performance and incidence angle dependence of two low concentrating collectors and one flat plate reference collector, all constructed for direct integration into non-insulated roofs, were investigated in detail by outdoor and indoor measurements and by simulations in MINSUN. Generally, good correspondence between measured and modelled collector performances was shown, which leads to the conclusion that the results are accurate.

The simulation results show that the maximum annual energy output would be 320 kWh/m^2, 330 kWh/m^2 and 280 kWh/m^2, per glazed collector area, respectively, or 360 kWh/m^2, 680 kWh/m^2 and 1140 kWh/

m^2, per absorber for collectors A, B and C respectively at an operating temperature of 50°C and with 45° tilt angle.

According to the detailed analyses of the thermal performance, Collector B, with the narrow strip absorber, shows the lowest heat loss coefficient. The heat loss coefficient *F'U* varies slightly between different measurements. This is explained by the difference in size of the prototypes, the theoretical difference between dark hour measurements and measurements with irradiation and also because of the use of back insulation on the collectors.

The analysis of transverse incidence angle dependence of Collector C shows results similar to the results from the ray tracing simulations. The deviations can be explained by imperfections of the reflector or by a slight dislocation of the absorber pipe, which can result in slightly higher optical losses.

These solar collectors combined in a ready-to-use roofing material should preferably be mounted as entire roofs over cold spaces, which could give a significant contribution to the heat supply.

Judging from the collectors with their present design, Collector B is the most promising, with low heat losses and little use of absorber material. Collector C is the collector that would be the cheapest to produce, but the heat losses could be too high to make it profitable. It would therefore be interesting to further analyse the unexpectedly high $F´U_0$ value of the concentrating Collector C.

It is possible to reduce the heat losses by decreasing the acceptance angle and by increasing the concentration ratio. A suggestion for further development is to decrease the acceptance angle of the reflectors of Collector B. For a previously evaluated non-insulated low-concentrating east-west collector (a roof-MaReCo) with a bifacial narrow absorber and a factor 3 between glazed area and single side absorber area, an acceptance interval of only 45° has been shown to be sufficient. This collector has a $F´U_0$ value of around 3.5-4.0 W/m²K (Adsten et al., 2005). However, for a concentrating collector with the absorbers in the north-south direction, the acceptance interval needs to be around 80º, as for Collector C, in order for the collector to be operated at least 5 hours in the middle of the day in Sweden.

As the designs are today they can be placed either in the east-west direction or in the north-south direction

Considering the low production costs expected for these collector types, it is estimated that the production of a cost-effective collector has a high potential, although there are improvements to be made. A detailed cost analysis should preferably also be performed in future work to ensure the low cost of the final product.

6 Evaluation of solar simulator performance

This chapter describes the work performed for the evaluation of the accuracy of indoor measurements of thermal performance and incidence angle dependence of solar collectors using a large solar simulator. The work is described in Paper V - *Measurement of concentrating solar collectors using a solar simulator with parallel light*, which was presented at Eurosun 2004.

6.1 Introduction

By using indoor measurements under steady ambient conditions, evaluations of concentrating solar collectors could be made easier and more systematic, facilitating the repetitiveness of the experiments. In order to enable indoor evaluation of concentrating solar collectors, a light source with parallel light is required. These kinds of light sources are not common and indoor evaluations are therefore rare. The solar simulator that is used at Energy and Building Design, shown in Figure 3.10, is designed to give parallel light and is adjustable to simulate different solar altitude angles. The simulator is further discussed in Section 3.2.1

In order that values of the irradiation on the collector surface should be recorded correctly during measurements, it is important that the irradiation on the test area is known throughout the measurement. A problem with this solar simulator is that the light distribution is slightly non-uniform and when the simulator is lifted to simulate different solar altitude angles, it is possible that the light pattern is altered, which could make it difficult to correctly evaluate the performance of concentrating solar collectors. This has been indicated by previously performed measurements where results were difficult to interpret.

The objective of this work is to improve indoor evaluations of incidence angle dependence of concentrating solar collectors by evaluating a method to better estimate the irradiance from the simulator on a test area in front

of the simulator. It is investigated if it is possible to compensate for the non-uniform light distribution and the movements of the light pattern by using an array of photodiodes that is placed in front of the test area to estimate the total irradiance on the collector surface.

6.2 The solar simulator light distribution

Each of the seven lamps on the solar simulator is placed facing one of the parabolic reflectors, which render the light nearly parallel. The good parallel light quality of the radiation has been achieved to some extent at the expense of a uniform area distribution. The irradiance over the test area perpendicular to the lamps is therefore slightly non-uniform. Fewer large lamps generating nearly parallel light are used instead of a larger number of smaller lamps, which would have generated more evenly distributed but also more diverging light. Previously performed measurements of the irradiance on several locations in front of the simulator have shown a light distribution according to Figure 6.1, where the light intensity peaks emanate from the rim of the reflectors surrounding the lamps. This is further discussed in Håkansson (2003 a, b) Håkansson (2001), Håkansson and Fredlund (1999).

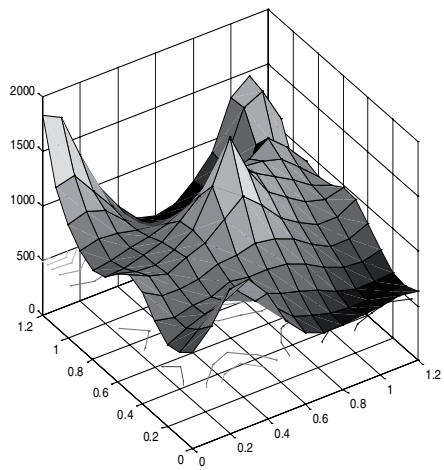

Figure 6.1 *Light intensity distribution pattern from the solar simulator over a test area perpendicular to the simulator (Håkansson, 2003 a, b).*

When the simulator is lifted to simulate various solar altitudes, the light intensity pattern tends to move over the test area, although placed at the pivot point of the adjustable lifting frame of the simulator. Therefore it is possible that total irradiation on the object is changed as the simulator altitude angle is altered. As the irradiation is normally measured by a single pyranometer, the results could be misleading. The radiation from the simulator also changes slightly over time due to the instability of the discharge lamps.

6.3 The photodiode array

In order to estimate the mean irradiance on the test area and thereby compensate for the spatially non-uniform irradiation from the solar simulator, an array of six photodiodes, connected in parallel by thin copper threads, was placed on the glazing of the collector during the measurements. The placement of the photodiodes divides the front area of the solar collector into smaller areas of equal size with one photodiode placed in the centre of each area. With this arrangement, the total current from the photodiode array should be a fairly good representation of the total irradiance on the collector surface.

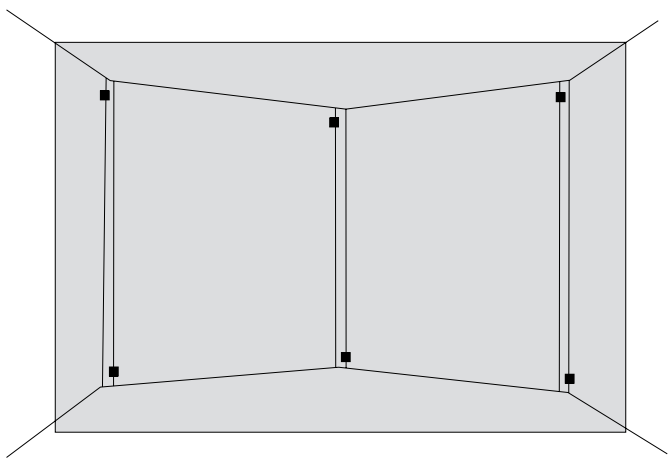

Figure 6.2 *An illustration of the photodiode array placed in front of a solar collector to be tested. The six photodiodes are connected in parallel and the resulting current from the array represents the total irradiance on the test area.*

6.4 Measurements of concentrating collectors

In order to compare results from indoor measurements with results from outdoor measurements that have higher credibility, the transverse incidence angle dependence of different concentrating solar collectors was evaluated by indoor and outdoor measurements. During the indoor measurements, the photodiode array was placed in front of the test area in order to achieve a mean value of the irradiance on the collector surface.

6.4.1 The roof collector of corrugated steel

Measurements

The concentrating roof-integrated solar collector, referred to as Collector C in chapter 5, is based on copper pipe absorbers placed together with concentrating reflectors in a roofing material of corrugated steel. The collector was evaluated by indoor and outdoor measurements as described in Sections 3.1.3 and 5.3.6.

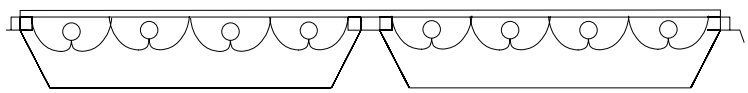

Figure 6.3 *The concentrating roof-integrated collector based on copper pipe absorbers.*

Results

The measurement results are described in Section 5.3.6 and Figure 5.24 shows the transverse incidence angle dependence where Collector C is measured both indoors and outdoors. The graphs from indoor and outdoor measurements correspond relatively well up to θ_T=50º. For incidence angles higher than that the results are less accurate.

6.4.2 The roof MaReCo

Measurements

A prototype of a 2D concentrating collector, a *roof MaReCo*, which is geometrically optimised for spring and autumn performance and intended

to be placed on a 30° tilted roof, was also evaluated. The collector, which was previously described and evaluated for thermal performance by Adsten (2002), is shown in Figure 6.4.

The reflector geometry is a parabola combined with a circular section. The bifacial absorber receives irradiation both on the front side and on the back side over an acceptance interval between 0° and 60° solar altitude angle when placed on a roof with 30° slope.

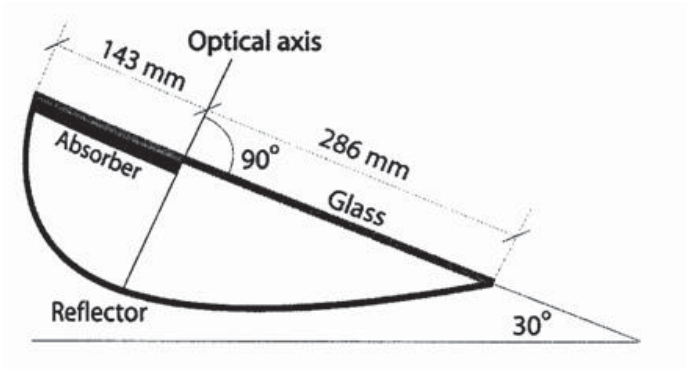

Figure 6.4 Design of MaReCo for tilted roofs (Adsten, 2002).

Indoor measurements with a Roof-MaReCo prototype were performed as described in Section 3.1.3. The collector was mounted in front of the solar simulator with the absorbers placed vertically on a stand that was rotated to get varying incidence angles on the collector, as shown in Figure 6.5. During the measurements the glazing of the prototype was replaced by a Teflon film, for which the incidence angle dependence is similar to that of glass. The $f(\theta)$ function was therefore approximated with K_b, with b_0 equal to 0.08. The photodiode array was placed in front of the Teflon film during the measurement.

Figure 6.5 *The roof MaReCo mounted in front of the solar simulator, with the absorbers placed vertically.*

A single measurement was performed outdoors, at θ_T =30°, with similar equipment set-up. The result from this measurement was intended to be a normalization point for the indoor measurements.

The relation between the current from the photodiode array and the irradiation at corresponding incidence angles during outdoor measurements was calculated based on the outdoor measurements.

The results of optical efficiency for the various incidence angles gave the incidence angle dependence in the transverse plane, $K(0,\theta_T)$, which includes the influence of the Teflon cover. $K(0,\theta_T)$ was then divided by $f_L(\theta_L)$, the influence of the glazing, in order to get $R_T(\theta_T)$, the influence of the reflector only, according to the method described in Section 2.5.3.

The optical efficiency was also calculated by multiplying the irradiation at normal incidence by *cos* θ_T, as this could be a good approximation had the total irradiation from the simulator been constant throughout the measurement.

A comparison has been made with corresponding outdoor measurements of $f_L(\theta_T)$ and $K(0,\theta_T)$ on the roof MaReCo, which were previously per-

formed at the Älvkarleby test facility on a larger prototype with identical geometrical features.

Results

The transverse incidence angle dependence of the roof MaReCo is shown in Figure 6.6. These values of optical efficiency, $R_T(\theta_T)$, show the influence of the reflector exclusively, since the influence from the Teflon and the glazing are deducted. For low angles of incidence, from ±0° to approximately ±35°- 40°, the results from the photodiode compensation method show good agreement with outdoor measurements but for higher angles of incidence, when the irradiance is low, the agreement is not so good. Here, the cosine dependence shows better agreement with outdoor measurements than the photodiode compensated data. According to these results the cosine compensation seems to be a good method for estimation of the irradiance but it does not take the moving light pattern, nor the variable irradiance and the time aspect into account.

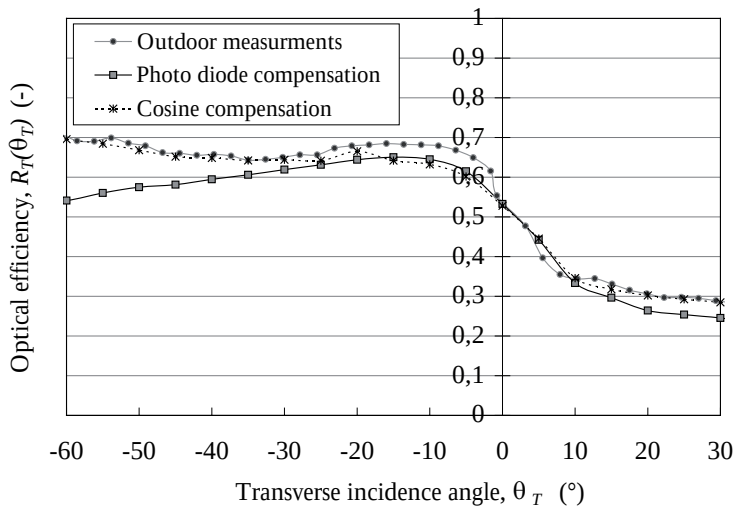

Figure 6.6 *The incidence angle dependence of the roof MaReCo from indoor and outdoor measurements is plotted here, showing the optical efficiency influenced only by the reflector. The interval of incidence angles corresponds to the interval when placed at a 30° tilted roof. Then -60° in the figure means that the solar altitude angle is 0°, 0° is normal incidence and 30° means 90° solar altitude (zenith).*

6.5 Conclusions

The measurement technique of using an array of photodiodes for calculation of the total irradiance during indoor measurements with the solar simulator has been shown to work well for lower incidence angles. However, the method is in need of improvement before it can be applied during evaluations of the entire angular spectrum.

The results of optical efficiency from outdoor and indoor measurements show that the agreement between indoor and outdoor measurement is good at lower incidence angles but not so good at higher incidence angles. The evaluation of the roof collector of corrugated steel showed that measurements of incidence angles up to ±50° gave accurate results while the measurements of the roof-MaReCo indicate that it is accurate only up to ±35°-40°.

Although the cosine compensation method, which showed very good agreement from the evaluation of the roof-MaReCo, appears good, it is not suitable for application where this solar simulator is used, as neither the light intensity variation in time nor the moving light pattern can be taken into consideration when it is used. In this case it is highly likely that the good correspondence was more or less a coincidence.

An explanation for the lower correspondence when the photodiode method is used at higher incidence angles could be that the active test area is smaller and the power involved is lower.

Also, the number of photodiodes could be too small. A higher number of photodiodes might give a more representative value of the total irradiance on the collector surface.

If possible the photodiodes should be replaced by pyranometers, the accuracy of which at high incidence angles is well known.

Actually, the photodiodes might not be suitable for use at high incidence angles. There is a risk that the light might be reflected into the silica receptor of the photodiodes from the sides and from the back of the diodes, which is transparent glass. There is therefore a risk that the shown current might be higher than the irradiance it should represent, which would explain the lower optical efficiency at high incidence angles. This problem could possibly be taken care of by painting the sides of the photodiodes black so that no side irradiation affects the result.

The method can thus be improved in a number of respects, and there is potential for development of a good indoor method for evaluations of the incidence angle dependence of solar collectors.

7 Building integrated solar collectors for district heating systems

A presentation and summary of Paper VI - *Design and performance of a large solar thermal system with façade-integrated collectors in several directions, connected to the district heating system* is found in this chapter. The work was performed in collaboration with E.ON and Grontmij (former Carl Bro), the owners and ivolved designers of the investigated solar thermal system and with help with climate data from Denmark Technical University. The paper was presented at Northsun 2005 in Vilnius.

7.1 Introduction

A reliable and robust control system is crucial for the optimal function of a solar thermal system. By connecting solar thermal collectors to the district heating system, problems with stagnation in the collectors can easily be avoided due to the constantly large heating demand. This chapter describes the interesting design features of one of the largest façade-integrated solar thermal systems in Europe, which is also connected to the local district heating system. This system has been operated successfully and monitored since June 2002 without stagnations problems or interruptions. The thermal performance of the collectors and the importance of some system features have been evaluated by studies of measured data from the system and by parametric studies from WINSUN simulations.

7.2 System description

7.2.1 System design

The solar thermal system works as any other conventional production unit in the district heating system in Malmö, with the exception that the production cannot be predicted. It is therefore very important that the system is robust and provides a high availability, in order not to cause disturbances like the discharge of low-temperature water into the district heating net. The system is therefore highly automated, remote-controlled and requires minimal maintenance.

The installation of the 1050 m^2 large flat plate collectors with antireflection treated and frosted glass was carried out as a replacement of the old façade and they have been given an interesting design, well integrated in the building.

Figure 7.1 *The large façade-integrated collectors at Kockum Fritid in Malmö. (Photo: Martin Råberg, Grontmij).*

The five collectors are divided into three subsystems, which are integrated in the façades in directions close to east, south and west and tilted at 90° and 73°. The control system allows cooperation of the five collectors. The areas, azimuth angles and tilt angles of the collectors are shown in Table 7.1. In Figure 7.2, an overview of the system design is shown.

Table 7.1 The size and orientations of the collectors.

Direction	Azimuth angle, γ	Collector tilt,β	Collector area (m²)
East	-98°	90°	181,6
South	-8°	90°	371,2
South	-8°	73°	221,6
West	82°	90°	112,4
West	82°	73°	163,4

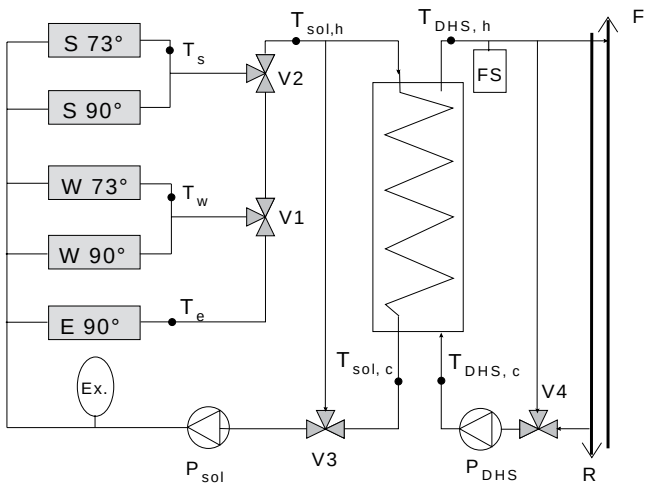

Figure 7.2 An overview of the system design.

The collectors are marked with S, W and E, for the orientations towards south, west and east, and with the tilt angles. The temperatures from the outlets of the collectors towards south, (T_s), west (T_w) and east (T_e) are shown in the figure as well as the hot and cold temperatures on the solar circuit side ($T_{sol,h}$) and ($T_{sol,c}$) and the corresponding temperatures on the district heating system side ($T_{DHS,\,h}$) and ($T_{DHS,\,c}$). The expansion vessel (Ex), the flow sensor (FS), the forward (F) and the return (R) pipes of the district heating system, the solar circuit pump (P_{sol}), the pump on the district heating side (P_{DHS}) and the three-way valves (V1, V2, V3 and V4) are also shown .

7.2.2 The flows in the collector circuits

The flow in the solar circuit is divided into three main circuits, east, west and south, and the flow rates in these circuits vary continuously. Two PID regulators seek to modify the positions of two motorized three-port control valves, V1 and V2, which mix the flows in a way that minimises the temperature differences between the outflows from the three circuits. The flows from the eastern and the western collector circuit are mixed in V1, so that T_w and T_e are balanced, by increasing the flow where the temperature is highest. The valve V2 mixes the flow from the collectors towards east/west with the flow from the southern collectors so that the highest temperature of T_w and T_e is balanced to T_s. This strategy results in a higher flow rate, lowered operation temperatures and thereby reduced heat losses in the most illuminated collector.

7.2.3 Start up and shut down control of the solar circuit

The start up and shut down of the solar circulation pump, P_{sol}, is controlled by a timer, which starts the pump in the morning on low power for two minutes, or as long as any of the three measured outlet temperatures, T_e, T_s and T_w, is higher than 40°C. A new attempt to start is made every 30 minutes. In this way, overheating and loss of available energy is avoided. When $T_{sol,\,h}$ rises above the required 67°C, the district heating pump, P_{DHS}, is started and the solar circuit pump activity is thereafter increased to 100%. The bypass valve, V3, protects the heat exchanger against freezing as it is kept open to the heat exchanger as long as $T_{sol,\,h}$ is higher than 5°C. When the temperature is lower than that, V3 shuts and the liquid is shunted outside the heat exchanger.

7.2.4 The control of the district heating circuit

In the heat exchanger, the return flow from the district heating system is heated from approximately 45°C to the temperature required for the outgoing flow, which is 65°C minimum. The three-way valve V4 is used to adjust the temperature of the outgoing water. The pump in the district heating circuit, P_{DHS}, increases the pressure from 4 bar on the return side to approximately 7 bar on the outgoing side. The pump is active as long as $T_{sol,\,h}$ is 65°C or higher. The flow sensor registers the actual flow rate in the district heating system circuit. When P_{DHW} is operating the solar pump P_{sol}, is set to operation mode, i.e. 100%, providing the design flow in the

solar circuit. If the valve V4 on the district heating side has been closed for ten minutes, the district-heating pump is shut off and the solar circuit pump is set to its mode of 25% rotation speed, waiting for the temperature to rise before a start-up can be initiated once again. In the event that the freezing alarm is activated, the three-way valve of the district heating system circuit is opened just enough to keep the outgoing water above 15°C. By having double control functions for the pump, on both the temperature and the flow of the circuit, the system is made more robust.

7.2.5 Overheat protection by partial evaporation

The system is protected from overheating by control features allowing partial evaporation of the heat transfer medium (Tyfocor). The system is equipped with a 1000 l compressor-fed expansion vessel that is automatically refilled after boiling. In case of boiling and stagnation, the pressure will rise to a certain limit before air is let out of the expansion vessel through a solenoid valve, maintaining this slightly higher pressure. The solar circulation pump is then stopped in order to prevent as much of the liquid as possible from boiling, which could expose the collectors to hammering as the hot steam condenses when meeting the cold liquid. The heat transfer medium is thereby pressed backwards into the expansion vessel. As the weight of the expansion vessel increases over a critical level, a pressure sensor triggers an alarm to the control centre. As the collectors are cooled down, the pressure in the solar circuit decreases and the Tyfocor is then pressed back into the system, due to the higher pressure in the expansion vessel, and it condenses in the solar collector. The compressor refills the expansion vessel with air to a certain pressure and the solar circuit is then ready for operation again. This overheat protection system was never activated during the first years of operation, since the system never reached stagnation. However, the pilot plant was in stagnation several times and the control strategy had then been proved successful.

7.2.6 The importance of location

A condition for the success of this solar thermal system is the carefully planned location, which makes it possible to keep the heat losses from the system very low. The solar system is situated in the outer parts of the district heating system where only relatively low temperatures are required. Also, it is very close to an area where the buildings were designed to maintain thermal comfort using the minimum temperature of 65°C from the district heating system.

7.3 Evaluation of the system

7.3.1 Methodology

An evaluation of the system was carried out based on studies of collected data from the solar heating system, such as temperatures, flow rates, valve positions, pump activity etc. during the period 2002-07-01 to 2003-06-30. As detailed data of solar irradiation from the site were not available, an analysis of the performance of the system based on measured data was not possible. Instead simulations of the energy output of each of the collectors were performed using WINSUN, a simulation program for solar collectors, see Section 3.3.2. Climate data from Meteonorm, for a typical year in Lund, was used. Input data of the performance parameters of the collectors are shown in Table 7.2. These values are received from the manufacturer who had the collectors tested by SP Technical Research Institute of Sweden.

Table 7.2 The collector performance parameters used in WINSUN simulations. η_0 is normally 0.83 but was considered lower due to the frosted glazing.

η_0 (W/m²K)	$F'U_0$ (W/m²K)	$F'U_1$ (W/m²K²)	b_0 (-)
0.81 (0.83)	2.7	0.03	0.10

Monthly mean flow weighted operation temperatures in the collectors were derived from measured data and the average operation temperature over the year was calculated to 63°C and used in WINSUN. Simulation results of monthly energy output from the solar collectors during an average year and monitored monthly values of total energy output to the district heating system during the investigated period were compared. Some minor deviations between these values were found, which could be explained by the fact that the irradiation varies considerably from year to year (Adsten, 2002). Also, a comparison between the climate data from Meteonorm and measured data from DTU, Copenhagen was performed in order to verify the simulation results. As Copenhagen and Malmö are close and the climatic conditions are similar it was assumed that these data give a sufficiently good approximation of the Malmö conditions. The comparison showed that there were considerable differences between the beam irradiation from measured data and corresponding climate data. This, and the

fact that the model is rather rough, explains the small difference between simulated and measured energy output from the collectors.

7.3.2 The overall energy yield

During the investigated period from 2002-07-01 to 2003-06-30, the system delivered 189000 kWh to the district heating system, i.e. 180 kWh/m² collector area, with a peak power of 0.3 MW. The COP (i.e. the thermal energy produced per kWh electricity used for the system operation) was 24, according to measured data. The results from the simulations show an expected energy output of 183000 kWh/a, i.e. 174 kWh/m^{2}a, which is a divergence of only 3% from the measured output. The results of annual energy output are as high as can be expected from a system with collectors in non-optimal directions.

7.3.3 The cooperation of the collectors

Figure 7.3 shows the positions of the motorized three-way valves V1 and V2 as illustrated in Figure 7.2, which alter the flows of the main collector sub circuits. The data is from the 20th of July 2003, a sunny clear day when the solar pump was working at 100% speed during the whole day.

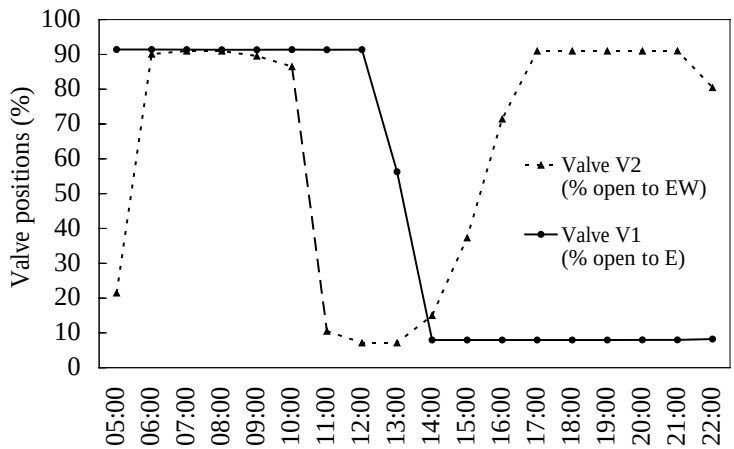

Figure 7.3 *The positions of the motorized three-way valves, V1 and V2, controlling the flows of the collector circuits, measured during a clear summer day, the 20th of July 2003.*

In Figure 7.4, the outlet temperatures T_e, T_s and T_w, from the different collectors, (from the same day) are shown as well as the temperatures at the inlet of the heat exchanger on the solar side, $T_{sol,h}$, and at the outlet of the heat exchanger on the district heating side, $T_{DHS,h}$. It also shows that the temperatures in and out of the heat exchanger, $T_{sol,\,h}$ and $T_{DHS,\,h}$, are stable from 07:00 to 20:00. As the temperature $T_{sol,h}$ decreases below 67° in the evening, the district heating pump is stopped and no more energy is delivered to the district heating system. Both Figure 7.3 and 7.4 show that the flows are well controlled and result in a constant output temperature to the district heating system.

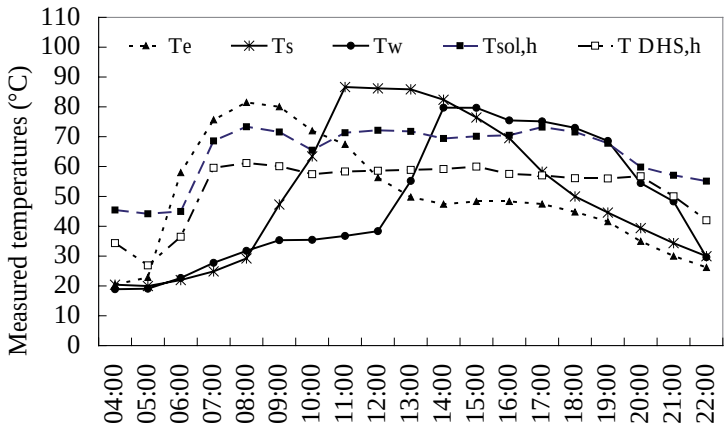

Figure 7.4 *The outlet temperatures from the three main collector circuits, T_e, T_s, T_w, the temperatures at the inlet to the heat exchanger on the solar circuit side, $T_{sol,h}$, and the outlet from the heat exchanger, $T_{DHS,h}$, in the district heating circuit. Data from 2003-07-20.*

7.3.4 Parametric studies

Collector orientation

WINSUN simulation results of the monthly energy output from the five collectors during a year are shown in Figure 7.5. The west- and south-facing collectors tilted 73° give the highest peaks in summer, while the south-facing vertical collector gives a more balanced output over the year. The two south-facing collectors provide some energy output during winter, when the eastern and western collectors hardly deliver any energy at all.

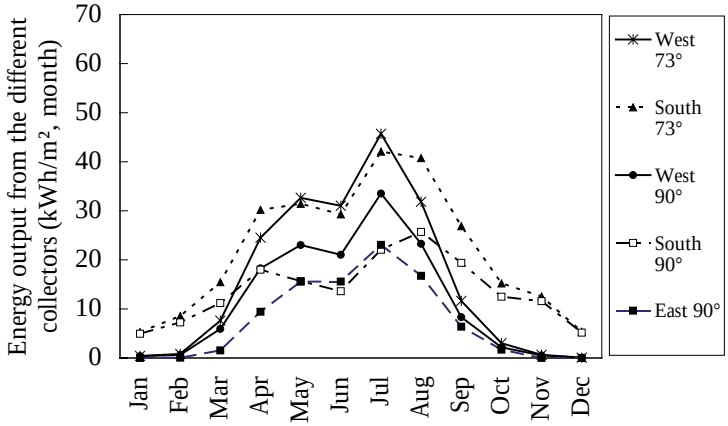

Figure 7.5 *The simulated energy output for the different collectors shown as monthly values over the year.*

The monthly values of mean area weighted energy output of the system are shown in Figure 7.6, as well as results of the energy output from a system where the collectors are placed horizontally or towards south, tilted 40°. The results of annual energy output are shown in Table 7.3.

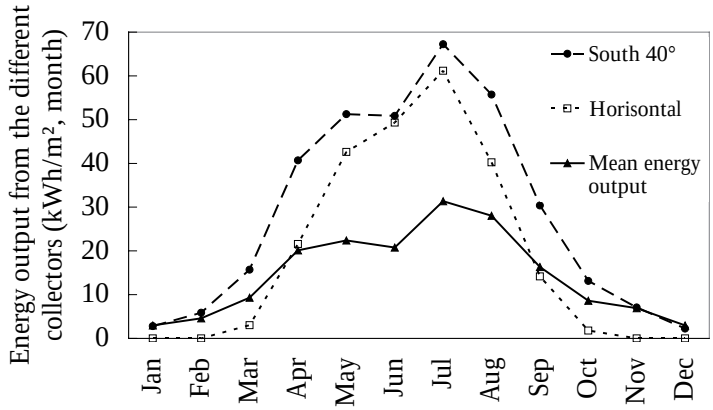

Figure 7.6 *Simulation results of the mean area weighted energy output and the theoretical output for horizontal or south-facing 40° tilted collectors.*

During the winter, the mean energy output of the system is higher in comparison to horizontally placed collectors but it does not exceed the output from a collector directed towards south tilted 40°.

Table 7.3 The simulated annual energy output of the differently tilted collectors and of a horizontal and south-facing collector tilted 40°.

Collector direction and tilt	East 90°	South 90°	South 73°	West 90°	West 73°	The total system	South 40 °	Hori-zontally
Annual energy output (kWh/m²a)	90	167	263	137	190	174	343	234

It can be concluded that the high tilt of the south-facing collectors gives balance to the energy distribution over the year whereas the vertical east- and west-facing collectors give less energy during the cold season. If the tilt was 40° they would give the maximum annual output of 343 kWh/m^{2}a, almost twice as much as they give today.

Operation temperature

The results in Figure 7.7 show how the energy output for the different collectors and the mean (area weighted) energy output of the whole system would change if the mean operation temperature in the collectors were altered. At present the average mean operation temperature is 63°C. The collector facing south and tilted 73° gives the highest annual output, followed by the 73° tilted collector directed towards west, which gives almost the same results as the area weighted system average. The collector facing east and tilted 90° is the collector with the lowest output. Had the operation temperatures instead been 40°C or 50°C, the output would have been 60-130 kWh/m²a higher. A 10°C increase in temperature reduces the mean annual energy output by around 50 kWh/m².

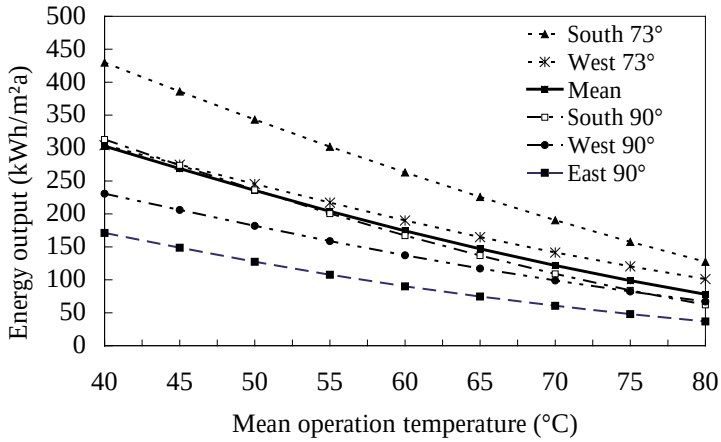

Figure 7.7 *The theoretical energy output of the different collectors for different mean operation temperatures in the collectors and the mean values of the system.*

7.3.5 Comparison of measured and simulated data

Measured and simulated results of monthly values of energy output from the solar collectors during an average year are compared in Figure 7.8. The obvious differences are most significant in March and September, when the collectors produced more heat than expected.

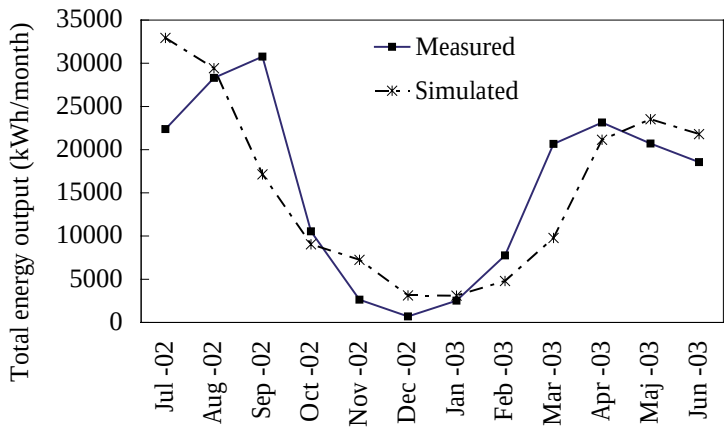

Figure 7.8 *Measured and simulated results of the total monthly energy output from the solar thermal system.*

The divergence can be explained by the natural climate changes from year to year. The solar irradiation varies considerably from year to year and the collector output also varies accordingly by ± 20% around the average value, according to Adsten (2002). This was further investigated by comparing data of global and beam irradiation measured at Denmark Technical University, Copenhagen to corresponding climate data from Meteonorm used in the simulations (a reference year based on the location of Lund). The measured data of global irradiation corresponded well with the climate data (see Paper VI, Figure 4). However, important differences were shown between the beam irradiation measured normal to the sun and the corresponding climate data, see Figure 7.9. The deviations are particularly large in March and September. This variation in beam irradiation from year to year, together with the fact that the model is rather rough, could very well explain the deviation of energy output shown in Figure 7.8. This implies that the results showing monthly values should be considered as an indication that these results are of slightly lower accuracy than the results showing annual energy output, which correspond well with measured data.

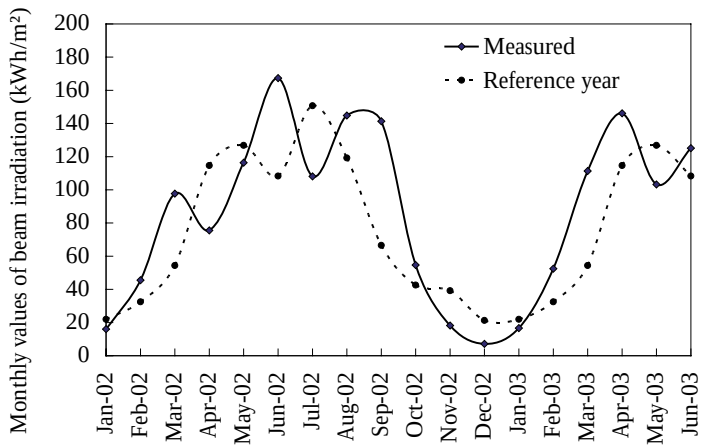

Figure 7.9 *Monthly values of beam irradiation, normal to the sun, from Copenhagen and the corresponding values used in the climate data in WINSUN.*

7.4 Conclusions

A large solar thermal system for production of heat for the district heating system was studied. The five large collectors are integrated in the façade in different directions. Simulations were performed in order to show the benefits of the used control strategies. The overall evaluation shows that the advanced system design for start up, stagnation and control has resulted in a well working solar collector system with high accessibility.

The design criteria are very different for a solar heating system with an immense heat load compared to a solar system for single houses. Still, there are several interesting design features in this system that are interesting to consider also for small scale systems, e.g. robust components and good control strategies such as partial evaporation and anti-freezing protection of the heat exchanger.

The control of the flows through the five collectors is designed to even out the temperature differences between the different collectors. The analysis shows that this control strategy results in a balanced flow over a day, with the highest flow rate in the most illuminated collectors. The output temperature is shown to be fairly constant over the day. It is also shown that the control feature for delivering heat to the heat exchanger at a temperature of at least 67°, works according to the design and with a high reliability. The temperature going into the heat exchanger and the temperature going out to the district heating system are relatively constant during the time heat is delivered.

The parametric studies using WINSUN show that, as expected, the collectors tilted at 73° south give the highest energy output and that the vertical collectors in east and west give the lowest output. The two collectors tilted 73º give the highest output in summer, the two south-facing collectors give the highest output during spring and autumn and the east and west collectors contribute to a uniform energy distribution over the day. If all the collectors had been mounted towards south tilted 40°, the total energy output would have been increased by a factor of approximately 2. However, the collectors were installed as a replacement of the old façade and the low total material costs for façade and collectors taken together is considered as a compensation for the lower energy output.

Detailed climate data from the location was not available, and simulations in WINSUN were therefore performed to show the expected thermal output. The simulations give a good indication of the energy output. The accuracy of the simulation results of annual energy output is considered fairly high while the monthly values are difficult to predict due to climate changes from year to year, especially variations in the beam irradiation.

This was shown by comparisons of climate data used in simulations and data measured in Copenhagen.

This evaluation shows the importance of having access to accurate and detailed climate data when evaluating the performance of solar collectors. It also shows that climate data from Meteonorm can be used for simulations of annual output when there are no measured irradiation data available.

8 Optimisation of module geometries for concentrating façade integrated collectors

This chapter presents an overview of Paper VII, *Optimisation of reflector and module geometries for static low-concentrating, façade integrated photovoltaic systems*, which is published in *Solar Energy Materials and Solar Cells*. The work was also presented at the ISES Solar World Congress in Gothenburg in 2003.

8.1 Introduction

The geometrical design of a static, façade integrated, concentrating solar collector has been optimised for maximum annual energy output when operated in southern Sweden. The module tilt and the geometry of the parabolic reflector have been investigated by measurements and simulations and the different geometries are compared.

The concentrating system could be used either as a photovoltaic collector, a thermal collector or a hybrid PV/thermal collector, generating both electricity and thermal energy. This work deals only with the geometrical design and the electricity generation from the collector as a photovoltaic system, which should however also be representative for the thermal generation as the optimisation aims to find the highest annual irradiation on the absorber.

8.2 Collector design

The collector had previously been produced as a prototype of which an illustration is shown in Figure 8.1. This system has a concentration ratio of 2.96 and includes parabolic reflectors and photovoltaic string modules, as well as EPS (expanded polystyrene) insulation. Due to the insulation material attached to the back of the reflector sheet metal, the façade element can serve as an integral part of the building envelope. The mirrors are made of anodised sheet aluminium, which offers good mechanical properties and has a total solar reflectance of 81% for wavelengths shorter than 1100 nm.

Figure 8.1 *Cross section of a static, two dimensional concentrating photovoltaic system intended for façade integration. The system includes photovoltaic string modules and parabolic aluminium reflectors, as well as EPS insulation. (Brogren et al., 2003)*

This system can be used either unglazed and passively cooled or with a glass surface placed vertically in front of the whole façade element in order to protect and prolong the lifetime of the reflector material. As photovoltaic modules give higher output at lower temperatures, it is beneficial to use active cooling combined with heat generation, especially when glazing is used.

The reflector is shaped as a parabola (see Figure 2.9) with its optical axis tilted at an angle ν to the horizontal, as shown in Figure 8.2. As also shown in Figure 2.9, all irradiation incoming parallel to the optical axis or from higher solar altitude angles will fall between the focal point, *F*, and the reflector, and it is therefore suitable to place an absorber here. The letter *h* denotes the height of the glazing and *a* the width of the module plane, which can be tilted back and forth around the focal point. In the figure, ϕ is the angle between the vertical glazing and the optical axis of the reflector. The solar altitude angle projected in the north-south plane is denoted by α_{NS} and the angle between the horizontal and the module plane is denoted β. The geometrical concentration ratio, *C*, of the system is given by Equation 40.

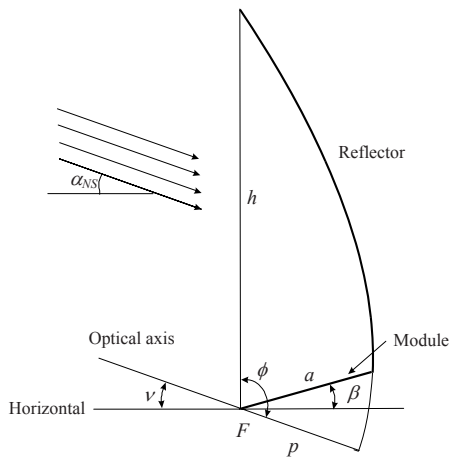

Figure 8.2 *Illustration of the geometry of the reflector and the module plane of the collector.*

Similar asymmetric concentrating collector systems for façade integration have been evaluated by measurements (Mallik et al., 2004; Mallik et al. 2006; Zacharopoulos et al. 2000) and found to increase the performance by 62% for a geometrical concentration ratio of 2.0.

8.3 Measurements and calculations of optical efficiency

In order that measurements may be performed for several different system geometries, a prototype with a parabolic reflector and an adjustable absorber plane was designed, see Figure 8.3. The module plane of this prototype can be tilted, as can the entire prototype. This means that the system can be evaluated for different values of angle β and for different transverse incidence angles, but the angle ν is constant at 25°.

Measurements of the short circuit current I_{SC} from a photovoltaic thin film CIGS (Copper Indium Gallium Diselenide) module that was placed on the module plane were performed for different geometries. The measurements were carried out indoors using the solar simulator described in Section 3.2.1. As the absorber plane was tilted the active absorber width, *a*, was altered. The thin film cell was shaded with aluminium foil to obtain the correct module area to be exposed for each value of the angle β, see illustration to the right in Figure 8.3. The short circuit current of the cells represents the irradiance, *I*, and is proportional to the module area. The CIGS cells are suitable for this purpose as the vertical cells are all aligned in one row and can be partly shielded perpendicular to the length of the cells without interrupting the current.

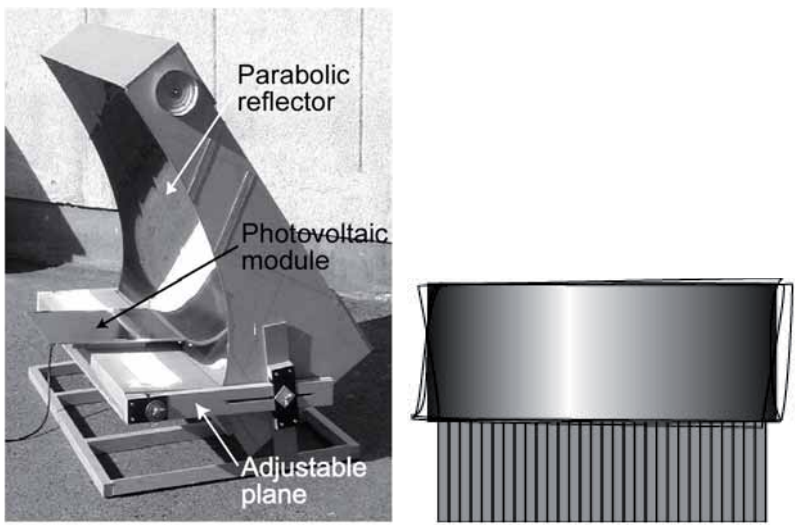

Figure 8.3 *To the left, the prototype with adjustable absorber plane. To the right, an illustration of a photovoltaic thin-film cell shielded with aluminium foil to achieve the right area.*

The entire prototype was tilted so that measurements could be performed for different transverse incidence angles. Two basic geometries, Geometry A and Geometry B, were analysed in detail. In both geometries, the angle ν, is 25° and the distance *p* is 158 mm. For Geometry A, the module tilt angle, β, is 20°, which results in a geometrical concentration ratio *C* of 2.96. For Geometry B, β is -15° and *C* is 3.44. Because of the difference in absorber tilt angles, the absorber width *a* is slightly higher for geometry A than for Geometry B. The positive module tilt gives the system a better performance at low solar altitudes angles, as direct irradiation can fall on the absorber. The negative module tilt of Geometry B was chosen because it gives the system a higher geometrical concentration ratio and thereby possibly a cheaper absorber.

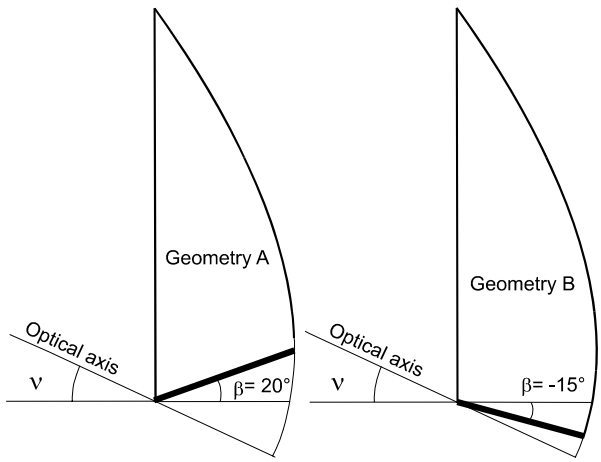

Figure 8.4 *Geometries A and B. For Geometry A, the angle β is -20° and in Geometry B, β is -15°. In both geometries the angle ν is 25º.*

Measurements were also performed on the CIGS modules when mounted vertically on the wall, shielded to the corresponding sizes, as references. The results of short circuit current per cell area for Geometry A, B and for the vertical reference cell are presented in Paper VII, Figure 12 and 13.

The optical efficiency for beam irradiation for each angle was then calculated by Equation 55 for every tenth south-projected incidence angle between 0° and 70°, giving the transverse incidence angle dependence.

$$\eta_{0b} = \frac{I_{SC\,(conc.)}}{C \cdot I_{SC\,(ref.)}} \qquad \text{Eq. (55)}$$

The accuracy of the measured optical efficiency for higher transverse incidence angles was considered too low, due to the limitations of the solar simulator (see Chapter 6). Therefore the optical efficiency for angles higher than 40° was also calculated according to Equation 56. This is referred to as the calculated optical efficiency and is also denoted $R_T(\theta_T)$. The calculation for angles lower than ν is shown in Equation 57. A constant k=0.69 that represents the effective reflectance was introduced in Equation 56 to get a good fit to the results of optical efficiency. The relatively low value of the effective reflectance, k, is explained by multiple reflections, optical imperfections and resistive losses in the photovoltaic cell. The calculation results are shown in Figure 8.5.

$$R_T(\theta_T) = \frac{k\cdot(h\cdot\cos(\theta_T) - a\cdot\cos(90°-\beta-\theta_T)) + a\cdot\cos(90°-\beta-\theta_T)}{h\cdot\cos(\theta_T)} = \\ = k + (1-k)\frac{1}{C}\frac{\cos(90°-\beta-\theta_T)}{\cos(\theta_T)} \qquad \theta_T > \nu \quad \text{Eq. (56)}$$

$$R_T(\theta_T) = \frac{1}{C}\cdot\frac{\cos(90°-\beta-\theta_T)}{\cos(\theta_T)} \qquad \theta_T < \nu \quad \text{Eq. (57)}$$

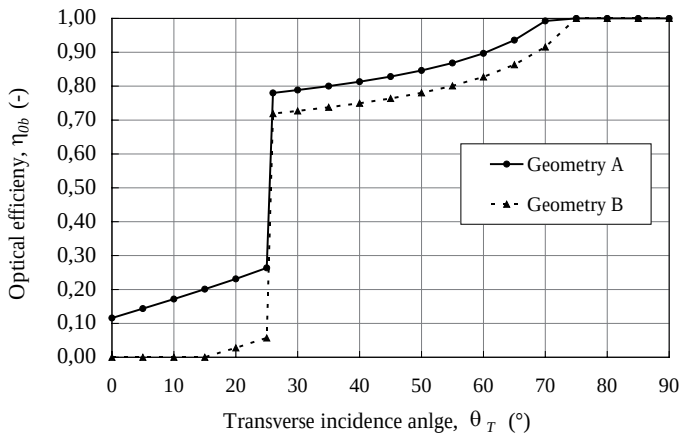

Figure 8.5 *The calculated optical efficiency $R_T(\theta_T)$ for the two system geometries. The values are significantly higher for incidence angles greater than the angle of the optical axis (25°) as this means that the irradiation is concentrated.*

Figure 8.6 shows the resulting incidence angle dependencies in the transverse plane for Geometry A and B, based on measurements up to 40° and on calculations for higher angles.

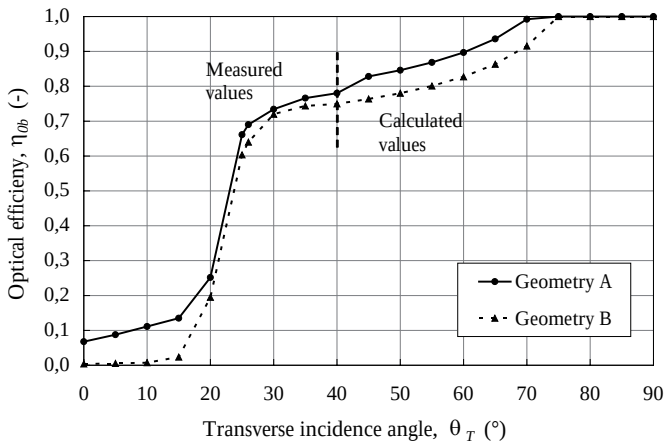

Figure 8.6 *The model of optical efficiency according to measured values for θ_T <40° and calculated values for θ_T >40°.*

For angles θ_T below ν, the concentrator is not used and no light is reflected, yet some irradiation reaches the module directly, more so for Geometry A than for Geometry B. For θ_T over 70°, all irradiation reaches the module directly without reflections, which means that the optical efficiency is equal to 1. The measured values of lower incidence angles correspond well to the calculated values.

8.4 Analysis of long term outdoor measurements

A long term outdoor evaluation of the prototype of Geometry A had previously been carried out at the Älvkarleby test facility. The results, thus including both diffuse and direct irradiation, show that $I_{sc(conc.)}$ is a factor of 2.0 higher than $I_{sc(ref.)}$ (see Paper VII, Figure 17). This means that the geometrical concentration factor of 2.96 in combination with the optical losses results in a real concentration factor of approximately 0.7, which is similar to the results achieved by (Mallik et al., 2004; Mallik et al. 2006; Zacharopoulos et al. 2000).

An analysis of the measured optical efficiency for beam irradiation $\eta_{0b}(\theta_T)$ was also performed, which showed a relatively good overall agreement with the results in Figure 8.6 (see Paper VII, Figure 18). For θ_T = 40°, the outdoor measurements show a η_{0b} value of 0.60-0.72, while the estimated value is 0.78. The influence of the diffuse irradiation scattering and of the aged and dirty reflectors explains this difference.

8.5 Simulations of annual energy yield

Simulations of the annual energy output from different system geometries were performed using the MINSUN simulation program. Glazing in front of the collector was considered in these simulations. The results of optical efficiency for beam irradiation for different transverse incidence angles were used as input to the program, which calculates the incidence angle dependence as a product of the optical efficiency in the transverse plane and the influence given for the longitudinal plane, basically the incidence angle dependence of the glazing. In the calculations, b_0 was set to 0.25. Read more about MINSUN in Section 3.3.1.

The MINSUN results gave the annual irradiation on a south facing vertical surface, with the optical losses of the concentrating system deducted. The annual irradiation on the absorber plane of the collector is then calculated by multiplication by the concentration ratio, *C*. Thereafter, the annually produced electricity yield is calculated by multiplying the result by the efficiency of the photovoltaic module. In the calculations, the efficiency of the photovoltaic module was set to 13%, a common value for thin film photovoltaic cells (Shell Solar, 2003).

Simulations of altered system geometries were also performed. The parabolic curves of the reflector were rotated in the simulations so that the performance of geometries with differently tilted optical axes (varied angle ν) could be calculated. This was accomplished by shifting the input data of optical efficiency in the north-south plane to the left or right on the input row, for tilting the optical axis forwards or backwards. As the program will consider the whole system as tilted, the angle β will be altered but the angle between the module plane and the optical axis remains unchanged. An illustration of how the geometries were altered is shown in Figure 8.7. The figure shows that the concentration ratio will increase as the angle ν increases and vice versa, because the height, h, relative to the module width, a, is increased. As the whole systems are tilted, the module tilt angles β are also altered.

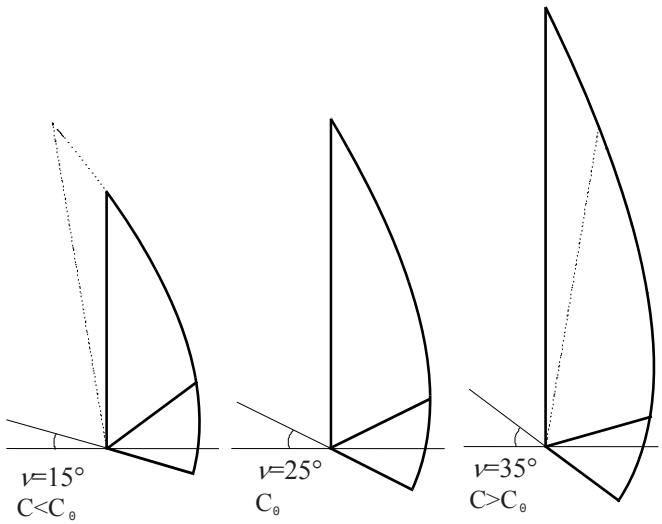

Figure 8.7 *The geometries that result from tilting the entire system forwards and backwards, adjusting the reflector length to the truncation of the glazing. The geometry in the middle is the original system design of Geometry A.*

8.6 MINSUN results and annual electricity production

The results of the simulated annual electricity production for different geometries of the concentrating system, based on Geometry A and B, are shown in Figure 8.8. The electricity yield per cell area and per glazed area are shown in the figure for varying tilt angles of the optical axis, ν. The horizontal lines show the calculated yield per cell area from the vertical flat reference module and also for a reference module that is shaded up to 12°, as this is a probable situation for vertically placed photovoltaic cells. The concentrator module is insensitive to shadowing up to the incidence angle equal to the optical axis.

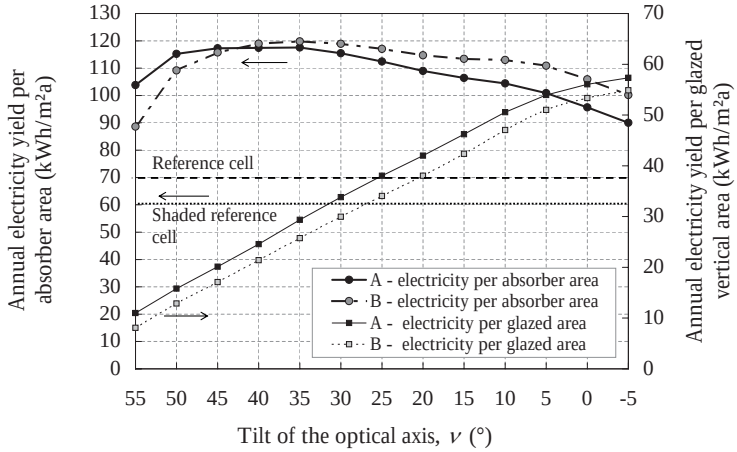

Figure 8.8 *The results of energy yield, shown per absorber area and per vertical glazed area, for different geometries of the concentrating system.*

The annual electricity yield per absorber area increases with higher values of angle ν (as the concentration ratio *C* increases) until the tilt of the optical axis is so high that the system does not accept a large share of the irradiation. For ν angles higher than 45° the annual yield is decreased. The annual yield per glazed area decreases with increasing values of angle ν. It can also be seen that the graphs for Geometry A and B are similar but slightly displaced from one another and that Geometry B gives a slightly higher yield per absorber area, compared to Geometry A, at values of ν up to 45°, due to the higher concentration ratio. Geometry A, on the other hand, gives a higher yield per glazed area, which is explained both by the lower concentration ratio and the lower reflection losses.

The highest annual energy yield per cell area is 120 kWh/m²a, achieved by Geometry B at ν = 35°, when the concentration ratio, *C*, is 4.65. The simulations show that the reference cell would give 70 kWh/m²a and, if shaded for θ_T from 0° to 12°, 60 kWh/m²a. The calculated electricity production for this concentrating system is thus 72% higher than that of the unshaded vertical reference module, and 100% higher than a shaded module. In this geometry, the module is tilted slightly backwards (β=-25°), which implies a lower energy generation for low solar altitudes.

However, at ν=35°, Geometry A gives almost as high a yield, 118 kWh/m²a, with *C*=4.00 (and β=10°).

The measured systems, where ν = 25°, show slightly lower values of the estimated annual yield, 112 and 118 kWh/m²a for Geometry A and B respectively, thus 60% and 68% higher than the unshaded reference cell.

As long as the angle ν is between 25° and 45° the annual yield is not lower than 93% of the maximum yield.

However, a higher inclination of the optical axis means that the acceptance of irradiation from low solar altitude angles is more limited. This results in a higher summertime production at the expense of a lower wintertime production. This effect can be observed in Figure 8.9, which shows the annual distribution of the electricity yield per module area for different values of angle ν (0°, 25° and 45°) of the Geometry A system and for the vertical reference cell. A low absorber tilt angle, β, also limits the production in winter.

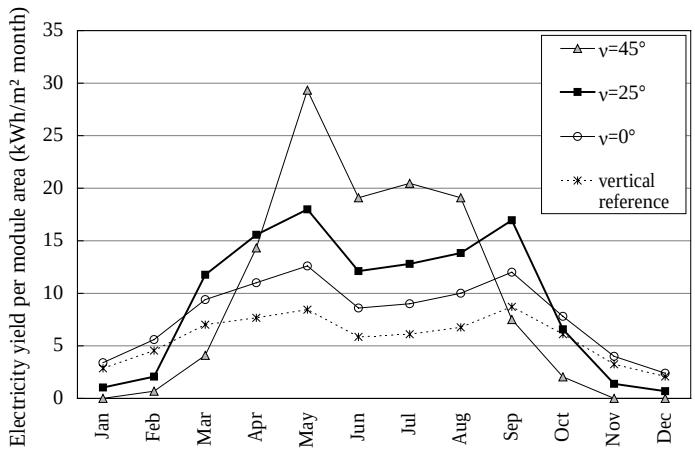

Figure 8.9 *Annual distribution of the electricity yield per module area for different system geometries and for the vertical reference cell. The higher the tilt angle of the optical axis, ν, the higher the summer production and the lower the winter production.*

8.7 Conclusions

The aim of this investigation was to find the system geometry that would give the highest energy yield per module area. The simulations showed that the difference in annual yield between the two basic geometries A and B (where the difference is the module tilt angle, β) is fairly small. What is more important is to find the right tilt angle of the optical axis. The choice of the absorber tilt angle is more a matter of fine adjustment.

The presented results suggest that the most efficient system, on an annual basis, should have a tilt angle ν, of 35°. However as long as the inclination is between 25° and 45° the annual yield is not lower than 93% of the maximum yield. At ν = 35° the energy yield of Geometry B is 120 kWh/m^{2}a, i.e. slightly higher than that of Geometry A, which is 118 kWh/m^{2}a. As Geometry B has a slightly higher concentration ratio there is a chance that it could be cheaper to produce, although this must be further investigated before a conclusion can be made.

The results show that the annual energy yield per module area will increase with a higher tilted optical axis, up to where the tilt of the optical axis, ν, is 35° and 45° respectively for Geometry A and B. The backwards-tilted parabolic reflector has a larger vertical area compared to the module area and thus a higher geometrical concentration ratio. This means that the cost effectiveness of the whole concentrating system also may be improved by increasing the tilt of the optical axis.

However, a highly tilted optical axis gives a high energy generation in summer at the expense of a lower generation in winter, and vice versa. Which design is the more suitable, must therefore be estimated from considerations of the patterns of energy demand. Of course, if the system is grid connected, the immense energy demand makes this aspect unimportant, and the inclination of the optical axis should then be 35°. Otherwise it would be reasonable to suggest a system where the inclination of the optical axis is between 25° and 35° and the absorber tilt angle is positive, to give a fairly well balanced energy output over the year. The original design, Geometry A, is therefore considered a good design for southern Sweden.

Another aspect is the cost of the façade. The building element consists of glazing, insulation wires etc. and the cost of these materials, as well as the modules, should preferably be covered by the energy savings per *glazed area* of the building element, or at least be kept at a reasonable level. However, since it is not uncommon that a large amount of money is spent on façade material, this design may be a very price worthy solution. Also, the collector could very well give an aesthetically appealing façade.

The anodised aluminium offers good solar reflectance but there are also other reflector materials available, which give considerably higher solar reflectance. For example, Miro sheets from Alanod have a solar reflectance of 90% at normal incidence (Brogren et al., 2000). By using these materials the system performance could be increased by almost 10 %, although at a higher cost.

In a line-focusing concentrating system, such as the parabolic reflector system optimised in this work, the concentration of solar radiation may result in high cell temperatures, which will decrease the efficiency of the system. One way of eliminating, or at least significantly reducing ,

this problem is to cool the photovoltaic modules. There are several cooling methods available, but work by Edenburn (1980) and by Rönnelid et al. (1999) indicates that active water cooling is the most cost effective method for low-concentrating line-focusing systems. In addition to increasing the electric power by reducing the cell temperature, if operated at medium temperatures (about 30–55°C depending on cell type), active water cooling makes it possible to utilize the warm water produced for heating or pre-heating of domestic hot water or space heating. If a hybrid absorber is considered, the demand of thermal energy and the pattern of the heating demand should preferably also be considered in the geometrical design of the collector.

Further research on the costs of the materials and the production of the collector is required before a final statement can be made about which geometry and materials to choose in order to minimize the energy costs.

It can be concluded that the use of photovoltaic modules and parabolic aluminium reflectors in static, low-concentrating systems designed for building integration has a potential to significantly increase the annual electricity production per cell area, compared to planar vertical modules of the same type. Given the low cost of the highly reflective anodised aluminium mirrors and the insulation material in combination with a simple manufacturing process, the kinds of systems evaluated in this work have a potential to reduce the cost of solar energy.

9 Summary and discussion

The objective of this work has been to find good design solutions for cost effective solar thermal collectors and solar thermal systems. The focus concerning the collectors has been set on concentrating, building integrated collector designs, as these are features that give potential for cost effective products. Collector designs for façade integration and roof integration are investigated. The work on solar thermal systems is intended to highlight important aspects of system design and also to show examples of how to integrate collectors into buildings, depending on different circumstances.

9.1 Collector designs

The collector designs discussed in this work are concentrating designs intended for integration into building elements. The ideas for this type of concentrating collectors are not entirely new, but they have been modified for different applications.

9.1.1 Roof integrated designs

The evaluated collector designs intended for integration in non-insulated roofs are interesting as they are rather thin, they only use little insulation material, and the use of commonly used corrugated steel for the collector box should make the production cheap and easy. It should therefore be easy to integrate the collectors as roofing material that could be produced in optional lengths and the assembly and the installation should be easily performed. The results of the evaluation showed that the maximum annual energy output per glazed collector area would be 320 kWh/m^2, 330 kWh/m^2 and 280 kWh/m^2, for the evaluated Collectors A, B and C respectively, in Stockholm climate, at an operating temperature of 50°C and with 45° tilt angle. These results are slightly lower than desired. Collector B, with the narrow strip absorber and circular reflector, is considered the most promising design, as it shows the lowest heat loss coefficient and

only requires little absorber material in comparison to the flat reference collector, Collector A. Although the concentrating Collector C, with the tubular absorber, would most likely be the cheapest to produce it also involves rather high heat losses. Before any of these collectors are produced on a larger scale it is desirable to further reduce the heat losses.

A suggestion for further development is to decrease the acceptance angle of the reflectors of Collector B to enhance the concentration on the absorber. As the collectors are designed today they can be mounted with the absorbers either in the north-south or the east-west direction. If Collector B is mounted with the absorbers in the north-south direction it is important to keep the acceptance interval at 80° at the least, in order to have the collector operating at least 5 hours in the middle of the day in summer.

After the experimental tests with these collectors were finished, a similar concentrating collector, well suited for integration in non-insulated roofs, with higher concentration ratio, has been developed by a private investor (Solarus, 2008) and is now available on he market.

9.1.2 Façade integrated designs

The geometry of a concentrating façade integrated PV/thermal hybrid collector for higher latitudes, e.g. southern Sweden, has been optimised for maximal annual energy generation. The collector has enough back insulation to allow it to be part of a façade element and it is flexible for production in variable lengths.

If the inclination of the optical axis of the parabolic reflector is increased, it gives a higher concentration ratio, meaning a lower requirement of module area per façade area. The results from measurements and simulations show that best results are achieved for geometries where the inclination of the optical axis is between 25° and 45°. In this range of angles the results do not depend so much on the tilt angle of the module plane. The maximum annual electricity production for a photovoltaic cell in the evaluated concentrating systems was found to be 120 kWh/m² per module area, 72% higher than that of the unshaded vertical reference module. This result was obtained for a system with a tilt of the optical axis, ν, of 35°, and with the concentration ratio, C = 4.65. With this geometry the module plane is tilted backwards, β = -25°, which means that no direct irradiation can fall on the module without reflection on the reflector, implying lower energy generation for low solar altitudes. A high tilt of the optical axis gives a high energy generation in summer at the expense of a lower generation in winter. Which design is the more suitable, must therefore be estimated from considerations of the patterns of energy demand. As it

is often is desired to achieve a more evenly distributed solar energy yield over the year the previously designed prototype with $\nu = 25°$, $\beta = 20°$ and C=2.96 also seems a promising design, which also gives relatively high total annual output.

For photovoltaic cells accepting concentrated light, cooling is very important in order not to reduce the efficiency. There are even risks of damaging the cells at too high concentration on the cells. Therefore, if photovoltaic cells are to be applied in this system, a promising design feature is to use a combined solution for cooling of the photovoltaic cells and thermal energy generation.

It could also be considered to produce this collector design with only thermal absorbers, as the optimisation is just about finding the design that accepts the most irradiation.

9.1.3 Future development

For both the roof integrated and the façade integrated collector designs it would be of interest to further investigate the production costs.

Another interesting idea for further work is to design and investigate the performance of a concentrating collector based on an evacuated tube collector with reflectors for higher irradiance. It could be either for roof or façade integration. Evacuated tube collectors are well suited for high temperatures as the heat losses are so low.

9.2 Solar thermal system designs

There is a great variation in design of the solar thermal systems used today and it is difficult to find direct answers to how to best design a solar thermal system, as every system is unique and as the energy demand depends on the users and their habits. However, the importance of knowing the energy demand and its distribution over the year, before designing a solar thermal system, should be stressed.

As solar thermal energy is only complementary to other energy sources it is also important to find the best auxiliary energy source for the system, or a system design that is suitable for combining solar thermal energy with the chosen auxiliary energy source. In the same way as e.g. heat pumps, solar collectors are preferably operated at low temperatures, which can cause a difficulty in priority between the two components. Often it is more suitable to combine solar collectors with a pellet boiler which is operated at high temperatures, and it is also beneficial to be able to shut off the

boiler during summer. However, it also depends much on the design and the temperature requirements of the heating system in the building.

Solar thermal system designs have been discussed in this work with the focus on different aspects. In Chapter 4 solar systems are investigated with the focus on houses with low energy demand and in Chapter 7 several features of solar systems are investigated in the analysis of a grid connected solar thermal system with façade integrated collectors.

9.2.1 Solar systems for houses with low energy demand

The work performed for the International Energy Agency, Task 28 – *Sustainable solar housing* shows different solutions of how to reduce the emissions of greenhouse gases and the use of non-renewable energy in buildings.

It is discussed that from an economical point of view it is not always evident to design a high performance house with a hot water radiant heating system, as it could be sufficient to heat the house with low power heat in the supply air. This is demonstrated in Solution 1a, an extremely well insulated building that only requires very low power for space heating, which is why there is no water based heating system, just an electric resistance heater in the ventilation system. In order to reach the target of non-renewable energy use of maximum 60 kWh per living area and year, solar energy is used for heating domestic hot water, replacing electric resistance heating.

For a building with slightly lower insulation standards, as in Solution 2, the higher space heating demand means that higher power is required. Therefore it is suitable to use a water based heating system that can give higher power to the building. Only renewable energy is used, bio pellets and solar energy, in a solar combi system, i.e. a water based heating system where solar energy can contribute to the heating of both domestic hot water and space heating. This solution is by far the best from an environmental point of view, as the resulting green house gas emissions are less than half the emissions of Solution 1a. This shows the importance of using renewable energy even where the building envelope is very well insulated.

The break point where the space heating demands are so low that a water based heating system is not economically justified must be defined in each case separately as the cost of a heating system and the solar collector gains depends on the building design and the users' habits of energy use.

Evacuated tube collectors are suitable for use on these buildings with their shortened heating season, as they use low irradiation very well.

Another aspect of combi systems is that the use of a common storage tank for space heating and hot water heating may be beneficial to the system efficiency as the heat withdrawal from the tank due to space heating demands can lower the tank temperature and increase the solar collector efficiency.

9.2.2 Solar system design features

The solar thermal systems for low energy houses were designed to almost cover the summer energy demand. This strategy was chosen so as not to overdimension the system and risk overheating, although there are means to deal with this issue today, such as the use of partial evaporation of the collectors. This strategy was applied for both solar domestic hot water systems and solar combi systems, as the benefits from designing larger solar combi systems for high performance houses are few. Most of the presented results for solar thermal systems in high performance houses are applicable also for standard houses, particularly for solar domestic hot water systems. For combi systems in standard houses it can be interesting to design the collector slightly larger if good overheating protection is applied.

One of the parametric studies shows how much the collector area needs to be increased when the tilt angles are higher or lower than the optimal angle for summer production, and shows the solar fraction to be expected for different tilt angles.

It is also shown that the volume of the storage tank has a fairly low influence on the energy output, although a minimum volume is crucial and too large a tank gives unwanted heat losses.

According to simulation results an external heat exchanger with a stratifying unit is a more profitable design compared to internal heat exchangers. For internal heat exchangers a higher flow rate gives higher output while a lower flow is more beneficial when an external heat exchanger is used, as the tank water can be kept well stratified.

9.2.3 Beneficial circumstances for investments

A good advice concerning investments in solar thermal systems is to install them when other investments are required, such as a new hot water tank, a new boiler or new roof or façade material, so that good planning and lower costs can be achieved.

The solar thermal system described in Chapter 7, which is delivering heat to the forward side of the district heating system in Malmö, has been installed as a replacement of the old façade. This is why the five large col-

lectors are integrated in different directions in the façade. The flow through the different collectors are controlled by an advanced control system.

As the system in question is connected to the district heating system, the temperatures are important. The temperature delivered to the forward side must be high enough to give thermal comfort in the buildings, yet low enough not to cause to high thermal losses. Because of this, one of the most important issues is the location of the system. This system is placed in the outer parts of the district heating grid, which means that the temperature requirements are not as high as for some of the other production plants in the district heating system. The minimum temperature for delivery to the grid is 70° and the buildings in this particular area were actually designed to maintain thermal comfort with only 65°. This is another beneficial circumstance, as it facilitates the delivery of heat with only low heat losses.

For locations in the city where land is expensive, integration into the façades is an interesting feature from an economic point of view.

9.2.4 Important design features of automated systems

An important feature of the above mentioned system (discussed in Chapter 7) is the highly automated and robust control system which makes the system as reliable as it has proved to be. One very important aspect is the overheating protection. In case of overheating, the collectors are automatically evacuated, by partial evaporation, a practice which is increasingly common today. Nevertheless it is important to point out the importance of this feature.

Other features are the many control strategies to stop the delivery of energy to the grid when temperatures are too low or the alarm transmitted when the system is short of electricity.

9.3 Future outlook

The world may soon be facing an environmental disaster if we do not take action now to mitigate the climate changes. Solar energy is one part of the solution that must be found. With solar thermal energy there is potential for significant reductions of green house gas emissions and therefore we need to use it much more than today.

It is hoped that the presented results and observations concerning design features of solar collectors and solar thermal systems can provide inspira-

tion for product developers, architects, constructors, building owners or anyone interested in these matters.

It would be beneficial to the building industry if more prefabricated building integrated solar collectors were available on the market, as they give potential for cost reductions in terms of saved time and material and bought energy. The use of building integrated collectors can also give a building an interesting and aesthetically appealing façade.

It is important that the issue of energy use is put on the top of the agenda when planning for new buildings, in order to enable the implementation of cost effective solutions that can reduce energy use. Today this issue is often brought up too late in the construction process, leading to an excessive use of energy in the final construction.

We should use solar energy in the best possible way. This means taking into account all technical facts and other important information, such as user behaviour, available energy systems and location, that can improve the function and cost effectiveness of solar energy systems.

References

Adsten, M. (2002) *Solar thermal collectors at high latitudes. Design and performance of non-tracking concentrators*. Doctoral thesis, Uppsala University, Sweden. ISBN 91-554-5274-4.

Adsten, M., Helgesson, A. & Karlsson, B. (2005) Evaluation of CPC-collector designs for stand-alone, roof- or wall installations. *Solar Energy 79* (6), pp 638-647.

Brogren, M., Nostell, P. & Karlsson, B. (2000) Optical efficiency of a PV-thermal hybrid CPC-module for high latitudes. *Solar Energy 69* (1-6), pp. 173-185.

Brogren, M., Wennerberg, J., Kapper, R. & Karlsson, B. (2003) Design of concentrating elements with CIS thin-film solar cells for façade integration. *Solar Energy Materials and Solar Cells 75* (3 4) pp. 567-575.

Butti, K. & Perlin, J. (1980) *A golden thread: 2500 years of solar architecture and technology*, Palo Alto, California. ISBN: 0-917352-07-6

Chant, V.G. & Håkansson, R. (1985) *The MINSUN simulation and optimisation program, Application and users guide*. A report for IEA SH & C, Task VII, Ottawa.

Dalenbäck, J.O. (2005) *Solar thermal market development in Europe*, Proceedings of Northsun 2005, Vilnius.

Dessus, B. & Pharabod, F. (2000) *Vad vet jag om solenergi*, Presses Universitaires de France, ISBN 91-88992-28-4.

Doebelin, E.O. (1990) *Measurement Systems Application and Design*, Chpt 8.4, ISBN 0-07-100697 4

Duffie, J.A. & Beckman, W.A. (1991) *Solar Engineering of Thermal Processes*, 2nd edn. Wiley Interscience, New York.

Edenburn, M. W. (1980) *Active and passive cooling for concentrating photovoltaic arrays*, Fourteenth IEEE Photovoltaic Specialists Conference 1980, San Diego, USA.

ESTIF (2006) *Solar thermal markets in Europe, trends and market statistics 2005*, Report from ESTIF, European Solar Thermal Industry Federation, www.estif.org.

ESTIF (2007) *Solar thermal action plan for Europe, heating and cooling from the sun*, Report from ESTIF, European Solar Thermal Industry Federation, www.estif.org.

Eur'ObservER (2007) *Solar Thermal Barometer*, Systemes Solaires – Le Journal des Energies Renouvelables n° 180, 2007. www.energies-renouvelables.org.

European Commission (1997) *Energy for the future: renewable sources of energy, White paper for a community strategy and action plan*, COM(97)599 final (26/11/1997). http://europa.eu/documents/comm/white_papers/pdf/com97_599_sv.pdf

Frank, E. (1959) *Electrical measurement analysis*, chapters 10 and 13, McGraw-Hill, New York.

Gajbert, H. (2007) Using active solar energy in *Sustainable Solar Housing, Vol. 1: Strategies and Solutions*, Hastings, R. & Wall, M. (editors), pp 28-32, ISBN 978-1-84407-325-2, Earthscan, London.

Gajbert, H. & Smeds, J. (2007) Apartment building in the cold climate, Renewable Energy Strategy, in *Sustainable Solar Housing, Vol. 1: Strategies and Solutions*, Hastings, R. & Wall, M. (editors), pp 156-170, ISBN 978-1-84407-325-2, Earthscan, London.

GEMIS (2004) GEMIS: *Global Emission Model for Integrated Systems*, Öko-Institut, Darmstadt, Germany.

Hastings, R. & Wall, M. (2007) Editors, *Sustainable Solar Housing, Vol. 1: Strategies and Solutions*, ISBN 978-1-84407-325-2, Earthscan, London.

Hausner, R. & Fink, C. (2002) *Stagnation behaviour of solar thermal systems*, A Report of IEA SHC – Task 26, AEE INTEC, Austria. http//www.iea-shc.org/.

Heidt, F.D. (1999) *Bilanz Berechnungswerkzeug*, NESA-Datenbank, Fachgebiet Bauphysik und Solarenergie, Universität-GH Siegen, D-57068 Siegen, Germany

Hellström, B, (2005) *Calculation and measurement methods for the performance of solar collectors.* Doctoral thesis, LTH, Lund University, Sweden. ISBN 91-85147-06-0.

Håkansson, H. & Fredlund, B. (1999) *A new solar simulator facility for calorimetric measurements on windows and shading devices* in 5th symposium on Building Physics in the Nordic Countries, Gothenburg.

Håkansson, H. (2003 a) *A parallel beam solar simulator for testing of solar components*, Proceedings of ISES Solar World Congress 2003, Gothenburg, Sweden.

Håkansson, H. (2001) Solar laboratory, in *Solar Protection in Buildings*, Wall M., Bülow-Hübe H. (editors), pp. 49-66, Lund University. ISRN LUTAD/TABK--3060-SE.

Håkansson, H. (2003 b) Solar laboratory, *In Solar Protection in Buildings: Part 2*, Wall M., Bülow-Hübe H. (editors), pp. 29-67, Lund University. ISBN 91-85147-00-1.

Johansson, L., Gustafsson, L., Tullin, C. & Cooper, D. (2003) *Emissions from domestic bio-fuel combustion, calculations of quantities emitted*, SP Report 2003:08, SP Technical Research Institute of Sweden, Borås, Sweden. ISBN 91-7848-939-3.

Karlsson, B. & Wilson, G. (2000) *MaReCo design for horizontal, vertical or tilted installation*. Proceedings of Eurosun 2000, Copenhagen, Denmark.

Kjellsson, E. (2004) *Solvärme i bostäder med analys av kombinationen solfångare och bergvärmepump*, Licentiate thesis, Lund University, Sweden, report TVBH--04/3047--SE(170), ISBN 91-88722-32-5.

Kovacs, P. & Pettersson, U. (2002) *Solvärmda kombisystem, en jämförelse mellan vakuumrör och plan solfångare genom mätning och simulering*, SP rapport 2002:20, SP Technical Research Institute of Sweden, Borås, Sweden, ISBN 91-7848-912-1.

Kvist, H. (2005) *DEROB-LTH for MS Windows, User Manual Ver. 1.0 –20050813*. Energy and Building Design, Lund University, Sweden. www.derob.se.

Larsson, S. (2006) http://www.maston.se/melacs

Mallick, T.K., Eames, P.C., Hyde, T.J. and Norton, B. (2004) The design and experimental characterisation of an asymmetric compound parabolic photovoltaic concentrator for building façade integration in the UK, *Solar Energy 77*, pp 319-327.

Mallick, T.K., Eames, P.C., and Norton, B. (2006) Non-concentrating and asymmetric compound parabolic concentrating building façade integrated photovoltaics: An experimental comparison, *Solar Energy 80* (7), pp 834-849.

McIntire, W.R., (1982) Factored approximations for biaxial incident angle modifiers. *Solar Energy 29* (4), pp 315-322.

Meteotest (2004) *Meteonorm 5.0 – Global Meteorological Database for Solar energy and Applied Meteorology*, Bern, Switzerland. (www.meteotest.ch).

Meteotest (2006) www.meteotest.ch, 2006-12-04.

Morhenne, J. (2000) Chapter V, Controls, *Solar Air Systems, A Design Handbook*, James & James Ltd., London, ISBN 1 873936869.

Nilsson, J., Brogren, M., Helgesson, A., Roos, A. & Karlsson B. (2006) Biaxial model for the incidence angle dependence of the optical efficiency of photovoltaic systems with asymmetric reflectors, *Solar Energy 80*, pp 1199 1212.

Nilsson, J. (2005) *Optical design and characterisation of solar concentrators for photovoltaics*, Licentiate thesis, Lund University, report EBD-T--05/6, ISBN 91-85147-15-X.

Nostell, P., Roos, A. & Karlsson, B. (1998) Aging of Solar Booster Reflector Materials. *Solar Energy Materials and Solar Cells 54*, pp 235-246.

Perers, B. & Karlsson, B. (1993) External reflectors for large solar collector arrays, simulation model and experimental results. *Solar Energy 51* (5), pp 327-337.

Perers, B. (1993) Dynamic method for solar collector array testing and evaluation with standard database and simulation programs. *Solar Energy 50* (6), pp 517-526.

Petersdorf, C. & Primas, A. (2007) Primary energy and CO2 conversion factors, in *Sustainable Solar Housing, Vol. 1: Strategies and Solutions*, Hastings, R. & Wall, M. (editors), pp 281-284, ISBN 978-1-84407-325-2, Earthscan, London.

Polysun (2002) *Polysun 3.3, Thermal solar system design, User's manual*, SPF, Institut für Solartechnik, Rapperswil, Switzerland. www.solarenergy.ch.

Russ, C. (2005) *Demonstration buildings, design, monitoring and evaluation* (Task 28, Subtask D), http//www.iea-shc.org.

Rönnelid, M. (1998) *Optical Design of Stationary Solar Concentrators for High Latitudes*, Doctoral thesis, Uppsala University, Sweden, ISBN 91-554-4170-X.

Rönnelid, M., Perers, B., Karlsson, B. & Krohn, P. (1999) *Cooling of PV modules equipped with low-concentrating CPC reflectors*. Proceedings of the ISES Solar World Congress 1999, Jerusalem.

Shell Solar, (2003) Shell Solar Product Information Sheet, Shell ST10 Photovoltaic Solar Module.

Smeds, J. & Gajbert, H. (2007) Apartment buildings in the cold climate, conservation strategy, in S*ustainable Solar Housing, Vol. 1: Strategies and Solutions*, Hastings, R. & Wall, M. (editors), pp 150-156, ISBN 978-1-84407-325-2, Earthscan, London.

Smeds, J. (2007) Cold climate design in *Sustainable Solar Housing, Vol. 1: Strategies and Solutions*, Hastings, R. & Wall, M. (editors) pp 103-114, ISBN 978-1-84407-325-2, Earthscan, London.

Solarus (2008) www.solarus.se, 2008-05-11.

Swedish Energy Agency (2006) *Energiläget 2006*, Eskilstuna, www.energimyndigheten.se.

Swedish Ministry of Enterprise, Energy and Communications (2007) *Årlig rapportering från det statliga bidraget till investeringar i solvärme* (SFS 2000:287), verksamheten 2006. Report Dnr: 00-05-06111.

Thür, A. & Weiss, W. (2005) *Success of solar heating in Austria*, Proceedings of Northsun 2005, Vilnius.

Wall, M. (2007) Solution examples in *Sustainable Solar Housing, Vol. 1: Strategies and Solutions*, Hastings, R. & Wall, M. (editors), pp 95-101, ISBN 978-1-84407-325-2, Earthscan, London.

Weiss, W., (editor) (2003) *Solar Heating Systems for Houses, A Design Hand Book for Solar Combisystems*, James & James Ltd., London.

Weiss, W., Bergmann, I. & Faninger, G. (2006) *Solar heat worldwide, markets and contribution to the energy supply 2004*, International Energy Agency, Solar Heating & Cooling Programme, Graz, Austria.

Welford, W.T., & Winston, R. (1989) *High Collection Nonimaging Optics*. Academic Press Inc., San Diego, California. ISBN 0127428852.

Winston, R. (2001) *Solar Concentrators, in Solar Energy, The State of the Art*, Gordon, J. (editor), pp 357-436, James & James Ltd., London.

Zacharopoulos A., Eames P.C., McLarnon D. & Norton B. (2000) Linear dielectric non-imaging concentrating covers for PV integrated building façades, *Solar Energy 68* (5), pp 439-452.

Appendix A

Equations of the involute and the semi parabola

A.l Derivation of involute equations

The equations 41 and 42 for the involute presented in Section 2.5.2 are derived from the figure shown below.

$$x = r\sin\sigma - r\sigma\cos\sigma \qquad \text{Eq. (41)}$$

$$y = -r\cos\sigma - r\sigma\sin\sigma \qquad \text{Eq. (42)}$$

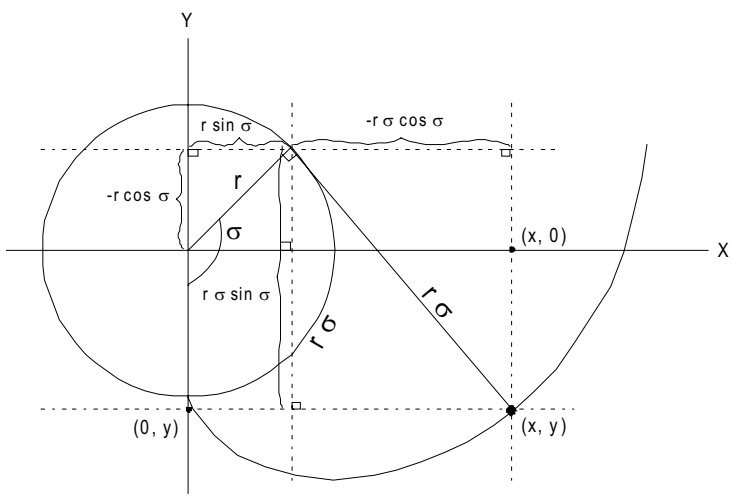

A.II Equations of the semi parabola

These are the equations that were used for the semi parabola shown in Figure 2.14. This geometry was also used in the design of the Collector C in Chapter 5.

$$x = r \cdot \sin\sigma - r \cdot \cos\sigma \cdot \frac{\sigma + \theta_{a/2} + \pi/2 - \cos(\sigma - \theta_{a/2})}{1 + \sin(\sigma - \theta_{a/2})} \qquad \text{Eq. (42)}$$

$$y = -r \cdot \cos\sigma - r \cdot \sin\sigma \cdot \frac{\sigma + \theta_{a/2} + \pi/2 - \cos(\sigma - \theta_{a/2})}{1 + \sin(\sigma - \theta_{a/2})} \qquad \text{Eq. (43)}$$

Appendix B

Design parameters used in the work for IEA, Task 28 – Sustainable solar housing

B.I Design parameters used in DEROB-LTH simulations

B.I.I Solution 1a

These following assumptions and parameters were applied in the simulations of a high performance building that is presented in Solution 1a in Section 4.3.3.This information can also be found in (Smeds & Gajbert, 2007).

Table B.1 Design parameters of the building envelope construction in Solution 1a: Conservation strategy. Space heating with electric resistance in the supply air and solar heating of the DHW.

	Material	Thickness	Conductivity	Percent	Studs	Studs	Resistance without Rsi, Rse	Resistance with Rsi, Rse	U-value
		m	λ (W/mK)	%	λ (W/mK)	%	(m^2K/W)	(m^2K/W)	(W/m^2K)
wall	exterior surface							0.04	
	wooden panel	0.045		100%					
	air gap	0.025		100%					
	mineral wool hd	0.050	0.030	100%			1.67		
	mineral wool	0.250	0.036	85%	0.14	15%	4.84		
	plastic foil			100%					
	mineral wool	0.050	0.036	85%	0.14	15%	0.97		
	plaster board	0.013	0.220	100%			0.06		
	interior surface							0.13	
		0.433					7.54	7.71	0.130
roof	exterior surface							0.04	
	roof felt	0.003		100%					
	mineral wool hd	0.050	0.030	100%			1.67		
	mineral wool	0.350	0.036	100%			9.72		
	plastic foil			100%					
	concrete	0.15	1.700	100%			0.09		
	interior surface							0.10	
		0.553					11.48	11.62	0.086
floor	exterior surface								
	mineral wool	0.300	0.036	100%			8.33		
	concrete	0.150	1.700	100%			0.09		
	interior surface							0.17	
		0.450					8.42	8.59	0.116
window				emissivity					
	pane	0.004	low emissivity	5%	reversed				
	gas	0.012	krypton						
	pane	0.004	clear	83.70%					
	gas	0.012	krypton						
	pane	0.004	low emissivity	83.70%					
		0.036							0.800
	frame	0.093	wood		0.14		0.66	0.83	1.20

The U-value of the whole building envelope is 0.21 W/m^2K.

B.I.II Solution 1b

These following assumptions and parameters were applied in the simulations of a high performance building that is presented in Solution 1b, which is briefly discussed for comparison of the other solutions in Sections 4.3.6 and 4.4. This information can also be found in (Smeds, 2007).

Table B.2 Design parameters of the building envelope construction in Solution 1b: Energy conservation with district heating for space heating and heating of DHW.

	Material	Thickness	Conductivity	Percent	Studs	Studs	Resistance without Rsi, Rse	Resistance with Rsi, Rse	U-value
		m	λ (W/mK)	%	λ (W/mK)	%	(m^2K/W)	(m^2K/W)	(W/m^2K)
wall	exterior surface							0.04	
	wooden panel	0.045		100%					
	air gap	0.025		100%					
	mineral wool hd	0.030	0.030	100%			1.00		
	mineral wool	0.100	0.036	85%	0.14	15%	1.94		
	plastic foil			100%					
	mineral wool	0.050	0.036	85%	0.14	15%	0.97		
	plaster board	0.013	0.220	100%			0.06		
	interior surface							0.13	
		0.263					3.97	4.14	0.242
roof	exterior surface							0.04	
	roof felt	0.003		100%					
	mineral wool hd	0.030	0.030	100%			1.00		
	mineral wool	0.100	0.036	100%			2.78		
	plastic foil			100%					
	concrete	0.15	1.700	100%			0.09		
	interior surface							0.10	
		0.283					3.87	4.01	0.250
floor	exterior surface								
	mineral wool	0.110	0.036	100%			3.06		
	concrete	0.150	1.700	100%			0.09		
	interior surface							0.17	
		0.260					3.14	3.31	0.302
window				emissivity					
	pane	0.004	low emissivity	5%	reversed				
	gas	0.012	krypton						
	pane	0.004	clear	83.70%					
	gas	0.012	krypton						
	pane	0.004	clear	83.70%					
		0.036							0.800
	frame	0.093	wood		0.14		0.66	0.83	1.20

The U-value of the whole building envelope is 0.34 W/m^2K.

B.I.III Solution 2

These following assumptions and parameters were applied in the simulations of a high performance building that is presented in Solution 2 in Section 4.3.4. This information is also presented in (Gajbert & Smeds, 2007).

Table B.3 Design parameters of the building in Solution 2.

	Material	Thickness	Conductivity	Percent	Studs	Studs	Resistance without Rsi, Rse	Resistance with Rsi, Rse	U-value
		(m)	λ (W/mK)	(%)	λ (W/mK)	(%)	(m^2K/W)	(m^2K/W)	(W/m^2K)
wall	exterior surface							0.04	
	wooden panel	0.045		100%					
	air gap	0.025		100%					
	mineral wool hd	0.030	0.030	100%			1.00		
	mineral wool	0.100	0.036	85%	0.14	15%	1.94		
	plastic foil			100%					
	mineral wool	0.030	0.036	85%	0.14	15%	0.58		
	plaster board	0.013	0.220	100%			0.06		
	interior surface							0.13	
		0.243					3.58	3.75	0.267
roof	exterior surface							0.04	
	roof felt	0.003		100%					
	mineral wool hd	0.015	0.030	100%			0.50		
	mineral wool	0.100	0.036	100%			2.78		
	plastic foil			100%					
	concrete	0.15	1.700	100%			0.09		
	interior surface							0.10	
		0.268					3.37	3.51	0.285
floor	exterior surface								
	mineral wool	0.110	0.036	100%			3.06		
	concrete	0.150	1.700	100%			0.09		
	interior surface							0.17	
		0.260					3.14	3.31	0.302
window				emissivity					
	pane	0.004	clear	83.70%					
	gas	0.015	air						
	pane	0.004	low emissivity	4%					
		0.023							1.400
	frame	0.093	wood		0.14		0.66	0.83	1.20

The U-value of the whole building envelope is 0.41 W/m^2K.

B.I.IV The reference apartement building for the cold climate

The following parameters were used for the energy balance calculations of the apartment reference building for the cold climate. The calculations were performed according to EN 832. The values are based on national building codes in countries in colder regions such as e.g. Scandinavia. These values have been somewhat modified (lower u-values etc.) since the standard in Sweden includes heat recovery. Read more about this in the handbook.

Table B.4 Parameters used for the reference building.

Ventilation (ach)	0.4
Infiltration (ach)	0.2
Heat recovery (%)	0.0
U-value wall (W/m^2K)	0.20
U-value window (W/m^2K)	1.81
U-value roof (W/m^2K)	0.19
U-value floor (W/m^2K)	0.20
U-value building (W/m^2K)	0.29

B.II Design parameters used in Polysun simulations

These parameters were used for the POLYSUN simulations of the solar systems designed for the work within IEA, Task 28, which is presented in Section 4.3. This information is also found in Gajbert& Smeds, (2007) and Smeds and Gajbert(2007).

Table B.5 Parameters used in Polysun simulations.

Parameter	**Value**
The Pipes of the solar circuit	
Pipe material	copper
$\varnothing_{inside}$	16 mm
$\varnothing_{outside}$	18 mm
Length indoors	24 m
Length outdoors	6 m
Thermal conductivity, λ, of pipe	0,040 W/mK
Thermal insulation thickness	25 mm
Collector circuit	
Pump power	210 W
Collector circuit flow	525 l/h
Specific throughput	7 l/h,m^2
Heat transfer medium	water (50%), glycol (50%)
Power output to heat transfer medium	60%
Heat exchanger in solar circuit	
Heat transfer rate k · A for heat exchanger	5000 W/K
Tank	
Volume	4 m^3
Height	4 m
Temperature in the tank room	15°C
Thermal insulation of the tank	150 mm

B.III Primary energy and CO_2 conversion factors

The factors for calculation of primary energy use and emissions of CO_2 equivalent that are used for the simulation work within IEA, Task 28 are presented in Table B.6. The factors are based on the GEMIS tool (GEMIS, 2004). This work was presented by (Petersdorf & Primas, 2007).

Table B.6 Primary energy and CO_2 conversion factors.

Primary Energy and CO_2 conversion factors	**PEF** (kWh_{pe}/kWh_{end})	**CO_2 eq** (g/kWh)
Oil-lite	1.13	311
Natural gas	1.14	247
Hard coal	1.08	439
Lignite	1.21	452
Wood logs	0.01	6
Wood chips	0.06	35
Wood pellets	0.14	43
EU-17 Electricity, grid	2.35	430
District heating CHP-coal cond. 70%, oil 30%	0.77	241
District heating CHP-coal cond. 35%, oil 65%	1.12	323
District heating heating plant; oil 100%	1.48	406
LDH CHP-coal cond. 35%, oil 65%	1.10	127
LDH Heating plant, oil 100%	1.47	323
Local solar	0.00	0
Solar heat (flat) central	0.16	51
PV (multi)	0.40	130
Wind electricity	0.04	20

Paper I

2.5 Using active solar energy

Helena Gajbert

DESIGN ADVICE

The amount of energy to heat domestic hot water is a large fraction of the total energy needed in high-performance housing, and an active solar system can easily cover up to 50 per cent of this demand. Here are example rules of thumb from simulations (see also Part II in this volume).

Suitable dimensions for an example solar system in northern or temperate climates:

An apartment building (approximately 1600 m^2, 16 apartments or 48 occupants):

- Tank volume: 3000–5000 l/building or 60–100 l/occupant.
- Collector area: 30–80 m^2/building or 0.6–1.75 m^2/occupant.

A single family house (approximately 150 m^2, 4 occupants):

- Tank volume: 400–600 l/house or 100–150 l/ occupant.
- Collector area: 5–10 m^2/house or 1.3–2.5 m^2/occupant.

Collector slope:	For domestic hot water (DHW) systems, approximately 40°–50° slope. For combi-systems, the slope is preferably steeper, although a larger collector area is then required.
Economics:	If water-based heat distribution is preferred (i.e. a low temperature floor heating system), a solar combi-system with direct injection of solar heat to the floor heating system is a good approach.

2.5.1 Introduction

Heat captured by an active solar heating system can cover a significant part of the very low energy demand of high-performance houses. Because the space heating demand of such houses is very low, the year-round energy demand for domestic hot water (DHW) becomes relatively important. An active solar system can cover a large part of this energy demand, often more than 50 per cent, since the demand also occurs in summer. The question then is: if there is to be a solar system, would it not be good to enlarge it to also supply some space heating (a 'combi-system')? A key issue, then, is estimating the space heating contribution realistically, given the shorter heating period of high-performance housing.

2.5.2 Solar thermal system designs

If the client desires a water-based heating system, this is a good situation to argue for a solar combi-system. It provides flexibility and there are many interesting system designs on the market, varying by region and the locally used auxiliary energy sources (Weiss, 2003). The storage tank can serve both the DHW and the space heating system, and it can be heated by both the auxiliary and the solar systems, depending on conditions. The system illustrated in Figure 2.5.1 uses a wood pellet boiler and an electric resistance heater as auxiliary energy sources to back up the solar circuit. It is equipped with a device to enhance thermal stratification in the tank. The DHW is heated in an external heat exchanger.

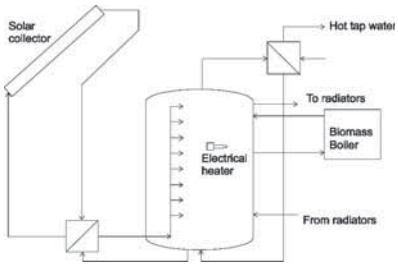

Source: Helena Gajbert, Lund University SE

Figure 2.5.1 *A solar combi-system with a joint storage tank for the domestic hot water (DHW) and space heating systems*

A critical design condition is the case of minimum heat demand by maximum solar gains, as often occurs in summer. To minimize the system overheating in such instances, the solar system should be dimensioned to just cover the summer energy demand, accepting a small solar coverage in winter. Nonetheless, an important advantage is that the combustion backup heating can be shut down during the summer. As a result, short cycling of the back-up system in summer can be eliminated, increasing the life expectancy of the system.

The shorter heating season of a high-performance house results in a more pronounced seasonal mismatch between solar gains and space heating demand than is the case for conventional houses. This is illustrated in Figure 2.5.2, with the case of a reference apartment building in the cold (Stockholm) climate. The DHW demand is here assumed constant over the year, although it is often slightly lower in summer – for example, due to vacations.

The overheating problem could be reduced by installing a larger storage tank than the system design would otherwise require. However, this approach is expensive, takes up more house volume and leads to higher tank heat losses.

There are also good control solutions available – for example, using partial evaporation to empty the collector during stagnation. Active removal of energy transported via the steam during stagnation is also possible with a small volume heat sink. Alternatively, the tank can be cooled down by circulating the heat transfer medium through the collectors at night or by using an air cooler (Hausner and Fink, 2002; Weiss, 2003). However, the more cautious design strategy is to not over-dimension the collector area.

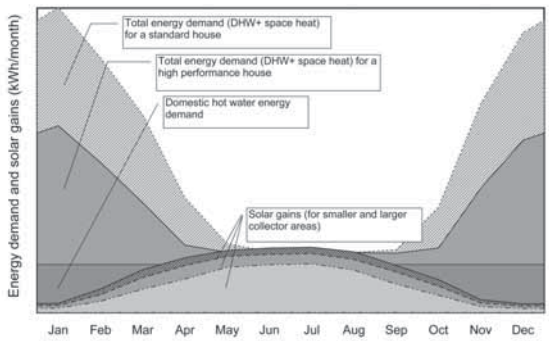

Source: Helena Gajbert, Lund University SE

Figure 2.5.2 *Seasonal variations in solar gains and space heating demand in standard housing versus high-performance housing*

An advantage of a combi-system is that during the heating season, when energy for space heating is withdrawn from the tank, the operating temperature in the collectors can be lowered, increasing the collector efficiency. This typically occurs in autumn and spring. This gain in efficiency can be maximized if the solar collectors supply heat directly to low temperature surface heating, as shown in Figure 2.5.3. This requires a good control strategy. Such systems are common in France, Denmark and Germany (Weiss, 2003).

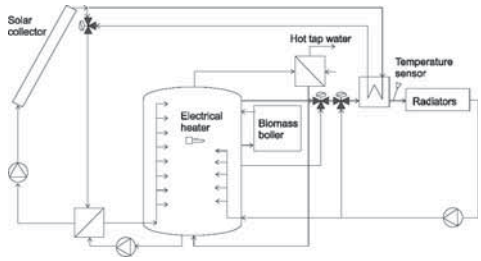

Source: Helena Gajbert, Lund University SE

Figure 2.5.3 *A solar combi-system with the possibility of delivering solar heat directly to the heating system without passing through the tank first*

One way to better balance the solar gains to the heating demand is to mount the collectors vertically on the façade or to mount them with a high tilt. This positioning makes better use of low winter sun angles and suppresses summer overheating. This results in a more even distribution of solar gains over the year; but a larger collector area is required to cover the summer domestic hot water demand. Figure 2.5.4 shows how the solar fraction increases with increased collector area for collectors tilted 40° and 90°. The results are from Polysun simulations of a flat-plate combi-system coupled to a single family house in the cold climate.

A larger collector area is possible without risking overheating if the collector tilt angle is increased in relation to the optimal tilt angle, which approximately lies between 35° in southern latitudes (latitudes around 45°) and 50° in northern latitudes (latitudes around 60°). The suitable collector area to cover 95 per cent of the summer hot water heating demand with minimal system overheating is illustrated in Figure 2.5.5. The results are from Polysun simulations of a flat-plate combi-system coupled to an apartment building in the cold climate.

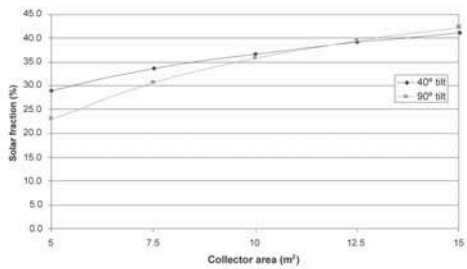

Source: T. Boström

Figure 2.5.4 *Effect of collector tilt and area on solar fraction*

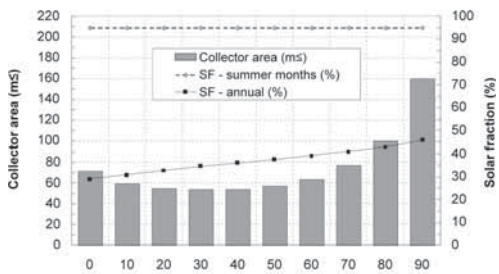

Source: Helena Gajbert, Lund University SE

Figure 2.5.5 *Suitable collector areas at different tilt angles for a collector dimensioned to cover 95% of the summer demand; solar fractions for the year and for the summer are also shown*

Where houses are closely spaced, a micro-heating grid with a central solar system may be plausible. Collectors on the houses then can share a large semi-seasonal solar storage tank enabling some summer solar gain excess to be stored for the autumn. The large tank volume has an advantageous surface-to-volume ratio reducing tank heat loss. A shared system can also even out peak demands or supply excesses. Disadvantages are the relatively high heat losses of the pipe grid relative to the very small space heating demand, and the investment and administrative costs for meeting such a small

demand. Such micro-heat distribution grids for row houses have proven effective in demonstration projects in Germany (Russ, 2005).

2.5.3 Collector types and placement

There are many reliable and efficient collectors and types on the market today.

Flat-plate collectors have been highly optimized with selective coated absorbers, low iron anti-reflective coated glazing, durable frames and gaskets, and effective back insulation.

Evacuated tube collectors, with their extremely good insulation, can operate at higher temperatures with only very small heat losses. Because the losses are so small, evacuated tube collectors can deliver heat even by very low irradiance levels occurring in winter and during overcast periods. They are thus very suitable for high-performance houses with their shortened heating season. The individual tubes can be rotated to an optimal absorber tilt angle, allowing great flexibility in where they are placed. However, the separation between tubes must avoid one shadowing the next. Heat pipe collectors need to be mounted with a slight tilt to allow for the gravity flow. A critical issue is snow retention on the tubes. A façade-mounted system minimizes this problem (Kovacs and Pettersson, 2002).

Concentrating flat-plate collectors can also be envisioned, although such systems are not commercially available for housing. Prototype systems have been built and tested – for example, in Sweden, the UK and Australia. A low-cost reflector increases the irradiance on the absorber. The system geometry can be optimized for spring and autumn solar angles. While this suppresses the summer performance, the solar gains are better balanced to the heating demand over the year. Using an evacuated tube collector as the target of the reflector is a promising solution.

Solar air collectors, while interesting for conventional houses or renovations, are difficult to justify economically for high-performance houses. The heat exchanger of the ventilation system competes with the solar air collectors. One system or the other must operate with decreased efficiency. A plausible configuration would be an entire roof slope covered with a low cost sheet-metal solar air collector. During summer an air-to-water heat exchanger should easily cover all or most of the water heating energy demand. In the autumn and spring, the system could supply much of the space heating. Pre-cast hollow-core concrete floor planks or large core masonry walls can also serve for heat storage and distribution (Morhenne, 2000).

2.5.4 Tank location

The tank location is an important design decision. On the one hand, it is sensible to locate it inside the insulated envelope of the building. Heat losses from even a very well-insulated tank are therefore not lost to the ambient, but remain within the house (although this is a disadvantage in summer). Short pipe runs keep circulation heat losses small. A good location for the tank could be in or next to the bathroom. The warm tank surface improves the comfort in the bathroom. Comfort here is critical because this is often where exhaust air for the whole living space is extracted, and the occupant may be feeling cold after showering. Also, the pipe run is minimized between the tank and one of the biggest points of demand. This decreases pipe heat losses and offers the convenience of immediate hot water at the faucet. An upper floor bathroom is ideal, as the pipe run to roof collectors is also minimized. However, the insulated building interior is a very expensive volume to sacrifice for a tank, so the basement may be the preferred location. This otherwise cold space can then be slightly tempered, improving comfort for the many uses found for a basement. Pipe runs from the tank should be within the heated house envelope as much as possible.

2.5.5 Regional design differences

It is easiest to market a solar combi-system in regions where homeowners prefer hot water radiant heating, particularly low temperature systems. Regions where oil or wood pellet heating is preferred have proven to be good markets for combi-systems, often even large systems. Solar combi-systems have been widely sold in Germany, Austria, Switzerland, Sweden, Denmark and Norway. It seems

more difficult to market combi-systems in regions where mainly direct electricity or gas is used for heating – for example, in The Netherlands (Weiss, 2003).

2.5.6 Conclusions

A solar thermal combi-system can be a valuable component of sustainable housing. The dimensioning and economics of the system have to reflect the very low space heating demand and short heating season. For a high-performance house, a solar domestic hot water system is more easily argued than a solar combi-system, given the more constant demand for hot water over the entire year and the cost of a water-based radiant heat distribution system. If the client desires a radiant heating system, a combi-system is suitable. The DHW and the space heating system can then share a storage tank, which can be heated both by the solar collector and by the auxiliary heat sources. In such an application, a higher collector tilt improves the balance between the space heating demand and seasonal solar gains, although a larger collector area is required to cover the summer demand. Façade-integrated collectors are very suitable and make the system less prone to summer overheating. Capturing and using energy from the sun is a very natural and marketable concept for sustainable low energy housing.

References

Hausner, R. and Fink, C. (2002) *Stagnation Behaviour of Solar Thermal Systems: A Report of IEA SHC – Task 26*, AEE INTEC, Austria, www.iea-shc.org/

Kovacs, P. and Pettersson, U. (2002) *Solvärmda Kombisystem: En Jämförelse Mellan Vakuumrör och Plan Solfångare Genom Mätning och Simulering*, SP rapport 200220, SP Swedish National Testing and Research Institute, Borås, Sweden

Morhenne, J. (2000) 'Controls', in *Solar Air Systems: A Design Handbook*, James and James Ltd, London, Chapter 5

Russ, C. (2005) *Demonstration Buildings: Design, Monitoring and Evaluation*, IEA, Task 28, Subtask D, www.iea-shc.org.

Weiss, W. (ed) (2003) *Solar Heating Systems for Houses: A Design Handbook for Solar Combisystems*, IEA Task 26, James and James Ltd, London,

Paper II

8.7 Apartment building in the Cold Climate Renewable Energy Strategy

Helena Gajbert and Johan Smeds

Table 8.7.1 *Targets for apartment building in the Cold Climate Renewable Energy Strategy*

	Targets
Space heating	20 kWh/m^{2}a
Non-renewable primary energy: (space heating + water heating + electricity for mechanical systems)	60 kWh/m^{2}a

This section presents a solution for the apartment building in the cold climate. As a reference for the cold climate, the city of Stockholm is considered. A balanced mechanical ventilation system with heat recovery is used to reduce the ventilation losses. The solution is based on renewable energy supply.

8.7.1 Solution 2: Renewable energy with solar combi-system and biomass boiler

Building envelope

The apartment building has reinforced concrete structure and wooden frame façades with mineral wool. The U-values are shown in Table 8.7.2. The double-glazed windows have a frame ratio of 30 per cent, one low-e coating and are filled with air. Construction data are found in Table 8.7.7.

Table 8.7.2 *U-values of the building components*

Building component	U-Value (W/m²K)
Walls	0.27
Roof	0.29
Floor (excluding ground)	0.30
Windows (frame + glass)	1.34
Window frame	1.20
Window glass	1.40
Whole building envelope	0.41

Mechanical systems

Ventilation: a balanced mechanical ventilation system with heat recovery and a bypass for summer ventilation is installed. The heat exchanger has an efficiency of 80 per cent. The ventilation rate is 0.045 ach and the infiltration rate is 0.05.

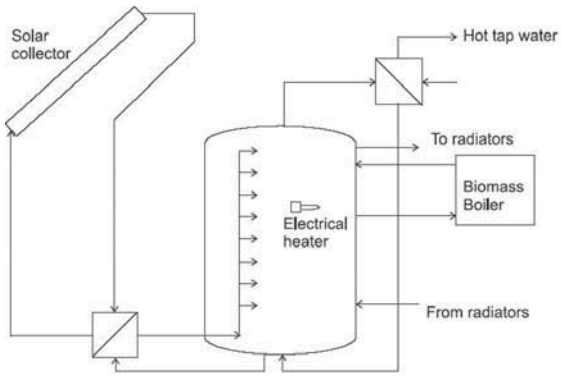

Source: Helena Gajbert and Johan Smeds

Figure 8.7.1 *The design of the suggested solar combi-system with a pellet boiler and an electrical heater as auxiliary heat sources and two external heat exchangers, one for DHW and one for the solar circuit; the latter is attached to a stratifying device in the tank*

Space heating and DHW: a solar combi-system is chosen as the energy supply system for the building – that is, a system where the space heating system and the domestic hot water (DHW) system are combined, here by a joint storage tank, to which both solar collectors and auxiliary energy sources are connected.

The solar thermal heating system consists of 50 m² collectors placed on the south-facing roof, tilted 40°. The storage tank is 4 m² and there is a 35 kW pellet boiler, as well as an electrical heater of 5 kW, connected to it for increased operational flexibility. The heat from the collector circuit is delivered to the tank via an external heat exchanger coupled to a stratifying device, which improves the important thermal stratification in the tank. Another external heat exchanger is used for heating the DHW, taking water from the top of the tank and returning it at the bottom. In the collector circuit,

the liquid heat transfer medium is a mixture of 50 per cent water and 50 per cent glycol. Water from the tank is also used for the radiant hot water space heating system in the building. Other important design parameters of this system can be found in Table 8.7.8. An illustration of the system is shown in Figure 8.7.1.

The electrical heater and the biomass boiler largely working alternately, heating the upper part of the tank when necessary. When only very little auxiliary heat is required during short time intervals, as is often the case in the summer, the biomass boiler operation mode with frequent starts and stops causes unnecessary energy losses. It is therefore suitable to shut off the furnace during summer, when solar energy can cover most of the energy demand. The electrical heater can then be a good complement during cold and cloudy days. The electrical heater can also be used in tandem with the boiler if needed in extremely cold winter days.

An alternative system design for increased efficiency could also include a possibility of delivering solar energy directly to a low temperature radiator heating system when there is prevailing heating demand. Since the collector temperature then can be lowered, heat losses of the system are reduced and the efficiency is increased.

The building is designed according to simulations with DEROB-LTH (Kvist, 2005). Simulations of the active solar energy systems are performed with a modified version of Polysun 3.3 (Polysun, 2002): the Polysun-Larsen version, which uses the data files of space heating demand from the DEROB-LTH simulations. Stockholm climate data from Meteonorm (Meteotest, 2004) are used in both simulation programs. The dimensioning of the solar thermal heating system was performed primarily with a concern for low auxiliary energy use in summer, avoidance of stagnation and overheating, and economical aspects. For general assumptions and parameters used in the DEROB-LTH and Polysun simulations, see Table 8.7.7 and 8.7.8.

Energy performance

Space heating demand: the space heating demand of the building is 30,400 kWh/a (19 kWh/m^{2}a) according to simulation results from DEROB-LTH. The assumed heating set point was 20°C. Maximum room temperature set points were 23°C during winter and 26°C during summer (this assumes the use of shading devices and window ventilation).

The monthly space heating demand for this high-performance case in comparison to a reference building (current building codes year 2001) are shown in Figure 8.7.2. Hourly peak loads of the heating system are calculated with results from DEROB-LTH simulations without direct solar radiation in order to simulate a shaded building. The annual peak load occurs in January and is 26.8 kW (17 W/m^2).

Domestic hot water demand: the net energy demand for domestic hot water is assumed to be 37,800 kWh/a (23.6 kWh/m^{2}a). The DHW demand is thus larger than the space heating demand.

System losses: the system losses consist mainly of losses from the hot water storage tank, but also from circulation losses in the distribution system for DHW. The tank and circulation losses are 1.2 and 4.4 kWh/m^{2}a, respectively. The circulation losses are taken into account as internal gains in the building heat load simulations. The tank losses and losses from the collector circuit can, however, not be used as internal gains since the tank and boiler are placed in the basement outside the thermal envelope of the building. The efficiency of the biomass boiler is set to 85 per cent, resulting in conversion losses of 5.5 kWh/m^{2}a.

Household electricity: the household electricity use is 2190 kWh/a (21.9 kWh/m^{2}a) for two adults and one child in each apartment. The primary energy target does not include household electricity since this factor can vary considerably depending on the occupants' behaviour.

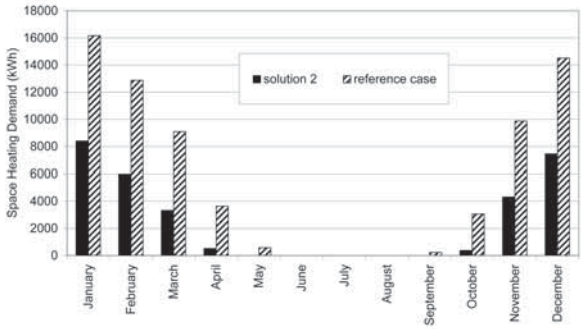

Source: Helena Gajbert and Johan Smeds

Figure 8.7.2 *Monthly values of the space heating demand during one year; the annual total space heating demand is 30,400 and 70,000 kWh/a, respectively, for the high-performance building and the reference building*

Total energy use, non-renewable primary energy demand and CO_2 emissions: as shown in Table 8.7.3, the net energy required for DHW, space heating and mechanical systems is 47.6 kWh/m²a (76,200 kWh/a). Adding tank, boiler and system losses gives a total energy use of 58.7 kWh/m²a (93900 kWh/a).The total auxiliary energy demand (electricity and pellets), including the conversion losses in the pellets boiler, is 36.4 kWh/m²a (58300 kWh/a), where 36.2 kWh/m²a (57900 kWh/a) are provided by biomass in the pellet boiler and approximately 0.3 kWh/m²a (400 kWh/a) by the electrical heater.

The active solar gains are 17.3 kWh/m²a (27600 kWh/a) and the solar fraction of the heating system is 35 per cent since the simulation result of the same building but without solar collector would require 77,400 kWh/a (described in section 8.7.2). The electricity use for mechanical systems is 5.0 kWh/m²a (8000 kWh/a).

Due to the solar contribution, the delivered energy is reduced to 41 kWh/m²a (66,200 kWh/a). The total use of non-renewable primary energy is approximately 17 kWh/m²a (27,900 kWh/a) and the CO_2 equivalent emissions are 3.8 kg/m²a (6100 kg/a). Compared to the reference building, the non-renewable energy use and CO_2 equivalent emissions are considerably lower (see Table 8.7.4 and Figure 8.7.3).

Table 8.7.3 *Total energy demand, non-renewable primary energy demand and CO_2 equivalent emissions for the apartment building*

Net Energy (kWh/m²a)	Total Energy Use (kWh/m²a)		Delivered energy (kWh/m²a)	Non renewable primary energy		CO_2 equivalent emissions	
	Energy use	Energy source		factor (-)	(kWh/m²a)	factor (kg/kWh)	(kg/m²a)
Mechanical systems 5.0	Mechanical systems 5.0	Electricity 5.0	Electricity 5.0	2.35	11.8	0.43	2.2
Space heating 19.0	Space heating 19.0	Electricity 0.3	Electricity 0.3	2.35	0.6	0.43	0.1
		Solar 17.3					
DHW 23.6	DHW 23.6	Bio pellets 36.2	Bio pellets 36.2	0.14	5.1	0.04	1.6
	Tank and circulation losses 5.6						
	Boiler conversion losses 5.5						
Total 47.6	58.7	58.7	41.4		17.4		3.8

Table 8.7.4 *A comparison between the high-performance house and the reference house regarding energy use and CO_2 equivalent emissions*

Building	Net energy (kWh/m²a)	Total energy use (kWh/m²a)	Delivered energy (kWh/m²a)	CO_2 equivalent emissions (kWh/m²a)
High performance building	47.6	58.7	41.4	3.8
Reference building	72.4	81.2	81.2	20.5

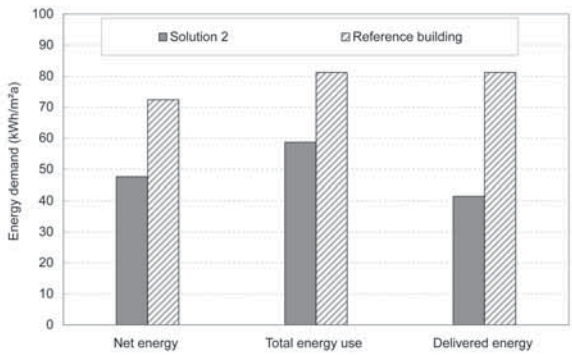

Source: Helena Gajbert and Johan Smeds

Figure 8.7.3 *An overview of the net energy, the total energy use and the delivered energy for the high-performance building and the reference building*

8.7.2 Sensitivity analysis

Since the performance of the solar energy system is strongly affected by the system design parameters (for example, collector area, tank volume, slope and direction of the collectors and collector type of the solar heating system), some of the most important results from the Polysun simulations shown during the designing of the system are presented here. If nothing else is mentioned, the parameters of the simulated systems are the same as for the suggested system. The 'auxiliary energy', which is shown in many of the figures, is the heat output from the auxiliary energy system, thus including heat for DHW heating, space heating and also heat losses. It does not include the conversion losses from the heat production (i.e. combustion and heat exchanger losses in a wood pellet furnace).

Collector area

The collector area and tank volume should preferably be considered both individually and as a unit. The collector area is, however, the more important feature to optimize in order to minimize the auxiliary energy use. The collector area was varied in the simulation while keeping a constant storage tank volume. The aim was to find a collector size that is large enough to almost cover the summer heating demand (i.e. the DHW demand), while still maintaining a relatively low risk of stagnation in the collectors.

The solar fraction (SF) is calculated according to Equation 8.1. The parameters Aux and Aux_0 represent the auxiliary energy required with and without the solar system, respectively. In Polysun, the value of Aux_0 was obtained by setting the collector area to zero, which resulted in an annual auxiliary energy demand of 77,400 kWh per year and 11,600 kWh during the summer months (June, July and August):

$$SF = 1 - \frac{Aux}{Aux_0} \qquad [8.1]$$

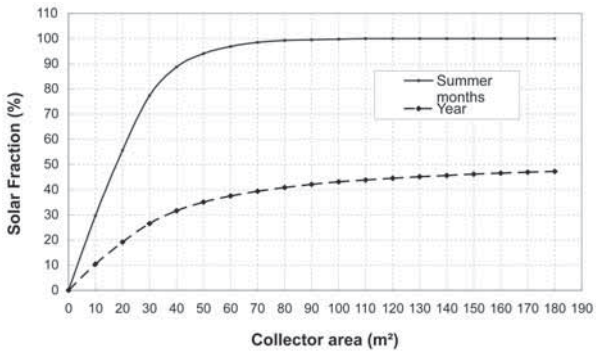

Source: Helena Gajbert and Johan Smeds

Figure 8.7.4 *The solar fraction of the system for the whole year and for the summer months*

In Figure 8.7.4 it is shown how the calculated solar fractions for the whole year and also for the summer months, June, July and August, increase with increasing collector area.

In order to lower the risk of stagnation and overheating, 50 m^2 seems a suitable collector size. The pellet boiler can still be turned off during summer, although a small amount of electricity may be needed during a few colder days. The solar fraction during the three summer months will then be 95 per cent. If a solar fraction of 100 per cent in the summer is to be obtained, the risk of overheating and stagnation would be large. Even if good control strategies can mitigate these problems, it is still desirable to avoid the problem completely. Should a heated swimming pool for summer use be included in the heating system, the problems of overheating and stagnation could be reduced as this increases the heat load during summer. Figure 8.7.5 shows monthly values of the auxiliary energy demand during summer for different system dimensions.

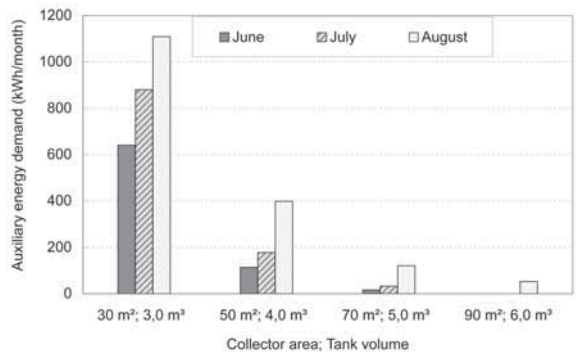

Source: Helena Gajbert and Johan Smeds

Figure 8.7.5 *Monthly values of auxiliary energy demand for solar systems of different dimensions*

In Figure 8.7.6, the energy saved due to the installation of the collectors is shown for the margin collector area (i.e. the extra savings made with an increase in collector area by 10 m^2). A rough estimation is that the collector area preferably should be between 40 m^2 and 60 m^2 to provide a reasonable amount of energy per margin collector area, thus giving sufficient energy yield in relation to the total investment costs.

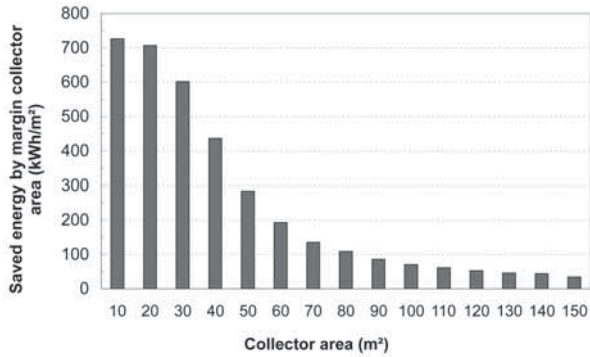

Source: Helena Gajbert and Johan Smeds

Figure 8.7.6 *The energy savings per margin collector area (i.e. how much additional energy is saved if 10 m² is added to the collector area, read from left to right)*

The resulting non-renewable primary energy demand and CO_2 equivalent emissions when solar combi-systems of different dimensions are used can be seen in Figure 8.7.7. The tank volumes were optimized for each case.

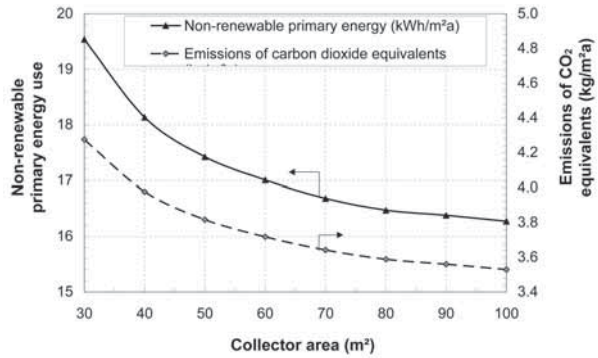

Source: Helena Gajbert and Johan Smeds

Figure 8.7.7 *The resulting non-renewable primary energy demand and CO_2 equivalent emissions for different collector areas*

If the solar system had been installed in the reference building (described in section 8.1) instead, the auxiliary energy demand would be much higher, as can be seen in Figure 8.7.8, where the auxiliary energy demand of the two buildings is shown for different solar system dimensions. Again, the tank volumes were optimized for each case.

In Figure 8.7.9 the overview of the energy demands of the high-performance building and for the reference building are shown, as well as the solar gains of collectors of 30, 50 and 70 m². Observe that the heat for DHW, circulation losses and tank losses is valid for a 50 m² collector area. For a larger collector, the tank losses will be slightly higher.

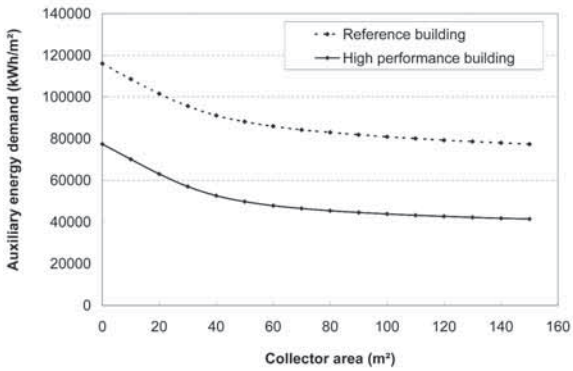

Source: Helena Gajbert and Johan Smeds

Figure 8.7.8 *Annual auxiliary energy demand per living area for different system dimensions based on Polysun simulations*

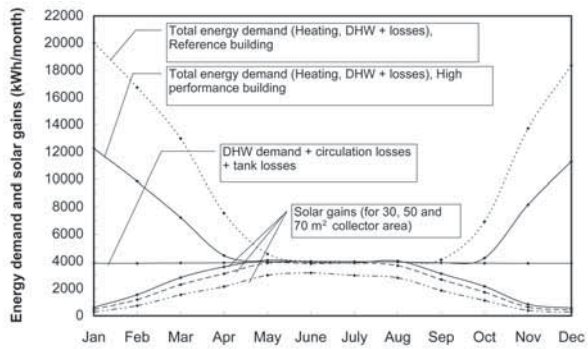

Source: Helena Gajbert and Johan Smeds

Figure 8.7.9 *The energy demands and the solar gains of the high-performance building and the reference building; the solar gains are shown for different collector areas*

Storage tank volume

For economical reasons it is important to consider the storage tank volume. A larger tank is much more expensive, although the impact on the auxiliary energy use is rather small, as shown in Figure 8.7.10. The tank could preferably be designed based on the daily energy demand due to the limited storage time capacity. The tank should not be too small due to the risk of overheating and because of lowered storage capacity. On the other hand, an oversized tank might require higher auxiliary energy demand in order to heat the tank and also because of the higher heat losses. A high insulation level is therefore important and it becomes more important the larger the tank is, as shown in Figure 8.7.10.

Simulation results for collector areas between 50 m^2 and 100 m^2, with varying tank volumes, are shown in Figure 8.7.11. The chosen system is marked with a circle. These results also show that the collector area has a much larger influence on the auxiliary energy use than the tank volume. Although the tank size has a relatively low influence on the auxiliary energy use, it is important not to choose too small a tank since there will be a risk of overheating and as it might be difficult to provide the required heat for DHW and space heating. For the larger collectors, some energy can be saved by choosing a larger tank. The suggested system with 50 m^2 collector area and a storage volume of 4 m^3 would neither imply overheating nor excessive tank losses, according to the simulation results.

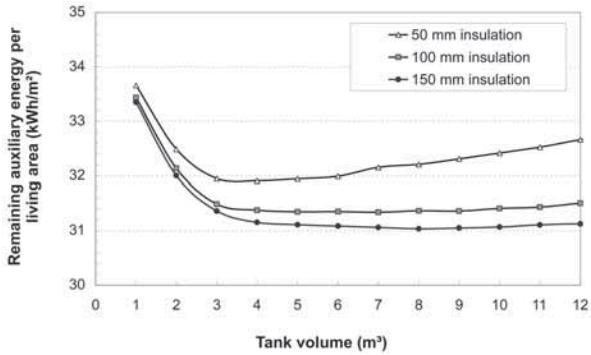

Source: Helena Gajbert and Johan Smeds

Figure 8.7.10 *The influence of tank volume and tank insulation level; the auxiliary energy demand per living area for different tank volumes is shown*

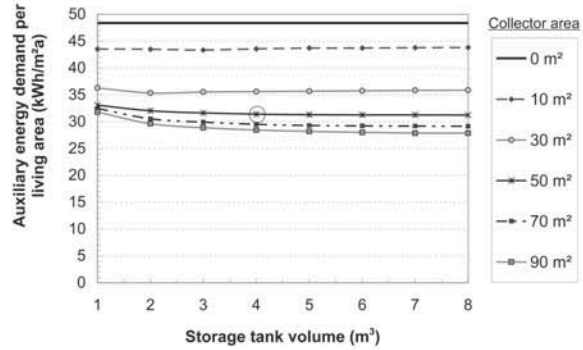

Source: Helena Gajbert and Johan Smeds

Figure 8.7.11 *Annual auxiliary energy per living area for different system dimensions based on Polysun simulations*

Collector tilt

The tilt of the collector determines how large the collector should be in order to cover the summer demand. In order to maintain a solar fraction of 95 per cent during the summer months, the required collector size increases as the collector tilt is increased or decreased from 30° to 40°, which is the tilt where the smallest collector area (50 m^2) is needed (see Figure 8.7.12).

When using highly tilted or vertical collectors, the solar gains will be better balanced to the seasonal heating demand since more of the winter space heating demand will be covered. However, this requires a larger collector area in order to cover the summer demand. For a very large collector with a high tilt angle, energy can be saved in total over the year, thus implying a higher annual solar fraction. A good, yet very expensive, solution would therefore be to use a vertical wall-mounted collector of very large size. The benefits of this are naturally much higher for combi-systems than for DHW systems. There are generally no benefits in using a horizontal collector or a collector with a low tilt.

Looking further at two mounting options for good building integration to either mount the collectors on the 40° tilted roof or vertically on the wall, tilted 90°, it can be seen in Figure 8.7.13 how the auxiliary energy demand decreases with increasing system size. The 40° tilt implies a lower demand of auxiliary energy on an annual basis and the difference is more significant in smaller systems.

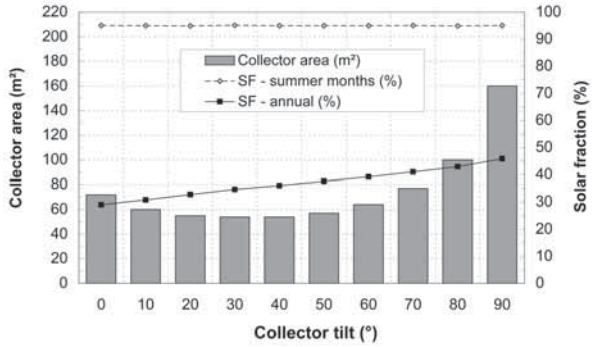

Source: Helena Gajbert and Johan Smeds

Figure 8.7.12 *The collector area required for differently tilted collectors in order to obtain a solar fraction of 95% during summer (this is thus an appropriate area that does not imply boiling in the tank); the solar fraction for the whole year and the constant solar fraction in summer are also shown*

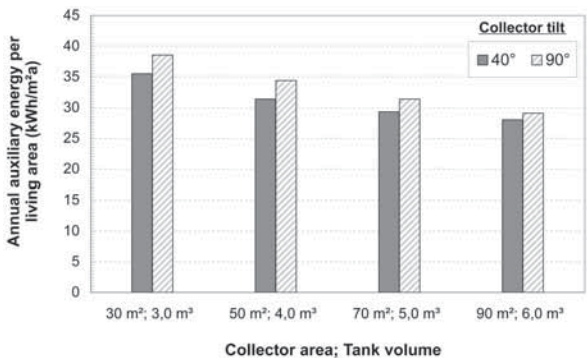

Source: Helena Gajbert and Johan Smeds

Figure 8.7.13 *Results from simulations of systems with differently tilted collectors: 40° for the roof-mounted and 90° for the wall-mounted collectors*

Furthermore, the risk of snow cover should be considered if a very low tilt angle is used. The risk of snow cover is even larger for evacuated tube collectors.

Azimuth angle

If the deviation from south is varied (i.e. the azimuth angle), the auxiliary energy demand and solar fraction changes according to Figure 8.7.14.

Collector performance

The choice of collector is very important for the system performance. Simulations have been performed with collectors of different types, from older collector types without a selective surface to the most advanced evacuated tube collectors available, with characteristics and simulation results listed in Table 8.7.5. The results are also shown in Figure 8.7.15. In the suggested system, an advanced flat-plate collector with a selective surface, anti-reflection treated glass and highly efficient thermal insulation, number 3 in Table 8.7.5, is used. When compared to an older collector type without selective surface, the chosen collector increases the solar fraction from 21 per cent to 30 per cent. If an evacuated tube collector is used, the solar fraction increases even more. For this solar

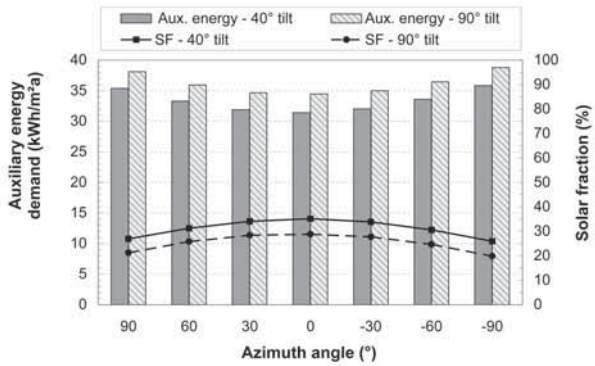

Source: Helena Gajbert and Johan Smeds

Figure 8.7.14 *The auxiliary energy demand and solar fractions of systems with different azimuth angles*

Table 8.7.5 *Collector parameters and corresponding solar fraction and auxiliary energy*

Collector type	η_0 (-)	c_1 (W/m²K)	c_2 (W/m²K²)	KCH1 (-)	KCH2 (-)	Specific heat capacity (kJ/m²K)	Solar fraction (%)	Remaining auxiliary energy (kWh/a)	Auxiliary energy (kWh/m²a)
1. Advanced evacuated tube collector	0.88	1.41	0.013	0.92	1.15	7.84	40,5	46053	28.8
2. Evacuated tube collector	0.77	1.85	0.004	0.9	1.00	5.71	36.7	49004	30.6
3. Advanced flat plate collector	0.85	3.7	0.007	0.91	0.91	6.32	35.1	50232	31.4
4. Flat plate collector	0.8	3.5	0.015	0.9	0.9	6.32	33.1	51767	32.4
5. Flat plate collector - no selective surface	0.75	6,00	0.03	0.9	0.9	7,00	26.4	56976	35.6

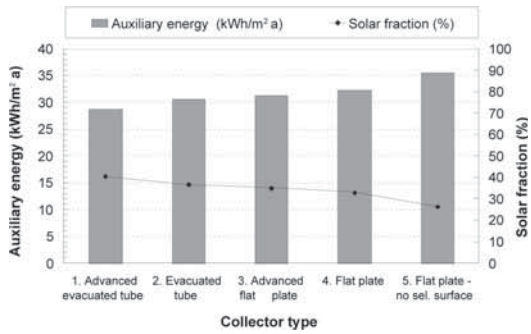

Source: Helena Gajbert and Johan Smeds

Figure 8.7.15 *Results from simulations of systems with different collector types*

heating system an evacuated tube collector of 35 m² would be sufficient. Evacuated tube collectors are very efficient, but are also often very expensive.

Concentrating collectors

By using concentrating reflectors to enhance the irradiance on the absorber, the output from the collectors can be increased. If the geometry of the collectors excludes irradiation from higher solar angles, the collector could improve the seasonal balance by increasing the winter performance and

	70°, 42 m²		90°, 56 m²	
	Without reflector	With reflector	Without reflector	With reflector
Total annual auxiliary energy (kWh/a)	47,538	42,297	45,643	40,570
Solar fraction (%)	38.6	45.4	41.0	47.6

Table 8.7.6 *The auxiliary energy demand for an evacuated tube collector with and without reflectors*

suppressing the summer performance. It is interesting to apply this strategy to an evacuated tube collector, which has the potential to deliver energy during lower irradiance levels and which also, currently, is relatively expensive. An estimation of the effect that this would imply was investigated for an evacuated tube collector (with collector characteristics according to Table 8.7.5, collector type 1). Polysun simulations were performed assuming a double collector area from October to March and with the collector tilted 70° and 90°. The area was chosen so as to imply a solar fraction of 95 per cent during summer. The results, shown in Table 8.7.6, indicate that the reflector implies energy savings of 11 per cent if it is tilted either 70° or 90°.

Design of the collector loop heat exchanger and flow rate

The design of the storage tank and its connected components is also important for the system efficiency since different types of heat exchangers work optimally at different flow rates. The flow rate in the collector loop should not be too low so as not to cause laminar flow, air traps and/or increased heat losses. Therefore, if the heat from the collectors is transferred to the tank through an internal heat exchanger, a high flow rate implies lower auxiliary energy demand, as shown in Figure 8.7.16.

The efficiency of the solar heating system is improved if an external heat exchanger is used instead and even better if a stratifying device is employed. In a smaller tank, the importance of a stratifying device is more significant. In these cases, a low flow rate is better since the fluid inserted into the tank otherwise can cause mixing of the stratified water. However, the flow rate should not be too low. The optimum can be seen in Figure 8.7.16. Lower flow rates also contribute to a lower electricity use for the pump and the dimensions of the pipes are reduced and less expensive.

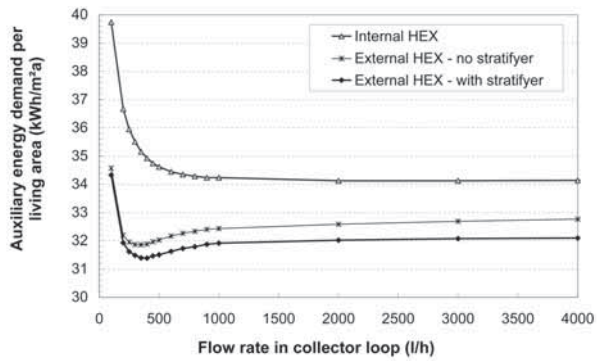

Source: Helena Gajbert and Johan Smeds

Figure 8.7.16 *The auxiliary energy demand, with varied flow rate and type of heat exchanger in the solar circuit*

Non-renewable energy use for solar DHW systems and combi-systems

If a solar DHW system would be used instead of the combi-system, the target of non-renewable primary energy would not be reached if combined with electricity for space heating. If combined with district heating for space heating, the solar collectors would have to be at least 40 m^2 in order to reach the target of 60 kWh/m^2a (living area), as shown in Figure 8.7.17. By looking at Figure 8.7.18, where the emissions of CO_2 equivalents are shown, the most environmentally friendly design also appears to be with a solar combi-system with a pellet boiler and an electrical heater.

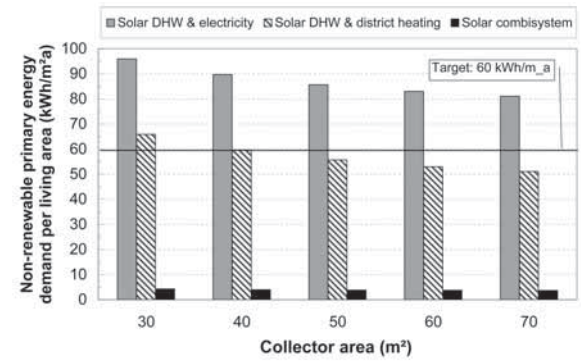

Source: Helena Gajbert and Johan Smeds

Figure 8.7.17 *The use of non-renewable primary energy for three different energy system designs: the combi-system in question, with a pellet boiler and an electrical heater; a solar DHW system combined with district heating; and a solar DHW system combined with electrical heating*

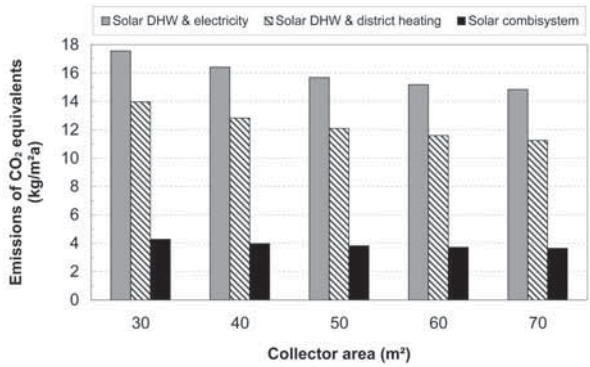

Source: Helena Gajbert and Johan Smeds

Figure 8.7.18 *The emissions of CO_2 equivalents for three different energy system designs: the combi-system in question, with a pellet boiler and an electrical heater; a solar DHW system combined with district heating; and a solar DHW system combined with electrical heating*

8.7.3 Design advice

The solution presented in this section fulfils the primary energy target. When comparing the construction of the building envelope to current building standards, it is clear that today's apartment buildings could live up to the targets set if they were built very air tight and with efficient ventilation heat exchangers.

In cold climates where the heating demand is high, the solar energy from a solar combi-system can provide a significant part of the total energy demand of a high-performance house. If looking

specifically at the space heating demand, solar energy can also contribute, to some extent, to the space heating supply even for a well-insulated building. However, it may be easier to justify a solar DHW system economically if the energy demand is low enough to warrant a space heating system based only, for example, on heat recovery and electrical resistance heating of the incoming air.

If a solar combi-system is used, the combined storage tank can give beneficial effects due to the higher energy withdrawal from the tank, which can lower the temperatures in the collector circuit and thus increase the collector efficiency somewhat during the heating season. By combining the tank for space heating and hot water and thus improving the system flexibility, the heat losses might be reduced in comparison to using two separate tanks for DHW and space heating.

The collector solar system dimensions should preferably be designed so as to cover most of the energy demand in summer, both for solar combi-systems and solar DHW systems. The highest solar fraction on an annual basis is achieved with a collector tilt of approximately 30° to 50°. If a larger collector is affordable, it is beneficial to design a combi-system, over-dimension the collector area and to place it vertically on the wall since this increases the solar gains during the heating season and reduces the risk of stagnation in summer.

For the technical facility management of the building, a solar combi-system does, of course, mean some additional costs in comparison to the district heating system; but since the biomass boiler can be shut down during summer, service costs should be at a reasonable level.

The solution presented here implies very low use of fossil fuels and low emissions of CO_2 equivalents to the atmosphere. Therefore, it is a very good solution for a building in rural areas where district heating is not available, especially as the solar system can cover the energy demand in summer and the furnace can be switched off.

District heating systems use a large share of renewable fuels in Scandinavia; approximately 80 per cent of the fuel is renewable. If the building is situated in an urban area with such a district heating system, the district heating is to be preferred to the use of biomass boilers as biomass boilers give rise to some emissions from the furnaces, something that may be forbidden in certain urban areas. Today, the purification of the exhaust gases is very good and modern furnaces are often

Table 8.7.7 *General assumptions for simulations of the building in DEROB-LTH – construction according to solution 2, space heating target 20 kWh/m²a*

	Material	Thickness	Conductivity	Per cent	Studs	Studs	Resistance without Rsi, Rse	Resistance with Rsi, Rse	U-value
		(m)	λ (W/mK)	(%)	λ (W/mK)	(%)	(m²K/W)	(m²K/W)	(W/m²K)
wall	exterior surface							0.04	
	wooden panel	0.045		100%					
	air gap	0.025		100%					
	mineral wool hd	0.030	0.030	100%			1.00		
	mineral wool	0.100	0.036	85%	0.14	15%	1.94		
	plastic foil			100%					
	mineral wool	0.030	0.036	85%	0.14	15%	0.58		
	plaster board	0.013	0.220	100%			0.06		
	interior surface							0.13	
		0.243					**3.58**	**3.75**	**0.267**
roof	exterior surface							0.04	
	roof felt	0.003		100%					
	mineral wool hd	0.015	0.030	100%			0.50		
	mineral wool	0.100	0.036	100%			2.78		
	plastic foil			100%					
	concrete	0.15	1.700	100%			0.09		
	interior surface							0.10	
		0.268					**3.37**	**3.51**	**0.285**
floor	exterior surface								
	mineral wool	0.110	0.036	100%			3.06		
	concrete	0.150	1.700	100%			0.09		
	interior surface							0.17	
		0.260					**3.14**	**3.31**	**0.302**
window				emissivity					
	pane	0.004	clear	83.70%					
	gas	0.015	air						
	pane	0.004	low emissivity	4%					
		0.023							**1.400**
	frame	0.093	wood		0.14		0.66	0.83	**1.20**

designed to use optimal oxygen amounts in the combustion process. If a biomass boiler is to be used, it should be an 'environmentally approved' boiler and it should be coupled with a thermal heat storage tank in order to achieve an effective and controlled combustion process and to minimize the emissions of volatile organic compounds (VOCs) and particles (Johansson et al, 2003).

Table 8.7.8 *Design parameters of the solar combi-system used in the Polysun simulations*

Parameter	Value
Pellet boiler	
Pellet boiler peak power	35 kW
Electrical heater peak power	5 kW
The pipes of the solar circuit	
Pipe material	Copper
Ø inside	16 mm
Ø outside	18 mm
Length indoors	24 m
Length outdoors	6 m
Thermal conductivity, λ, of pipe	0.040 W/mK
Thermal insulation thickness	25 mm
Collector circuit	
Pump power	210 W
Collector circuit flow	525 l/h
Specific throughput	7 l/h,m^2
Heat transfer medium	Water (50%), glycol (50%)
Power output to heat transfer medium	60%
Heat exchanger in solar circuit	
Heat transfer rate k*A for heat exchanger	5000 W/K
Tank	
Volume	4 m^3
Height	4 m
Temperature in the tank room	15°C
Thermal insulation of the tank	150 mm

References

Johansson, L., Gustafsson, L., Thulin, C. and Cooper, D. (2003) *Emissions from Domestic Bio-fuel Combustion – Calculations of Quantities Emitted*, SP Report 2003:08, SP Swedish National Testing and Research Institute, Borås, Sweden

Kvist, H. (2005) *DEROB-LTH for MS Windows, User Manual Version 1.0–20050813*, Energy and Building Design, Lund University, Lund, Sweden, www.derob.se

Meteotest (2004) *Meteonorm 5.0 – Global Meteorological Database for Solar Energy and Applied Meteorology*, Bern, Switzerland, www.meteotest.ch

Polysun (2002) *Polysun 3.3: Thermal Solar System Design, User's Manual*, SPF, Institut für Solartechnik, Rapperswil, Switzerland, www.solarenergy.ch

Swedish Environmental Protection Agency (2005) www.naturvardsverket.se

Swedish National Testing and Research Institute (2005) www.sp.se

Weiss, W. (ed) (2003) *Solar Heating Systems for Houses: A Design Handbook for Solar Combisystems*, James and James Ltd, London

Paper III

8.6 Apartment building in the Cold Climate Conservation Strategy

Johan Smeds

Table 8.6.1 *Targets for apartment building in the Cold Climate Conservation Strategy*

	Targets
Space heating	15 kWh/m^{2}a
Non-renewable primary energy: (space heating + water heating + electricity for mechanical systems)	60 kWh/m^{2}a

This section presents two solutions for the apartment building in the cold climate. As a reference for the cold climate, the city of Stockholm is considered. The solutions are based on energy conservation, minimizing the heat losses of the building. A balanced mechanical ventilation system with heat recovery is used to reduce the ventilation losses.

8.6.1 Solution 1a: Conservation with electric resistance heating and solar DHW

Building envelope

In this solution the envelope and ventilation system were designed so that the peak space heating load is limited to approximately 10 W/m^2. This allows one central heating element for each apartment and heat distribution by the supply air, which is more economical than individual room heaters. This solution requires a well-insulated and air-tight building envelope.

The apartment building has reinforced concrete structure and wooden frame façades with mineral wool. The windows have a frame ratio of 30 per cent, triple glazing, one low-e coating and they are filled with krypton. The U-values are shown in Table 8.6.2. Construction data are shown in Table 8.6.6.

Table 8.6.2 *The building components*

Building component	**U-value (W/m^{2}K)**
Walls	0.13
Roof	0.09
Floor (excluding ground)	0.12
Windows (frame + glass)	0.92
Window frame	1.20
Window glass	0.80
Whole building envelope	0.21

Mechanical systems

A balanced mechanical ventilation system with heat recovery and a bypass for summer ventilation is used. The heat exchanger has an efficiency of 80 per cent. The supply air is used for the distribution of heat. Domestic hot water is supplied by a solar domestic hot water system in combination with an electric furnace. The solar system consists of 60 m^2 collectors, a storage tank of 6 m^2 and an electric furnace of 8 kW.

Energy performance

Space heating demand and peak load: simulation results from DEROB-LTH show that the space heating demand is 10,300 kWh/a (6.5 kWh/m^2a). The monthly space heating demand of solution 1a in comparison to the reference case (building code 2001) is shown in Figure 8.6.1.

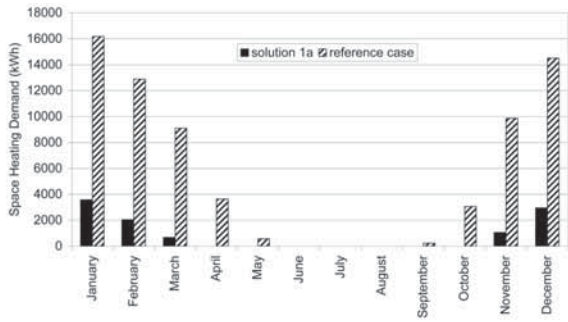

Source: Johan Smeds

Figure 8.6.1 *Space heating demand of solution 1a*

Hourly loads of the heating system are calculated from the DEROB-LTH simulation results without direct solar radiation in order to simulate a totally shaded building. The annual peak load is 16 kW or 10 W/m^2 and occurs in January.

General assumptions for these simulations were:

- heating set point: 20°C;
- maximum room temperatures: 23°C during winter, 26°C during summer (assumes use of shading devices and window ventilation);
- ventilation rate: 0.45 ach;
- infiltration rate: 0.05 ach; and
- heat recovery: 80 per cent efficiency.

Domestic hot water demand: the net heat demand for DHW is approximately 37,800 kWh/a (23.6 kWh/m^2a). Thus, the DHW demand is much larger than the space heating demand.

The system losses consist mainly of losses from the hot water storage tank, but also from pipe losses in the distribution system. The tank and circulation losses are 1.5 and 4.4 kWh/m^2a, respectively. The circulation losses are taken into account as internal gains in the simulations with DEROB-LTH. The tank losses and losses from the collector loop, on the other hand, cannot be used as internal gains since the tank and boiler are placed in the basement outside the thermal envelope of the living area. The conversion losses of the electric boiler are set to zero.

The choices of system solutions are based on simulations of the space heating demand for the building performed with the programme DEROB-LTH. Simulations of the active solar energy

systems are performed with Polysun 3.3. A modified version of Polysun, the Polysun-Larsen version, was used in order to enable the use of the data files of space heating demand from heat load simulations performed in DEROB-LTH.

Household electricity: the use of household electricity for each apartment (two adults and one child) is 2190 kWh or 21.9 kWh/m^2. The primary energy target does not include household electricity since this factor can vary considerably depending on the occupants' behaviour.

Non-renewable primary energy demand and CO_2 emissions: the total energy use for DHW and space heating, system losses and mechanical systems is 63,200 kWh/a. After taking the solar contribution for DHW into account, the delivered energy is 34,200 kWh/a, which is provided by electricity. This results in a total use of non-renewable primary energy of 80,300 kWh/a (55 kWh/m^{2}a) and CO_2 equivalent emissions of 10 kg/m^{2}a (see Table 8.6.3).

Table 8.6.3 *Total energy demand, non-renewable primary energy demand and CO_2 equivalent emissions for the apartment building with electric resistance space heating and solar DHW system with electrical backup*

Net Energy (kWh/m²a)		Total Energy Use (kWh/m²a)				Delivered energy (kWh/m²a)		Non renewable primary energy		CO_2 equivalent emissions	
		Energy use		Energy source				factor (-)	(kWh/m²a)	factor (kg/kWh)	(kg/m²a)
Mechanical systems	5.0	Mechanical systems	5.0	Electricity	5.0	Electricity	5.0	2.35	11.8	0.43	2.2
Space heating	6.5	Space heating	6.5	Electricity	6.5	Electricity	18.3	2.35	43.0	0.43	7.9
DHW	23.6	DHW	23.6	Electricity	11.8						
		Tank and circulation losses	5.5	Solar	17.3						
		Conversion losses	0.0								
Total	35.1		40.6		40.6		23.3		54.8		10.0

8.6.2 Solution 1b: Energy conservation with district heating

Building envelope

Using a district heating system with hot water radiant heating allows a less insulated building envelope than solution 1a with supply air heating.

The apartment building has reinforced concrete structure and wooden frame façades with mineral wool. The windows have a frame ratio of 30 per cent, triple glazing, one low-e coating and are filled with krypton. U-values are shown in Table 8.6.4. Construction data are shown in Table 8.6.7.

Table 8.6.4 *U-values of the building components*

Building component	U-value (W/m²K)
Walls	0.24
Roof	0.25
Floor (excluding ground)	0.30
Windows (frame + glass)	0.92
Window frame	1.20
Window glass	0.80
Whole building envelope	0.34

Mechanical systems

A balanced mechanical ventilation system with heat recovery and a bypass for summer ventilation is used. The heat exchanger has an efficiency of 80 per cent. District heating is distributed by a hot water radiant heating system. A wastewater counter-flow pipe heat exchanger for preheating of water to the space heating system can be installed; but this is not included in any of the calculations for energy performance shown below.

Energy performance

Space heating demand: simulation results from DEROB-LTH show that the space heating demand of the building is 21,500 kWh/a (13.4 kWh/m^{2}a). The monthly space heating demand of the building in comparison to the reference case is shown in Figure 8.6.2. The heating season for the proposed solution 1b extends from November to March.

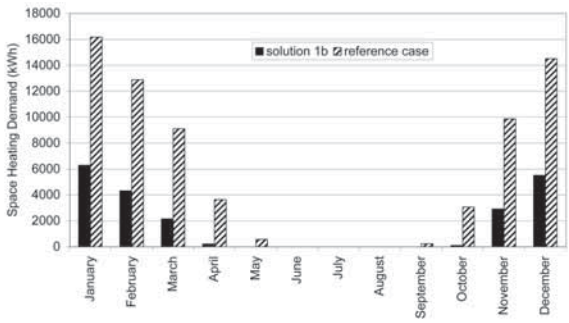

Source: Johan Smeds

Figure 8.6.2 *Space heating demand*

Hourly loads of the heating system are calculated with results from DEROB-LTH simulations without direct solar radiation in order to simulate a totally shaded building. The annual peak load is 21.2 kW or 13 W/m^2 and occurs in January.

Domestic hot water demand: the net domestic hot water demand for the 48 inhabitants is 37,800 kWh/a (23.6 kWh/m^{2}a).

System losses: the system losses consist mainly of circulation losses in the distribution system. The circulation losses are taken into account as internal gains in the simulations with DEROB-LTH. The conversion losses of the heat exchanger connected to the district heating system are set to zero.

Household electricity: the household electricity use for each apartment is 2190 kWh (21.9 kWh/m^2) for two adults and one child. The primary energy target does not include household electricity.

Non-renewable primary energy demand and CO_2 emissions: the total energy use for DHW and space heating, system losses and mechanical systems is 74,240 kWh/a. The use of district heating results in a non-renewable primary energy demand of 69,760 kWh/a (44 kWh/m^{2}a) and CO_2 equivalent emissions of 12 kg/m^{2}a in one year (see Table 8.6.5).

Table 8.6.5 *Total energy demand, non-renewable primary energy demand and CO_2 equivalent emissions for the apartment building with district heating*

Net Energy (kWh/m²a)		Total Energy Use (kWh/m²a)				Delivered energy (kWh/m²a)		Non renewable primary energy		CO_2 equivalent emissions	
		Energy use		Energy source				factor (-)	(kWh/m²a)	factor (kg/kWh)	(kg/m²a)
Mechanical systems	5.0	Mechanical systems	5.0	Electricity	5.0	Electricity	5.0	2.35	11.8	0.43	2.2
Space heating	13.4	Space heating	13.4	District heating	41.4	District heating	41.4	0.77	31.9	0.24	10.0
DHW	23.6	DHW	23.6								
		Circulation losses	4.4								
		Conversion losses	0.0								
Total	42.0		46.4		46.4		46.4		43.6		12.1

8.6.3 Design advice

Both solutions here fulfil the primary energy target. When comparing the construction of the building envelope to current building standards, it is clear that today's apartment buildings could live up

Table 8.6.6 *Solution 1a: Conservation with electric resistance heating and solar DHW – building envelope construction*

	Material	Thickness	Conductivity	Per cent	Studs	Studs	Resistance without Rsi, Rse	Resistance with Rsi, Rse	U-value
		m	λ (W/mK)	%	λ (W/mK)	%	(m²K/W)	(m²K/W)	(W/m²K)
wall	exterior surface							0.04	
	wooden panel	0.045		100%					
	air gap	0.025		100%					
	mineral wool hd	0.050	0.030	100%			1.67		
	mineral wool	0.250	0.036	85%	0.14	15%	4.84		
	plastic foil			100%					
	mineral wool	0.050	0.036	85%	0.14	15%	0.97		
	plaster board	0.013	0.220	100%			0.06		
	interior surface							0.13	
		0.433					**7.54**	**7.71**	**0.130**
roof	exterior surface							0.04	
	roof felt	0.003		100%					
	mineral wool hd	0.050	0.030	100%			1.67		
	mineral wool	0.350	0.036	100%			9.72		
	plastic foil			100%					
	concrete	0.15	1.700	100%			0.09		
	interior surface							0.10	
		0.553					**11.48**	**11.62**	**0.086**
floor	exterior surface								
	mineral wool	0.300	0.036	100%			8.33		
	concrete	0.150	1.700	100%			0.09		
	interior surface							0.17	
		0.450					**8.42**	**8.59**	**0.116**
window				emissivity					
	pane	0.004	low emissivity	5%	reversed				
	gas	0.012	krypton						
	pane	0.004	clear	83.70%					
	gas	0.012	krypton						
	pane	0.004	clear	83.70%					
		0.036							**0.800**
	frame	0.093	wood		0.14		0.66	0.83	**1.20**

to the targets set by IEA Task 28 if they were built very air tight and if they used efficient ventilation heat exchangers.

If the building is situated in an urban area where district heating systems use large quantities of renewable fuels (as, for example, in Scandinavia, where 80 per cent of the fuel is renewable), solution 1b is preferable. In rural areas where district heating is not available, solution 1a, with a solar domestic hot water system and electrical auxiliary heating, is a good alternative, especially since the solar system can cover the energy demand in summer. Of course, the production method of electricity is an important issue that significantly affects the resulting primary energy demand of a building using a high share of electricity – for example, as in solution 1a. An average value for the primary energy factor for electricity based on 17 European countries is used in all calculations. An environmentally friendly choice of electricity production would have a great impact on the primary energy use.

Table 8.6.7 *Solution 1b: Energy conservation with district heating – building envelope construction*

	Material	Thickness	Conductivity	Per cent	Studs	Studs	Resistance without Rsi, Rse	Resistance with Rsi, Rse	U-value
		m	λ (W/mK)	%	λ (W/mK)	%	(m^2K/W)	(m^2K/W)	(W/m^2K)
wall	exterior surface							0.04	
	wooden panel	0.045		100%					
	air gap	0.025		100%					
	mineral wool hd	0.030	0.030	100%			1.00		
	mineral wool	0.100	0.036	85%	0.14	15%	1.94		
	plastic foil			100%					
	mineral wool	0.050	0.036	85%	0.14	15%	0.97		
	plaster board	0.013	0.220	100%			0.06		
	interior surface							0.13	
		0.263					**3.97**	**4.14**	**0.242**
roof	exterior surface							0.04	
	roof felt	0.003		100%					
	mineral wool hd	0.030	0.030	100%			1.00		
	mineral wool	0.100	0.036	100%			2.78		
	plastic foil			100%					
	concrete	0.15	1.700	100%			0.09		
	interior surface							0.10	
		0.283					**3.87**	**4.01**	**0.250**
floor	exterior surface								
	mineral wool	0.110	0.036	100%			3.06		
	concrete	0.150	1.700	100%			0.09		
	interior surface							0.17	
		0.260					**3.14**	**3.31**	**0.302**
window				emissivity					
	pane	0.004	low emissivity	5%	reversed				
	gas	0.012	krypton						
	pane	0.004	clear	83.70%					
	gas	0.012	krypton						
	pane	0.004	clear	83.70%					
		0.036							**0.800**
	frame	0.093	wood		0.14		0.66	0.83	**1.20**

Table 8.6.8 *Design parameters of the solar DHW system in solution 1a*

Parameter	Value
Electrical heater efficiency	8 kW
The pipes of the solar circuit	
Pipe material	Copper
ø inside	16 mm
ø outside	18 mm
Length indoors	24 m
Length outdoors	6 m
Thermal conductivity, λ, of pipe	0.040 W/mK
Thermal insulation thickness	25 mm
Collector circuit	
Pump power	210 W
Collector circuit flow	525 l/h
Specific throughput	7 l/h,m^2
Heat transfer medium	Water (50%), glycol (50%)
Power output to heat transfer medium	60%
Heat transfer rate k*A for heat exchanger of stratifying device	5000 W/K
Tank	
Volume	6 m^3
Height	4 m
Temperature in the tank room	15°C

References

Kvist, H. (2005) *DEROB-LTH for MS Windows, User Manual Version 1.0–20050813*, Energy and Building Design, Lund University, Lund, Sweden, www.derob.se

Meteotest (2004) *Meteonorm 5.0 – Global Meteorological Database for Solar Energy and Applied Meteorology*, Bern, Switzerland, www.meteotest.ch

Polysun 3.3 (2002) *Polysun 3.3: Thermal Solar System Design, User's Manual*, SPF, Institut für Solartechnik, Rapperswil, Switzerland, www.solarenergy.ch

Paper IV

Design and evaluation of solar collectors for integration on non-insulated roofs

H. Gajbert*, B. Karlsson and J. Nilsson

Energy and Building Design, Lund University, Box 118, SE-221 00 Lund, Sweden

Submitted to Solar Energy Materials & Solar Cells

Abstract

There is a large potential of using cost-effective collectors with low insulation level integrated in non-insulated roofs in Sweden. The thermal performance and incidence angular dependence of three collectors for integration into non-insulated roofing material were evaluated by measurements and simulations. The maximum annual energy output per collector area would be 320 kWh/m^2, 330 kWh/m^2 and 280 kWh/m^2 respectively for Collector A, B and C at 50°C operation temperature. The corresponding yield per absorber area is 360, 680 and 1140 kWh/m^2 respectively. This indicates that there is a potential for production of cost-effective collectors of this type, Collector B particularly.

Keywords: Solar collector, Building-integration, Concentrating collector, Cost-efficiency, Roofing material

1. Introduction

1.1 Background

In order to increase the use of solar thermal collectors, it is important to develop cost-effective collector designs for building integration. One of the largest available potential locations for installation of solar collectors in Sweden is non-insulated roofs with cold attics underneath. Collectors integrated in such roofs do not require heavy insulation for the thermal comfort in the building and therefore they have an important advantage over standard integrated collectors, which must often be well-insulated.

By also using low-concentrating collectors the absorber material is used more efficiently. As existing roofing sheet is used for the collector bottom, no separate collector box is required. This and the fact that the absorber area is reduced enable a low production cost of the collector.

There is therefore a potential for development of a cost-effective, thin concentrating collector with lower use of insulation material, suitable for easy integration in non-insulated roofs.

Since very few collectors have been designed for non-insulated roofs it is interesting to investigate the thermal performance of such collector designs.

1.2 Objectives of this work

The objective of this work was to design cost-effective solar collectors for use on non-insulated roofs, which could be industrially produced, and to evaluate their thermal performance. These collectors was constructed as prototypes and evaluated with respect to their thermal performance and their incidence angle dependence.

2. Theory

2.1 Design criteria

In order to create a selling product, it is necessary to keep the investment costs low. Cost reductions can be achieved by using building integrated collectors that replace building material as the material use and installation time are minimised. By also using readily available products, the production

* Corresponding author. Phone: +46-46-2227583, fax: +46-46-2224719, e-mail: Helena.Gajbert@ebd.lth.se

costs can be further reduced, as the expensive start-up of a construction process is avoided. A desired feature is the use of low-concentrating reflectors, as this decreases the required absorber area, and thereby also the heat losses, without thick insulation.

Prefabrication and simple mounting are desirable features for building integrated collectors. In order to reduce the material use and to simplify the mounting process, the collector should preferably be thin and flexible for production in variable lengths. Maintenance requirements should be minimised by using durable materials.

2.2 The collector designs

Three similar collectors were designed to be integrated into commonly used corrugated steel roofing material that was found to enable the above mentioned criteria to be met. Since the material used in this collector box is commonly mass produced steel, the production costs can be lower than for a conventional collector with a thick insulated box. This material also allows flexible use, as collectors can be produced in flexible lengths for covering complete roofs. For all the three similar collectors the absorbers, reflectors and the expanded polystyrene (EPS) insulation material are placed directly in the compartments of an existing corrugated roofing sheet steel. Two of the collectors are designed with concentrating reflectors and one is a flat plate reference collector. The different collector designs are illustrated and described in Figure 1. All prototypes are covered with a 4 mm acrylic plate, which in full scale will be replaced by a glass cover of higher transmittance.

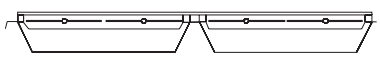

Figure 1a. Collector A - Flat plate reference collector with standard strip absorbers.

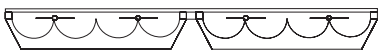

Figure 1b. Collector B - Concentrating collector with narrow strip absorbers and circular reflectors.

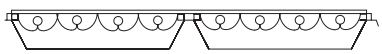

Figure 1c. Collector C - Concentrating collector with tube absorber, selective surface and CPC-reflector.

The absorber of the flat plate reference Collector A is a standard size Sunstrip absorber of 143 mm width. Underneath is 50 mm insulation of EPS material. For the other designs the thickness of the insulation is determined by the reflector geometry. In the concentrating Collector B, a Sunstrip absorber of half width, 72 mm, is used in combination with a circular shaped concentrating reflector, resulting in a factor of two between the glazed area and single side absorber area. The geometrical concentration ratio is 2.0 and the physical concentration is 1.0, since the absorber is bifacial. The acceptance interval is from -90° to 90°.

For concentrating collectors, it is important to consider the effect of different incidence angle dependences in the longitudinal and transverse plane. The longitudinal and transverse incidence angles, θ_L and θ_T, are here defined as shown in Figure 2.

For Collector A and B, which accept irradiation from all angles, the incidence angle dependences for beam irradiation in the longitudinal and transverse plane are both described by Equation 6. For Collector B however, the circular reflector could cause slightly larger optical losses. For the concentrating Collector C, the longitudinal and the transverse incidence angle dependences differ.

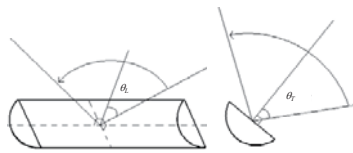

Figure 2. The transverse and longitudinal incidence angles, θ_L and θ_T, of a concentrating collector.

Collector C has a circular absorber that consists of an ∅ 18 mm copper pipe with a selective aluminium foil taped onto it. The absorbance, α, is 0.92 and the emittance, ε, is 0.20. The geometrical design of the reflector is an involute shaped after a ∅ 15 mm copper pipe [1], combined with a truncated quasi parabola. The 61 mm width of the aperture, denoted $2L$, results in a geometrical concentration ratio between glazed area and absorber area of 1.1. The geometry, which can be seen in Figure 3, gives an acceptance interval of 80°, and the acceptance half-angle, $\theta_{a/2}$, is thus 40°.

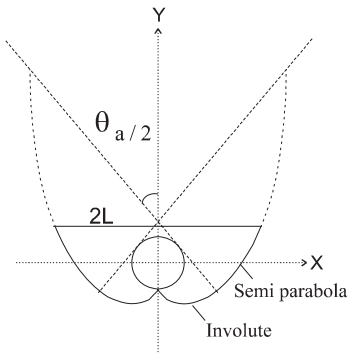

Figure 3. The shape of the truncated reflector used in Collector C, which is a combination of an involute and a parabola with an acceptance half-angle, $\theta_{a/2}$, of 40°.

Four copper pipes with reflectors fit into each compartment of the corrugated steel. A photograph of the absorber is shown in Figure 4.

Figure 4. A closer view of the large prototype of Collector C, showing the tube absorbers.

2.3 Thermal performance

The thermal performance of the collectors were evaluated based on Equation 1, which is similar to the model described by [2] although the piping heat loss coefficient and the wind and sky temperature factors are neglected here.

$$q = \eta_{0b} \cdot G_b + \eta_{0d} \cdot G_d - F'U_0 \cdot (T_m - T_a) - \\ - F'U_1 \cdot (T_m - T_a)^2 - (m \cdot C)_e \cdot \frac{dT_m}{dt} \quad (1)$$

The heat loss coefficient, $F'U$ is expressed by the first and second order heat loss coefficients $F'U_0$ and $F'U_1$, as shown in Equation 2. The mean collector temperature is calculated from the inlet and outlet temperatures, as shown in Equation 3.

$$F'U = F'U_0 + F'U_1 \cdot (T_m - T_a) \quad (2)$$

$$T_m = \left(\frac{T_{in} + T_{out}}{2} \right) \quad (3)$$

For a flat plate collector the incidence angle dependent optical efficiency for beam irradiance, η_{0b}, is described by $K_{\tau\alpha}$, as written in Equation 4. For angles higher than 60°, η_{0b} diminishes to 0, proportionally to the angle of incidence. [3]

$$K_{\tau\alpha} = 1 - b_0 \cdot \left(\frac{1}{\cos\theta} - 1 \right) \quad \text{for } \theta < 60° \quad (4)$$

The over-all collector efficiency at any given time is calculated from the relation between the power and the irradiance as written in Equation 5.

$$\eta = \frac{q}{G} \quad (5)$$

The absorber areas for the collectors are calculated as seen from a front view

3. Methodology

Prototypes of the three collectors were constructed and evaluated with respect to the thermal performance and the incidence angle dependence.

3.1 Long term measurements for evaluation of the thermal performance

Long term collector measurements have been performed in Älvkarleby, Sweden (60.5°N, 17.4°E), during the period from 2005-04-02 to 2005-05-10. Collector prototypes of a size of 1.0 × 2.0 m are mounted directed towards south, tilted 45°, with the absorbers directed in the east-west plane (see Figure 5). The inlet and outlet temperatures, flow rates, global and diffuse irradiation are monitored in the collector plane are monitored in ten minute intervals.

Figure 5. The collectors mounted outdoors for long-term evaluation in Älvkarleby, Sweden.

3.2 Evaluation of incidence angle dependence in the transverse plane

To measure the transverse incidence angle dependence of Collector C, an identical but smaller collector of 0.6 × 1.0 m, has been created and evaluated by measurements. The collector was mounted on a south-facing stand, which is adjustable for variable tilt angles, with the absorbers mounted vertically in the north-south plane. The transverse incidence angle at any specific time could be calculated by Equation 6 [3], since the collector tilt was adjusted continuously during the measurement, so that the surface was rotated around the horizontal east-west axis. That way the collector was always directed towards the sun's projection in the north-south plane. Although not commonly practiced, this measuring technique was found very suitable and efficient for the purpose.

$$\cos\theta = (1 - \cos^2\delta \sin^2\omega)^{1/2} \qquad (6)$$

3.3 MLR analysis

The collector parameters describing the thermal performance were calculated from the long-term measurements by Multi Linear Regression, MLR, according to the model described by [2], which is based on equation 1. The parameters q, G_b, G_d, T_m, T_a, and dT_m/dt were monitored and the parameters η_{0d}, $F'U_0$, $F'U_1$, $(mC)_e$ and b_0 were given by the MLR results.

3.4 Calculation of transverse incidence angle dependence for Collector C

For the concentrating Collector C, the optical efficiency for beam irradiation for different transverse incidence angles was calculated from the MLR results, according to Equation 7. The observed dependence of the transverse incidence angles was established from these results and during the following days the modelled values were compared to the monitored values of power.

$$\eta_{0b} = \frac{q - \left(\eta_{0d} G_d - F'U_0(T_m - T_a) - F'U_1(T_m - T_a)^2 - (mC)_e \frac{dT_m}{dt}\right)}{G_b} \qquad (7)$$

3.5 MINSUN simulations of annual energy output

The MINSUN simulation program was used to calculate the expected annual energy output from the collectors [4, 5]. The program considers the characteristic parameters of solar collectors and the longitudinal and transverse incidence angle dependence can be included as input data for simulations of concentrating collectors. The parameters derived from the MLR analysis were used as input in MINSUN. Simulations have been performed for all three collectors and the tilt of the surface was altered in the simulations in order to show the effect of installing the collectors on roofs of different tilt angles.

For Collector A and B, the $K_{\tau\alpha}$ function with the b_0 values from the MLR results was used to describe the incidence angle dependence. For Collector C simulations were performed with the influence of both the longitudinal and the transverse incidence angle dependence. The angular dependence can be described by a function $f(\theta)$, as expressed in Equation 8.

$$f(\theta) = g(\theta_L) \cdot h(\theta_T) \qquad (8)$$

The function $g(\theta_L)$ is the incidence angle dependence in the longitudinal plane, where the results of b_0 from MLR was used. The function $h(\theta_T)$, represents the transverse incidence angle dependence. The established values from the measurements in Lund were normalised to the MLR result of the η_{0b} value at normal incidence and used for $h(\theta_T)$ in the MINSUN simulations. The $F'U_0$ values from the MLR analysis are the most relevant $F'U_0$ values to use, since they are derived from

periods of normal operation during an extended time and for larger collectors, which are more similar to the intended product.

The tilt of the surface was also altered in the simulations in order to show the effect of installing the collectors on differently tilted roofs.

3.6 Ray tracing simulations

Ray tracing simulations of Collector C were performed in ZEMAX in order to show the theoretical transverse incidence angle dependence. The reflectance of the reflector was set to 0.85, the transmittance of the glazing to 0.9 and the absorbance of the absorber to 0.9. The incidence angular dependence of the transmittance and the absorbance were accounted for by a variation from 0.9 at normal incidence to 0.0 at 90° incidence similar to the $K_{\tau\alpha}$ function.

4. Results

4.1 MLR results

The values in Table 1 were derived from the MLR analysis from 2005-04-02 to 2005-05-05.

Table 1. The results from the MLR analysis.

	η_{0b} [-]	η_{0d} [-]	$F'U$ [W/m²K]	$F'U_0$ [W/m² K]	$F'U_1$ [W/m²K]	mC_e [J/kgK]	b_0 [-]
A	0.76	0.65	5.84	4.90	0.017	6834	0.125
B	0.72	0.62	4.93	4.27	0.012	5617	0.134
C	0.72	0.58	5.79	5.29	0.009	19148	0.154

The MLR analysis shows that the concentrating collectors B and C show lower values of optical efficiency for beam irradiation at normal incidence, compared to the reference, Collector A. This is explained by reflectance losses and deviations from the ideal optical designs of the reflectors. The pipes of Collector C are slightly displaced from the centre of the reflector. The concentrating Collector C shows a lower optical efficiency for diffuse irradiation. Collector B shows the lowest first order heat-loss coefficient, $F'U_0$. The heat loss factors of the concentrating Collector C and the reference, Collector A, are comparable.

The very high specific heat parameter, $(mC)_e$, of Collector C is explained by the 4 times higher water content in Collector C compared to Collector A and B.

The incidence angular dependence in the longitudinal plane, given by the b_0 value, is similar for all the collectors.

4.2 Model accuracy

In Figure 6, 7 and 8, the monitored data of energy output for the 6th of May 2005, a day with varying weather and low temperature, is compared to the corresponding values predicted by the model.

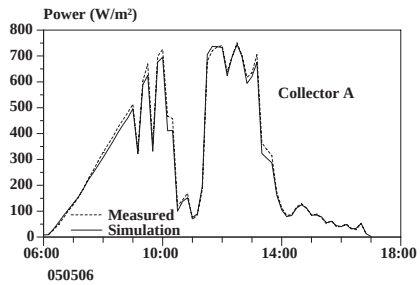

Figure 6. Comparison between monitored and simulated results of energy output for Collector A.

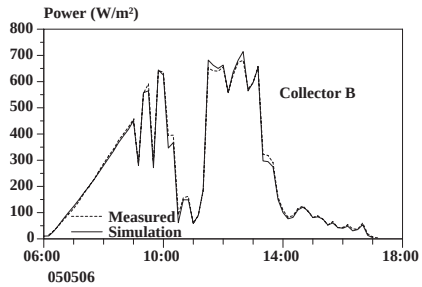

Figure 7. Comparison between monitored and simulated results of energy output for Collector B.

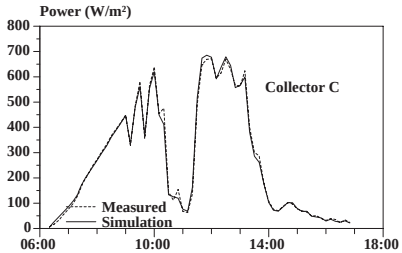

Fig 8. Comparison between monitored and simulated results of energy output for Collector C.

Figure 9, 10 and 11 show comparisons between measurements and simulations of the power from the collectors from the period 2005-04-02 to 2005-05-10. The good agreement between simulated and measured results of energy output from the collectors (in figures 6 -11) indicates that the evaluation model works well.

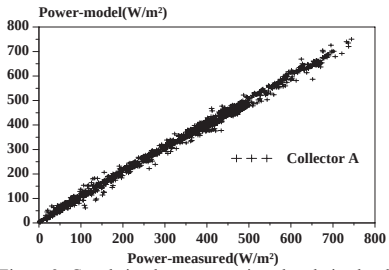

Figure 9. Correlation between monitored and simulated thermal effect of Collector A.

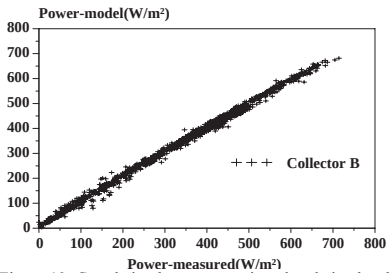

Figure 10. Correlation between monitored and simulated thermal effect of Collector B.

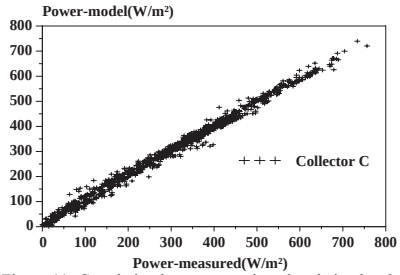

Figure 11. Correlation between monitored and simulated thermal power of Collector C.

4.3 Monitoring of efficiency curves

Standard efficiency curves were plotted based on data from periods during the long-term measurements, when the irradiance was higher than 900 W/m^2. Data was taken at near normal incidence and at stable temperatures. The collector efficiencies for $\Delta T = 0°$ (see Figure 12) show good agreement with the results of η_{0b} from the MLR results, although not entirely comparable.

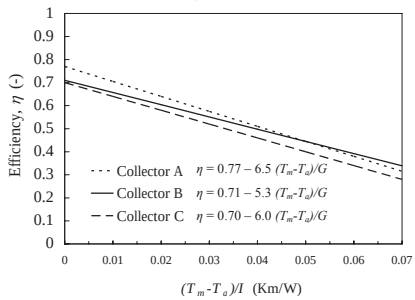

Figure 12. The efficiency as a function of $(T_m-T_a)/I$ for the three collector prototypes. The slope of the graph isequal to the $F'U_0$-value.

The $F'U$ values from the efficiency graphs at high irradiances are systematically higher than the corresponding data from the MLR results. This is because the data used in the MLR is measured during all hours of operation. An increase in absorbed irradiance causes an increase in the temperature difference between the fin and the heat carrier fluid, which increases $F'U$ [6]. This effect

was confirmed by also looking at $F'U$ values from dark hour measurements. The comparison of $F'U$ values is shown in Table 2. The dependence of $F'U$ on the irradiance is strongest for Collector A, which has a wide absorber and the lowest F'-value.

Table 2. Comparison of F´U values from MLR, from the efficiency curves and from cooling during dark hours.

Collector	$F'U$ [W/m²K] Efficiency	$F'U$ [W/m² K] MLR	$F'U$ [W/m²K] Cooling
A	6.5	5.84	5.5
B	5.3	4.93	4.8
C	6.0	5.79	5.5

4.4 The longitudinal incidence angle dependence

Figure 13 (from 1st of May -05) shows that during the long-term measurements, the variation of the transverse incidence angle over the main part of the day was very small, while the variation of the longitudinal incidence angle is far more significant. This means that the b_0 values obtained from the MLR analysis practically give information about the angular dependence in the longitudinal direction for all the collectors, as they are mounted with the absorbers in the east-west direction. The reflectors of Collector B and C thus have a small impact on the obtained b_0 values.

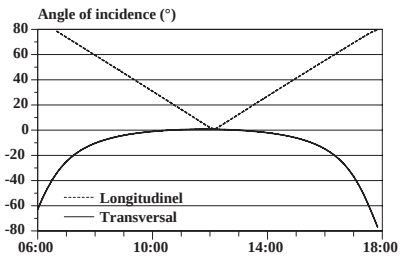

Figure 13. Longitudinal and transverse components of the angle of incidence towards the collector plane in the middle of the monitored period.

The longitudinal incidence angle dependence of η_{ob} is derived directly from collected data from varying incidence angles at low operating temperatures during the period from 2005-04-02 to 2005-05-10. The values have been corrected for contribution of diffuse irradiance and heat losses and the results, presented in Figure 14, show that the collectors have similar longitudinal incidence dependencies.

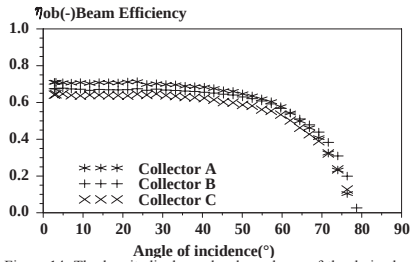

Figure 14. The longitudinal angular dependence of the derived beam efficiency, η_{0b}.

4.5 The transverse incidence angle dependence of Collector C

The transverse incidence angular dependence is important for Collector C, since the acceptance interval is limited in this direction. Measured data of the optical efficiency for beam irradiance, from Lund from the whole day of September 1st 2005, a clear sunny day, was plotted against the transverse incidence angles, θ_T, as shown in Figure 15.

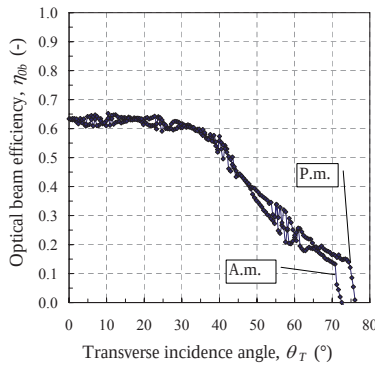

Figure 15. The measurement results of the transverse incidence angle dependence of the concentrating Collector C during September 1st 2005. The results from a.m. and p.m. coincide well.

As expected, irradiation from within the acceptance interval, 0°- 40°, give higher efficiency than for higher incidence angles. Also, the data from a.m. and p.m. correspond well. The optical efficiency at normal incidence is slightly lower than the MLR analysis for the larger collector showed, which is explained by the relatively lower heat losses of the larger collectors. Over all, the results appear to be accurate.

From these results, a model of the expected optical efficiency for different transverse incidence angles was set-up (see Figure 16).

The model was also adjusted to descend gradually to 0 at 90° from the abrupt down-fall between 70° and 80°, which was the result of the sun descending before reaching 90°, as this was expected also during the following measurements. The values were also normalised to the MLR results of η_{0b} at normal incidence, which are considered the most accurate due to the larger size and the better precision during the production of the prototypes.

The model was validated by comparing measured data of the collector power from another day, August 18, 2005, with modelled values. As can be seen in Figure 17, the accuracy is good.

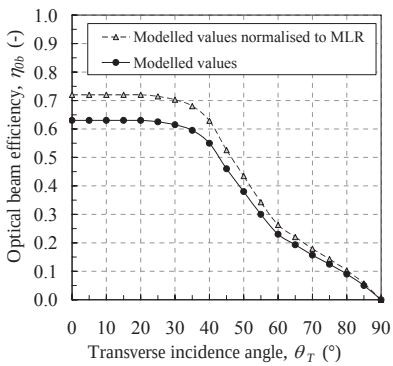

Figure 16. The model was validated by plotting measured and modelled data of the collector power over measurements from another day, the 18th of August 2005.

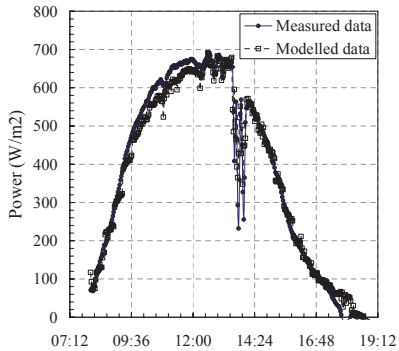

Figure 17. The model was validated by plotting measured and modelled data of the collector power over another day, the 18th of August 2005.

4.6 Ray tracing results

Figure 18 shows graphs of the transverse incidence angle dependence, both the modelled values and ray tracing results, which correspond relatively well.

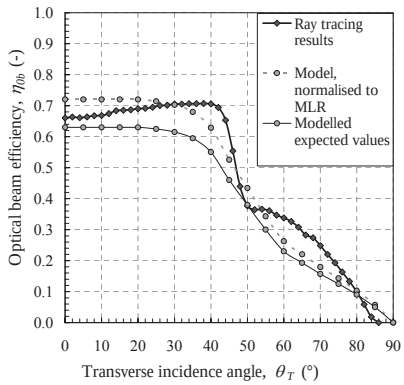

Figure 18. Results of incidence angle dependence of Collector C, both from ray-tracing results and from the model set up based on measurements.

The ray tracing results also gave the irradiance patterns and figures of distribution across the tubular absorber for different transverse incidence

angles (see Figures 19-22). The x-axis shows the pixels (used in simulations) along the absorber surface from the top and clockwise around. The left side of the absorber tube is thus represented by the higher values on the X-axis.

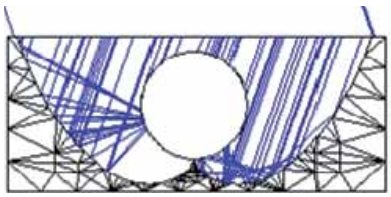

Figure 19. The irradiance patterns from $\theta_T = 20°$.

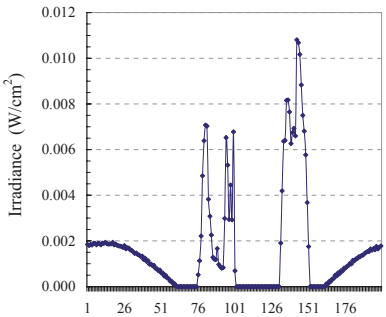

Figure 20. Light distribution on the absorber. $\theta_T = 20°$.

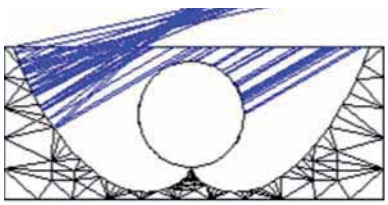

Figure 21. The irradiance patterns from $\theta_T = 60°$.

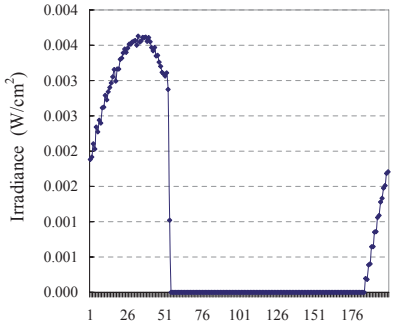

Figure 22. Light distribution on the absorber. $\theta_T = 60°$.

4.7 Thermal inertia of the collectors.

The effect of the greater thermal inertia of Collector C, shown by its high $(mC)_e$ value, can be observed in Figure 23, 24 and 25, showing the temperature difference between the collector and the ambient air, ΔT, and the measured and modelled power of the collectors during a sudden temperature decrease on the 25th of April 2005. Figure 25 shows that the power of Collector C exhibits a strong peak, while the other collectors show a smaller effect of the temperature decrease. Also here, the model follows the measurements well.

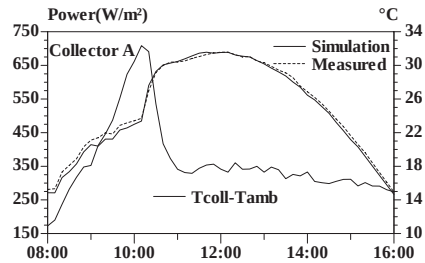

Figure 23. The measured and modelled power and ΔT for Collector A during a temperature peak.

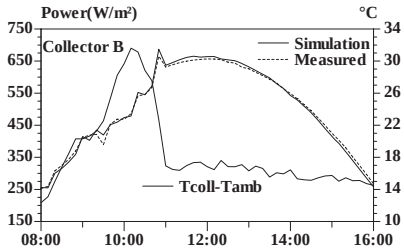

Figure 24. The relative collector temperature and the measured and modelled power of Collector B during a temperature peak.

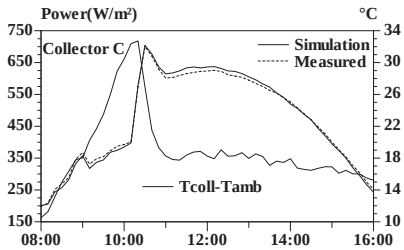

Figure 25. The relative collector temperature and the measured and modelled power of Collector C during a temperature peak.

4.8 MINSUN simulation results

The MINSUN simulation results show that the maximum annual energy output per glazed collector area would be 320 kWh/m^2, 330 kWh/m^2 and 280 kWh/m^2 respectively for collector A, B and C at an operation temperature of 50°C and with a collector tilt of 45°, which proved to be the optimum roof tilt angle. If calculated per absorber area, the corresponding yield would be 360, 680 and 1140 kWh/m^2 absorber respectively for collector A, B and C. (The absorber area of collector C is based on the pipe diameter). The simulation results of annual energy output per collector area for varying roof tilt angles are shown in figure 26.

While collector A and B show higher performance per glazed area than collector C, both collector B and C show high energy output per absorber area. Considering the economical potential of cost reductions for the pipe absorber of collector C, both collector B and C seem to have a good potential to become a cost effective product. The optimal tilt angle of the roof is 45° and for tilt angles between 35° and 50° the annual output is not reduced by more than 2%.

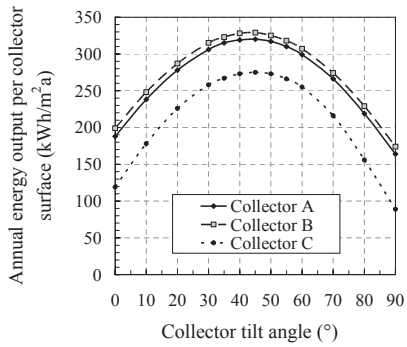

Figure 26. MINSUN simulation results showing the annual energy output for the collector tilts.

5. Discussion

The detailed analyses of the thermal performance of the collectors shows that the flat plate collector, Collector A, and the concentrating tube collector, Collector C, have high heat losses. Collector B, with the narrow strip absorber, shows lower heat losses. The $F'U$ value increase with increasing intensity. The F' value is temperature dependent and should increase slightly with increased operation temperature, as shown by [6].

The measurements performed in Lund on Collector C show a slightly higher $F'U$ value, which is natural considering the smaller prototypes used, which have a higher area-to-volume ratio.

It is required that the heat losses are further suppressed. This can be done by decreasing the acceptance angle and increasing the concentration ratio. For a previously evaluated non-insulated low-concentrating east-west collector, with a bifacial narrow absorber and a factor 3 between glazed area and single side absorber area, an acceptance interval of 45° has been shown to be sufficient. This collector, a roof-MaReCo, has a $F'U_0$ value of around 3.5-4.0 W/m²K [7]. However, a reflector in the north-south plane requires an acceptance interval of around 80°, as the Collector C, in order to be operated at least 5 hours in the middle of the day in

Sweden. The unexpectedly high $F'U_0$ value of the concentrating Collector C should be further analysed.

The analysis of transverse incidence angle dependence of Collector C show results similar to the theoretical values achieved by ray tracing simulations. As expected, the optical efficiency is as highest and almost constant within the acceptance interval from -40° to +40°, and thereafter is diminished. However the deviations shown can be explained by imperfections of the reflector or by a slightly dislocated absorber pipe, which can result in slightly higher optical losses for certain incidence angles.

A cost analysis should preferably also be performed in future work to assure the low cost of the final product.

Considering the very low production costs expected for these collector types, the potential of producing a cost-effective collector are estimated as high, although there are improvements to be made.

6. Conclusions

The thermal performance and incidence angular dependence of two low concentrating and one flat plate reference collector, constructed for direct integration into non-insulated roof, where investigated in detail by outdoor and indoor measurements.

The good correspondence of the measured and the simulated collector performances and temperature variations for the long term measurements leads to the conclusion that the model works well and that the results are accurate.

The simulations show that the maximum annual energy output would be 320 kWh/m^2, 330 kWh/m^2 and 280 kWh/m^2, per glazed collector area, respectively, or 360 kWh/m^2, 680 kWh/m^2 and 1140 kWh/m^2, per absorber respectively for collector A, B and C at an operation temperature of 50°C and with 45° tilt angle. As there is a potential to further decrease the heat loss coefficients, i.e. by decreasing the acceptance angle and increasing the concentration ratio, there is a high potential of these collectors to be developed into cost-effective products.

Judging from the collectors with their present design, the collector B is the most promising, with low heat losses and little use of absorber material. Collector C is the collector that would be the cheapest to produce, but the heat losses could be too high to make it profitable.

These solar collectors combined in a ready-to-use roofing material should preferably be mounted as entire roofs of cold spaces, which could give a significant contribution to the heat supply.

List of symbols

b_0	Incidence angle modifier coefficient (-)
dT/dt	Momentary mean collector temperature increase (K/s)
$F'U$	Heat loss coefficient (W/m^{2}K)
$F'U_0$	First order heat loss coefficient (W/m^{2}K)
$F'U_1$	Second order heat loss coefficient (W/m^{2}K^2)
G	Global irradiance (W/m^2)
G_b	Beam irradiance (W/m^2)
G_d	Diffuse irradiance (W/m^2)
$K_{\tau\alpha}$	Incidence angle modifier (-)
$(mC)_e$	Collector specific heat capacity (J/m^{2}K)
T_a	Ambient temperature (°C)
T_m	Mean collector temperature (°C)
T_{in}	Inlet temperature (°C)
T_{out}	Outlet temperature (°C)
T	Time (s)
q	Collector power (W/m^2)
δ	Declination (°)
η_{0b}	Optical efficiency, beam irradiance (-)
η_{0d}	Optical efficiency, diffuse irradiance (-)
θ	Angle of incidence (º)
θ_L	Longitudinal angle of incidence (º)
θ_T	Transverse angle of incidence (º)
$\theta_{a/2}$	Acceptance half-angle (º)
ω	Angle of time (°)

Acknowledgements

This work was financially supported by the Swedish Energy Agency. This project was partly carried out in cooperation with the construction company NCC Construction Sweden.

References

[1] W.T Welford and R. Winston, High Collection Nonimaging Optics (Academic Press Inc., San Diego, 1989).

[2] B. Perers, Solar Energy 50, (1993) 517-526.

[3] J.A. Duffie and W.A. Beckman, 1991. Solar Engineering of Thermal Processes (Wiley Interscience, New York, 1991).

[4] V.G. Chant and R. Håkansson, The MINSUN simulation and optimisation program, application and users guide, IEA SH&C Task VII, Ottawa, 1985.

[5] B. Perers, Optical Modelling of Solar Collectors and Booster Reflectors under Non Stationary Conditions, Ph.D. Thesis , Department of Technology, Uppsala University, Sweden, 1995.

[6] B. Hellström, Calculation and Measurement Methods for the Performance of Solar Collectors, Ph.D. Thesis, Department of Construction and Architecture, Lund University, Sweden, 2005.

[7] M. Adsten, A. Helgesson and B. Karlsson, Solar Energy 79 (2005) 638-647.

Paper V

Measurement of concentrating solar collectors using a solar simulator with parallel light

Helena Gajbert, Energy and Building Design, Lund University, Sweden
Håkan Håkansson, Energy and Building Design, Lund University, Sweden
Björn Karlsson, Energy and Building Design, Lund University, Sweden

By indoor measurements with steady surrounding conditions evaluations of concentrating solar collectors could be facilitated and made more systematic. In this article, a method is described of how indoor measurements of incidence angular dependence of concentrating collectors can be performed by using a large solar simulator providing nearly parallel light. The problem of spatial non-uniform irradiation from the described simulator is taken into account and compensated for by measurements of the total irradiation by several photodiodes placed in front of the test area.

01

Background

Concentrating solar collectors have a potential to be cost efficient in comparison to flat plate collectors due to lower investment costs (Adsten, 2002). The ability of evaluating solar collectors indoors provides independence of unwanted climate changes and facilitates the repetitiveness of the experiments. In order to enable indoor evaluation of concentrating solar collectors, a light source with parallel light is required. These kinds of light sources are not common, hence indoor evaluations are rare. A solar simulator providing nearly parallel light, and adjustable for solar angles is in use at Energy and Building Design at Lund Institute of Technology. The distribution of irradiated light from the simulator is however rather uneven. Hence, some results from previously performed evaluations of concentrating solar collectors have been somewhat difficult to interpret. (Gajbert et al., 2003)

The objective of this work is to develop a method to compensate for the non-uniform light distribution and the movements of the light pattern while using the solar simulator. The aim is to improve evaluations of incidence angle dependence of concentrating solar collectors using the simulator.

A method that serves this purpose has been developed and is presented in this article. The idea is to estimate the total irradiance on the test area, based on continuous measurements with a number of photodiodes placed on the glazed surface of the solar collectors. By using this method, two different types of concentrating collectors with limited acceptance angles have been evaluated with respect to incidence angle dependence of the zero-loss efficiency and the results are presented and discussed in this article. Another method which assumes that the irradiance on the collector is proportional to the cosine of the angle of incidence is also tested. The results of these two methods are presented and discussed here.

The solar simulator

The large indoor solar simulator used for some of the measurements in this work, is shown in figure 1. The simulator is further described in Håkansson (2003 a, b) and Håkansson (2001). Seven large parabolic reflectors are used to render the light nearly parallel, which is a rare quality for solar simulators. The simulator was originally designed for simulation of

daylight for evaluations of solar shadings. However, the parallel light is an important characteristic also for evaluation of the incidence angle dependence of concentrating collectors and it is desirable to be able to adequately perform this kind of evaluations. In order to achieve correct registered values of the irradiation on the collector surface during measurements, it is important that the total irradiation is known throughout the measurement, hence also when shifting solar altitude, i.e. lifting the simulator.

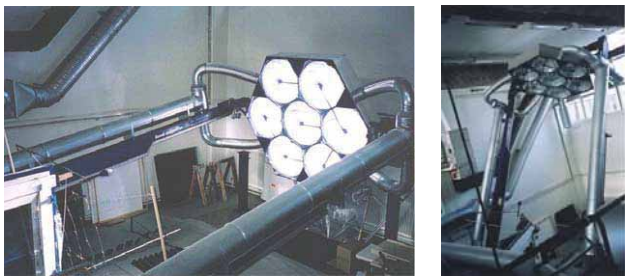

Figure 1. The solar simulator horizontally and lifted to the maximum elevation of 70°.

The good parallel light quality of the simulator has been achieved, to some extent, at the expense of a uniform area distribution. Fewer larger lamps generating nearly parallel light are used instead of smaller, but more numerous lamps generating more diverging but more evenly distributed light. The light intensity has been measured at several locations over a central test area, perpendicularly to the simulator, and the resulting intensity distribution diagram is shown in figure 2 (Håkansson, 2003 a, b).

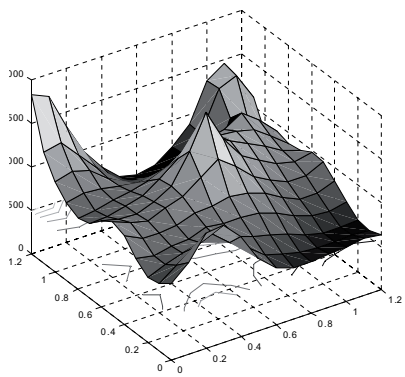

Figure 2. Light intensity distribution pattern from the solar simulator over a test area perpendicular to the simulator.

The light intensity peaks emanates the rim of the reflectors surrounding the lamps (Håkansson, 2003 a). When the simulator is lifted to simulate different incidence angles,

the light intensity pattern tend to move over the test area, thus possibly changing the total irradiation on the object. As the irradiation normally is measured by a single pyranometer, the results could be misleading. Earlier results from evaluations of incidence angle dependence of concentrating collectors were initially found to be poorly corresponding to similar outdoors measurements, thus indicating that the effect of the lifted simulator and the consequently moving light intensity pattern significantly altered these results. (Gajbert et al., 2003)

01

Compensation method for non-uniform illumination

In order to compensate for the moving light pattern an array consisting of six photodiodes connected in parallel, has been created and placed on the glazed surface of the collectors at the time of the measurement. The placement of the photodiodes divides the front area of the solar collector into smaller areas of approximately equal size with one photodiode placed in the centre of each area. With this arrangement, the total current from the photodiode array should be a rather good representation of the total irradiance on the collector surface.

The non-uniform irradiance makes it difficult to get absolute values of optical efficiency, η_0, from indoor measurements. Therefore, the calculated optical efficiencies from indoor measurements were adjusted to match the value of η_0 from outdoor measurements.

Designs of the evaluated concentrating solar collectors

The roof MaReCo, previously described by Adsten (2002), is 2D, concentrating solar collector intended to be placed on a tilted roof, see figure 3. It has a reflector designed as a parabola combined with a circular section and an absorber that absorbs irradiation on the back side from an acceptance interval between 0° and 60° solar altitude angle, when placed on a roof with 30° slope. The absorber also receives direct irradiation on the absorber. A prototype of this design was evaluated by indoor and outdoor measurements of thermal performance at varying incidence angles. The glazing of the prototype was replaced by a Teflon film.

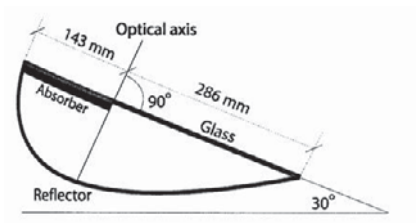

Figure 3. Design of MaReCo for tilted roofs (figure from Adsten, 2002).

The other concentrating solar collector evaluated here is a hybrid solar window, which basically consists of a parabolic reflector and a hybrid absorber, designed with a

concentration ratio of 2.45. The function of the reflector is both to concentrate the irradiance onto the absorber and to be used as solar shading, as the reflectors may be rotated backwards, as shown in figure 4. The hybrid absorbers consist of thermal absorbers with photovoltaic cells laminated on the surface. The wall element is further described by Fieber et al. (2004). The efficiency of the thermal absorbers in a prototype of this design was evaluated by indoor and outdoor measurements at varying incidence angles. The glazing of the prototype consists of two anti-reflex coated glass panes.

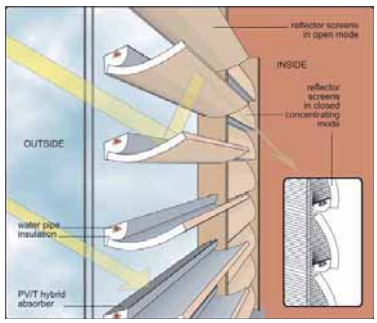

Figure 4. The hybrid solar window.

Incidence angle dependence of the concentrating collectors

For these types of 2D concentrating collectors, the incidence angle dependence of the optical efficiency is composed by the angular dependence of both the transversal and the longitudinal plane, as illustrated in figure 5.

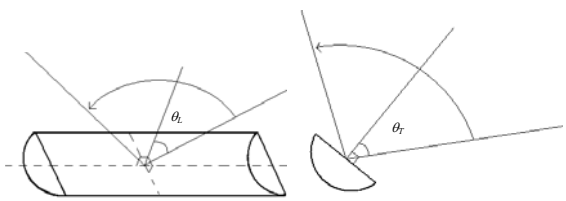

Figure 5. The longitudinal incidence angle, θ_L, and the transversal incidence angle, θ_T, of a 2D concentrating collector.

A propsed biaxial model, based on separate measurements of the effect on the optical efficiency of the reflector and the glazing, is shown in equation (1).

$$K(\theta_L,\theta_T) = R_T(\theta_T) f_L(\theta_i) \quad (1)$$

Here, $f_L(\theta_l)$ gives the influence of the glazing and is obtained by measuring the angular optical efficiency in the longitudinal plane at a given θ_T, when the reflector gives a constant contribution. $R_T(\theta_T)$ gives the influence of the reflector and is obtained by measuring the angular optical efficiency of the collector in the transversal plane when $\theta_L = 0$. If glazing is used, the function $K(\theta_L = 0, \theta_T)$ gets contribution from both the glazing and the reflector according to equation (1). Then $R_T(\theta_T)$ will be obtained from equation (2) according to equation (3).

01

$$K(\theta_L=0, \theta_T) = R_T(\theta_T) * f_L(\theta_T). \quad (2)$$

$$R_T(\theta_T) = \frac{K(0,\theta_T)}{f_L(\theta_T)} \quad (3)$$

This means that the ratio between the measured dependency in the θ_T and θ_L directions gives the influence of the reflector only.

The following complete expression for the angular dependency is obtained from equation (4).

$$K_{tot}(\theta_L,\theta_T) = f_L(\theta)\frac{K_{tot}(\theta_L=0,\theta_T)}{f_L(\theta_T)} = f_L(\theta)R_T(\theta_T) \quad (4)$$

In the longitudinal plane, the angular dependence consists only of the dependence of the glazing, $f(\theta_L)$. This means $K_{\tau\alpha}$, in the longitudinal plane can be described as flat plate collector by equation (5), where b_0 is an incidence angle modifier coefficient, characteristic for the glazing (Duffie and Beckman, 1991).

$$K_{\tau\alpha} = 1 - b_0\left(\frac{1}{\cos\theta} - 1\right) \quad (5)$$

Measurements of incidence angle dependence of the concentrating collectors

The two previously described prototypes of concentrating reflectors have been evaluated for incidence angle dependence by indoor and outdoor measurements. During indoor measurements, the collectors where placed at the pivot point of the simulator and the photo diode array was placed on collector surfaces. The irradiance to the collectors where also measured with a pyranometer. The incidence angles were simulated by raising the simulator or by rotating the collectors when placed vertically in front of the simulator.

$K(0,\theta_T)$ was derived from the measured values and divided by $f_L(\theta_L)$, in order to get $R_T(\theta_T)$. A single outdoor measurement was performed at θ_T=30° for the roof MaReCo and θ_T=20° for the solar hybrid window. The relations between the current from the photodiode array and the irradiation at corresponding incidence angles at outdoor measurements were

calculated. A compensation of the cosine dependence of the incidence angles was also performed, assuming that the total irradiation from the simulator is constant throughout the measurement and that the irradiance on the collector is dependent on *cos* θ_T.

The calorimetric measurements were performed with the temperature difference, ΔT, between the water in the collector and the ambient air maintained close to zero. The flow for the calorimetric measurements is recorded with an inductive flow meter and the temperature difference between in- and outlet is measured with a thermopile consisting of five thermocouple pairs. The thermal performance was registered continuously during the measurements.

A comparison has been made to corresponding outdoor measurements of both $f_L(\theta_T)$ and $K(0,\theta_T)$ of the roof MaReCo, that were previously performed on a larger prototype with identical geometrical features.

Results from indoor and outdoor measurements

The results of the evaluations of the roof MaReCo are shown in figure 6. These values are thus the angular dependence of the reflector exclusively, since the influence from the Teflon and the glazing are deducted, as earlier described. The measurements show good agreement for both methods for low angles of incidence. For high angle of incidence, when the irradiance is low, the cosine dependence shows better agreement with outdoor measurements than diode compensated data.

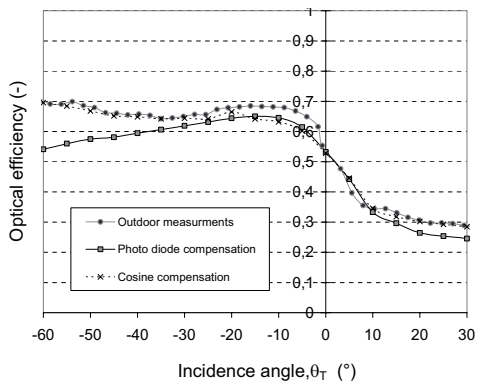

Figure 6. The incidence angular dependence of the roof MaReCo from indoor and outdoor measurements are shown here. The interval of incidence angles corresponds to the interval when placed at a 30° tilted roof. Then -60° means θ_T*=0° and 30° means* θ_T*=90.*

An equal relation between the indoor and outdoor measurements of the solar hybrid window was found for the roof MaReCo. This result gives another indication of that the

method is working satisfactory and that the simulator can be used for characterisation of concentrating collectors. However, at higher incidence angles, the agreement is not as good as for lower angles, suggesting that the method still needs further improvements.

Discussion

01

The results of incidence angular dependence from outdoor and indoor measurements show that the agreement is good at lower incidence angles. At higher incidence angles, the correspondence is less accurate. There are possibilities to improve the method further. By adding more photodiodes to the array, the accuracy of the measured total irradiance would be better. Improvements of the reflectors of the solar simulator, to obtain a more even light field, are also possible. An explanation for the lower correspondence at higher incidence angles could be that the active test area is smaller and that the power involved is lower.

References

Adsten M. (2002*) Solar Thermal Collectors at High Latitudes - Design and Performance of Non-Tracking Concentrators*, Acta Universitatis Upsaliensis, Uppsala, Sweden. ISBN 91-554-5274-4

Brogren M. (2004) *Optical efficiency of low-concentrating solar energy systems with parabolic reflectors,* Acta Universitatis Upsaliensis, Uppsala, Sweden. ISBN91-554-5867-X

Duffie J. A. and Beckman W. A. (1991) *Solar Engineering of Thermal Processes*, 2nd edn. Wiley Interscience, New York.

Fieber A., Gajbert H., Håkansson H., Nilsson J., Rosencrantz T. and Karlsson B., (2004) Design, Building Integration and Performance of a Hybrid Solar Wall Element, submitted to *Eurosun2004*, 20-23 June 2004, Freiburg, Germany.

Gajbert H., Brogren M. and Karlsson B. (2003) Optimisation of reflector and module geometries for stationary, low-concentrating, facade-integrated photovoltaic systems, Submitted to Solar Energy, In *Optical efficiency of low-concentrating solar energy systems with parabolic reflectors*, Brogren M., (2004) Acta Universitatis Upsaliensis, Uppsala, Sweden. ISBN 91-554-5867-X.

Håkansson H. (2003 a) A parallel beam solar simulator for testing of solar components, In the proceedings of *ISES Solar World Congress 2003*, Gothenburg, Sweden 14–19 June 2003.

Håkansson H. (2003 b) Solar laboratory, In *Solar Protection in Buildings: Part 2*, Wall M., Bülow-Hübe H. (eds), pp. 29-67. Dept. of Construction and Architecture, Lund University. ISBN 91-85147-00-1.

Håkansson H. (2001) Solar laboratory, In *Solar Protection in Buildings*, Wall M., Bülow-Hübe H. (eds), pp. 49-66. Dept. of Construction and Architecture, Lund University. ISRN LUTAD/TABK--3060-SE.

Karlsson B., Nilsson J., Gajbert H. and Helgesson A. (2004) A unified model for the incidence angle dependence of solar collectors, PV modules, windows and sun-shades, submitted to *Eurosun2004*, 20-23 June 2004, Freiburg, Germany.

Paper VI

DESIGN AND PERFORMANCE OF A LARGE SOLAR THERMAL SYSTEM WITH FAÇADE-INTEGRATED COLLECTORS IN SEVERAL DIRECTIONS, CONNECTED TO THE DISTRICT HEATING SYSTEM

Helena Gajbert, Bengt Perers and Björn Karlsson
Energy and Building Design, Lund University, Box 118, 221 00 Lund, Sweden
Phone: +46-46-2227583, Fax: +46-46-2224719, E-mail: Helena.Gajbert@ebd.lth.se

Astract - A reliable and robust control system is crucial for an optimally working solar thermal system. Improvements of system solutions are required in order to facilitate and widen the use of solar thermal systems. A large façade-integrated, highly automated solar thermal system is connected to the outgoing side of the district heating system in Malmö, Sweden, and has been operated and monitored since June 2002 without interruptions. The aim of this work is to investigate and describe the function of this innovative system. Simulations of energy output from the collectors and parametrical studies of temperatures and tilt angles have been performed. The flows of the five collectors, directed towards east, south and west, tilted in 90° and 73°, are coordinated to minimize the operating temperatures of the collectors, thus lowering the heat losses and resulting in a well-balanced heat production over the day. The system has an overheat protection system based on partial evaporation, where a compressor-connected expansion system is used for automatic refilling after boiling. From 2002-07-01 to 2003-10-30, the collectors delivered 180 kWh/m²a to the district heating system, with a peak power of 0.3 MW, which is as expected from a system with non-optimally oriented collectors. According to simulations performed with WINSUN, the average annual energy output should be 174 kWh/m²a, i.e. a divergence of 3% from the measured output. The simulations performed show relatively good agreement with measured energy output and the parametrical studies performed give an indication of the influence of the separated collectors on the total energy output.

1. INTRODUCTION

1.1 Background

A reliable and robust control system is crucial for an optimally working solar thermal system. Improvements of system solutions are important in order to facilitate and widen the use of solar thermal systems. By connecting solar thermal collectors to the district heating system, problems with stagnation in the collectors can easily be avoided due to the constantly large heating demand. Since no heat storage is needed, the heat losses otherwise caused by a storage tank are avoided.

This paper describes some interesting design features and experiences from one of the largest façade-integrated solar thermal systems in Europe, which also is connected to the local district heating system and has several relatively new control solutions.

The 1050 m² collectors are oriented in different directions, towards east, west and south, on the wall of a sports centre in Malmö, Sweden. It is integrated in the façade, and the energy output is delivered to the district heating system. The system, which is highly automated and remote-controlled, has been operated successfully and monitored since June 2002 without stagnations problems or interruptions. The system is one of 10 solar heat-producing subsystems connected to the forward side of the district heating system, thus serving as small power plants. The total collector area of the ten systems is 2030 m^2.

1.2 Objectives of this work

This study is concentrated on evaluating the performance and system design of this highly automated solar thermal system, with the aim to describe some important design features of the system, as it may be beneficial to apply these features elsewhere.

Parametrical simulation studies have been performed in order to show the importance of potential improvements that could be the result of changes of some of the design features such as the orientation of the collectors and the operation temperature.

2. SYSTEM DESCRIPTION

2.1 General system design

The 1050 m^2 large flat plate collectors from Aquasol with antireflection treated and frosted glass are modified for attractive façade integration. The five collectors are divided into three subsystems, which are integrated in the façades in directions close to east, south and west and tilted in 90° and 73°. The areas, azimuth angles and tilt angles of the collectors are shown in table 1.

Table 1. The size and orientations of the collectors.

Direction	Azimuth angle, α_z	Collector tilt, β	Collector area (m²)
East	-98°	90°	181,6
South	-8°	90°	371,2
South	-8°	73°	221,6
West	82	90°	112,4
West	82	73°	163,4

In figure 1, an overview of the system design with the measured temperatures marked out is shown.

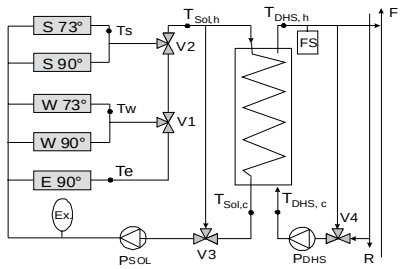

Figure 1. An overview of the system design.

The collectors are marked with S, W and E for the orientations towards south, west and east, and with the tilt angles. The temperatures from the outlets of the collector towards south, (Ts), west (Tw) and east (Te) are shown as wells as the hot and cold temperatures on the solar circuit side ($T_{sol,h}$) and ($T_{sol,c}$) and the corresponding temperatures on the district heating system side ($T_{DHS,\ h}$) and ($T_{DHS,\ c}$). The expansion vessel (Ex), the flow sensor (FS), the forward (F) and the return (R) pipes of the district heating system, the solar circuit pump (P_{SOL}), the pump on the district heating side (P_{DHS}) and the three-way valves (V1, V2, V3 and V4) are marked as well.

The control system allows cooperation of the five collectors.

Heat is delivered at minimum 65°C to the forward side of the district heating system by a plate heat exchanger.

2.2 The system design process

Before the system was built, the system design had first been tested with several different operation modes in simulations with the software Dymola and a pilot plant had been erected where measurements had been performed, all in order to find the most efficient solar thermal system. As most of the components used in the solar thermal systems are of the same type as those used in the conventional part of the district heating system, the repair time is reduced.

2.3 The flows in the collector circuits

The flow in the solar circuit is divided into three main circuits, as the heat transfer medium, Tyfocor (1,2-propylene glycol, 42-45 %), in the collectors with the same azimuth angle are mixed by static control valves (figure 1).

The flows through the three main collector circuits vary continuously. Two PID regulators seek to modify the positions of two motorized three-port control valves, V_1 and V_2, which mix the flows in a way that minimises the temperature differences between the outflows from the three circuits. The flows from the eastern and the western collector circuit are mixed in V_1, so that T_w and T_e are balanced. The valve V_2 mixes the flow from the collectors towards east/west with the flow from the southern collectors so that the highest temperature of T_w and T_e is balanced to T_s. This results in a higher flow through the circuit of the most illuminated collector. Therefore, the operation temperatures, and thus the heat losses, in the most illuminated collectors are minimised, resulting in an optimised energy output.

As the valve positions are altered and the flows in the sub circuits change, the total flow rate in the main solar circuit is changed as well, although the pump power is constant during the time the system delivers energy to the district heating system.

These are strategies to create a well-balanced temperature and flow variation between the collector circuits over the day.

2.4 Start up and shut down control of the solar circuit

The start up and shut down of the solar circulation pump, P_{SOL}, is controlled by a timer, which is programmed with start and stop hours, based on the time of sunrise and sunset, varying from month to month. The timer starts the pump running at 25% of the power required to obtain the dimensioned flow rate. The pump is operating like this for two minutes, or as long as any of the three measured outlet temperatures, T_e, T_s and T_w, are higher than 40°C. Meanwhile, the temperature of the Tyfocor at the solar inlet to the heat exchanger, $T_{sol,,h}$, is measured. In this way, overheating and loss of available energy is avoided.

When the temperature $T_{sol,\ h}$ rises above 67°C, the district heating pump, P_{DHS}, is started and the solar circuit pump activity is thereafter increased to 100%, which corresponds to the dimensioned flow in the solar circuit.

The bypass valve, V3, protects the heat exchanger against freezing. It is kept open to the heat exchanger as long as $T_{sol,\ h}$ is higher than 5°C. When the temperature is lower than that, V3 shuts and the liquid is shunted outside the heat exchanger.

If the temperatures T_e, T_s and T_w are lower than 40°C, the solar circulation pump is shut off but new attempts to start up again are performed every 30 minutes until the timer shuts off the system for the day. The fact that the temperature sensor $T_{sol,h}$ which controls the start of the pump P_{DHS}, is placed in the basement of the building,

gives a more robust system compared to if the temperature sensors on the roof would have been controlling the start of the system. The energy lost by running the pump on 25% is during short periods is very low.

A plate heat exchanger which works with equal flow rates on both sides, allows the temperature in the collector circuit, and thus also the heat losses, to be kept as low as possible.

2.5 The control of the district heating circuit

It is very important that the water going out to the district heating system has reached the minimum temperature of 65°C in order to secure the thermal comfort for the customers.

In the heat exchanger, the return flow from the district heating system is heated from approximately 45°C to the temperature required for the outgoing flow, which is 65°C minimum (and approximately 85°C maximum).

The three-way valve, V4, is used to control the flow through the heat exchanger on the district heating system side, adjusting the temperature of the outgoing water. The valve is open enough to secure that the temperature coming out from the heat exchanger, $T_{DHS,h}$, is 65°C or higher. If $T_{DHS,h}$, is too low, the water is re-circulated through the heat exchanger.

The pump in the district heating circuit, P_{DHS}, is a distribution pump that increases the pressure from 4 bar on the return side to approximately 7 bar on the outgoing side, which is a rather electricity demanding process. The highest pressure in the district heating system is 12 bar. The pump is active as long as $T_{sol,\ h}$ is 65°C or higher. The pump power is then adjusted with the aim to generate equal flow rates on the both sides of the heat exchanger.

The flow sensor (FL in figure 1) registers the actual flow rate in the district heating system circuit by measuring the pressure difference over a measuring flange. Flow disturbances from the district heating system and from the heat exchanger can thereby be adjusted.

The optimal pump power is calculated based on the position of the control valves and the flows in the solar sub circuits. This regulates the set point for the power of the pump on the district heating side.

When P_{DHW} is operating the solar pump P_{sol}, is set to operation mode (100%), providing the dimensioned flow in the solar circuit.

If the valve V4 on the district heating side has been closed for ten minutes, the district heating pump is shut off and the solar circuit pump is set to its mode of 25% rotation speed, waiting for the temperature to rise before a start-up can be initiated once again.

In case of activated freezing alarm, the three-way valve of the district heating system circuit is opened just enough to keep the outgoing water above 15°C.

By having double control functions for the pump, on both the temperature and the flow of the circuit, the system becomes more robust.

2.6 *Overheat protection by partial evaporation*

One important design criterion has been not to let the heat transfer medium out of the system unless it is absolutely necessary. The system is protected from overheating by control features allowing partial evaporation of the heat transfer medium. The system is equipped with a compressor-fed expansion vessel that is automatically refilled after boiling. The large expansion vessel of 1000 l is designed to handle the entire collector volume of the system. In case of boiling and stagnation, the pressure will rise to a certain limit before air is let out of the expansion vessel through a solenoid valve, maintaining this slightly higher pressure. The solar circulation pump is then stopped, in order to prevent as much of the liquid as possible from boiling and to protect the collectors from hammering as the hot steam condenses when meeting the cold liquid. The heat transfer medium is thereby pressed backwards into the expansion vessel. As the weight of the expansion vessel increases over a critical level, a pressure sensor triggers an alarm to the control centre.

When the collectors have been cooled down and the Tyfocor condensates, the pressure in the solar circuit decreases and the medium in the expansion vessel is pressed back into the system, due to the higher pressure in the expansion vessel. The compressor refills the expansion vessel with air to a certain pressure and the solar circuit is then ready for operation again.

If electricity is unavailable the solenoid valve can not open and decrease the pressure. To handle this scenario a mechanical safety valve on the airside of the expansion vessel opens. If this also fails each of the five collector subsystems are equipped with a mechanical safety valve. The Tyfocor released from these valves are collected in a large container. From this container the system can be refilled manually with an electric pressure pump.

The risk of implosion, which may arise due to too low pressure when the heat transfer media is running back into the system and the compressor is not in operation, is prevented by another valve that opens if the pressure is below a certain limit, letting air into the system. The system has never been exposed to boiling but the pilot plant was in stagnation several times during the design faze, both with and without electricity, and the overheat control strategy was proven successful.

2.7 The system as a part of the district heating system

The system works as any other conventional production unit in the district heating net, with the exception that the production can not be predicted and the production unit is installed at a customer. It is therefore extremely important that the solar thermal system is robust and provides a high availability, in order for the system not to cause disturbances, like low-temperature water going out on the district heating net. This could cause discomfort for the customers and create a demand for adjusting the problem, which would probably have been done by using electricity peak power.

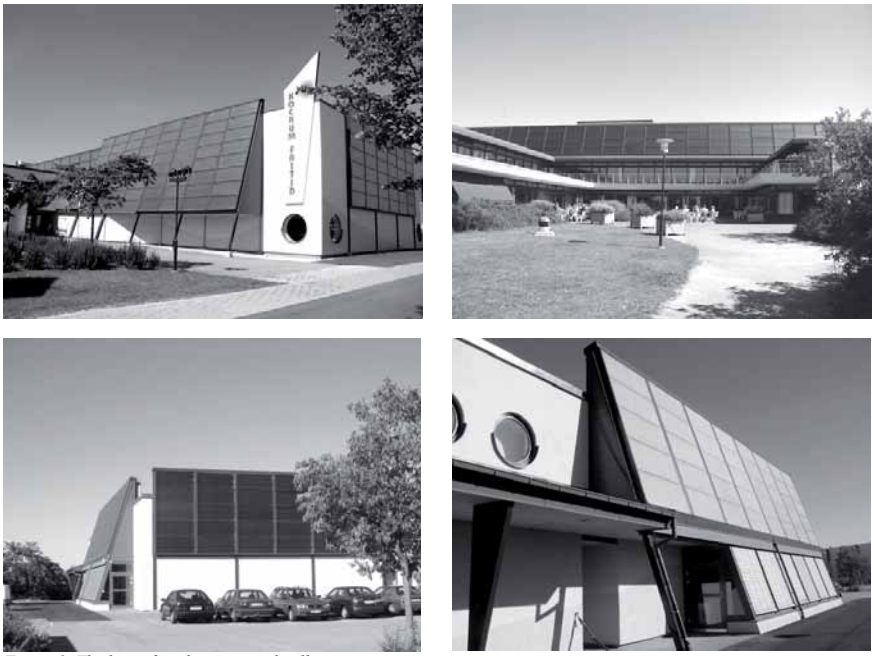

Figure 2. The large façade-integrated collectors.

The knowledge about the district heating system and the nearby consumers are utilized to optimise the operation circumstances of the solar collector system. The solar system is situated in the outer parts of the district heating system but still very close to a larger group of consumers. The buildings in this area are built with consideration to the fact that they need to keep thermal comfort at the minimum temperature of 65°C from the district heating system. Because of the closeness and the low temperature required the heat losses can be kept very low.

Another important characteristic of the system is that the pipe from the heat exchanger to the main forward pipe of the district heating system is designed as short as possible, in order to avoid low-temperature water going out to the customers.

2.8 Measurements and monitoring

Hourly values of temperatures, flow rates, valve positions, pump activity etc. from the system are measured continuously and collected in a data base at the control centre of the district heating network. From there the system control parameters can be changed and the operation controlled. A new control system is used and it has access to every measuring point in the solar system. It has its own data collection algorithm that uses the deviations between the sampling points to decide if a new data point should be stored or not. The total energy output is measured on the district heating circuit by an energy meter. The temperatures in and out of the heat exchanger are measured, which makes it possible to monitor the performance of the heat exchanger.

2.9 Architectural aspects of the building integration

The installation of the collectors was carried out as a replacement of the old façade and they have been given an interesting and appealing design, well integrated in the building. The frosted glazing makes the collectors more appealing but lowers the energy output and hides the absorber fins.

The bold design of the collectors occupying a very large part of the façade (see figure 2), accentuates the solar panels and emphasises the concept of renewable energy use and sustainable solutions.

2.10 Economical aspects

Economical support from the government for local investment programs have been received for the installations of the collectors, belonging to the sports

centre. For the energy company Sydkraft (that owns the delivered energy and the system components except the collectors) the alternative to installing this solar thermal system was to increase the heat production elsewhere in the district heating system. The possibility of installing a large field of collectors outside the city and connecting it to the district heating system was never a realistic option since the long piping required and the high cost of ground area would have made the project far too expensive. In comparison to that option, the placement of the collectors on the façade provides an economically advantageous solution.

3. EVALUATION METHODS

3.1 The WINSUN program

The TRNSYS based simulation program WINSUN was used for the simulations of solar gains from the different collectors. The program calculates the theoretical monthly energy output from the solar collectors using climatic data from Meteonorm as input data. The program also uses the monthly operation temperatures of the collectors, parameters of the collector performances and orientations, climatic data and certain other surrounding conditions. It returns the monthly energy output for the period.

3.1 Data analysis and simulations

Measured data from the solar thermal system from the period 2002-07-01 to 2003-06-30 have been analysed and used for simulations. Each collector was simulated separately. The performance parameters of the collectors from Aquasol that was used as input to WINSUN are shown in table 2. The parameters are the results of collector test performed by SP, the Swedish National Testing and Research Institute. The parameter c_0 is 0.83 for the collector in its original design, but was for this case estimated lower, due to the frosted glazing.

Table 2. The collector performance parameters of the Aquasol collectors used in WINSUN. The parameter c_0 is normally 0.83 but was estimated lower due to the frosted glazing.

c_0 (W/m²K)	c_1 (W/m²K)	c_2 (W/m²K²)	b_0 (-)
0.81 (0.83)	2.7	0.03	0.10

Solar radiation data from site of the collectors were not available. Therefore a detailed analysis of the performance of the system was not possible. Instead simulations were performed with the WINSUN program. Monthly mean flow weighted operation temperatures in the collectors were derived from measurements and used as input in the simulation program. The average operation temperature over the year was calculated to 63°C.

WINSUN used climatic data from Meteonorm for a typical year in Lund, close to Malmö. This means that WINSUN predicts the annual performance of the collectors for a normal year in Lund. The Meteonorm data were then compared with solar radiation data from the Technical University of Denmark, Copenhagen, registered during the measured period.

4. RESULTS

4.1 The over all energy yield from the system

During the investigated period from 2002-07-01 to 2003-06-30, the system delivered 189000 kWh to the district heating system, i.e. 180 kWh/m² collector area, with a peak power of 0.3 MW. The COP, the Coefficient Of Performance, i.e. the thermal energy produced per unit (kWh) electricity used for the system operation, e.g. pumps etc. was 24, according to the measurements.

The results from the simulations show an expected energy output of 183000 kWh/a, i.e. 174 kWh/m^{2}a, which is a divergence of only 3% from the measured output.

The results of annual energy output are as high as can be expected from a system with collectors in non-optimal directions.

4.2 Correspondence of measured and simulated energy output and irradiation

Monthly values of simulated energy output from the solar collectors during an average year and measured monthly values of total energy output on the district heating system during the investigated period are shown in figure 3. The simulated values show a similar dispersion over the year as the measured values, although there are obvious deviations, largest in March and September. When the measured output is lower than the simulations, the deviation could possibly be explained by the fact that the district heating pump does not start until 67°C is obtained at the inlet to the heat exchanger.

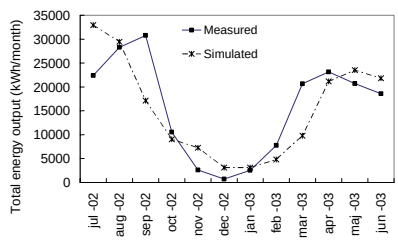

Figure 3. Measured and simulated results of the total monthly energy output from the solar thermal system.

The divergence can also be explained by the natural climate changes from year to year. The solar irradiation

varies considerably from year to year and the collector output also varies accordingly with ± 20% around the average value, according to an investigation of data from a 16 year period presented by Adsten (2002).

Figure 4 shows that data used in WINSUN (originally from Meteonorm) of global irradiation on horizontal, which represent an average year, correspond rather well with the measured data from Copenhagen. Data is shown for the year 2002 and the first six months of 2003.

From the measured data from Copenhagen from 2003 there were some data points missing. Therefore the mean values of the measured values each month have been used instead for 2003.

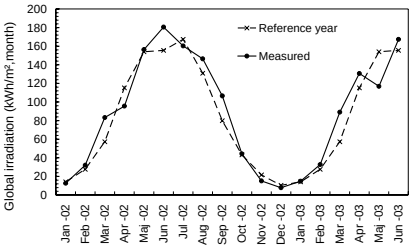

Figure 4. Monthly values of global irradiation on horizontal from Copenhagen and the corresponding reference year values used in WINSUN.

However, the direct beam irradiation also plays an important role for the energy production from the solar collector. Figure 5 shows the variation in measured values of direct beam irradiation, normal to the sun, from Copenhagen. The difference between these values is very large during the year and is very large in March and September. This variation in beam irradiation from year to year could explain the deviation of energy output shown in figure 3.

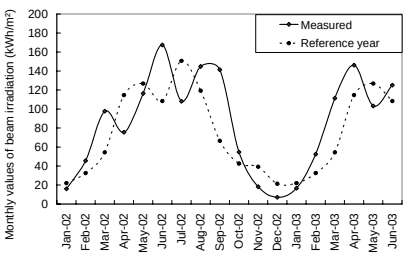

Figure 5. Monthly values of beam irradiation from Copenhagen and the corresponding values used in the climate data in WINSUN.

The result show that the measured beam irradiation, diverge significantly from the reference year used in WINSUN. This, together with the fact that the model is rather rough, can probably explain the difference between simulated and measured energy output from the collectors. The simulations can thus be accepted as giving interesting indications of the actual output.

4.3 The cooperation of the collectors

Figure 6 shows the positions of the motorized three-way valves, V1 and V2 in figure 1, which alter the flows of the main collector sub circuits. The data is from the 20th of July 2003, a sunny clear day when the solar pump was working at 100% speed during the whole day.

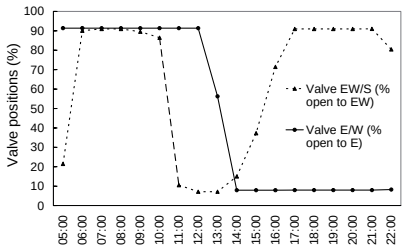

Figure 6. The positions of the motorized three-way valves, V1 and V2, controlling the flows of the collector circuits, measured during a clear summer day, the 20th of July 2003.

In figure 7, data of the outlet temperatures from the different collectors, T_e, T_s and T_w, (from the same day) are shown as well as the temperatures going in to the heat exchanger on the solar side, $T_{Sol,h}$, and out of the heat exchanger on the district heating side, $T_{DHS,h}$.

Figure 7 shows that the temperatures in and out of the heat exchanger, $T_{sol,\,h}$ and $T_{DHS,\,h}$, are stable from 07:00 to 20:00. As the temperature $T_{Sol,h}$ is decreasing below 67° in the evening, the district heating pump is stopped and no more energy is delivered to the district heating system. This can be seen in figure 8, showing the total energy delivered to the system during the day.

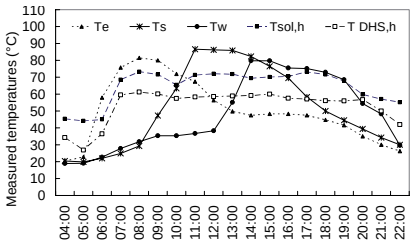

Figure 7. The outlet temperatures from the three main collector circuits, T_e, T_s, T_w, and the temperatures at the inlet to the heat exchanger on the solar circuit side, $T_{sol,h}$, and the outlet from the heat exchanger, $T_{DHS,h}$, in the district heating circuit. Data from the 20th of July 2003.

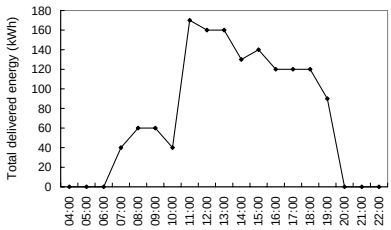

Figure 8. The total delivered energy to the district heating system the 20th of July 2003.

The figures 6, 7 and 8 show that the flows are well controlled and result in a constant output temperature. The higher output during the afternoon is explained by the larger areas towards west than towards east.

4.4 Parametrical studies

It is interesting to see how much energy could be gained by decreasing the operating temperatures and how much is gained by keeping the operation temperature as low as possible.

The results from WINSUN, shown in figure 9, show how the theoretical energy output for the different collectors and the area weighted mean energy output of the whole system would change if the mean operation temperature in the collectors would change. At present the average mean operation temperature is 63°C. The collector facing south and tilted 73° give the highest annual output, followed by the 73° tilted collector directed towards west, which give almost the same results as the area weighted system average. The collector facing east and tilted 90° is the collector with the lowest output. Should the operation temperatures instead be 40°C or 50°C, the output would have been 60-130 kWh/m²a higher. A 10°C increase in temperature decrease the mean annual energy output by around 50 kWh/m².

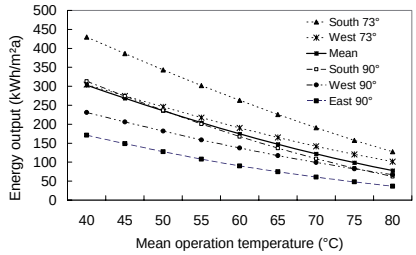

Figure 9. The theoretical energy output of the different collectors for different mean operation temperatures in the collectors and the mean values of the system.

The simulation results in figure 10 show the monthly distribution of the energy output from the five collectors.

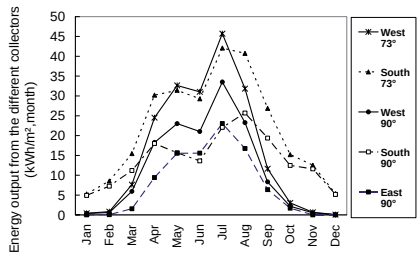

Figure 10. The simulated energy output for the different collectors shown as monthly values over the year.

The west- and south-facing collectors, tilted 73° give the highest peaks in summer, while the south-facing vertical collector gives a more balanced output over the year. Both south-facing collectors provide some energy output during winter, when the eastern and western collectors hardly deliver any energy at all.

In figure 11, the monthly values of mean area weighted energy output of the system are shown, as well as results of the energy output from a system where the collector are placed horizontally or towards south, tilted 40°. The values of annual results are shown in table 3.

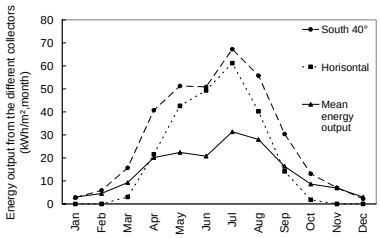

Figure 11. Simulation results of the mean area weighted energy output and the theoretical output for horizontal or south-facing 40° tilted collectors.

During the winter, the mean energy output of the system is higher compared to if the collectors were to be placed horizontally but not more than if they were to be directed towards south tilted 40°.

Table 3. The simulated annual energy output of the differently tilted collectors and of a horizontal and south-facing collector tilted 40°.

Colector direction and tilt	East 90°	South 90°	South 73°	West 90°	West 73°	The total system	South 40 °	Hori-zontally
Annual energy output (kWh/m²a)	90	167	263	137	190	174	343	234

It can be concluded that the high tilt of the south-facing collectors gives balance to the energy distribution over the year whereas the vertical east- and west-facing collectors give less energy during the cold season.

The global irradiation from Meteonorm is shown in figure 12 in order to verify the results in figure 10.

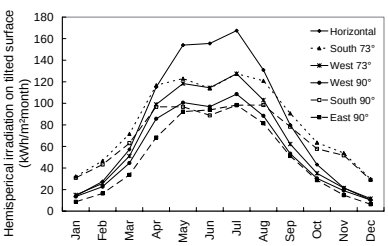

Figure 12. Data of global irradiation for differently tilted surfaces, derived from Meteonorm.

If the collectors were tilted differently, the energy output would change according to figure 13. It the tilt was 45° the would give the maximum annual output of 340 kWh/m^{2}a, compared to the 180 kWh/m²a they give today.

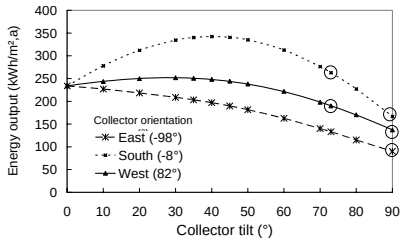

Figure 13. Simulated values of energy output for the collectors in given directions and in different tilt angles. The rings show the actual orientation of the collectors.

5. DISCUSSION

The simulation results, without access to irradiation data, give a relatively rough prediction of the system performance.

The agreement between measurement and simulations based on Meteonorm data is satisfying. The simulations and parametrical studies give indications of the possible improvements that different orientations or operation temperatures could give.

The control of the flows through the collectors is very important. The chosen control strategy evens out the temperature differences between the different collectors and results in a balanced flow over a daily bases, with the highest flow rate in the most illuminated collectors. The output temperature is shown to be rather constant over the day.

If the collector all had been mounted in the optimal direction, towards south tilted 45°, the energy output would have been increased by a factor of 2. But since the collectors were replacing wall materials they were installed in all directions.

The system is a well-functioning heat producing plant, which have worked during three years without unexpected interruptions.

A solar thermal system that produces heat to the forward side of the district heating system, with a constantly high heat load, can of course be designed very differently compared to a system that requires a storage tank, but there are many interesting design features applied in this system that would be interesting to consider also for other solar thermal systems, as e.g. the use of robust components.

The design method to both test the system by simulations and by a building a pilot plant is a very promising strategy, yet seldom possible within the budget frames. Hopefully, the good ideas and design features applied in this system can also be successfully applied elsewhere.

6. CONCLUSIONS

A large façade-integrated, highly automated solar thermal system is connected to the outgoing side of the district heating system in Malmö, Sweden and has been operated and monitored since June 2002 without interruptions. From 2002-07-01 to 2003-10-30, the collectors delivered 180 kWh/m²a to the district heating system, with a peak power of 0.3 MW, which is as expected from a system with non-optimally oriented collectors. According to simulations performed with WINSUN, the average annual energy output should be 174 kWh/m^{2}a, i.e. a difference of 3% from the measured output.

Collector parameters from standard testing and climatic data based on Meteonorm data for a normal year were used as an input for the simulations. This also means that the procedure for using Meteonorm, when measured irradiation data is missing, seems to work satisfactory. The monthly values from simulations and measurements show larger differences, which are explained by the climatic changes from year to year.

The system consists of five different sub-systems in different directions connected to the district heating net via an advanced control system and heat exchanger. The analysis shows that the control system, which is designed to deliver heat at temperature of at least 67° to the heat exchanger, is working satisfactory. The temperature going into the heat exchanger and the temperature going out to the district heating system are relatively constant during the time heat is delivered.

The system has an overheat protection system based on partial evaporation, where a compressor-connected expansion system is used for automatic refilling after boiling. This system was never tested during first years of operation, since the system never reached stagnation. However, the pilot plant was in stagnation several times and the control strategy was then proven successful.

The parametrical studies show that the collectors tilted in 73° south give the highest energy output. The vertical collectors in east and west give the lowest output. If all collectors were installed in south direction and tilted 40° the annual performance should increase by a factor of 2. This was not an option in this case though, as the collectors were replacing the façade.

The south-facing collectors with a high tilt give higher output during spring and fall and the east and west collectors contribute to a uniform energy distribution over the day.

The idea with the collectors connected to district heating grid close to buildings which are designed to sustain thermal comfort at low temperatures is that it allows the collectors to operate at a relatively low temperature. The over all evaluation show that the advanced system design for start up, stagnation and control has resulted in a well working solar collector system with high accessibility.

ACKNOWLEDGEMENTS

Martin Råberg at Carl Bro Group is acknowledged for support and serving of detailed information of the system design and construction.

Li Lövehed and Per Rosén at Sydkraft Värme Syd are acknowledged for providing measured data from the solar thermal system and general information about the district heating system.

Elsa Anderson and Simon Furbo at the Department of Civil Engineering at the Technical University of Denmark are acknowledged for contribution of climate data.

REFERENCES

Adsten, M., (2002) *Solar Thermal Collectors at High Latitudes. Design and Performance of Non-Tracking Concentrators,* Acta Universitatis Upsaliensis, Uppsala, Sweden.

Duffie J.A. and Beckman W.A. (1991) *Solar Engineering of Thermal Processes*, 2nd edn. Wiley Interscience, New York.

Weiss W. (2003) *Solar Heating Systems for Houses. A Design Handbook for Solar Combisystems*. James and James, London.

Paper VII

Available online at www.sciencedirect.com
ScienceDirect
Solar Energy Materials & Solar Cells 91 (2007) 1788–1799
Solar Energy Materials and Solar Cells
www.elsevier.com/locate/solmat

Optimisation of reflector and module geometries for stationary, low-concentrating, façade-integrated photovoltaic systems

Helena Gajbert[a,*], Maria Hall[b,1], Björn Karlsson[a,2]

[a]Energy and Building Design, Lund University, P.O. Box 118, SE-221 00 Lund, Sweden
[b]Swedish Energy Agency, P.O. Box 310, SE-631 04 Eskilstuna, Sweden

Received 19 November 2006; accepted 14 June 2007
Available online 9 August 2007

Abstract

The high cost of photovoltaic modules motivates the use of reflectors to increase the electricity production. The system geometry of static low-concentrating PV systems for building-integration with parabolic aluminium reflectors was optimised for maximum annual electricity production. The optical efficiency of systems with different geometries was calculated from short-circuit current measurements on thin film modules and the annual electricity production was simulated. An inclination of the reflectors' optical axis of 35°, resulting in a concentration ratio of 4.65, showed the highest electricity yield per cell area, 120 kWh/m^2 cell area, 72% higher than for a vertical module without reflector.

Keywords: Photovoltaic; Parabolic; Reflector; Building integration; Solar simulator

1. Introduction

1.1. Background

Building integration is a rapidly increasing market for photovoltaic systems [1]. By integration of the photovoltaic systems in the building envelope already during construction, building material is saved and redundant work is avoided, which results in cost reductions for the combination of new building and electricity system. Still, grid-connected solar electricity is not cost-competitive on the electricity market due to the high cost of photovoltaic modules. This high cost motivates the use of relatively cheap, highly reflecting mirrors for increasing the irradiance on the modules and thus the electricity production.

A previously designed static, concentrating photovoltaic system for integration in a south-facing façade is shown in Fig. 1 [2]. The collector has a PV/thermal hybrid absorber and the system includes parabolic aluminium reflectors and photovoltaic string modules, as well as expanded polystyrene (EPS) insulation. Due to the insulation material, which is attached directly to the back of the reflector sheet metal, the façade element can serve as an integrated part of the building envelope.

Similar asymmetric concentrating collector systems for façade integration have been evaluated by measurements [3–5] and found to increase the performance by 62% for a geometrical concentration ratio of 2.0.

The geometry of the CPC:s presented in this work is highly asymmetric and includes only one, upper reflector. This simple design facilitates the production of the collector, which leads to cost reductions.

The transversal incidence angles are here defined as angles in the north–south–vertical plane and the longitudinal incidence angles are defined as those in the east–west plane. This is illustrated in Fig. 2.

The thin film photovoltaic CIGS (copper–indium–gallium–diselenide) module used in this work is suitable to use in combination with reflectors if the long narrow cells are aligned normal to the reflectors. Unlike the

*Corresponding author. Tel.: +46 46 222 7583; fax: +46 46 222 4719.
E-mail addresses: helena.gajbert@edb.lth.se (H. Gajbert), maria.hall@energimyndigheten.se (M. Hall), bjorn.karlsson@edb.lth.se (B. Karlsson).
[1]Tel.: +46 16 544 2174, fax: +46 16 544 2099.
[2]Tel.: +46 46 222 7261, fax: +46 46 222 4719.

0927-0248/$ - see front matter © 2007 Elsevier B.V. All rights reserved.
doi:10.1016/j.solmat.2007.06.007

crystalline silicon cells used by Refs. [3–5], which have to be connected in a single string if equal irradiance on all cells should be obtained, the CIGS cells offer higher flexibility in production to suitable sizes and are less sensitive to shading from the horizon. Therefore, this design has a high potential to be applicable also for large-scale installations, which in turn gives it potential to be developed into a cost-efficient component.

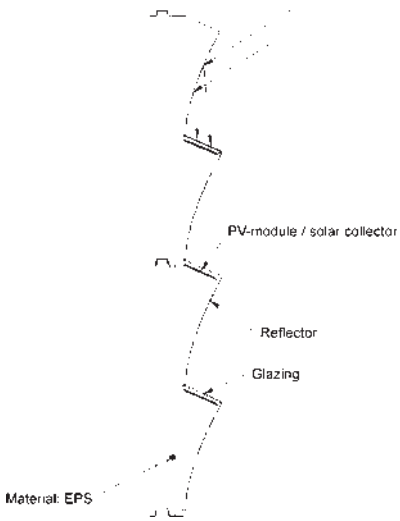

Fig. 1. Cross-section of a static, two-dimensional concentrating photovoltaic system intended for façade integration. The system has a concentration ratio of 3 and includes photovoltaic string modules and parabolic aluminium reflectors, as well as EPS insulation.

1.2. Objectives of this work

The objective of this work was to optimise the geometry of a wall-integrated concentrating solar collector [6] for operation in regions of latitudes around 60° so that maximum annual electricity production is achieved. The tilt angle of the photovoltaic module and the inclination of the parabolic reflector's optical axis has been evaluated and optimised by measurements and simulations. Both the influence of the lower acceptance angle and the tilt of the module plane have been investigated.

2. System design

2.1. Angular distribution of annual irradiation

A static concentrating collector requires a low-concentration ratio in order to benefit from solar irradiation also at low solar angles. A suitable collector geometry is estimated from data of irradiation in Stockholm, Sweden. Here, the greatest amount of irradiation on a south-facing vertical surface is received from south projected incidence angles, $\alpha_{NS} = 50–55°$, as shown in Fig. 3, which represents data collected in Stockholm during the period 1983–1991 [7]. This figure indicates that a static, façade-integrated concentrator for all year operation should accept radiation between 10° and 60°. The irradiation is considerably reduced during the winter due to cloudy climate and absorption of the radiation in the atmosphere [8]. This explains the low irradiation at α_{NS} between 0° and 5°. Shadow effects from the surrounding can further decrease the irradiation for low altitudes.

An ideal asymmetric vertical concentrator with reflectors that accepts solar irradiation from incidence angles $\theta_{min} = 10°$ to $\theta_{max} = 60°$ gives a concentration ratio, C, of maximum 2.89, as calculated by Eq. (1) [9]. If the acceptance interval is 25–60°, C_{max} is 4.51. These geometries require a wedge formed absorber and two reflectors. With a single reflector that accepts irradiation in the interval 25–90°, C_{max} is 3.46:

$$C = \frac{2}{\sin\theta_{max} - \sin\theta_{min}}. \quad (1)$$

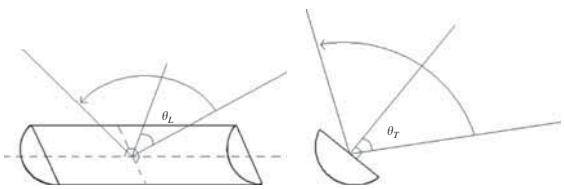

Fig. 2. Definition of the longitudinal angle θ_L and the transverse projected angle θ_T.

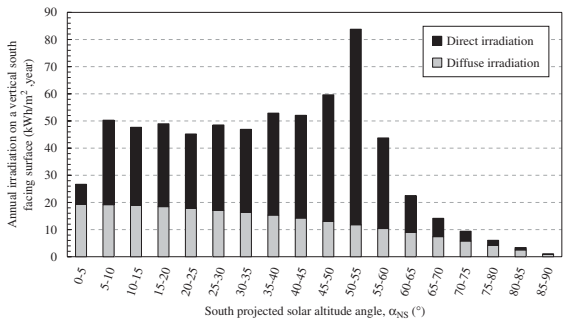

Fig. 3. Angular distribution of annual direct and diffuse irradiation (mean values for 1983–1991) on a south-facing vertical surface in Stockholm, Sweden.

2.2. System geometry

The reflectors used for the system designs are 2D parabolic mirrors extended in the east–west direction, a design feature often used in solar energy applications [10]. This system is primarily intended to be unglazed and passively cooled. However a glazed surface could be placed vertically in front of the whole façade element in order to protect and prolong the lifetime of the reflector material. Glazing is here described in order to better illustrate the geometry.

The system geometry, illustrated in Fig. 4, is based on a 2D parabolic graph. The inclination of the optical axis to the horizontal is denoted v and h is the height of the glazing. As all irradiation incoming parallel to the optical axis or from higher solar altitude angles will fall between the focal point, F, and the reflector, it is suitable to place an absorber here. The angle β denotes the tilt angle of the absorber plane and a denotes the width of the module plane. The angle ϕ is the angle between the vertical glazing and the optical axis of the reflector. The transversal incidence angle, θ_T, on the vertical glazing is equal to the solar altitude angle projected in the north–south vertical plane, α_{NS}.

The mathematical description for the parabola is shown in Eq. (2). The focal length, p, is the distance between the origin of the parabola and the focal point along the optical axis. r is a vector from the focal point to a point on the curve, at angle ϕ:

$$r(\phi) = \frac{p}{\cos^2(\phi/2)}. \tag{2}$$

The geometrical concentration ratio, C, of the concentrating system is defined as the ratio between h and a, which both can be expressed by r. For $r = h$, ϕ *is* $v + 90$ and for

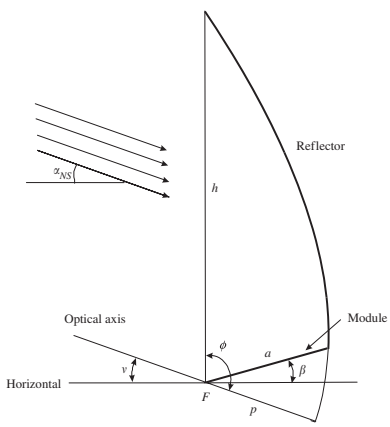

Fig. 4. Illustration of the collector with the parabolic reflector. All symbols are described in the text.

$r = a$, ϕ is $v + \beta$. C can be calculated from

$$C = \frac{h}{a} = \frac{\cos^2((v+\beta)/2)}{\cos^2((v+90)/2)}. \tag{3}$$

Two different geometries, illustrated in Fig. 5, were analysed in detail in order to investigate the difference between system designs of different concentration ratios. In both geometries, the angle v, between the optical axis and the horizontal, is 25° and the distance p is 158 mm.

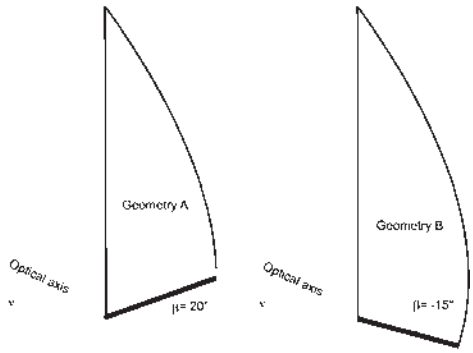

Fig. 5. Geometries A and B. The angle β is 20° in Geometry A and −15° in Geometry B.

In Geometry A, the module tilt angle, β, is 20°, which results in a geometrical concentration ratio C of 2.96. For Geometry B, β is −15° and C is 3.44. The positive module tilt gives the system a better performance at low solar altitudes as direct irradiation can fall on the absorber. The negative module tilt of Geometry B was chosen because it gives the system a higher geometrical concentration ratio. The different absorber tilt angles also means that the absorber width a is slightly higher for Geometry A than for Geometry B.

2.3. Reflector material

The mirrors are based on anodised sheet aluminium, which offers good mechanical properties. The total and the specular reflectance were calculated to 83% and 82%, respectively, from measurements at near normal incidence at wavelengths of $\lambda = 200$–2550 nm, for which a Perkim-Elmer λ-900 spectrophotometer equipped with an integrating sphere was used. The results are shown in Fig. 6. The reflectance increases very slowly with increasing angle of incidence [11]. The weighted total solar reflectance for wavelengths shorter than 1100 nm is 81%.

3. Experimental methods

3.1. Electrical measurements

In this work, measurements of the short-circuit current of photovoltaic CIGS string modules placed on the absorber plane of a system prototype were performed. Measurements were performed using a system prototype with a fixed angle v of 25° and with a module plane that can be tilted at different angles β (see Fig. 7). Measurements

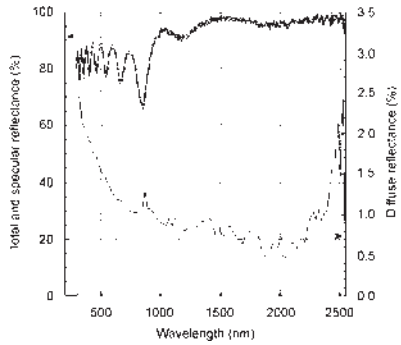

Fig. 6. Total specular, and diffuse reflectance of anodised aluminium at near normal angle of incidence.

were performed for Geometry A ($v = 25°$, $\beta = 20°$), Geometry B ($v = 25°$, $P = -15°$) and for a vertically placed reference module without reflector.

The measurements were performed indoors, using a large indoor solar simulator with parallel light [12]. The solar simulator is built up of parabolic collimators that render the light almost parallel, which means that only beam irradiance is used during the measurements. The light bulbs used in the simulator contain a metal halide gas, which gives the light spectral characteristics similar to sunlight. The simulator can be lifted to simulate different solar altitudes, between 0° and 73.5°, and measurements were

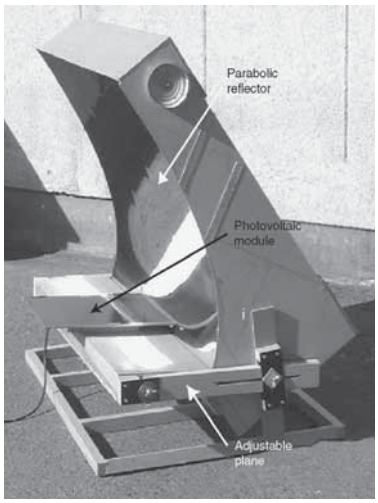

Fig. 7. The system prototype with parabolic reflector and an adjustable module plane.

performed for every 10th solar altitude angle from 0° to 70°, which for the vertical collector facing the simulator is equal to the transversal incidence angles, θ_T. No glazing was used during the measurements.

As the absorber tilt, β, was altered from $-15°$ to $+20°$, the module width, a, was varied accordingly. The accurate active module sizes were obtained by shielding the CIGS cells (including the vertical reference cells) with aluminium foil, as illustrated in Fig. 8. The aperture opening h is constant.

The CIGS module was suitable for this purpose, as the module is built up by narrow rectangular cells extended perpendicular to the length of the east–west oriented concentrator. This means that all series-connected cells get equal irradiance.

3.2. Calculation of optical efficiency

The measured optical efficiency for beam irradiation, η_{0b}, was determined for each measurement. It was calculated from the results of short-circuit current measurements from the cells in the concentrating system $I_{SC(conc.)}$, and from the measurements of the vertical reference, $I_{SC(ref.)}$ using

$$\eta_{0b} = \frac{I_{SC(conc.)}}{C I_{SC(ref.)}}. \quad (4)$$

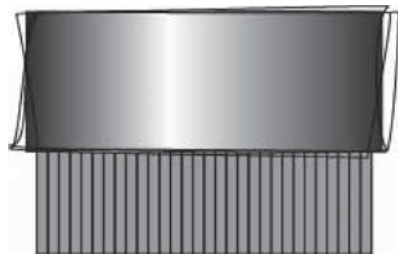

Fig. 8. A thin film CIGS module with the cells extended perpendicular to the reflector, shielded with aluminium foil.

The calculated optical efficiency for beam irradiation, here referred to as $R_T(\theta_T)$ of this system, was calculated by

$$R_T(\theta_T) = \frac{1}{C}\frac{\cos(90° - \beta - \theta_T)}{\cos(\theta_T)}, \quad \theta_T < v, \quad (5)$$

$$R_T(\theta_T) = \frac{k(h\cos(\theta_T) - a\cos(90° - \beta - \theta_T)) + a\cos(90° - \beta - \theta_T)}{h\cos(\theta_T)}$$
$$= k + (1-k)\frac{1}{C}\frac{\cos(90° - \beta - \theta_T)}{\cos(\theta_T)}, \quad \theta_T > v. \quad (6)$$

Eq. (5) is based on the cosine dependence of the intensity on the modules for θ_T angles lower than v, when a fraction of the irradiation reaches the module at an angle of incidence of $90°-\beta-\theta_T$ and the rest is reflected back out from the collector. The direct irradiation on the module is divided by the direct irradiation on the glazing and the concentration ratio. For θ_T angles higher than v, a fraction of the beam radiation reaches the module directly and the remaining fraction is reflected onto the module. These fractions are included in Eq. (6), where it is assumed that the rays that reach the reflector are reflected only once before they hit the module. An effective reflectance, $k = 0.69$, was introduced in the equation to get a good fit to measurement data in Fig. 16. In an ideal system without resistive losses in the photovoltaic cell, there is no angular dependence of the absorption of the cells, and with a perfect geometry, the value of this constant would be close to the value of the reflectance of the reflector as the average number of reflections is close to unity. The graphs in Fig. 9 show the calculated optical efficiency for Geometries A and B for varying incidence angles and the effect of the reflector is shown by the difference in optical efficiency at low incidence angles, when the rays are not reflected, and for incidence angles higher than the optical axis, 25°, where the reflector is useful. For incidence angles higher than 70°, the irradiation falls directly on the absorber without reflections and the optical efficiency reaches unity.

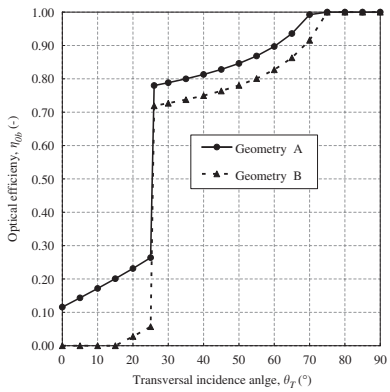

Fig. 9. The calculated optical efficiency $R_T(\theta_T)$ for the two geometries. The current is significantly higher for incidence angles higher than the angle of the optical axis (25°) as it implies that the irradiance is concentrated.

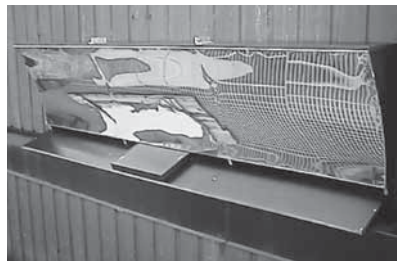

Fig. 10. Photograph of a ST5 photovoltaic module from Siemens in a concentrating reflector system of Geometry A, where the tilt of the optical axis, v, is 25° and the absorber tilt, β, is 20°. An identical reference module was mounted in the vertical plane of the aperture.

The relatively low value of the effective reflectance, k, is explained by multiple reflections and optical imperfections. The cell with the lowest irradiance limits the performance.

3.3. Long-term outdoor measurements

An unglazed system of Geometry A and a vertical reference system was long-term monitored in Älvkarleby, Sweden (60.6°N, 17.4°E) during July–October 2003 by monitoring the short-circuit current from the reference and the concentrator module and also the global and diffuse irradiance. The stored data was averaged during 10 min periods. The set-up is shown in Fig. 10.

3.4. The MINSUN simulation program and the biaxial incidence angle dependence model

The MINSUN program was originally developed for simulations of energy yield from thermal collectors. It is specially developed for simulating solar collectors with a complicated angular dependence [13]. The program can be modified for simulations of electricity yield from photovoltaic modules of known nominal power, since it calculates the annual irradiation on a specified surface. Basically, it means that it simulates the energy yield of a solar collector with a defined optical angular dependence and no thermal losses.

MINSUN uses hourly climate data of direct and diffuse irradiation to calculate the total annual irradiation on a specified surface. The total absorbed irradiance, S, is obtained by multiplying the incoming radiation by incidence angle modifiers for beam, K_b, diffuse, K_d, and ground reflected irradiance, K_g. The direct (beam) irradiance, I_b, is also multiplied by C as shown in Eq. (7). I_d is the diffuse irradiance and I_g is the ground irradiance [14]:

$$S = CK_b(\theta)I_b + K_dI_d + K_gI_g. \quad (7)$$

Asymmetric collectors have to be modelled by a biaxial model that accounts for the different optical efficiency in different planes of incidence. A commonly used model is shown in Eq. (8), where θ_L is the longitudinal angle and θ_L is the transverse projected angle of incidence, as defined in Fig. 2:

$$K(\theta_L, \theta_T) = K_L(\theta_L, 0)K_T(0, \theta_T). \quad (8)$$

This model was presented by Rönnelid. [15] and estimates the optical efficiency K by measurements of the optical efficiency in the perpendicular longitudinal and transverse directions. This model is difficult to use for the geometries evaluated in this work, since the angles for $\theta_T = 0°$ is outside the acceptance interval. Furthermore, it does not model the angular dependence of the glazing in a correct way.

An alternative model has recently been proposed [16] that separates the influence of the glazing and of the concentrator. The optical efficiency of this type of symmetric two-dimensional concentrators, like troughs, depends on the components of the rays in the transversal plane. The angle of incidence in this plane is θ_T and the reflector trough will be modelled as a function of this angle. The transmittance of the glazing depends on the true angle of incidence on this surface, here denoted θ_i. Eq. (9) defines the proposed model. Here, R_T models the effect of the concentrator and f_L models the effect of the glazing.

$$K_b(\theta_L, \theta_T) = R_T(\theta_T)f_L(\theta_i). \quad (9)$$

MINSUN calculates the total incidence angle modifier as a product of the functions of $R_T(\theta_T)$ and $f(\theta_i)$. The functions are given in MINSUN numerically in intervals of 5°.

In the simulations, the ground reflected radiation, K_g, was assumed to be 0. The incidence angle modifier for diffuse irradiance, K_d, is given as a constant value or obtained by integrating $R_T(\theta_T)f_L(\theta_i)$ over an isotropic sky. This means that Eq. (10) gives the useful irradiance S on the cell:

$$S(\theta_T, \theta_L) = CR_T(\theta_T)f_L(\theta_i)I_b + K_dI_d. \quad (10)$$

The function R_T is obtained from measurements of the optical efficiency in the transversal plane with $\theta_L = 0$. The f_L function is obtained from measurements of the optical efficiency in a plane where θ_L is constant. This means that f_L conveniently can be modelled as a conventional b_0 function according to Eq. (11) [14]:

$$f_L(\theta =)1 - b_0\left(\frac{1}{\cos(\theta)} - 1\right). \quad (11)$$

Principally, $R_T(\theta_T)$ represents the angular dependence of the reflector and $f_L(\theta_i)$ represents the angular dependence of the glazing. A typical reference year of the Stockholm climate from 1983 to 1992 by the Swedish Meteorological and Hydrological Institute Stockholm (SMHI) is included in the model for the simulations.

3.5. MINSUN simulations of the annual energy yield for systems with various geometries

The MINSUN simulation program was used to calculate the expected annual energy output from the solar cells with reflectors by multiplying the useful irradiance from Eq. (10) by the efficiency of the solar cell (13%). Simulations were initially performed for Geometries A and B (shown in Fig. 5), with the tilt of the absorber plane, β, 20° and −15°, respectively. The values of optical efficiency that were established from the measurement results were used as input data for $R_T(\theta_T)$ for every fifth incidence angle from 0° to 90°.

In order to theoretically investigate a number of variations of the system geometry, MINSUN simulations were also performed for geometries based on both Geometries A and B. The input data of optical efficiency, $R_T(\theta_T)$, of the two systems were shifted in the MINSUN input file in a way that imply that the collectors (both the reflector and the absorber) theoretically were rotated around the focal point, F. In a simulation when the reflector is tilted forward 10° (v is rotated from 25° to 15°), the values of R_T (θ_T) are shifted 10° towards lower angles. When the reflector is tilted backwards 10° v is rotated from 25° to 35° the values of $R_T(\theta_T)$ are shifted 10° towards higher incidence angles and extrapolated. This means that the optical axis tilt angle, v, varies between −5° and +55° in steps of 5°. This also changes the solar acceptance intervals and implies a change of the concentration ratio as the height, h, of the vertical glazing has to be altered to match the new geometries. The absorber tilt angle from the horizontal, β, will then also be altered while the angle between the optical axis and the module plane is constant. If the system is rotated backwards, as v is increased, the concentration ratio will increase, because the height, h, relative to the module width, a, is increased. The aperture

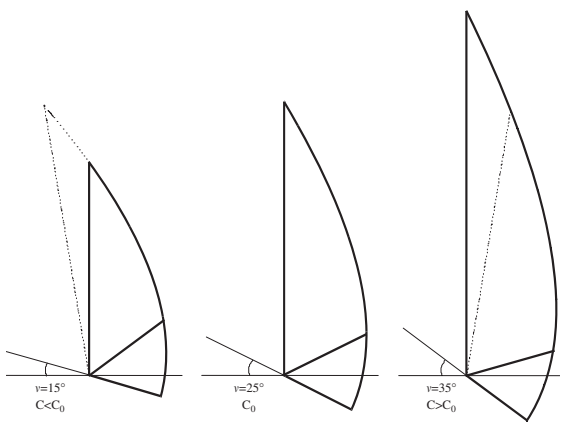

Fig. 11. Different tilt angles, v, of the optical axes of the systems simulated in MINSUN. The system in the middle is Geometry A, where v is 25° and the module tilt, β is 20°. The left- and right-hand geometries were simulated in MINSUN after rotation.

opening of the concentrator will always be in the vertical plane. During forward rotation, the reflector is truncated and during backwards rotation the reflector is extended. An illustration of the system geometry is shown in Fig. 11.

4. Results

4.1. Results of short-circuit current measurements

The short-circuit current was recorded as a function of the transversal incidence angle and the measurement results with varied β tilt angles are presented in Fig. 12. The measurements show that below the cut-off incidence angle of the concentrator (25°), the current is relatively low, as only some direct irradiance reaches the module with a high incidence angle. Above the cut-off angle the current is relatively independent of the β angle, since all irradiated light reach the module directly or after reflection. However, the average number of reflections is increasing with decreasing β angles, which means that the current slightly decreases.

The corresponding current densities of the reference and concentrator modules are presented in Fig. 13. The figure shows that the output per module area increases with decreasing module tilt, the β angle, since the module area decreases and the concentration factor increases with decreasing tilt angle. The maximum average current density increases from 30 to 70 mA/cm^2 by concentration.

If it is assumed that both the flat reference module and the concentrator are modelled by Eq. (10) with the function $CR_T(\theta_T) = 1$ for the reference module (without concentrating reflector) and a negligible diffuse fraction, then $I_{SC(conc.)}$ of the concentrator module is related to $I_{SC(ref.)}$ of the reference cell according to Eq. (12):

$$I_{SC(conc.)}(\theta_T) = I_{SC(ref.)} R_T(\theta_T) C. \quad (12)$$

This further implies that the angular dependence of θ_L at constant θ_T for the concentrator and reference module are identical. It is important to point out that the reference is situated in the plane of the entrance aperture of the concentrator.

The measured and the ideal I_{SC} of the concentrators of Geometries A and B are compared in Figs. 14 and 15. The ideal values of I_{SC} should be obtained from a concentrator with a reflector of reflectance 1. The values of the ideal I_{SC} in the figures were derived from the monitored $I_{SC(ref.)}$ according to Eq. (12), with $R_T(\theta_T)$ derived from Eqs. (5) and (6) and with the effective reflectance parameter k equal to 1. The current of the reference cell is lower in Fig. 15 than in Fig. 14, since the absorber area is larger in Geometry A.

4.2. The optical efficiency

The measured values of optical efficiency, of the systems of Geometries A and B was thereafter determined from measured data by Eq. (4). This equation is identical to the ratio between the monitored $I_{SC(conc.)}$ and the $I_{SC(ideal)}$ for $\theta_T > v$. The theoretical optical efficiency was also calculated from Eqs. (5) and (6) with $k = 0.69$. The measured and the theoretical optical efficiency agree well up to 40°. For higher θ_T, the measurements are unreliable due to the limitations of the solar simulator at large angles of incidence.

In order to set up an accurate model of optical efficiency to use in simulations, data of optical efficiency is taken from measurements, for $\theta_T < 40°$, and from calculations, for $\theta_T < 40°$. This resulting model is shown in Fig. 16.

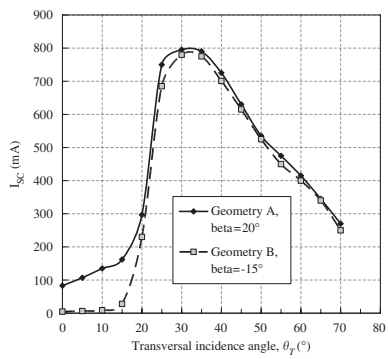

Fig. 12. The results of short-circuit current from the CIGS cell in the concentrating system for Geometries A and B, shown for different solar altitudes, i.e. transversal incidence angles.

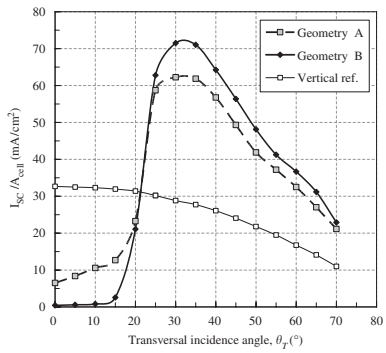

Fig. 13. The results of short-circuit current per cell area from the CIGS cell in the concentrating system, for Geometries A and B, shown for different solar altitudes, i.e. transversal incidence angles. The current of the vertical reference cell is also shown.

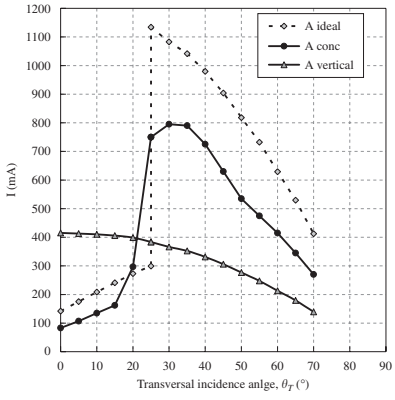

Fig. 14. Short-circuit current, I_{SC}, as function of the transversal incidence angle for the reference module, a concentrator module with Geometry A($\beta = +25$) and the calculated I_{SC} for a module in an ideal concentrator, $k = 1$.

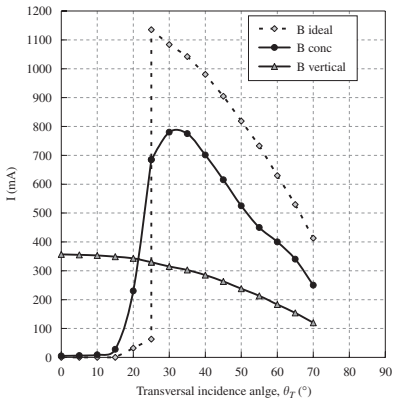

Fig. 15. Short-circuit current, I_{SC}, as function of the transversal incidence angle for the reference module, a concentrator module with Geometry B($\beta = -15°$) and the calculated I_{SC} for a module in an ideal concentrator, $k = 1$.

For angles θ_T below v, the concentrator is not used and no light is reflected, yet some irradiation reaches the module directly. The fraction of radiation that is reflected

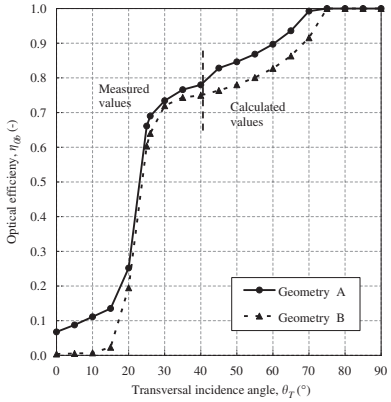

Fig. 16. The model of optical efficiency η_{0b} composed by the measured values for $\theta_T < 40°$ and calculated values for $\theta_T > 40°$.

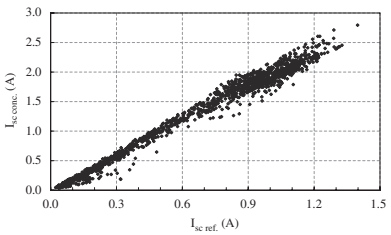

Fig. 17. Comparison of the I_{SC} of the reference and the concentrator module from 10 a.m. to 2 p.m. daily from July 10 to September 12 in 2003.

before it reaches the module is increased with increasing θ_T. For θ_T over 70°, all irradiation reaches the module directly without reflections, which means that the optical efficiency is equal to 1.

4.3. Analysis of long-term outdoor measurements

The results of the long-term outdoor measurements, thus including diffuse and direct irradiation, are illustrated in Fig. 17 and 18. Fig. 17 shows that the $I_{SC(conc.)}$ is a factor of two higher than $I_{SC(ref.)}$. This means that the geometrical concentration factor of 2.96 in combination with the optical losses results in a real concentration factor of approximately 2.

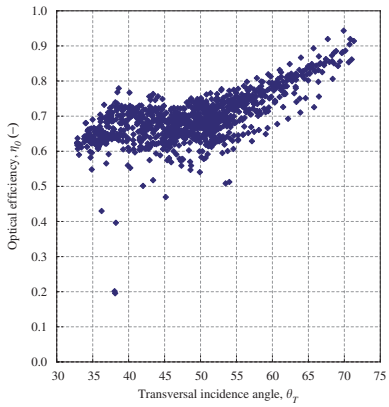

Fig. 18. The optical efficiency η_0 as a function of the transversal incidence angles θ_T from long-term outdoor measurements, from 12 a.m. to 5 p.m.

The performance is further analysed by plotting the measured optical efficiency η_0 as a function of the transversal incidence angles θ_T. The results presented in Fig. 18 show a large scattering but also a relatively good overall agreement with model shown in Fig. 16. The data from times when the irradiance was very low are discarded by selecting only data points when $I_{SC(ref.)}$ was higher than 0.3 A.

For θ_T of 40°, the outdoor measurements show that the optical efficiency η_0 is 0.60–0.72, while the estimated value of η_{0b} is 0.78. This difference is explained by the influence of the diffuse irradiation scattering and by aged and unclean reflectors.

4.4. MINSUN results of annual electricity production

The results of the simulated annual electricity production of CIGS modules (with 13% conversion efficiency) in the concentrating systems of Geometries A and B are shown in Fig. 19. The varying tilt angles of the optical axis, v, are shown on the x-axis and both the yield per cell area and the yield per glazed area are shown in the figure. The horizontal lines across the figure show the calculated yield per cell area from the vertical flat reference module and

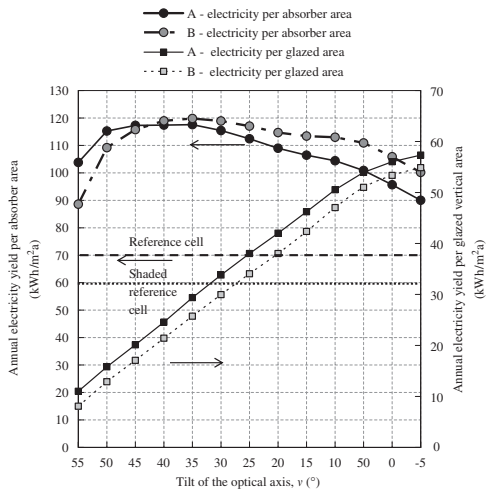

Fig. 19. Simulated annual electricity production per glazed vertical area and per module area as a function of the tilt angle, v, of the reflector's optical axis. The annual output of the vertical reference module is also shown for comparison, with and without shading up to $\theta_T = 12°$. daily from July 10 to September 12 in 2003.

also for a reference module that is shaded up to 12°, as this is a probable situation for vertically placed collectors. The concentrator module is insensitive to shadowing up to the incidence angle equal to the optical axis.

Fig. 19 shows how the annual electricity yield per absorber area increases with higher v angles (30–50°), as the concentration ratio C increases, until the tilt of the optical axis is too high to accept irradiation from solar altitudes of 45° and higher. The greatest part of the annual irradiation in Sweden occurs at projected solar altitude angles, α_{NS}, of 50–55° (see Fig. 3). Fig. 19 also shows how the energy yield per glazed area decreases with increasing v angles.

It can also be seen that the similar graphs of Geometries A and B are slightly displaced from one another and that Geometry B gives a higher yield per absorber area than Geometry A at v angles up to 45°, due to the higher concentration ratio. Geometry A, on the other hand, gives higher yield per glazed area, as the reflection losses are lower for this geometry.

The highest annual energy yield per cell area is 120 kWh/m^{2}a, achieved by Geometry B at a v angle of 35°. (Geometry A gives almost as high yield at this point.) The resulting geometrical concentration ratio, C, is 4.65. The simulations show that the reference cell would give 70 kWh/m^{2}a and if shaded for θ_T from 0° to 13°, 60 kWh/m^{2}a. The calculated electricity production for this concentrating system is thus 72% higher than that of the unshaded vertical reference module, and 100% higher than a shaded module.

The measured systems, where $v = 25°$, show slightly lower values of the estimated annual yield, 112 and 118 kWh/m^{2}a for Geometries A and B, respectively.

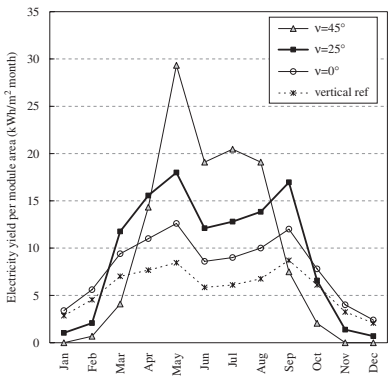

Fig. 20. Annual distribution of the electricity yield per module area from the CIGS cells in the concentrator and for the vertical reference cell. The higher the tilt angle of the optical axis, v, the higher is the summer production and the lower is the winter production and vice versa.

It is important to also consider that a higher inclination of the optical axis means that the acceptance of irradiation from low solar altitude angles is more limited. This results in a higher summertime production on the expense of a lower wintertime production. This effect can be observed in Fig. 20, which shows the annual distribution of the electricity yield per module area for varying v angles (0°, 25° and 45°) and for the vertical reference cell.

Although a lowered absorber tilt angle, β, results in higher yield per cell area, it also impedes the wintertime production, as it excludes the irradiation from low solar altitudes. Therefore, depending on the pattern of the energy demand, a tilt of the optical axis of 25–35° and a positive absorber tilt angle β would be suitable. It can also be concluded that the original design is very good for the application. The system with a v angle of 25° gives about twice as high yield as the reference cell, which is in agreement with the outdoors measurements.

5. Discussion

The focus of this investigation is to reduce the cost of the collector by replacing expensive solar cell material by reflector material. The most interesting of the shown results is therefore the annual energy output per module area and its relation to the output of the vertical reference cell, which shows the potential savings.

The results have shown that the annual energy yield per module area will increase with a higher tilted optical axis up to where the tilt of the optical axis, v, is 35° and 45°, respectively, for Geometries A and B. The backwards-tilted parabolic reflector implies a larger vertical area compared to the module area and thus a higher geometrical concentration ratio. This means that the cost-efficiency of the whole concentrating system also may be improved by increasing the tilt of the optical axis.

However, a highly tilted optical axis gives a high-energy generation in summer at the expense of a lower generation in winter. Which design is the more suitable, must therefore be estimated from considerations of the patterns of energy demand. Of course, if the system is grid connected, the immense energy demand makes this aspect unimportant.

A third important aspect is the cost of the façade. The building element consists of glazing, insulation and wires, and the cost of these materials, as well as the modules, should preferably be covered by the energy savings per *glazed area* of the building element, or at least be kept at a reasonable level. However, considering that it is not uncommon that façades are allowed high expenses, this design may be a very price worthy solution. Also, the collector could very well give an aesthetically appealing façade.

The optical measurements show that anodised aluminium offers a good solar reflectance. However, there are several booster reflector materials available on the market, which exhibit considerably higher solar cell reflectance than anodised aluminium. For example, Miro sheets from

Alanod have a solar reflectance of 90% at normal incidence [11]. Using these materials should therefore increase system performance by almost 10%, but at a higher cost. Further research of the cost-efficiency per glazed area of the whole building envelope is therefore required before a final statement can be made about which geometry and materials to choose in order to minimise electricity production costs.

In a line-focusing concentrating system, such as the parabolic reflector system optimised in this work, the concentration of solar radiation may result in high cell temperatures. Due to the negative temperature coefficient of all photovoltaic cells, high cell temperatures will decrease the efficiency of the system. One way of eliminating, or at least significantly reduce, this problem is to cool the photovoltaic modules. There are several different cooling methods available, but work by Refs. [8,17] indicates that active water cooling is the most cost-effective method for low-concentrating line-focussing systems. In addition to increasing the electric power by reducing the cell temperature, if operated at medium temperatures (about 30–55 °C depending on cell type), active water cooling makes it possible to utilise the warm water produced for heating or pre-heating of domestic hot water or space heating. If a hybrid absorber is considered, the demand of thermal energy and the pattern of the heating demand should preferably also be considered in the geometrical design of the collector.

6. Conclusions

The maximum annual electricity production in the evaluated concentrating systems, if installed in Stockholm, Sweden, was calculated to 120 kWh/m^2 per solar cell area, using the MINSUN simulation program and measurement data. This result was obtained for a system with concentration ratio, $C = 4.65$ a module tilt angle, β, of $-15°$, and a tilt of the optical axis, v, of 35°. The calculated annual electricity production is 72% higher than that of the vertical reference module, which would produce 70 kWh/m^2 cell area. Compared to a reference module that is shaded for θ_T from 0° to 13°, the yield is 100% higher.

For the system of Geometry A, where v is 25° and β is 20°, the electricity yield is 112 kWh/m^2 per solar cell area, according to simulation results.

For this geometry, an effective concentration of approximately 2.0 has been observed from outdoor measurements. Considering the geometrical concentration, which is 2.96, this results in an optical efficiency of approximately 0.7, which is similar to the results achieved by Refs. [3–5].

The conclusion is that the use of photovoltaic modules and parabolic aluminium reflectors in static, low-concentrating systems designed for building integration has a potential to significantly increase the annual electricity production per cell area, compared to a planar vertical module with the same cell type. Given the low cost of the highly reflective anodised aluminium mirrors and the insulation material in combination with a simple manufacturing process, the kind of systems evaluated in this work have a potential to reduce the cost of photovoltaic electricity.

Acknowledgements

This work was supported by Elforsk AB Sweden in co-operation with the Energy Systems Program, which is financed by the Swedish Foundation for Strategic Research, the Swedish National Energy Agency and Swedish industry. H. Håkansson at Lund University and J. Jonsson at Uppsala University are acknowledged for assistance during the measurements.

References

[1] O. Lundberg, L. Stolt, Trends in photovoltaic applications in selected IEA countries between 1992 and 2001, Report IEA-PVPS T1-11:2002, 2002.
[2] M. Brogren, J. Wennerberg, R. Kapper, B. Karlsson, Sol. Energy Mater. Sol. Cells 75 (2003).
[3] T.K. Mallick, P.C. Eames, T.J. Hyde, B. Norton, Sol. Energy 77 (2004) 319.
[4] T.K. Mallick, P.C. Eames, B. Norton, Sol. Energy 80 (2006) 834.
[5] A. Zacharopoulos, P.C. Eames, D. McLarnon, B. Norton, Sol. Energy 68 (2000) 439.
[6] M. Brogren, Low-concentrating photovoltaic systems with parabolic reflectors, Licentiate Thesis, Division of Solid State Physics, Uppsala University, Sweden, 2001, ISSN 03 46-8887.
[7] M. Rönnelid, Optical design of stationary solar concentrators for high latitudes, Ph.D. Thesis, Department of Materials Science, Uppsala University, Sweden, 1998.
[8] M. Rönnelid, B. Perers, B. Karlsson, P. Krohn, Cooling of PV modules equipped with low-concentrating CPC reflectors, in: Proceedings of the ISES Solar World Congress, Jerusalem, 1999.
[9] D.R. Mills, J.E. Giutronich, Sol. Energy 23 (1979) 85.
[10] R. Winston, Solar concentrators, in: J. Gordon (Ed.), Solar Energy—The State of the Art, James & James, London, 2001, pp. 357–436.
[11] M. Brogren, P. Nostell, B. Karlsson, Sol. Energy 69 (2000) 173.
[12] H. Håkansson, A parallel beam solar simulator for testing of solar components, in: ISES Solar World Congress, Gothemburg, Sweden, 2003.
[13] V.G. Chant, R. Håkansson, The MINSUN Simulation and Optimisation Program, Application and Users Guide, IEA SH&C Task VII, Ottawa, 1985.
[14] J.A. Duffie, W.A. Beckman, Solar Engineering of Thermal Processes, Wiley-Interscience, New York, 1991.
[15] W.R. McIntire, Sol. Energy 29 (1982) 315.
[16] J. Nilsson, M. Brogren, A. Helgesson, A. Roos, B. Karlsson, Sol. Energy 80 (2006) 1199.
[17] M.W. Edenburn, Active, passive cooling for concentrating photovoltaic arrays, in: Fourteenth IEEE Photovoltaic Specialists Conference, San Diego, 1980.

Paper VIII

Design, Building Integration and Performance of a Hybrid Solar Wall Element

Andreas Fieber, Division of Energy and Building Design,
Department of Construction and Architecture, Lund University
P.O. Box 118, 221 00 Lund, Sweden andreas.fieber@ebd.lth.se
Phone +46-46-2227347 fax +46-46-2224719
Helena Gajbert, Division of Energy and Building Design, Lund University
Håkan Håkansson, Division of Energy and Building Design, Lund University
Johan Nilsson, Division of Energy and Building Design, Lund University
Tobias Rosencrantz, Division of Energy and Building Design, Lund University
Björn Karlsson, Division of Energy and Building Design, Lund University

The building industry and the solar energy industry calls for innovative and attractive building integrated active solar thermal and PV systems, in order to widen the acceptance and use of solar energy. As an answer to a widened understanding of building integration, a multifunctional wall element has been developed.

A PV/T component on the inside of an antireflective insulation window with concentrating mobile reflector screens makes the system fully integrated into the building, even its interior. The Solar Window provides PV electricity and warm water, besides passive space heating and day lighting. Simultaneously, the reflector screens act as sunshades and added internal insulation for the window. The reflectors have an optical concentration factor of 2.45, which decreases the required, cost-intensive PV cell and heat absorber area. The hybrid technology has synergetic effects such as cooling the PV cells for increased performance, and making use of heat generated in the cell. The climate protected system is a visible element in the exterior and particularly in the interior, and its performance is directly connected to the user behaviour, due to the operation of the reflectors, which can be switched between a closed, concentrating mode or an open, transparent mode.

Performance of a 1 m^2 prototype of the system, regarding its sun shading and U-value properties and its photovoltaic and active thermal output, has been momitored. For a two-pane anti-reflective window, the U value is reduced from 2.8 to 1.2 W/ m^2K with the reflectors closed. The annual transmittance through the window is estimated to 609 kWh/ m^2, of which approximately 10% is expected to be delivered by the PV modules. About 20 % will be delivered as active solar heat and 30% as net passive space heating. The distribution is highly dependent on the daily operation of the reflectors, which to some extent could be automated.

1 The design of the Solar Window

As an answer to the search for truly building integrated solar energy systems, an experimental design was proposed, which combines all useable forms of solar energy into one system; active and passive heating, PV electricity and daylight. The concept also aims at visually exposing the system in a novel and attractive way. The key for this challenge was simply to use a window as the glazing for a solar collector. By using hybrid absorbers and pivoted reflectors behind the window, a multifunctional and responding building skin is achieved. The basic concept of building integration is

hence changed from the notion of the solar energy system being part of the building envelope, to the idea of the building envelope being part of the solar energy system.

The system consists of three main components: the window, the hybrid absorber and the reflector, see figure 1. The combination is intended to give synergy effects by ascribing the components multiple functions

The hybrid absorber is fixed in an angle of 20° to the horizontal plane. A 2 mm thick aluminium absorber has PV cells laminated on the upper side. The thickness

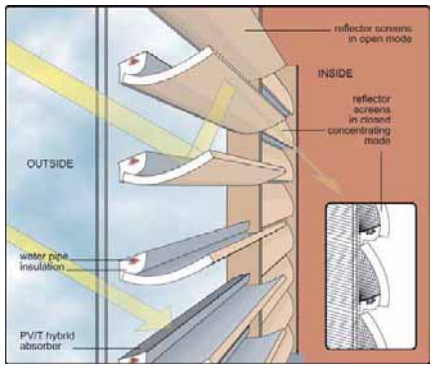

Figure 1: Description of the Solar Window in open and closed mode

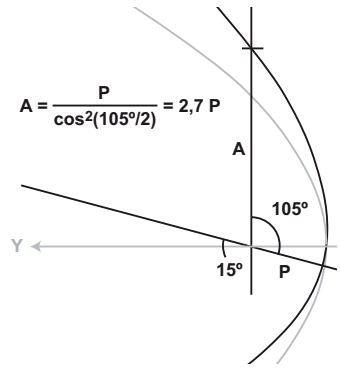

Figure 2: Concentrating geometry

reduces movements due to temperature differences, which otherwise puts the PV cells at risk of cracking. Water pipes are attached to the bottom for distributing active solar gains and for cooling the PV cells and the cavity between the window surface and the reflectors. Building integrated, they also serve as supporting structure for the absorbers and the reflectors, and as the pivot for the reflectors. EPS insulation around the pipes also makes endings for the rotation of the reflectors, and connects the insulation of the reflectors into a continuous convection shield.

The reflector screens are primarily intended for concentrating the solar radiation onto the hybrid absorber. Thus, the need for expensive absorber and PV cell area is reduced, as it is largely replaced by substantially cheaper reflecting material. The resulting distance between the fixed absorbers thus makes it possible to achieve transparency between them when the reflectors are of little use. Hence, daylight may filter through the structure, which also gives passive thermal gains. For passive solar house designs with use of large south facing window areas, risks of overheating and thermal losses are common. The reflectors are intended to reduce these problems, by serving as internal sunshades during daytime and as internal insulation during night time. The reflecting geometry is a two-dimensional parabolic curve, with the optical axis tilted by 15° from the horizontal plane, see figure 2. It has a geometrical concentration factor, i.e. the ratio between the glazed opening and the absorber area, of 2.45. The curve is extruded horizontally as a trough, and the reflector is constructed as a sandwich composition with a 35 mm EPS core between the reflective film on the concave side and a birch veneer on the convex side.

The window serves as the climate shield and as the solar radiation transmitter for the system. After the solar radiation is transmitted through the window, it is distributed as daylight, passive or active heating, or as PV electricity, in proportions

depending on the handling between the closed or open modes. For maximal input for the PV/T absorber through a vertical surface, the transmittance through the window needs to be maximized. Therefore, a highly transparent glass with anti-reflective coating is used. Due to the over-heating precautions by the solar shading and the cooling effect of the absorber, a higher transmittance of the glazing can be tolerated.

2 Building integration

The presence of the hybrid PV/T system inside a window makes it highly visible from the exterior as well as the interior. One of the basic ideas behind the design was to express the building integrated solar energy system architecturally in an attractive, maximally exposed way. Conceptually, the window is the traditional solar collector, hence an interesting starting point for integrating other solar technologies.

Other aesthetical considerations are mainly due to the reflectors. The curved concentrating geometry is decorative and expresses the capturing nature of a solar energy system. The backside facing the interior could be covered with any surface material suitable for the interior context. The modular nature of the reflectors, with no connection to the energy distribution, makes it possible to exchange them for alternative surface, thickness or reflecting geometry. The concave front facing the window will be highly visible from the exterior, and the mirror like surface might be the most critical aesthetical property for a wider acceptance. However, the curved mirror can generate interesting optical expressions in the façade. The extruded picture of the PV/T absorber is visible when the spectator is within the optical acceptance angle range, which means that the impression of the individual modules will differ much in height on a short distance. The overall impression of the façade will hence change when approaching it. The mobility of the reflectors also contributes to a dynamic façade expression.

Figure 3: Illustration of the initial design of the Solar Window building integrated

The system is initially intended for experimental integration into a low energy, single family house, designed simultaneously with the concept for the solar window, see figure 2. This house has an 18 m^2 south facing window structure prepared for the integration of the Solar Window system. The house is constructed with an EPS module system with integrated load-bearing wooden beams, with no thermal bridges. A central brick wall and a ceramic clad concrete floor absorb passive gains. The solar heating system is complemented by a pellet burner, and the PV system is grid-connected while also carrying a local DC circuit for reducing magnetic fields and eliminating losses in battery eliminators, used for DC powered devices.

3 Window properties

The Solar Window is evaluated for its properties as a building component. From this perspective, it can be regarded as a normal window with added features, such as solar shading and internal insulation by the reflector screens. The window consists of

a double-pane insulating glass unit (IGU). The panes are proposed to have anti-reflective coatings in order to increase the active thermal and PV performance for a vertically oriented element. The insulating and sun-shading properties of the reflectors and the anti-reflective coatings are objects for evaluation.

A 1 m^2 prototype of the solar window has been constructed for evaluation of the thermal properties. Five hybrid absorbers with reflectors were mounted in a wooden frame with a double pane IGU attached in the front. The U value of the window together with the closed reflectors has been calculated from measurements in a guarded hot-box, according to ISO 8990 (Johansson 2004, ISO8990 1994). The Solar Window was placed in a square shaped hole between a cold and a hot space of 21.6 m^3 each. The hot space contained a guarded measuring box, covering the hole and the heating device. The U value was calculated according to Eq. (1):

$$U = \frac{Q}{A \cdot \Delta T_n} \qquad \text{[Eq. (1)]}$$

U is the U-value of the construction (W/m^2K), Q is the power input for heating the guarded measuring box, A is the area of the window, and ΔT_n is the environmental temperature difference between the hot and cold space.

Tests were made for the window separately and with the solar window components attached with the reflectors in six different positions, with four intermediate opening angles between the fixed open or closed modes. The window separately represents a U value of 2.80 W/m^2K. The U value of the whole Solar Window differs between 2.42 in the fully open mode, to 1.33 for the fully closed mode, see figure 4.

The effect on the U value with the reflectors opened derives from the reduced convection due to interruption of cold downdraught. Hence, the effect of the open reflectors could be regarded as an added internal surface resistance, which varies by opening angle.

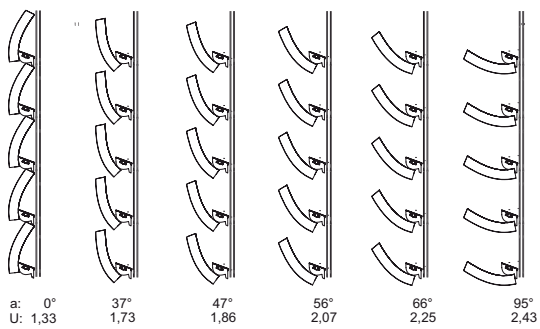

Figure 4: U values for different opening angles, a

The prototype construction was not made sufficiently airtight, why some compensation was made for this by sealing the gaps in its closed position. One measurement was made with the reflectors closed and sealed towards the absorber insulation, and another one also with added sealing between absorber insulation and window, in order to reduce the channel of cold downdraught to one individual module. These two steps made the U value drop from 1.33 to 1.22 and 1.17 W/m^2K respectively. Air tightness is hence an important criterion for further design studies.

The visual shading effect of the reflectors as sunshades in a closed position is total, which means that effective solar shading, visible shading and effective insulation is obtained simultaneously. However, the shading effect of the reflectors in an open position needs to be evaluated. Especially the risk of glare due to the concentration

of daylight from the reflectors needs to be observed and reduced to a minimum. A two-dimensional ray-tracing analysis, made by hand in a CAD program (see figure 5), shows that most of the radiation reflected will be distributed upwards to the next element above and then spread again. For solar angles at 20° and lower, there is a small risk of glare from the concentrated daylight. This problem is likely solved by reducing the rotation angle from 95° (which was set for minimizing the horizontal obstruction of view) to 90°.

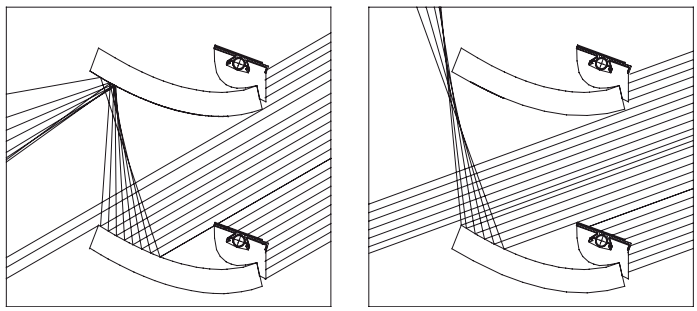

Figure 5: Ray-tracing illustrating the distribution of direct radiation with the reflectors opened at a solar height of 30° (left) and 20° (right).

4 User strategies

The final distribution between the different forms of solar gains, and the thermal losses through the structure, are dependent on how the system is regulated between the two reflector modes. The complexity also increases due to more subjective response from the users due to thermal comfort and wish for daylight and view.

The system was initially designed for integration into a single family house, where most bright hours during weekdays are characterised by the absence of the inhabitants. A rough operating schedule is outlined: during morning hours, with low solar flux and high user activity, the reflectors can be opened to allow for daylight, view and direct passive heat gain. During solar peak hours, with family members being at work or at school, the reflectors can stand closed for maximal active performance. Late afternoons and evenings have similar characteristics like the mornings, thus the reflectors are likely to be opened. For avoiding view inside (i.e. allow for privacy) and thermal losses during dark hours, the reflectors should be mainly closed until the next morning. When integrated into larger areas, zoning of the system allows for combinations of closed and open modules during this cycle.

Another operating strategy could be automating the movement for the reflectors on response to the radiation intensity and the outdoor temperature. It could be programmed for closure at radiation levels too high for thermal or visual comfort, or at levels too low for any practical use, e.g. at night time. In combination with other “intelligent house” technologies, such as sensors indicating occupant absence, obvious opportunities for keeping the reflectors totally closed can be maximally used. For calculations on passive gains in Stockholm, Sweden (lat 59.31), the reflectors were considered closed at transmitted irradiance levels below 50 W/m^2 and above 300 W/m^2, and opened at intermediate levels, from March to October. Concerns have been taken to the solar shading effect of the reflectors by using the computer tool

Parasol. For November to February, the system was operated as a window with no thermal and power production and the reflectors were considered closed or opened, depending on the most beneficial thermal energy balance, for every hour. The energy balance was calculated for every hour of the year, according to Eq. (2):

$W = I - U \cdot \Delta T$ [Eq (2)]

W is the net energy gain through the window, I is the transmitted irradiation, U is the heat transfer coefficient of the and ΔT is the temperature difference between indoors and outdoors.

The calculations indicates an annual positive net energy balance of 10 kWh/m^2 for the winter season. For the warmer season, there is a loss of 14 kWh/m^2 for the dark period with irradiance levels below 50 W/m^2, and a passive gain of 214 kWh/m^2 for the opened mode, at levels between 50 W/m^2 and 300 W/m^2. At levels above 300 W/m^2, 245 kWh/m^2 are available for the PV/T absorber.

5 Photovoltaic properties

For monitoring the photovoltaic performance of the system, a separate prototype with a hybrid absorber with polycrystalline silicon cells and a reflector was constructed.

The optical efficiency *η(α)* is defined as the ratio between the performance of the concentrating module and a vertical module of the same area as the concentrating aperture. It was determined through outdoor measurements. The short circuit current I_{sc} of the concentrator module was monitored as a function of the angle of incidence β in the meridian plane. The optical efficiency (figure 6), was then derived according to

$$\eta(\alpha) = \frac{I_{sc} \cdot 1000}{I_{1000} \cdot C_g \cdot G \cdot \cos(\beta)}$$ [Eq. (3)]

where I_{1000} is the short circuit current of the bare module at an irradiance of 1000 W/m^2 at normal incidence, C_g is the geometrical concentration of the concentrator system, β is the angle of incidence of beam irradiance, and G is the global intensity perpendicular to the sun.

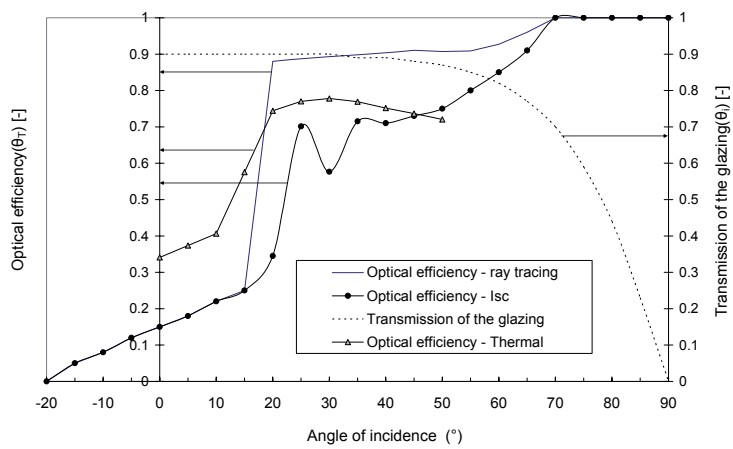

Figure 6: Optical efficiency $R_T(\theta_T)$ of the Solar Window and the transmittance of the glazing $f_L(\theta_L)$.

The measurements were performed during high irradiance and with a diffuse fraction of around 10%. The concentrator accepts all irradiance for solar altitudes exceeding 15° in the meridian plane, which means that the diffuse optical performance of the concentrator will be similar to that of a module tilted 20° with a correction for reflectance losses. This further means that the optical acceptance of diffuse irradiance will be around 70% of the beam efficiency. For this reason, the global intensity can be used in Eq (3) without significantly increasing the error of the model.

The optical efficiencies are functions of the projected angle of incidence in the transversal plane and the transmission of the glazing is given as a function of the conventional angle of incidence. Ray tracing represents the theoretical optical efficiency of the system at 85% reflectance. The graph labeled *Optical efficiency - Isc* in figure 6 contains contributions from measurements with corrections from ray tracing. The difference between measured values and ray tracing at $15°<\theta_T<60°$ is due to resistive losses in the cells when the reflector is effective. The cells on the prototype absorber did not cover the whole width of the absorber, which meant that for angles above 40° the reflected beam partly missed the cell. The angulars above 40° are instead generated by ray tracing. The transmission of the glazing has also been included in the graph as it was used in the calculations of the annual output.

A simulation software, MINSUN (Chant and Håkansson 1985), estimated the annual output of electricity using the optical efficiencies at different angles of incidence. The model used to describe the incidence angle dependence of the system in MINSUN is defined by Eq. (4)

$$\eta_{opt} = R_T(\theta_T) f_L(\theta_i) \qquad \text{[Eq. (4)]}$$

R_T describes the behaviour of the reflector as dependent of θ_T and f_L the transmission of the window glass as dependent of θ_i . θ_T is the projected angle of incidence in the transversal plane and θ_i is the conventional angle of incidence relative to the glass normal.

This model has previously been shown to describe the optical performance of an asymmetric compound parabolic reflector system such as this one well (Brogren et al, 2004).

The simulations show a 93% increase in electrical output for the concentrator module relative to the vertical reference module, which means that one square meter of this window annually would deliver 79 kWh of electric energy. The annual performance is 43% higher than that of an identical module tilted 20°.

The active area of the tested measured prototype covers only 87% of the total glazed area, which this has to be taken into consideration when an economical comparison is made with other systems. It is however possible to increase the active area of the window in a future full scale installation.

6 Solar thermal properties

The active thermal absorbers for water carried heat serves three purposes; delivering heat for domestic hot water and possibly also for space heating, reducing the heat load in the interior during summer and cooling the photovoltaic cells in order to increase the electrical efficiency. The full scale window prototype was used in indoor and outdoor measurements for determination of the incidence angle dependency and the U value of the thermal collectors. Based on these results the annual energy yield has been derived.

To estimate a U value for the prototype of the solar wall operating as a solar collector, measurements of the heat loss from the collector have been performed in a dark surrounding at different temperatures of the inlet water. The values of U_0 and U_1 were estimated to 4.0 W/m^2·K and 0.046 W/m^2·K^2 and the resulting collector U value as a function of ΔT is shown in figure 7.

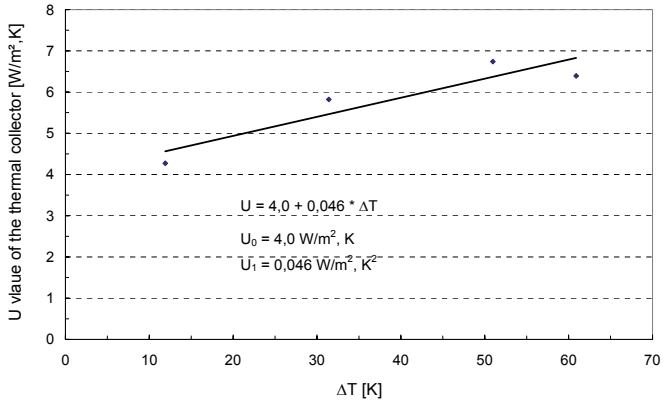

Figure 7. The U value of the thermal collector as a function of ΔT.

At ΔT = 30 K, the U value is 5.4 W/m^2·K per glazed wall area. During the measurements, the prototype was surrounded on both sides with the same temperature. In a building, however, the back side of the window will usually be surrounded with air of room temperature, which will suppress the heat losses. Approximately 10 % of the total heat losses, are estimated as border losses.

The indoor measurements have been performed by using a large solar simulator providing nearly parallel light and adjustable for solar altitude angles (Håkansson H. (2003 a and b). As described in Håkansson (2003 c) and Gajbert et al. (2004), the simulator provides relatively good parallel quality of light, though this has been achieved somewhat at the expense of the light distribution over the area. As different solar altitudes are simulated, there is a tendency of varying irradiation over the test area as the uneven light pattern moves. To continuously measure the variation of the total irradiation on the test area, a number of parallel connected photodiodes were evenly spread out over the front glass of the prototype, giving a current corresponding to the received total irradiation (Gajbert et al, 2004).

By indoor measurements of the thermal efficiency, i.e. the zero-loss efficiency, the incidence angle dependency was derived. The prototype of the solar wall was placed perpendicular to the solar simulator and the simulator was raised in order to simulate every tenth degree of solar altitude angle, i.e. the incidence angle on the glazing projected in the north south vertical plane, θ_T. The optical efficiency of the prototype was monitored for different solar altitude angles, giving the incidence angle dependency in the meridian plane, $\eta_T(\theta_T)$. The result was normalized by an outdoor measurement where the absolute value of the optical efficiency, i.e. the zero-loss efficiency at 30° incidence angle was registered.

The measured zero-loss efficiency has been divided by $f_L(\theta_L)$, the transmission of the glazing, as described in equation [3], resulting in a graph angular dependence of

the reflector only, $R(\theta_T)$. These functions , $R(\theta_T)$ and $f(\theta_L)$, shown in figure y, were used in MINSUN to simulate the annual thermal energy yield. The measured values of optical efficiency at high incidence angles are less reliable, due to the non-uniform light distribution on the small projected area. Therefore, for angles higher than 50°, the same theoretical values as were used for the electricity calculations, shown in figure 6, have been used. The difference between the theoretical graph of optical efficiency, calculated by ray tracing, and the calculated values is due to the reflections on the absorber, the collector efficiency, the multiple reflexes on the reflector at higher incidence angles, and on the unevenness of the reflector. Since the photovoltaic cell situated in front of the thermal absorber has an efficiency of 15%, only 85% of the in MINSUN simulated irradiation falling onto the absorber is taken into count for thermal energy yield.

The result of the simulations shows that the annual thermal energy provided by the Solar Window is 103 kWh/m^2 glazed surface, calculated at an operating temperature of 50°C. For operating temperatures of 40°C and 25°C the yield would be 155 and 250 kWh/a,m^2 respectively. However, as previously discussed, the real heat losses would probably be lower, because of the higher indoor temperature, thus implying higher yields.

7 Discussion and conclusion

A proper model for the regulating strategy of the system is needed to predict the distribution of gains and losses via the Solar Window. The complexity and interrelations between the different functions is a challenge for the modelling, which needs to integrate the spatial surrounding. A detailed model could be of much use for a regulation of an automated system for best performance and comfort.

The level of automation for the system is object for further studies. A range of products with different standard, from fully manual to fully automatic, is a likely development. It is however of importance that the control-function can be overridden manually at all times due to direct response from the user.

Performance of the system has been analysed separately for passive gains, active thermal gains and PV electricity yield. According to the proposed regulating schedule, passive gains are estimated to 210 kWh/m^2 annually. However, it is not examined how much of this is usable. The performance of the fully concentrated PV/T absorber is estimated to 79 kWh/m^2 of electricity, and at least 155 kWh/m^2 of heat for domestic hot water. Following the proposed regulating schedule, these figures might be reduced. For a more accurate and integrated analysis, long-term outside measurements will be made for the full window prototype with PV/T absorbers.

Cost estimations are dependent on where the system border is drawn, since the system also is the building envelope. For comparison with conventional solar energy systems, it might be fair to withdraw the window and sunshade cost if the same is done for the building material the conventional collector replaces. Production cost for the Solar Window excluding the glazing is estimated to approximately €250/m^2, but more thorough calculations need to be made.

Acknowledgements

This work was supported by the Swedish Energy Agency and Formas, the Swedish Research Council for Environment, Agricultural Sciences and Spatial Planning.

References

Adsten M., 2002. *Solar Thermal Collectors at High Latitudes – Design and Performance of Non-Tracking Concentrators*, Acta universitatis Upsaliensis, Uppsala, Sweden.

Brogren M. et al, 2004. *Biaxial model for the incidence angle dependence of the optical efficiency of photovoltaic and solar thermal systems with asymmetric reflectors*. Submitted to Solar Energy Journal.

Chant V.G. and Håkansson R., 1985. *The MINSUN simulation and optimisation program. Application and users guide*. IEA SH&C Task VII, Ottawa.

Fieber A. and Karlsson B. *Design, construction and performance of a multifunctional hybrid solar wall element,* In the proceedings of ISES Solar World Congress 2003, Gothenburg, Sweden

Gajbert H., Håkansson H., Karlsson B., (2004) *Measurement of concentrating solar collectors using a solar simulator with parallel light*, Submitted to Eurosun2004, Freiburg, Germany 20-23 June 2004.

Håkansson H., (2003) *A parallel beam solar simulator for testing of solar components*, In the proceedings of ISES Solar World Congress 2003, Gothenburg, Sweden 14–19 June 2003.

Håkansson H. (2003) *Solar laboratory,* In Solar Protection in Buildings, Wall M., Bülow-Hübe H. (eds), pp. 49-66. Dept. of Construction and Architecture, Lund University.

Håkansson H. (2003) *Solar laboratory*, In Solar Protection in Buildings: Part 2, Wall M., Bülow-Hübe H. (eds), pp. 29-67. Dept. of Construction and Architecture, Lund University.

ISO 8990 (1994) *Thermal insulation – Determination of steady-state thermal transmission properties – Calibrated and guarded hot box*, ISO 8990:1994 (E)

Johansson T. (2004) *Utvärdering av Solfönster, en integration av solhybrid och solskydd*, Dept. of Construction and Architecture, Lund University

www.parasol.se

Paper IX

COMPETITIVE SOLAR HEATING SYSTEMS FOR RESIDENTIAL BUILDINGS

Simon Furbo and Alexander Thür
Department of Civil Engineering, Technical University of Denmark, Brovej, building 118, Kgs. Lyngby, DK-2800, Denmark, phone number: +45 45 25 18 57, fax number: +45 45 93 17 55, email: sf@byg.dtu.dk

Frank Fiedler and Chris Bales
SERC, Dalarna University College, Department of Mathematics, Natural Sciences and Technology, Borlänge, S-78188, Sweden, phone number: +46 23 778 711, fax number: +46 23 778 701, email: ffi@du.se

John Rekstad and Michaela Meir
Department of Physics, University of Oslo, P.O. Box 1048, Blindern, Sem Sælandsvei 24, Oslo, N-0316, Norway, phone number: +47 2285 6475, fax number: +47 2285 6422, email: john.rekstad@fys.uio.no

Dagnija Blumberga and Claudio Rochas
Department of Energy Systems and Environment, Riga Technical University, Kronvalda bulv. 1, Riga, LV-1010, Latvia, phone number: +371 9419783, fax number: +371 7089923, email: dagnija@parks.lv

Björn Karlsson and Helena Gajbert
Department of Construction and Architecture, Division of Energy and Building Design, Lund Institute of Technology, P.O. Box 118, Lund, SE-22100, Sweden, phone number: +46 268 3529, fax number: +46 46222 4719, email: bjorn.karlsson@vattenfall.com

Abstract – This paper describes the ongoing research project "Competitive solar heating systems for residential buildings". The aim of the project is to develop competitive solar combisystems which are attractive to buyers. The solar combisystems must be attractive compared to traditional energy systems, both from an economical and architectural point of view.
The project includes education, research, development and demonstration. The project started in 2003 and will be finished by the end of 2006. The participants of the project, which is financed by Nordic Energy Research and the participants themselves, are the universities: Technical University of Denmark, Dalarna University, University of Oslo, Riga Technical University and Lund Institute of Technology, as well as the companies: Metro Therm A/S (Denmark), Velux A/S (Denmark), Solentek AB (Sweden) and SolarNor (Norway). The project consists of a number of Ph.D. studies in Denmark, Sweden and Latvia, and a post-doc. study in Norway. Close cooperation between the researchers and the industry partners ensures that the results of the project can be utilized. By the end of the project the industry partners will be able to bring the developed systems onto the market.
In Denmark and Norway the focus is on solar heating/natural gas systems, and in Sweden and Latvia the focus is on solar heating/pellet systems. Additionally, Lund Institute of Technology and University of Oslo are studying solar collectors of various types being integrated into the roof and facade of the building.

1. INTRODUCTION

Today only a small part of the worlds energy consumption is covered by renewable energy systems. Figures 1 and 2 show the world's installed capacity and yearly energy production of different renewable energy systems. A comparison between the different energy systems based on the figures is not completely fair, since some of the energy systems are producing electricity while others, such as solar heating systems, are "only" producing heat. It is however obvious that worldwide solar energy utilization by means of solar heating systems is one of the most important ways to utilize renewable energy sources today.

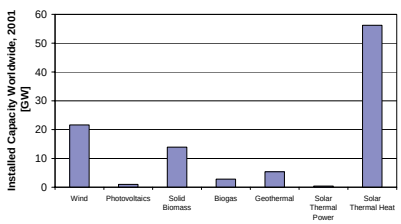

Figure 1. Installed capacity worldwide for different renewable energy systems, (Weiss, 2004).

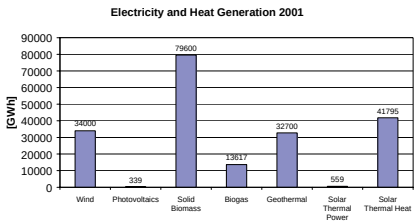

Figure 2. Energy produced worldwide by different renewable energy systems, (Weiss, 2004).

Today the solar heating market worldwide is growing by about 30% per year (Weiss, 2004), and this growth is expected to continue. In not a too far future, our energy supply must come from renewable energy systems. Solar heating systems can, if the energy costs from the systems are low enough, play an important role in this connection.

In Denmark, Sweden, Norway and Latvia respectively 25%, 23%, 27% and 35% of the country's total yearly energy consumption is used for heating of buildings, while the yearly solar radiation on the horizontal surface of the country is respectively 180, 1030, 1200 and 3130 times greater than the country's total yearly energy consumption. Certainly, the potential for solar heating systems is large, even at Northern latitudes.

Further, from the start of 2006 the EU directive 2002/91/EC on Energy Performance of Buildings must be implemented in all 25 EU countries. New and renovated buildings must have a low total energy consumption. This is expected to further accelerate the growth of the number of installed solar heating systems in Europe.

In the last 10 years the market for solar heating systems in the Northern European countries has not been as good as in the central European countries, like Austria and Germany, where major companies are now active in the market.

In Scandinavia the number of yearly installed solar heating systems has not increased in the same way, with significant differences between the countries. Significant factors here are the on-off subsidy conditions over recent years, lack of major players on the market, and the fact that the cost of solar heating is perceived to be relatively high compared to the price of heating produced by burning fossil fuel or electricity. Electricity is a common energy form for heating houses in Norway, Sweden and Finland due to the abundance of hydropower. Increasing electricity use combined with two dry years with reduced hydropower production, currently make alternative sources for heating much more interesting. In addition, the increased deregulation of electricity production in Europe will probably lead to higher consumer prices in Scandinavia.

There are two ways to reduce the energy costs of solar heating systems. One is based on rationalisation effects due to large scale production. This way is only possible if there is a continuous sufficient demand for solar heating systems. The alternative is to improve the performance/cost ratio of the solar heating systems by means of development of improved systems.

Recent studies within Task 26 of the International Energy Agency's Solar Heating and Cooling Programme have shown that significant improvements can be made to solar heating systems, and a few German and Austrian companies have already optimised their systems (Weiss, 2003). These optimised systems are complete systems including boiler as well as solar collectors, and are often installed in new buildings or when an existing boiler is being replaced. However, these systems are not readily available in the Nordic countries. Therefore it has been decided to use the knowledge gained from this previous international collaboration in connection with development of solar heating systems for North European countries.

2. RESEARCH PROJECT: COMPETITIVE SOLAR HEATING SYSTEMS FOR RESIDENTIAL BUILDINGS

During the period 2003-2006, the research project "Competitive solar heating systems for residential buildings" will be carried out in cooperation between leading research institutes and companies in the solar heating field in the Nordic and Baltic countries. The aim of the project is to develop solar heating systems which are attractive to buyers. Up to 50% of the energy consumption in the building will be covered by solar energy; the remaining energy consumption will be covered by conventional energy resources. Solar heating for new buildings as well as for retrofits will be addressed.

The project includes education, research, development and demonstration. The participants of the project, which is financed by Nordic Energy Research and the participants themselves, are the universities: Technical University of Denmark, Dalarna University, University of Oslo, Riga Technical University and Lund Institute of Technology as well as the companies Metro Therm A/S and Velux A/S from Denmark, Solentek AB from Sweden and SolarNor from Norway.

The project consists of a number of Ph.D. studies in Denmark, Sweden and Latvia and a post-doc. study in Norway. Close cooperation between the researchers and the industry partners ensures that the results of the project can be utilized. By the end of the project the industry partners will be able to bring the developed systems onto the market.

In Denmark and Norway the focus is on solar heating/natural gas systems, and in Sweden and Latvia the focus is on solar heating/pellet systems. Further, Lund Institute of Technology and University of Oslo are

studying building integrated solar collectors of various types.

3. EDUCATION ACTIVITIES

During the first part of the Ph.D. projects, two Ph.D. courses on solar energy have been organized at Technical University of Denmark and Riga Technical University, with participants from all around the world. During the courses, which included lectures by experienced researchers, visits to manufacturers and solar heating systems as well as social arrangements, the students worked on different topics within the solar energy field with the aim to prepare state of the art reports. The students presented their findings and their Ph.D. projects to the other participants of the courses. Valuable networks among the Ph.D. students and the teachers were established. A third specialized Ph.D. course focusing on thermal stratification in solar storage tanks will be organized at Technical University of Denmark in September-October 2005.

The Ph.D. students of the project have carried out/will carry out study stays at one of the other participating universities for a period of about 6 months. In this way good cooperation between the participating universities is ensured.

At SERC the ESES education, European Solar Engineering School education, a one-year Master degree on solar energy with new students from all around the world every year, is carried out. Lectures for the ESES students have been given by teachers from the participating universities of the project. Further, ESES students have carried out their Master Thesis projects in connection with the research project at the participating universities.

Further, the students following the normal solar heating courses at the participating universities have been informed about the activities of the research project. Several Master Thesis projects and special courses have been carried out in connection with the research project. Consequently, the project contributes to capacity building in the solar heating field.

Finally, national workshops for the solar heating industry and solar heating seminars for all interested have been arranged. In this way not only the participating industries will benefit from the research project.

4. RESEARCH ACTIVITIES

Research is carried out with focus on:

- Building integrated solar collectors
- New materials
- Heat storage
- Good interplay between solar collectors and auxiliary energy supply system
- Advanced control strategy
- Low temperature heating systems

In total 5 Ph.D. students and 1 post-doc. are working on the project. Two Ph.D. studies on solar combisystems are carried out at Technical University of Denmark by Alexander Thür and Elsa Andersen. Alexander Thür is working on development of solar heating/natural gas systems in cooperation with Metro Therm A/S, while Elsa Andersen is working on differently designed solar combisystems. At SERC Frank Fiedler is working on a Ph.D. study with the aim to develop a solar/pellet heating system in cooperation with Solentak AB and Metro Therm A/S. At Riga Technical University, Claudio Rochas is working on a Ph.D. project with the aim to develop a solar/pellet heating system. At Lund Institute of Technology, Helena Gajbert is working on a Ph.D. project on concentrating solar collectors for building integration. At University of Oslo, Michaela Meir is carrying out a post-doc. study concerning new façade and roof integrated solar collectors and solar heating/natural gas systems with high solar fractions. She is working in close cooperation with SolarNor.

5. DEVELOPMENT OF SOLAR HEATING SYSTEMS

The research groups at SERC and Technical University of Denmark work together with the industry partners Metro Therm A/S and Solentek AB with the aim to develop attractive natural gas/solar heating systems and pellet/solar heating systems.

The concept for both systems is the same: The system consists of a highly prefabricated technical unit with all the equipment of the systems including the natural gas/pellet boiler and one or more units with the heat storage. The units are built into 60x60 cm cabinets, see Figure 3. Prototypes of the units will be tested in laboratory test facilities during the summer of 2005 and demonstration systems will be installed during the autumn of 2005. The integration allows faster installation and reliable systems. Although the system is highly prefabricated, there is significant flexibility: choice of gas or pellet boiler; choice of system size, with larger systems either having multiple 60 x 60 cm cabinet stores, or single larger stores.

The goal is, by the end of the project, to have natural gas/solar heating system units and pellet/solar heating systems installed in several houses for field tests by Metro Therm A/S and by Solentek AB, respectively.

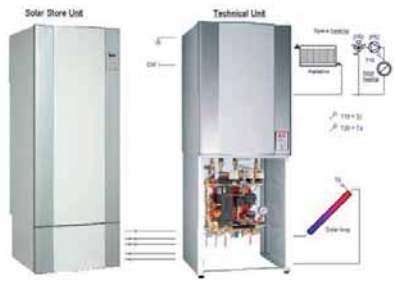

Figure 3. Solar storage unit and technical unit for the Danish/Swedish solar combisystems.

At Riga Technical University work, with the aim to develop solar pellet heating systems using the same principles as used in the Danish/Swedish concept is carried out.

Lund Institute of Technology is focusing on the development of concentrating integrated solar collectors in cooperation with NCC AB.

At University of Oslo, a low temperature drain back solar heating/natural gas system based on plastic collectors, a large solar store and a floor heating system with a high solar fraction has been developed in cooperation with SolarNor. Further, façade integrated solar collectors have been developed. Figure 4 shows an example of a façade integrated solar collector in a one family house.

Figure 4. SolarNor's façade integrated solar collectors in a one family house, (source: SolarNor).

6. DEMONSTRATION SYSTEMS

A number of solar combisystems based on the developed solar heating systems and components will be built in one family houses in the autumn of 2005. The systems will be monitored in such a way that the thermal performance and energy savings of the systems can be determined.

For instance, the Danish solar heating will be installed in a one family house with an existing natural gas boiler. The energy demand as well as the natural gas consumption has been measured since August 2004. It is therefore possible to determine the energy savings of the solar heating system based on measurements from the house without and with the solar heating system installed.

The measurement periods for the demonstration systems will be about 1 year.

7. FUTURE WORK

Prototypes of the developed solar heating systems and components will be tested in laboratory test facilities during the summer of 2005. Based on the test results, the designs of the systems/components might be improved before the demonstration systems will be built in one family houses in the autumn of 2005. Measurements from the demonstration systems will be carried out until the end of the project by the end of 2006.

Theoretical investigations based on detailed computer simulations and cost estimates concerning optimization of the design of the systems will be carried out in parallel with the tests of the prototypes and the measurements from practice. The investigations will, among other things, elucidate how to design the systems in order to achieve solar heating systems with high solar fractions.

The results of the project will be available in a number of Ph.D. reports, a report finalizing the post-doc. study and in a number of scientific papers. Further, the results of the project will be presented at international solar heating conferences and at national solar heating seminars and workshops. The results will also, along with general information on the project, be available on the project homepage: http://energi.fysikk.uio.no/rebus.

Preliminary results from the project are found in the following papers and reports: (Fiedler, 2003), (Boström, Wäckelgård and Karlsson, 2003), (Gajbert and Fiedler, 2003), (Meir and Rekstad, 2003), (Fiedler, 2004), (Thür, Furbo and Shah, 2004), (Meir, Rekstad and Svåsand, 2004), (Meir, Fiedler, Rekstad, van Wieringen and Kristoffersen, 2004), (Furbo, Andersen, Thür, Shah and Andersen, 2004), (Fiedler, Nordlander, Bales and Persson, 2004), (Andersen, Jordan, Shah and Furbo, 2004), (Kahlen, Wallner, Meir and Rekstad, 2005), (Gajbert, Råberg, Lövehed and Karlsson, 2005), (Schakenda, Spikkeland, Meir, Olivares and Rekstad, 2005), (Gajbert and Karlsson, 2005), (Meir, Fiedler, Gao, Kahlen, Mathisen, Olivares, Rekstad and Schakenda, 2005), (Thür and Furbo, 2005), (Rochas and Blumberga, 2005), (Meir, Rekstad, Fiedler, Kristoffersen, Olivares, Schakenda, van Wieringen, 2005), (Fiedler, Bales, Thür, and Furbo, 2005), (Andersen, Furbo and Fan, 2005) and (Andersen and Furbo, 2005).

8. CONCLUSIONS

The project "Competitive solar heating systems for residential buildings" has increased the educational and research cooperation within the solar heating field between the Nordic and Baltic universities. Further, the project has resulted in an increased number of young experts in the solar heating field.

It is expected that the attractive solar combisystems developed in the project will be brought to the market by the industry partners of the project from 2007.

Finally, the basis for development of improved solar heating systems in the Nordic and Baltic countries for the future has been improved. Consequently, the project will contribute to increased use of solar heating systems in the future.

ACKNOWLEDGEMENT

We are grateful to Nordic Energy Research for their financial support for the project "Competitive solar heating systems for residential buildings".

REFERENCES

Weiss W. (2004). *New emerging markets and applications for solar thermal systems. Chance or risk for the European solar thermal industry?* Key note presentation EuroSun 2004 Congress. June 20-23, Freiburg, Germany.

Weiss W. (2003). *Solar Heating Systems for Houses. A Design Handbook for Solar Combisystems*. Solar Heating and Cooling Executive Committee of the International Energy Agency. James & James Ltd, London.

Fiedler F. (2003). *The application of renewable energy for prefab houses in Germany*. SERC Report No. ISRN DU-SERC—76—SE, SERC, Department of Mathematics, Natural Sciences and Technology, Högskolan Dalarna, Sweden.

Boström T.K., Wäckelgård E. and Karlsson B. (2003). Design of a solar system with high solar fraction in an extremely well insulated house. *Proceedings of ISES Solar World Congress 2003*, June 14-19, Gothenburg, Sweden.

Gajbert H. and Fiedler F. (2003). *Solar combisystems – a state of the art report*. From Ph.D. course Solar Energy, Technical University of Denmark.

Meir M. and Rekstad J. (2003). Der SolarNor Kunststoffkollektor – The development of a polymer collector with glazing. *Proceedings of Polymeric Solar Materials, Erstes Leobener Symposium "Solartechnik – Neue Möglichkeiten für die Kunststoffbranche"*. October 7-8, Leoben.

Fiedler F. (2004). The state of the art of small-scale pellet-based heating systems and relevant regulations in Sweden, Austria and Germany. *Renewable and Sustainable Energy Reviews 8(3), pp. 201-221.*

Thür A., Furbo S. and Shah L.J. (2004). Energy savings for solar heating systems. *EuroSun 2004 Proceedings.* June 20-23, Freiburg, Germany.

Meir M., Rekstad J. and Svåsand E. (2004). Façade integration of coloured polymeric collectors. *EuroSun 2004 Proceedings.* June 20-23, Freiburg, Germany.

Meir M., Fiedler F., Rekstad J., van Wieringen B., Kristoffersen A.R. (2004). A non-pressurized heat store with immersed DHW-tank. *EuroSun 2004 Proceedings*. June 20-23, Freiburg, Germany.

Furbo S., Andersen E., Thür A., Shah L.J., Andersen K.D. (2004). Advantages by discharge from different levels in solar storage tanks. *EuroSun 2004 Proceedings*, June 20-23, Freiburg, Germany.

Fiedler F., Nordlander S., Persson T. and Bales C. (2004). Heat losses and thermal performance of commercial combined solar and pellet heating systems. *EuroSun 2004 Proceedings*, June 20-23, Freiburg, Germany.

Andersen E., Jordan U., Shah L.J. and Furbo S. (2004). Investigations of the SOLVIS stratification inlet pipe for solar tanks. *EuroSun 2004 Proceedings*, June 20-23, Freiburg, Germany.

Kahlen S.M., Wallner G.M., Meir M.G. and Rekstad J. (2005). Investigation of polymeric materials for solar collector absorbers. *North Sun 2005 Proceedings*, May 25-27, Vilnius, Lithuania.

Gajbert H., Råberg M., Lövehed L., Karlsson B. (2005). Design and performance of a large solar thermal system with wall integrated collectors in several directions. *North Sun 2005 Proceedings.* May 25-27, Vilnius, Lithuania.

Schakenda J.A., Spikkeland G., Meir M., Olivares A. and Rekstad J. (2005). Energy metering in solar heating systems – A comparison of three methods. *North Sun 2005 Proceedings.* May 25-27, Vilnius, Lithuania.

Gajbert H. and Karlsson B. (2005). Design and evaluation of two concentrated roof-integrated solar collectors for uninsulated roofs. *North Sun 2005 Proceedings*. May 25-27, Vilnius, Lithuania.

Meir M., Fiedler F., Gao P., Kahlen S., Mathisen, Olivares A., Rekstad J., Schakenda J.A. (2005). Facade integration of polymeric solar collectors. *North Sun 2005 Proceedings*. May 25-27, Vilnius, Lithuania.

Thür A. and Furbo S. (2005). Investigations on design of heat storage pipe connections for solar combisystems. *North Sun 2005 Proceedings.* May 25-27, Vilnius, Lithuania.

Rochas C. and Blumberga D. (2005). Solar combisystems in Latvia – market needs and potential. *North Sun 2005 Proceedings.* May 25-27, Vilnius, Lithuania.

Meir M., Rekstad J., Fiedler F., Kristoffersen A.R., Olivares A., Schakenda J.A. and van Wieringen B. (2005). A new and simple concept for a heat store combining solar and gas. *North Sun 2005 Proceedings*. May 25-27, Vilnius, Lithuania.

Fiedler F., Bales C., Thür A. and Furbo S. (2005). The actual status of the development of a Danish/Swedish system concept for a solar combisystem. *North Sun 2005 Proceedings*. May 25-27, Vilnius, Lithuania.

Andersen E., Furbo S. and Fan J. (2005). Investigations of fabric stratifiers. *ISES Solar World Congress 2005 Proceedings.* August 8-12, Orlando, USA.

Andersen E. and Furbo S. (2005). Investigations of solar combisystems. *ISES Solar World Congress 2005 Proceedings.* August 8-12, Orlando, USA.

LUND UNIVERSITY

ISSN 1671-8136
ISBN 978-91-85147-29-8